Title
Analysis and Design of Curved Box Girder Bridges

Author
Meyer, Christian

Publication Date
1970-10-01

REPORT NO.
UC SESM 70-22

STRUCTURES AND MATERIALS RESEARCH
DEPARTMENT OF CIVIL ENGINEERING

ANALYSIS AND DESIGN OF CURVED BOX GIRDER BRIDGES

by
C. MEYER

Report to the Sponsors: Division of Highways, Department of Public Works, State of California, and the Bureau of Public Roads, Federal Highway Administration, United States Department of Transportation.

DECEMBER 1970

COLLEGE OF ENGINEERING
OFFICE OF RESEARCH SERVICES
UNIVERSITY OF CALIFORNIA
BERKELEY CALIFORNIA

Structures and Materials Research
Department of Civil Engineering
Division of Structural Engineering
and
Structural Mechanics

Report No. UC SESM 70-22

ANALYSIS AND DESIGN OF CURVED BOX GIRDER BRIDGES

by

C. Meyer

Faculty Investigator: A.C. Scordelis

Sponsored by:

The Division of Highways
Department of Public Works
State of California
Under Research Technical Agreement
No. 13945-14423

and

U. S. Department of Transportation
Federal Highway Administration
Bureau of Public Roads

College of Engineering
Office of Research Services
University of California
Berkeley, California

December 1970

ABSTRACT

Curved bridges have become a major component of highway systems in recent years. Elevated freeways and multi-level interchange structures are very common in densely populated areas and could hardly be constructed without curved bridges. Usually, these bridges are of cellular cross section so that the high torsional moments due to curvature can be resisted economically. Methods of analysis and design to date have been very approximate, but because of the large number of curved bridges being constructed everywhere, refined methods of analysis are desirable.

In this dissertation, the main geometric parameters of curved bridges are studied, as they are prescribed by highway engineering requirements. The existing approximate methods of analysis are reviewed, and two new refined methods developed. The first one is based on the finite element method, for which a general computer program was written. This method may be used to analyze general non-prismatic folded plate structures with an incorporated three-dimensional frame. The second approach is the finite strip method of analysis applied to folded plate structures curved in plan, for which also a general computer program has been written. This method of analysis is restricted to structures simply supported along their straight radial edges. But the extension of the theory to include interior supports is also discussed.

On the basis of these refined analytical methods, the behavior of curved box girder bridges is studied. In particular, wheel load distribution characteristics are investigated especially with respect to how they change with the major bridge parameters. Finally, design recommendations are presented aimed at combining efficiency and accuracy of the design of curved box girder bridges.

ACKNOWLEDGEMENT

The author wishes to express his deepest appreciation and gratitude to Professor Alexander C. Scordelis for his constant guidance, encouragement and support throughout the course of this research. He would also like to thank Professors Graham H. Powell and Horst W. J. Rittel for their helpful suggestions, as well as Professor Carl L. Monismith, especially for his advice concerning highway engineering problems.

This research investigation was supported by the Division of Highways, Department of Public Works, State of California, and the Bureau of Public Roads, Federal Highway Administration, United States Department of Transportation. The generous support of the Computer Center at the University of California is gratefully acknowledged.

The findings, opinions, and recommendations expressed in this report are those of the author and not necessarily those of the sponsors.

TABLE OF CONTENTS

	Page
ABSTRACT	i
ACKNOWLEDGEMENT	ii
TABLE OF CONTENTS	iii
LIST OF SYMBOLS	vii
1. INTRODUCTION	1
1.1 General	1
1.2 The Bridge as Part of the Highway	2
1.3 Objective and Scope of Present Investigation	2
2. BRIDGE AND HIGHWAY	4
2.1 The Basic Design Problem	4
2.2 Principles of Geometric Highway Design	7
2.2.1 General	7
2.2.2 Horizontal Alignment	8
2.2.3 Vertical Alignment	11
2.2.4 Superelevation	11
2.2.5 Roadway Width	12
2.2.6 Miscellaneous	14
2.3 Geometry of Highway Bridges	14
2.3.1 Types of Bridge Structures	14
2.3.2 Bridge Structures on the Open Highway	15
2.3.3 Geometry of Bridge Structures on the Open Highway	16
2.3.4 Bridge Structures at Intersections	20
2.3.5 Geometry of Bridge Structures at Intersections	26

		Page
	2.3.6 Elevated Freeways	29
3.	METHODS OF ANALYSIS	35
	3.1 General	35
	3.2 Straight Bridge Approximation	37
	3.3 Curved Beam Theory	37
	3.4 Refined Beam Theories	43
	3.5 Plate and Grid Analyses	44
4.	FINITE ELEMENT ANALYSIS	51
	4.1 General	51
	4.2 Finite Element Models	51
	4.3 Description of Program FINPLA2	57
	4.4 Examples	59
5.	FINITE STRIP ANALYSIS OF CURVED FOLDED PLATES	63
	5.1 Introduction	63
	5.1.1 General	63
	5.1.2 Leve's Solution for Simply Supported Plates	64
	5.1.3 Harmonic Analysis of Prismatic Folded Plate Structures	65
	5.1.4 Finite Strip Analysis of Prismatic Folded Plate Structures	67
	5.1.5 Finite Element Analysis of Shells of Revolution	67
	5.2 Direct Stiffness Solution of Curved Folded Plate Structures	69
	5.3 Stiffness Matrix of Curved Strip Element	72

Page

5.4 Consistent Load Analysis and Determination of Internal Forces. 81

5.5 Description of Program CURSTR. 85

5.6 Examples 87

5.6.1 Straight Beam and Square Plate. 87

5.6.2 Axisymmetric Shells 90

5.6.3 Structures with Arbitrary Opening Angle 92

5.7 Study of Strain-Displacement Relations 100

5.7.1 Remark on Thin Shell Theories 100

5.7.2 Eigenvalues and Rigid Body Modes. 104

5.7.3 Studies on Element Level. 106

5.7.4 Studies on Structural Level 110

5.8 Study of Quadratic In-Plane Displacement Functions . . 114

5.8.1 Element Stiffness and Consistent Load Vector. . 114

5.8.2 Studies on Element Level. 117

5.8.3 Studies on Structural Level 119

5.9 Continuous Curved Folded Plate Theory. 124

5.9.1 Introduction. 124

5.9.2 Continuous Curved Strip Theory. 125

5.9.3 Examples. 128

5.9.4 Problems Related to Continuous Theory 134

6. BEHAVIOR OF CURVED BOX GIRDER BRIDGES 140

6.1 Objective. 140

6.2 Comparison Between Finite Element and Curved Strip Theory 140

Page

6.3 Concept of Wheel Load Distribution 145

6.4 The Single-Cell Curved Box Girder. 147

6.5 The Two-Cell Curved Box Girder 154

6.6 Additional Studies of Curved Box Girders 159

7. DESIGN OF CURVED BOX GIRDER BRIDGES 168

7.1 General. 168

7.2 Accurate Method of Design. 169

7.3 Simplified Method of Design. 170

7.4 Miscellaneous Design Considerations. 173

8. CONCLUSIONS 175

APPENDIX - BIBLIOGRAPHY A1

LIST OF SYMBOLS

Highway Engineering

D	degree of curve = 5729.58/R
e	superelevation rate, foot per foot
f	side friction factor
V	speed, mph
R	radius of curvature, feet

Curved Beam Theory

EI	bending rigidity, kip-ft^2
GJ_x	torsional rigidity, kip-ft^2
$M(\theta)$	internal bending moment, kip-ft
p	uniform external load, kip/ft
P	concentrated external load, kip
R	radius of curvature, ft
R_A, R_B	vertical beam end reactions, kip
$T(\theta)$	internal torsional moment, kip-ft
T	concentrated external torque, kip-ft
T_A, T_B	torsional beam end reactions, kip-ft
$V(\theta)$	internal shear, kip
X	redundant force = T_A
δ_A, δ_B	end rotations of beam
κ	= EI/GJ_x
θ	circumferential coordinate
θ_o	opening angle
ω	angle specifying section of applied force or moment

Curved Plate Theory

A_n, B_n, C_n, D_n	free constants of integration of plate equation
D	plate bending rigidity $= Et^3/12(1-\nu^2)$
E	Young's modulus
m	$= n\pi/\theta_o$
$M_\theta, M_r, M_{r\theta}$	internal plate bending moments
n	harmonic number
q	external load on plate
Q_r, Q_θ	internal plate shears
r	radial coordinate
r_1, r_2	edge radii of plate
r_o	mean plate radius $= (r_1 + r_2)/2$
t	plate thickness
V_r	Kirchhoff shear $= Q_r - \partial M_{r\theta}/r\partial\theta$
w	plate deflection
η	normalized radial coordinate $= r/r_o$
θ	circumferential coordinate
θ_o	opening angle
ν	Poisson's ratio

Curved Folded Plate Theory

a	half element width projection $= (r_2 - r_1)/2$
$[A]$	displacement transformation matrix
b	mean radius of shell element $= (r_2 + r_1)/2$
d_{ij}	elements of force-displacement matrix $[D]$, $i,j = 1,2,\ldots,6$
$[D]$	force-displacement matrix
E	isotropic Young's modulus

E_s, E_θ	orthotropic Young's modulus in s and θ directions
$\{F_i\}$	global nodal force vector
F_P, F_H, F_V, F_M	global nodal joint force components in U, V, W, Ω directions
G	shear modulus = $E/2(1 + \nu)$
$[k]_n$	element sitffness of shell element for harmonic n
$k_{uu}, k_{uv}, k_{uw}, k_{vv}, k_{vw}, k_{ww}$	submatrices of element stiffness $[k]_n$
L	span length along the curve = $R \cdot \theta_o$
$M_s, M_\theta, M_{s\theta}$	internal bending moments of shell element
n	harmonic number
$N_s, N_\theta, N_{s\theta}$	internal membrane stress resultants of shell element
p_u, p_v, p_w	external load components in u,v,w directions, kip/ft^2
$\bar{p}_u, \bar{p}_v, \bar{p}_w$	intensities of load components at nodal joints, kip/ft^2
r	radial coordinate
r_1, r_2	radii of element joints 1 and 2
R	radius of reference line of structure
$\{R_i\}_n$	consistent load vector in element coordinates, for harmonic n
s	transverse coordinate for shell element
s_{12}	transverse element width between joint 1 and 2
t	element thickness
$[T_n]$	strain-displacement matrix for harmonic n
u, v, w	element displacements in local coordinates
u_i, v_i, w_i	element joint displacements
U_i, V_i, W_i	global joint displacements

X	circumferential coordinate along reference line
Z	downward coordinate
$\{\varepsilon\}$	strain vector for shell element
$\varepsilon_s, \varepsilon_\theta, \varepsilon_{s\theta}$	membrane strains in shell element
η	normalized transverse coordinate = $2s/s_{12} - 1$
θ	angular circumferential coordinate
θ_o	opening angle of structure
$\kappa_s, \kappa_\theta, \kappa_{s\theta}$	curvature strains in shell element
ν	isotropic Poisson's ratio
$\nu_{s\theta}, \nu_{\theta s}$	orthotropic Poisson's ratios
$\{\sigma\}$	internal force vector for shell element
φ	inclination angle of shell element
$\langle\Phi_u\rangle, \langle\Phi_v\rangle, \langle\Phi_w\rangle$	displacement interpolation polynomial vectors
$\langle\Phi_p\rangle$	internal load interpolation polynomial vector
ω_i	element joint rotation
Ω_i	global joint rotation

1. INTRODUCTION

1.1 General

The present mode of vehicular traffic transportation is not likely to change rigorously within the foreseeable future, i.e., mass transportation will to a large extent be handled by vehicular traffic requiring an efficient highway network. Hence, in all industrialized nations as well as in those which are in the process of industrialization, the efforts of constructing efficient highway systems will continue if not increase.

With the growth of urban populations everywhere in the world, this construction of highways will to a great extent be concentrated on arterials in urban built-up areas. In fact, it will be a challenging and exciting requirement imposed on the responsible agencies charged with the construction of urban highways to help in modelling new cities and restructuring existing ones. A main design concept for this purpose will be the multiple use of the highway corridor both vertically and horizontally such that the entire corridor is planned as an integrated part of the city.

The consistent separation of vehicular and pedestrian traffic on different levels will, for example, be one solution for providing sufficient safety of people and property. Likewise, the consistent use of cross-traffic free intersections within the highway system will increase its efficiency and reduce losses due to accidents. In urban areas with high land values, these cross-traffic free intersections are usually most economically obtained using multi-level interchange structures.

Thus, bridge structures will play an increasing role in future highway systems as a major cost factor. Therefore it is desirable that engineers are familiar with all problems inherent in the design of a bridge of general geometry.

1.2 The Bridge as Part of the Highway

Being an integrated part or subsystem of the highway system, the bridge itself is influenced by a variety of factors such as urban design, traffic and highway engineering requirements, structural engineering, topographical and soil conditions, political and aesthetical considerations, etc., all of which may in certain cases be very important. However, for most bridge designs, structural considerations are usually not very important with respect to the choice of general location and geometrical layout. These are more likely to be determined by traffic and highway engineering requirements or urban design considerations. Because it is the purpose of both the highway and the bridge to convey traffic, traffic requirements have usually clear priority for the determination of location and geometrical layout of a bridge. Thus, in the "decision-making stage" of the design process, structural considerations are often not decisive, although they become of prime importance once the geometrical layout has been determined.

1.3 Objective and Scope of Present Investigation

The objective of this dissertation will be to present the curved bridge design problem in a broad sense. First, the role of the structural engineer in the decision-making stage of the design process in which location and geometrical layout are determined, will be discussed. Then, a summary of highway and traffic engineering principles will be presented as they have important consequences on the bridge geometry, so that structural engineers may obtain a complete picture of the range of geometrical parameters of curved bridges.

As for the analysis, present methods are usually very approximate and often based on empirical considerations. In view of the large number of curved bridges built everywhere, it therefore appears to be desirable to have at hand more accurate methods of analysis. If a comparison study shows that present methods of analysis capture the overall structural behavior in all cases well enough for engineering purposes, then engineers will be satisfied with this confirmation that their empirical rules were correct. If, however, it can be shown that the approximate methods lead to unreliable results for certain types of structures, then the need for refined methods will have been clearly demonstrated.

Thus, it will be the main goal of this dissertation to critically review existing methods of analysis and design of curved bridges and to develop new methods which take most of the major bridge parameters into consideration. With the aid of these refined methods of analysis, the behavior of bridges under loads will be studied as a function of horizontal curvature. Since torsional moments, which become increasingly important with higher curvatures, are most economically resisted by closed cross sections, the design methods to be proposed in Chapter 7 will primarily be oriented towards box girder bridges.

2. BRIDGE AND HIGHWAY

2.1 The Basic Design Problem

It is the objective of this chapter to investigate the salient features of interaction between bridge and highway as they are important in the more general aspects of a bridge design.

Bridge and highway form a system which is most suitably treated with the tools of systems design. The best or optimum solution will be the one which optimizes benefits compared to costs. Both costs and benefits have to be conceived in a wide sense, including right-of-way, construction and maintenance cost compared with the economical benefits, but also user and accident costs and human and cultural factors such as the impact on the adjacent environment should be considered. Therefore not only highway and traffic engineering requirements and structural engineering principles govern the design. Urban design considerations, political, social and aesthetical aspects, topographical and soil conditions may very well be even more important factors to be taken into account.

It is beyond the scope of this dissertation to cope with the design of the bridge-highway system in its broadest sense. This study will be restricted therefore to the general discussion of only highway, traffic and structural engineering aspects, although one should always keep in mind that they may often be less important than some of the other above mentioned factors.

Traffic and highway engineering principles furnish the criteria by which the serviceability of the overall highway design is evaluated. These criteria ask for the most efficient traffic flow, safety, and elimination of accident hazards at optimum cost which might be evaluated with the help of a road user benefit analysis, taking into account all the cost factors just mentioned.

The structural engineering aspect of the design defines the criteria for strength, stability, and safety under various loading conditions at optimum cost. The fact that skew and especially curved structures are more expensive due to higher stresses and construction cost therefore needs consideration.

In the optimization process, the various influencing factors have to be weighed against each other. Figure 2.1 shows a qualitative flow chart of how an optimal solution might be arrived at. As can be seen in this diagram, structural considerations influence the bridge alignment and overall geometrical layout (such as for example curvature, roadway width, span lengths and skew) only when the structural cost is a very important cost factor in the overall project, because otherwise the savings due to a suboptimization of the bridge alone will seldom justify the cost increase associated with realignment of the approaches that become necessary to meet certain traffic standard requirements. A typical example which makes an overall optimization indeed desirable is the elevated freeway.

Historically, the basic interaction between bridge and highway has been recognized and considered in design only quite recently. In earlier times, the importance of a bridge structure was usually largely overemphasized compared to the highway design. Thus, almost exclusively straight and right-angle bridges were built, resulting often in sharp turns at the approaches and generally tortuous alignment because the most favorable bridge site was the only criterion for location.

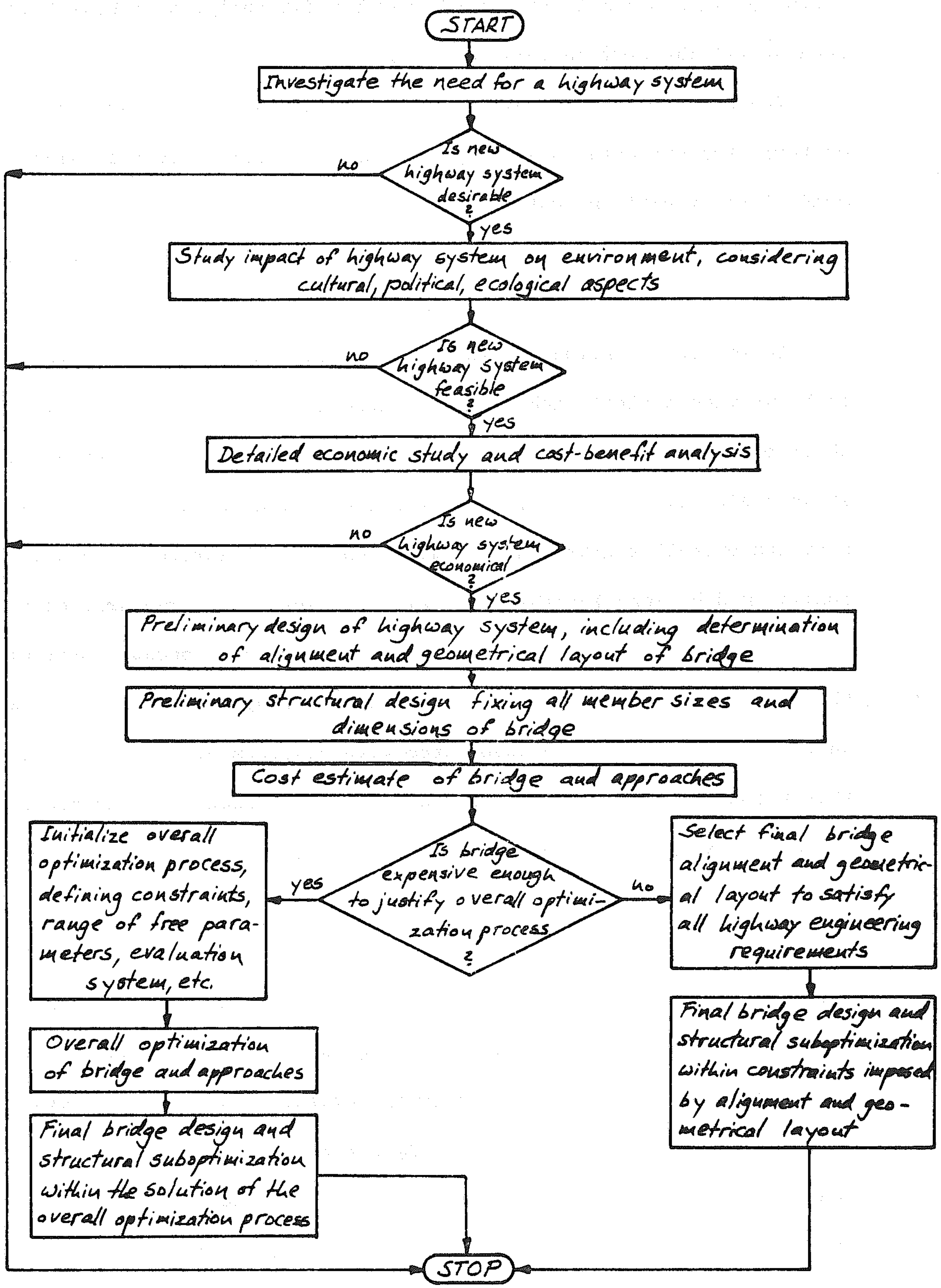

Fig. 2.1 A Design Scheme For The Bridge-Highway System

Curved bridges have been introduced into highway systems much more recently. Pressure from highway engineers for better alignments stimulated a rapid improvement of curved bridge design. In addition, structural engineers were becoming more and more familiar with the special problems due to the curvature of bridges. But still, research on curved highway bridges, in particular on those having the advantageous cellular cross sections, has been scarce. The large number of existing bridge structures have proven to be satisfactory with respect to serviceability and strength. It shall be the objective of further research to produce curved bridges that satisfy also the requirement of economy.

2.2 Principles of Geometric Highway Design

2.2.1 General

In order to study curved bridges it is necessary to understand the principles of geometric highway design which determine the bridge centerline alignment as well as the major bridge dimensions.

The objective of all highway design is a balanced composition of the various design elements which are to be consistent with an appropriate design speed. Because the efficiency of a highway is primarily evaluated in terms of its capacity, any highway is only as efficient as its weakest point. Critical points are the intersections and interchanges which therefore have to be designed with utmost care, otherwise the rest of the highway might be overdesigned. Bridge structures are employed primarily at these critical points, thus confirming the importance of the bridge-highway interaction discussed in the previous section.

Another important measure of highway efficiency is the safety which it provides for traffic. The high priority of the need for eliminating accident hazards imposes certain requirements on the design of highway bridges. Drivers tend to be confused by narrow roadway widths on overpasses and by column piers and massive abutments at underpasses which therefore have to be designed properly.

Geometric highway design may be subdivided into two categories, design of open highways and design of intersections. The governing design principles usually vary from one category to the other, therefore it is also appropriate to distinguish two classes of bridge structures. While the first class includes bridges over valleys, waterways, and railway tracks as well as any grade separation structures without ramps, the second class contains all types of grade separation structures with ramps, i.e., interchange structures. Elevated freeways are a special combination of the above two groups and will therefore be treated separately.

Below, those design elements will be discussed briefly which define the geometry of highway bridges. Reference may be made to two publications of the American Association of State Highway Officials, "A Policy on Geometric Design of Rural Highways," [1.1], and "A Policy on Arterial Highways in Urban Areas," [1.2], both excellent summary treatments of geometric highway design, on which most of the design data below are based.

2.2.2 Horizontal Alignment

In a highway design, all geometric elements should, as far as economically feasible, be balanced to permit safe and continuous operation at design speed. Given this design speed, V, in miles per hour, the roadway superelevation rate, e, in foot per foot, and a side friction factor, f, then the minimum permissible radius of curvature can be derived from a law of mechanics and is given by

$$R = \frac{1}{15} \frac{V^2}{e+f} \tag{2.1}$$

in feet. Often, instead of using the radius as measure of curvature, the "degree of curve," D, is specified which is defined to be the degree subtended by a 100 ft. long curve and which is related to R as D = 5729.58/R, so that Eq. (2.1) can be stated in the form

$$D = 85{,}900 \frac{e+f}{V^2} \tag{2.2}$$

Maximum curvature restrictions are different on the open highway than they are at intersections. Likewise, turning roads and ramps have their own maximum requirements, and highways in urban areas are designed differently than in rural areas. Curvatures in urban areas are generally sharper than in rural areas because of lower design speeds.

Two types of horizontal curves are most commonly used in highway practice--circular curves with minimum radius requirements according to Eq. (2.1), and easement curves providing smooth transitions between highway sections with different curvatures.

As transition curves, clothoid spirals are very popular because they have the property of linearly varying curvature if moving along the curve coordinate s, Fig. 2.2,

$$\frac{1}{R} = a^2 s \tag{2.3}$$

In parameter form, the spiral is defined as

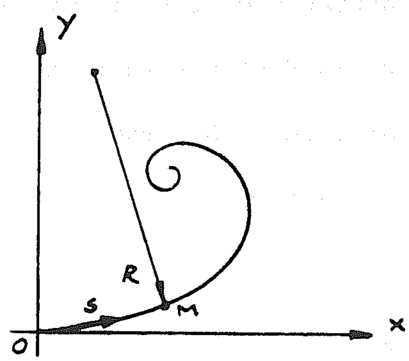

$$x = a\sqrt{\pi}\int_0^t \cos\frac{\pi t^2}{2}\,dt$$
$$y = a\sqrt{\pi}\int_0^t \sin\frac{\pi t^2}{2}\,dt \qquad (2.4)$$

with

$$t = \frac{s}{a\sqrt{\pi}}\ , \quad s = \widehat{OM}$$

Fig. 2.2 Clothoid Spiral

The parameter a^2 is the "sharpness" of the spiral and defines the rate of curvature increase per unit length of curve.

Transition curves should be fitted in between curves of substantially different curvature radii and between tangents and curves with smaller than certain minimum radii which are prescribed as functions of the design speed. While these spirals are essential for railbound traffic to avoid jerks, many highway departments prefer circular curves with intermediate curvatures as transition curves, arguing that traffic lanes are wide enough to let each driver select his own spiral within a lane.

Often, maximum curvatures cannot be utilized because the stopping sight distance might govern the design, i.e., the minimum distance which a vehicle traveling near design speed requires to stop before reaching an object in its path. The sight distance should at any point on a highway be as long as possible but cannot be shorter than certain limits.

Passing sight distance, on the other hand, is of importance mostly only for 2-lane highways and should be provided only over as large a portion of the highway as feasible and will therefore seldom control the horizontal alignment.

2.2.3 Vertical Alignment

In a discussion of vertical alignment as design element, maximum grades and vertical curves need to be considered.

Maximum grade restrictions depend on the nature of the area, i.e., urban or rural or mountainous, as well as on the highway type, design speed, nature of traffic, etc. But also very important is the length of grade, because long grades reduce the speed of trucks considerably.

Vertical curves provide the gradual change between tangent grades. They should be safe and comfortable in operation, pleasing in appearance and adequate for drainage. Usually they are of simple parabolic shape and maximum curvatures are generally controlled by stopping sight requirements for both crest and sags. In the latter case, the sight distance at night (headlights) governs. In addition, gravitational and vertical centrifugal forces act in the same direction in sags so that driving comfort plays a role. To consider passing sight distance for vertical alignment is often impractical because too flat curves would be required.

Vertical curvatures are generally so small that they can be usually neglected for structural considerations. For example, a crest vertical curve from + 5% to - 5% grades for a design speed of 50 mph has to be 850 ft. long while the corresponding sag vertical curve needs only to be 750 ft. long. Approximating these curves by circular arcs, radii of 8500 ft. and 7500 ft. would be required, respectively.

2.2.4 Superelevation

Maximum horizontal curvature limits depend on a given design speed, developed side friction factor, and on the rate of superelevation. The maximum permissible superelevation rates depend on climatic conditions (snow and ice), terrain conditions (flat or mountainous), type of area (rural or urban), and the frequency of slow moving vehicles. This variety of influence factors explains the variety of prescribed maxima.

The common maximum superelevation for open highways is 0.12 ft. per ft., preferably less. In urban areas with high traffic volumes and generally lower average speeds, the general maximum is 0.10 ft. per ft. and in areas with snow and ice, 0.08 ft. per ft.

If transition curves are used between curves and tangents, then the superelevation can be run off on these transition curves. Otherwise at least a portion of the runoff has to be applied on the tangent before the curve. Geometrically, the superelevation runoff produces a twisted roadway surface. However, considering that the maximum difference in slope between the roadway edges seldom exceeds 1%, this twist can be neglected in a structural idealization.

On the other hand, superelevation itself may in some cases affect the state of stress in a bridge such that it should not be neglected. For example, on a 2-lane roadway with a superelevation of 0.10 ft. per ft., the outer edge is 2.4 ft. higher than the inner edge. The vertical lever arm for centrifugal loads is thus increased by that amount.

2.2.5 Roadway Width

Bridge structures generally have to be designed to carry the complete roadway width, which includes the total number of traffic lanes, shoulders and a median separating lanes of opposing traffic in divided highways.

Lane widths of 11 to 13 ft. are essential for safe and efficient operation, and 12 ft. lanes have been accepted as general standard. Lanes of 10 ft. or less should be avoided or reserved for low volume roads because narrow lanes greatly reduce the highway capacity and lead to high accident rates.

The median in divided highways should for safety reasons be as wide as possible. However, the desirable minimum of 60 ft. is often impractical, especially in urban areas. The required absolute minimum is 4 ft., but the actual median width will usually be a compromise between safety and economy.

Shoulders are used for emergency stops or parking of disabled vehicles as well as to insure full traffic capacity. One stalled vehicle in rush hour traffic might have catastrophic consequences on the traffic situation. Therefore, shoulders are essential requirements for arterial highways in urban areas, and their use might be justified even on long bridges. They also serve as safety margins between the through traffic and guardrails, curbs, bridge piers, etc.

The desirable minimum shoulder width is generally 10 ft., preferably 12 ft. Where this is considered too costly, as for example on elevated freeways, a partial shoulder of 5-6 ft. width might be justified. On long-span structures, even this might be too expensive so that only a minimum offset of 2-3 ft. is provided to separate the roadway from the barrier curb.

In general, however, it does not pay to save money in reducing the roadway width. The savings will usually be too small to justify daily rush hour congestions and high accident rates. Besides, minimum designs often prove to be inadequate even almost at the time of completion.

2.2.6 Miscellaneous

If sidewalks are required for pedestrian traffic, they are provided on either one or both sides of the bridge, with widths of at least 6 ft., preferably 8-12 ft. in built-up districts and at least 4 ft., preferably 6 ft. in residential areas. On elevated freeway structures, sidewalks are never included except for river or valley crossings or other long-span structures where other means for pedestrian crossing are not readily available.

On bridge structures, the roadway is usually curbed with barrier curbs as part of the rail-parapet. Curbs should be offset from the edge of the through traffic lanes at least 2 or 3 ft. if no shoulders are used. There is increased tendency to eliminate barrier curbs along walls or faces of bridge parapets if these are separated by several feet from the edge of the through traffic lane, for example if a shoulder is carried across the structure.

2.3 Geometry of Highway Bridges

2.3.1 Types of Bridge Structures

The best bridge structure in a highway engineering sense is the one which drivers practically take no notice of because only then will their driving behavior be the same as on other points of a highway. This requirement demands among others, liberal shoulder clearances everywhere and adequate offset of piers, columns, abutments, walls, etc. The presence of a structure tends by itself to be already a hazard which has to be overcome by a careful and liberal geometric design, as far as economically feasible. In fact, to counterbalance any sense of restriction caused by abutments, piers, etc., geometric standards at a highway grade separation should ideally be even higher than on the open highway.

Highway bridges should in general be of the deck type because of appearance and possibility of future widening. Only long-span structures may require through girders or trusses.

In this subchapter, three classes of highway bridges will be considered, ordered according to their special geometric characteristics.

a) Structures on the open highway facilitating a smooth and efficient highway alignment over obstacles such as waterways, valleys, railway tracks and cross roads;

b) Grade separation structures at interchanges carrying the intersecting highways as well as ramps which provide turning movements from one highway leg onto another one;

c) Elevated freeways which are an important component of arterial freeway systems in urban areas, requiring structures of both aforementioned types and which will be discussed separately because of their special problems.

2.3.2 Bridge Structures on the Open Highway

The simplest case of those bridges to be considered here is a simple overcrossing over a minor cross road. There will hardly be any interaction between bridge and highway in the sense of the overall design problem discussed in Section 2.1, because the structure cost is relatively small compared to the highway cost. Bridge location and geometry are completely predetermined by the highway alignment. In general, the horizontal curvatures of these bridges will be very small if not negligible.

If long bridge structures are required, for example at waterway and valley crossings, then the bridge economy may affect the highway design in some way or other, because the highway can no longer be designed without any regard to the bridge. An extreme example is the Golden Gate Bridge, Fig. 2.3. Here, bridge location and geometry had to be chosen without any consideration for highway approaches and alignment because their costs are almost negligible compared to the bridge cost. Also, roadway dimensions had to be reduced to the absolute bearable minimum.

2.3.3 Geometry of Bridge Structures on the Open Highway

Maximum permissible curvatures of open highways for given design speeds, maximum superelevations, and side friction factors can be calculated according to Eq. (2.1) or (2.2), and rounded values are given in Table 2.1 which are valid for both rural and urban highways.

Transition curves between tangents and circular curves are required only for curvatures exceeding the upper limits given in Table 2.2, while below these limits, they are desirable but not essential. As can be seen, all curves except for those with very small curvatures require transition curves.

Maximum grades are a function of the design speed and of topographic conditions and are given in Table 2.3. Vertical curvatures are generally so small that they are unessential for bridge geometry considerations.

The generally accepted maximum superelevation rate is 0.10 ft. per ft., but according to traffic, climatic and topographic conditions, it may be as high as 0.12 or as low as 0.08 ft. per foot for rural

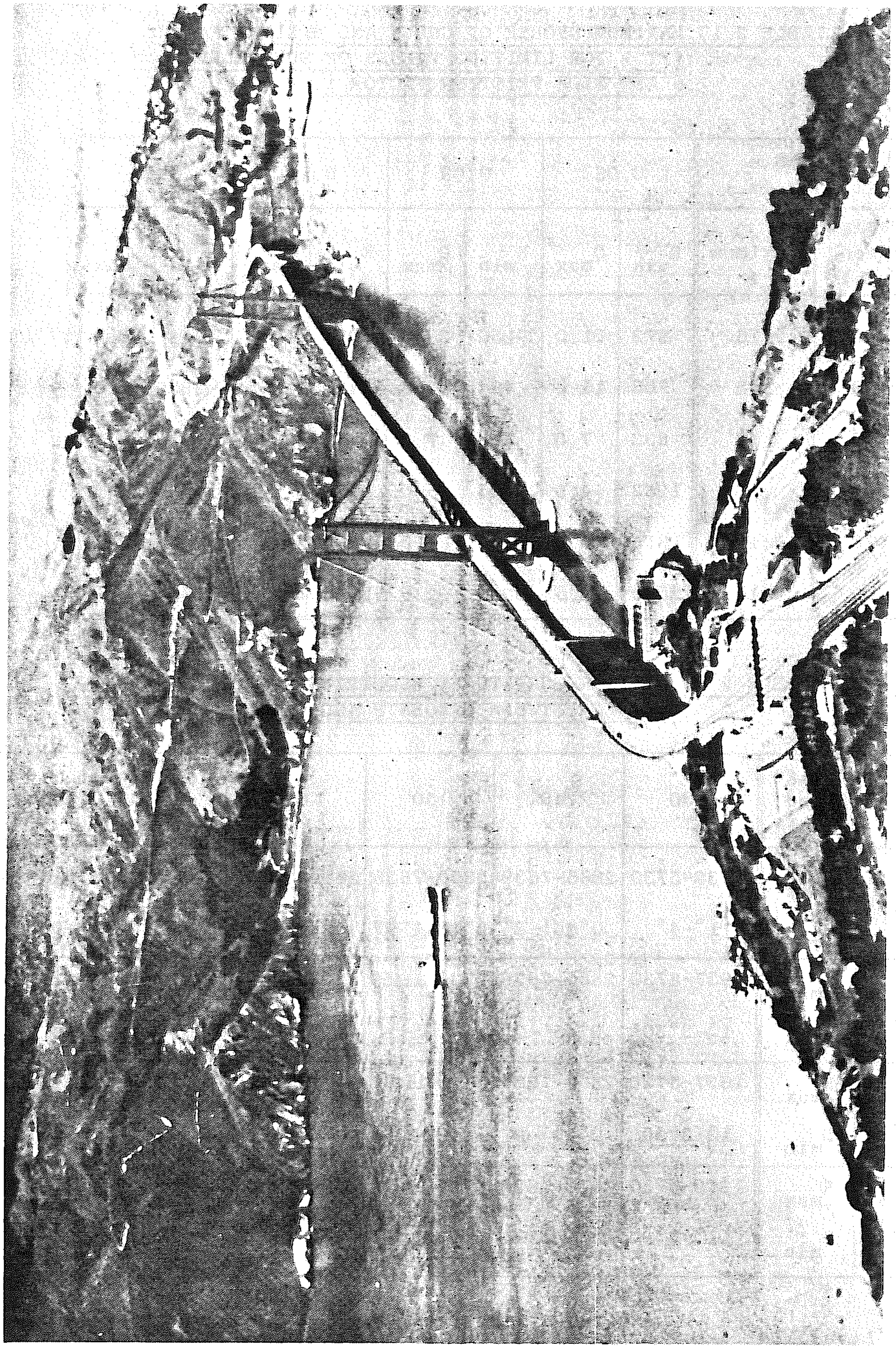

Fig. 2.3 Golden Gate Bridge, San Francisco

TABLE 2.1. MAXIMUM DEGREE OF CURVE AND MINIMUM RADIUS (FT.) FOR LIMITING VALUES OF SUPERELEVATION e AND SIDE FRICTION FACTOR f.

Maximum e (ft. per ft.)		0.06		0.08		0.10		0.12	
Design Speed (mph)	Maximum f	R_{min}	D_{max}	R_{min}	D_{max}	R_{min}	D_{max}	R_{min}	D_{max}
30	.16	273	21.0	250	23.0	231	25.0	214	26.5
40	.15	508	11.5	464	12.5	427	13.5	395	14.5
50	.14	833	7.0	758	7.5	694	8.5	641	9.0
60	.13	1263	4.5	1143	5.0	1043	5.5	960	6.0
70	.12	1815	3.0	1633	3.5	1485	4.0	1361	4.0
80	.11	2510	2.5	2246	2.5	2032	3.0	1855	3.0

TABLE 2.2. MINIMUM CURVATURES REQUIRING TRANSITION CURVES BETWEEN TANGENTS AND CURVES*

e	Design Speed (mph)	30	40	50	60	70	80
.06	R_{max}	1432-5730	2865-7639	3820-7639	5730-22918	7639-22918	11459-
	D_{min}	1°-4°	0°45'-2°	0°45'-1°30'	0°15'-1°	0°15'-0°45'	-0°30'
.08	R_{max}	1637-5730	2865-7639	5730-11459	5730-22918	7639-22918	11459-
	D_{min}	1°-3°30'	0°45'-2°	0°30'-1°	0°15'-1°	0°15'-0°45'	-0°30'
.10	R_{max}	1637-5730	2865-7639	5730-11459	7639-22918	7639-22918	11459-
	D_{min}	1°-3°30'	0°45'-2°	0°30'-1°	0°15'-0°45'	0°15'-0°45'	-0°30'
.12	R_{max}	1910-5730	3820-7639	5730-11459	7639-22918	7639-22918	11459-
	D_{min}	1°-3°	0°45'-1°30'	0°30'-1°	0°15'-0°45'	0°15'-0°45'	-0°30'

*Lower limits are desirable, upper limits essential.

highways, while in urban areas, it generally varies between 0.05 and 0.08 ft. per ft., with an average maximum rate of 0.06 ft. per ft.

TABLE 2.3. MAXIMUM GRADES OF HIGHWAYS, %

	Design Speed, mph					
Type of Topography	30	40	50	60	70	80
Flat	6	5	4	3	3	3
Rolling	7	6	5	4	4	4
Mountainous	9	8	7	6	5	-

Road widths on bridge structures should preferably be the same as on any other highway point. This implies a constant number of lanes with 12 ft. per lane. Narrower lanes may have to be widened on sharp curves.

The desirable shoulder width depends on the length or cost of the bridge. Short bridges in this sense are defined to be structures with lengths up to 50 ft. or preferably 150 ft., for freeways or other high type highways even up to 250 ft. These structures will generally carry full shoulder widths of 10 ft. For longer structures, high structural costs may permit only partial shoulder widths or minimum curb clearances of 3.5 - 4.5 ft., unless a relatively high ratio of the design hour volume to the design capacity justifies employment of partial or even full shoulders. In any case, it is good design practice to make an economic study for each long structure individually to obtain a feasible shoulder width as well as a reasonable median width for divided highways. Since it is generally more economical to build a single structure for median widths below 20 ft., double structures are unusual in urban areas. Commonly used roadway widths are summarized in Table 2.4.

Spans of overpass structures are governed by clearance requirements at supports and abutments for the underpassing roadway, asking for the least amount of restriction of drivers as possible. Center supports, for example, should only be used where the median is wide enough for adequate clearances. Likewise, the sense of openness and unrestricted lateral clearance is favoring open-end spans more than solid abutments, Fig. 2.4.

From a pure highway safety point of view, a one-span structure would be the most desirable solution--but also the most expensive one. The optimum solution, therefore, has to be found as a compromise between structural cost and value in utility and safety. Edge clearance requirements between roadway pavement and outside face of columns, piers, etc. are modified from time to time towards more liberal and therefore safer values. With those listed in Table 2.4 (see Refs. [1.1] and [1.2]), resulting spans of highway overpasses can be calculated and are summarized in Table 2.5. These spans apply only to straight right-angle overpasses and have to be modified appropriately in case of curvature or skew supports. Spans of structures other than highway overpasses are influenced by so many factors that it is unfeasible to summarize them here.

2.3.4 Bridge Structures at Intersections

Grade separation structures are required for a cross-traffic-free intersection of two highways. If no provision for moving from one highway onto the other one is made, relatively simple structures which actually belong to the class of bridges just discussed may be

TABLE 2.4. WIDTHS OF OVERPASS STRUCTURES, FT.

Highway Type			Short Structures					Long Structures				
			Lanes	Median	Left Shoulder	Right Shoulder	Total	Lanes	Median	Left Shoulder	Right Shoulder	Total
2-Lane Highway	Low	M†	20		2.5	2.5	25	20		2.5	2.5	25
	Volume	D†	22		3.5	3.5	29	22		3.5	3.5	29
	Local	M	22		4	4	30	22		3.5	3.5	29
	Character	D	24		6	6	36	24		4.5	4.5	33
	Major	M	24		8	8	40	24		3.5	3.5	31
		D	24		10	10	44	24		4.5	4.5	33
4-Lane Divided Hwy.	Single	M	48*	4		2(8)	68*	48*	6		2(3.5)	61*
	Structure	D	48*	14		2(10)	82*	48*	6		2(4.5)	63*
	Double	M	24*		4	8	36*	24*		3.5	3.5	31*
	Structure	D	24*		6	10	40*	24*		4.5	4.5	33*

† M - minimum; D - desirable.

* Add 12 ft. for each additional lane.

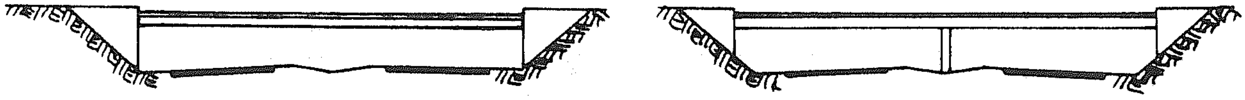

a) Solid Abutments (To be avoided)

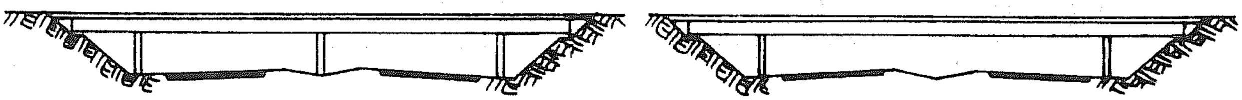

b) Three- and Four-Spans with Open Ends

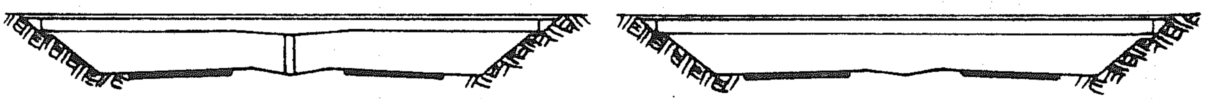

c) One- and Two-Spans with Open Ends (Least obstructive)

Fig. 2.4 Types of Overpass Structures

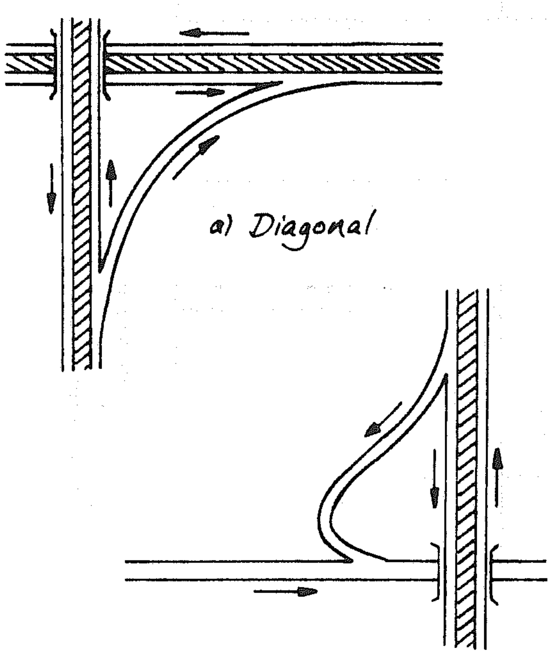

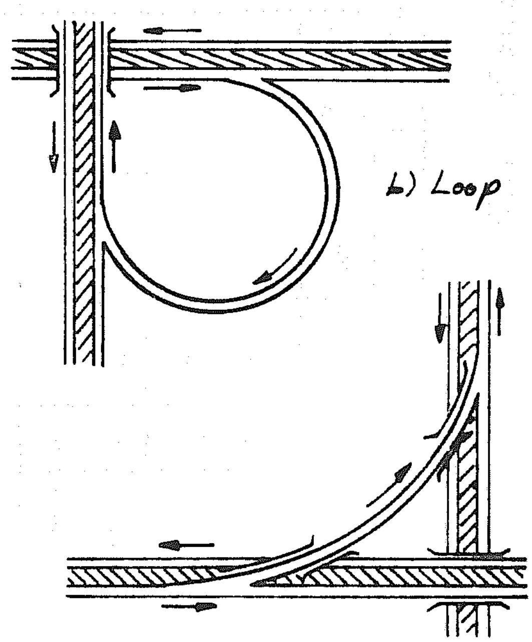

c) Semidirect Connection   d) Direct Connection

Fig. 2.5 Ramp Types

TABLE 2.5. SPANS OF HIGHWAY OVERPASS STRUCTURES, FT.*

Type of Under-passing Highway	Lanes		Left Clearance		Right Clearance		Median		Total Span	
	Min.	Des.	Min.	Des.	Min.	Des.	Min.	Des.	Min.	Des.
4-Lane Divided Highway (Single Span)	48†	48†	6	12	6	12	4	16	64†	88†
4-Lane Divided Highway (2 Spans)	24†	24†	4.5	6	6	12			34.5†	42†
Major 2-Lane Highway (provision for future improvement)	24+18	24+24	6	6	6	6			54	60
2-Lane Highway (no foreseeable improvement)	22	24	6	10	6	10			34	44
Local Road	20	22	4	6	4	6			28	34

*Sidewalks and auxiliary lanes not considered.

†Add 12 ft. for each additional lane.

sufficient. But if any interchanges between the highways are provided, quite elaborate multi-level structures might become necessary and may in fact even be the cheapest solutions in built-up urban areas. The choice of a specific interchange design is influenced mainly by questions of right-of-way, topography, and the nature of traffic.

Interchanges have to be designed with liberal alignment if the capacities of the approaching highways are to be fully utilized. Steep grades and sharp turns are apt to be hazards and tend to reduce highway capacities. On the other hand, too flat curves usually result in long extra travel distances which can be avoided by reasonably reducing design speeds which drivers generally accept when approaching interchanges.

The type of an interchange depends on the kind of ramps used. There are four basic ramp types: diagonal, loop, semidirect, and direct connection, Fig. 2.5. The superiority of the direct connection over the loop is obvious. In order to perform a left turn, the loop requires a right turn of 270°, while the direct connection leads directly around 90°. The semidirect connection is the intermediate solution. Ramp structures are normally subjected to higher curvatures, grades, and superelevations than the structures carrying the intersecting highways, therefore design speeds are generally lower on ramps. Some interchange types are shown in Fig. 2.6.

The interchange design is largely controlled by highway engineering requirements rather than structural considerations. Since the whole interchange is constructed solely for the purpose of providing a safe and efficient cross-traffic-free intersection, it would be unrealistic to impede the ramp alignment because of structural reasons.

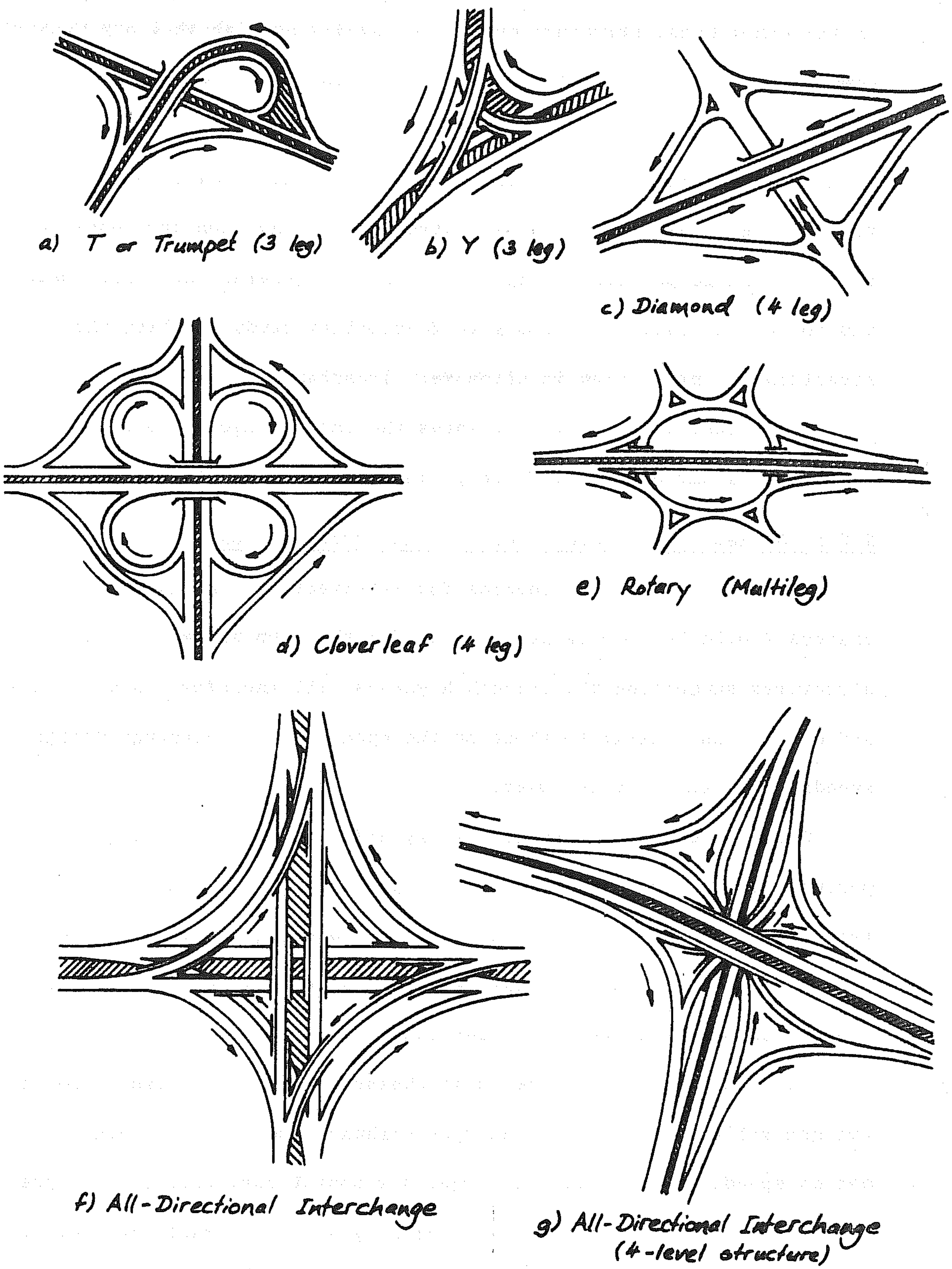

Fig. 2.6 General Types of Interchanges

On the other hand, structure costs are usually so high that any measure compatible with the alignment should be taken if it reduces the cost. For example, if a cost analysis reveals that the 6 simple bridge structures of Fig. 2.6f is still cheaper than the one 4-level structure of Fig. 2.6g, then this is a strong recommendation for choosing the interchange pattern of Fig. 6f. Thus, in general the final design has to be the result of a complete feasibility study in which the structural point of view is often very important.

For illustration, Fig. 2.7 shows the interchange between the Santa Monica and San Diego Freeways in Los Angeles, California.

2.3.5 Geometry of Bridge Structures at Intersections

Geometric design standards for intersecting highways at interchanges should be comparable to those for the open highway. Bridge structures supporting the through highways will therefore have layouts and dimensions similar to those on the open highway, although design speeds will generally be lower.

Those structures which are really different in terms of geometric parameters are the ramp structures supporting the turning roads of interchanges. These bridges have the most unusual geometrical layouts that are known in modern bridge design. Sharp horizontal curvatures, steep grades and maximum superelevations, twisted roadway surfaces and tapered cross-sections may be their characteristics. Design standards are generally lower than on the open highway, coupled with reduced design speed, thus permitting larger horizontal curvatures. But speed reductions at intersections and interchanges are generally considered by drivers as unavoidable, especially for turning movements. These unusual structures suggest themselves to reinforced concrete as the

Fig. 2.7 Interchange Between San Diego and Santa Monica Freeways in Los Angeles (Courtesy of California Highway Department)

proper material for construction. Furthermore, cellular cross sections are generally the most economical ones to carry the incurring torsional moments.

The design speeds for ramps should generally equal the average running speed of the intersecting highways and are summarized in Table 2.6. The corresponding curvature radii can be derived, once

TABLE 2.6. GUIDE VALUES FOR RAMP DESIGN SPEED

Highway Design Speed, mph		30	40	50	60	65	70	75	80
Ramp Design Speed, mph	Desirable	25	35	45	50	55	60	60	65
	Minimum	15	20	25	30	30	30	35	40

suitable superelevation rates and side friction factors have been selected, and are summarized in Table 2.7, which is just a continuation of Table 2.1 into lower design speeds. Minimum stopping sight distance must always be provided, but passing sight distance for 2-lane two-way turning roads is not a design control because they are short and should be marked for no passing.

TABLE 2.7. MINIMUM CURVATURE RADII AND SPIRAL LENGTHS FOR TURNING ROADS

Design (Turning) Speed, mph	15	20	25	30	35	40	45
Suggested Minimum Radius, ft	50	90	150	230	310	430	550
Corresp. Max. Degree of Curve	-	64	38	25	18	13	10
Suggested Min. Spiral Length, ft.		70	90	110	130	160	200

In view of the strong curvatures of ramps, transition curves, preferably spirals, are almost always used to define a natural travel path. For compound curves, spirals or circular curves with intermediate radii are required if $R_2 \geq 2R_1$ preferably if $R_2 \geq 1.75R_1$. Due to lower design speeds, spiral lengths may be shorter on intersection curves than on open highways but no shorter than given in Table 2.7.

Maximum grades on intersection curves should be as low as possible, especially in urban areas, and in no case exceeding the maximum for open highways, while superelevations should be as high as practical. Generally accepted maximum values are summarized in Table 2.8.

TABLE 2.8. MAXIMUM GRADES AND SUPERELEVATION RATES FOR TURNING ROADS

Condition	General	Heavy Volume or Urban Area	Snow and Ice	Exceptional
Max. Grades, %	4-6	3-4	5	8-10
Max. Superelev., ft/ft	0.06-0.12	0.10	0.06-0.08	0.14

Ramp widths are governed by special design considerations and are summarized in Table 2.9. Shoulders are generally not carried on ramps, but ramps should be wide enough to allow passing a stalled vehicle.

Spans of bridge structures for intersecting highways and ramps are governed by the same factors as those of overpass structures on open highways as discussed above.

2.3.6 Elevated Freeways

Arterial highways in densely populated areas have either to be depressed (below grade) or elevated (above grade) freeways in order to provide cross-traffic-free intersections with all major cross streets, thus obtaining large capacities. Various reasons such as restricted right-of-way, high water table, extensive underground utilities, etc., may prohibit the construction of a depressed freeway, so that resort to an elevated freeway has to be taken, in extreme cases even to a double-deck structure.

TABLE 2.9. RAMP DESIGN WIDTHS, FT.

Radius on Inner Edge of Pavement, ft.	1-Lane, One-way Operation No Passing			1-Lane, One-way Operation - Passing Stalled Vehicle			2-Lane Operation Either One-way or Two-Way		
	A	B	C	A	B	C	A	B	C
50	16	17	20	21	24	27	30	33	37
100	14	16	17	19	21	24	27	30	33
200	13	15	16	18	20	22	26	28	29
400	12	14	15	17	19	21	25	27	28
Tangent	12	14	14	16	18	20	22	24	24

A - Predominantly passenger vehicles, but also some single unit trucks.

B - Sufficient single unit trucks to govern design, but some consideration for semitrailer vehicles.

C - Sufficient semitrailer trucks (43 or 50 ft. long) to govern design.

Elevated freeways may be located on viaducts or embankments, but here only viaducts are of interest. In fact, such a viaduct may be an extremely long structure and therefore deserves special attention because structural cost has a decisive influence on the overall freeway project.

The columns have to be spaced such as to leave as much of the ground level area open for other purposes such as streets, parking lots, etc., as possible. For rolled steel girders, spans between 50 and 70 ft. have been found to be economical. Concrete box girders are competitive for the same span range, but prestressed girders make spans of over 100 ft. feasible too.

Minimum clearances for overcrossings are the same as for any other overcrossings, 14 ft. over streets and 22 ft. over railroad tracks. At ramp exits and terminals, the deck elevation should be as low as possible to reduce length and therefore cost of ramps. Coupled with the vertical clearance requirements for cross roads, this goal results in a rolling freeway profile which may lead to a pleasing effect in driving and appearance.

Horizontal and vertical curvatures as well as grades are similar to those of other urban freeways. Superelevation rates of more than 0.08 ft. per ft., however, are aesthetically unsatisfactory for multi-lane freeways.

Common minimum widths of elevated freeway structures are summarized in Table 2.10. Feasible minimum median widths are 6-8 ft., although emergency use, snow removal, lighting standards, etc., might justify wider medians, especially for 6- and 8-lane freeways. But never should the median be widened at the expense of shoulder width on the right, because shoulders or at least emergency parking bays are very important on high-volume roads. These emergency parking bays are 10 to 11 ft. wide, 50-75 ft. long, and the structure cross section widens to the new width over a length of 50-75 ft. on both ends of the bay, resulting in a taper of as much as 0.2 ft. per ft. Some typical sections of elevated freeways are shown in Fig. 2.8.

Ramp terminals for elevated freeways may be classified as parallel and lateral ramps, Fig. 2.9. Both types require 11 ft. wide

TABLE 2.10. MINIMUM WIDTHS OF ELEVATED FREEWAYS, OUT-TO-OUT FT.

Section	Type of Shoulder		4-Lane Two-Way Structure					4-Lane One-Way Structure				
			Lanes*	Median	Shoulders	Curb Parapets	Total*	Lanes*	Left Shoulder	Right Shoulder	Curb Parapets	Total*
Without Ramps	Full Shoulder	M†	2(24)	4	2(8)	2(2)	72	24	2	8	2+2.5	38.5
		D†	2(24)	6	2(10)	2(2)	78	24	2	10	2+2.5	40.5
	Partial Shoulder	M	2(24)	4	2(5)	2(2.5)	67	24	2	5	2(2.5)	36
		D	2(24)	6	2(6)	2(2.5)	71	24	2	6	2(2.5)	37
	Minimum Offset	M	2(24)	4	2(2)	2(2.5)	61	24	2	2	2(2.5)	33
		D	2(24)	6	2(3)	2(2.5)	65	24	2	3	2(2.5)	34
Auxiliary Lane or Park. Bay on One Side	Minimum Offset	M	24+35	4	2+0	2(2.5)	70	24+11	2	-	2(2.5)	42
Auxiliary Lane or Park. Bay on Both Sides	Minimum Offset	M	2(35)	4	-	2(2.5)	79	24+22	-	-	2(2.5)	51
Parallel Ramp on One Side	Minimum Offset	M	24+41	4	2(2)	2(2.5) + 6	84	24+17	2	2	2(2.5) + 6	56
Parallel Ramp on Both Sides	Minimum Offset	M	2(41)	4	2(2)	2(2.5) +2(6)	107	24+34	2	2	2(2.5) + 2(6)	79

*For each additional traffic lane, add 12 ft.

†M - minimum D - desirable.

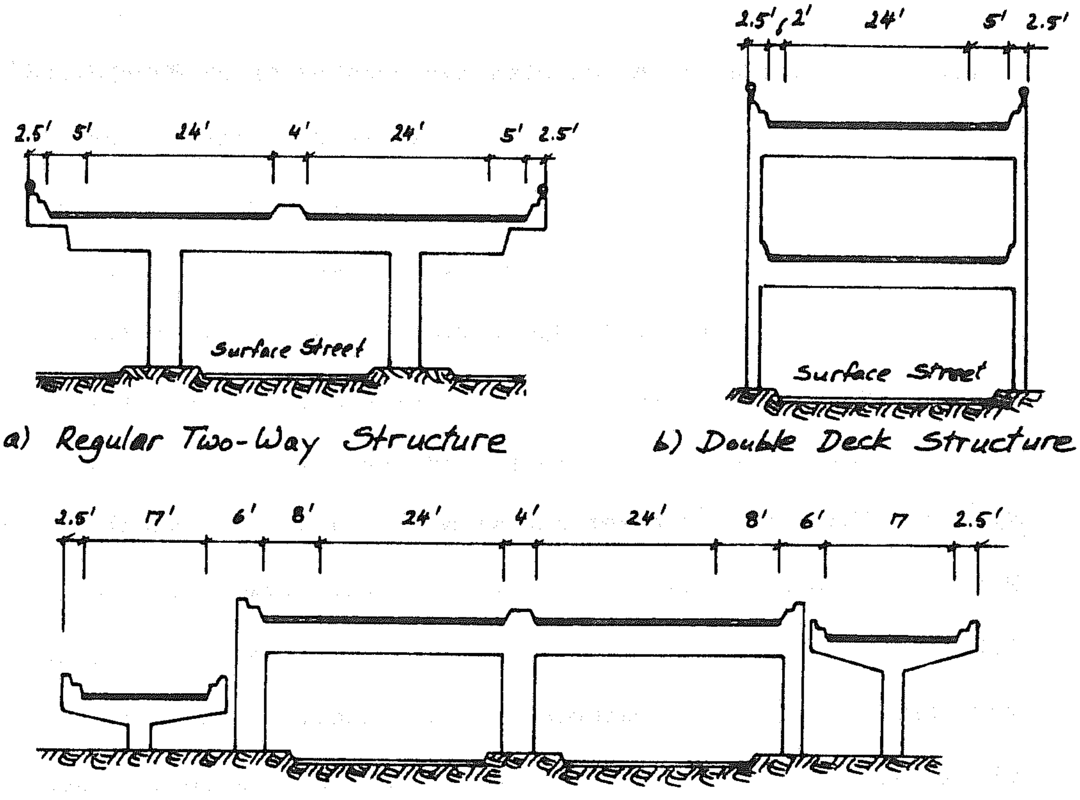

a) Regular Two-Way Structure

b) Double Deck Structure

c) Regular Two-Way Structure with On- and Off-Ramps

Fig. 2.8 Typical Elevated Freeway Sections

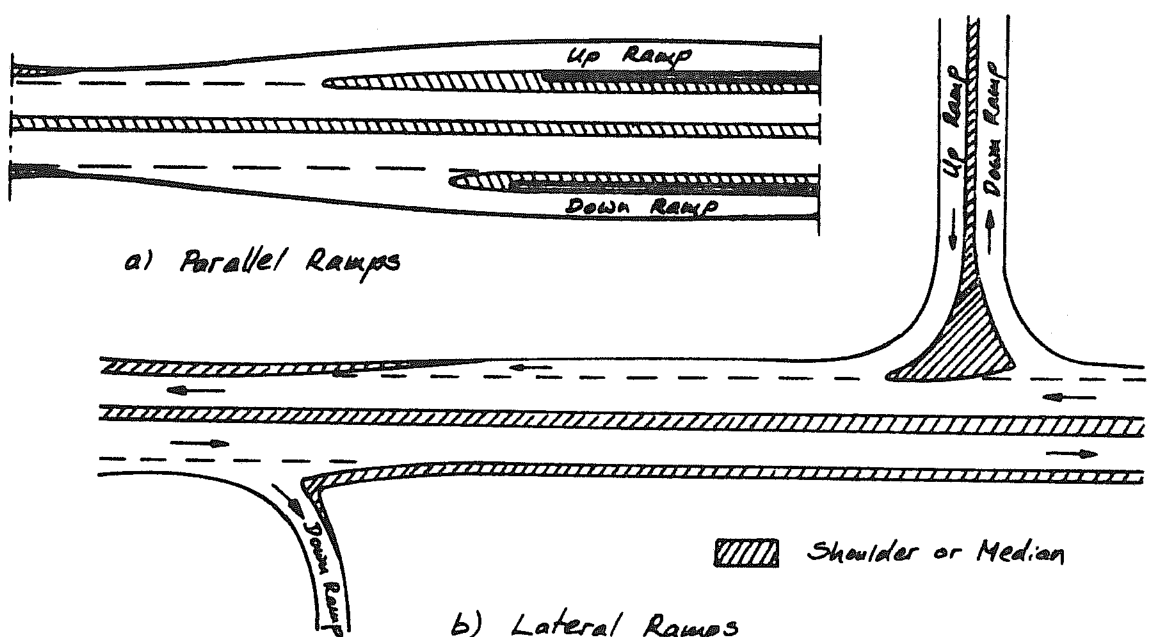

a) Parallel Ramps

b) Lateral Ramps

Fig. 2.9 Typical Ramp Arrangements For Elevated Freeways auxiliary lanes in which vehicles may accelerate or decelerate. Ramp design criteria are the same as those discussed before.

As can be seen in Fig. 2.9, bridge cross sections at ramp terminals are tapered. While for parallel ramps, this taper is generally fairly small so that the bridge structure basically preserves its prismatic nature, lateral ramps on the contrary join the structure like tree branches, thus adding truly a second dimension to the structural system. This fact is important with regard to analytical treatment. Methods of analysis developed for prismatic structure types are unlikely to be applicable to the general non-prismatic case, and only very general numerical methods like the finite element method will permit a rational assessment of stresses and deformations of such complex structural systems.

3. METHODS OF ANALYSIS

3.1 General

It is the objective of the structural analysis within the wider context of a design to provide an insight into the response of a given structure to specified actions such as dead weight and static wheel loads or dynamic effects due to wind and moving vehicles as well as temperature, shrinkage and creep effects. Provided this information is available to the designer, then he will be in the position to check if the structure is satisfactory with respect to certain design criteria concerning strength, stability, and economy.

It is important to note in this context that approximate methods of analysis are often superior over so-called exact methods. On the one hand, approximate methods very often give results which are in error only as much as or even less than the errors inherent in determining important material properties, or errors associated with fabrication and construction tolerances. On the other hand, closed-form solutions, if possible at all, are often so involved and time-consuming, that the savings in computational effort might very well favor the employment of a proper approximate solution technique rather than an exact solution.

For the analysis of straight bridges, a variety of efficient and accurate methods are available, but research on curved bridges has been relatively scarce and incomplete. In fact, the lack of experience with curvature effects both in construction and in analysis and design seriously limited the use of curved bridges, both for highway as well as for rail-bound traffic, and as a consequence, made smooth and efficient alignment difficult.

The first curved bridges built were probably steel truss bridges for railroads. Hence it was logical that this structure type attracted the attention of researchers first. The work of Kapsch, [6.2], in 1914, for example, on the bridges of the elevated rapid-transit system in Hamburg, Germany, initiated extensive research efforts in Germany on this type of bridge, [6.3] through [6.7]. Curved concrete bridges probably did not appear before the 1920's. But once the first structures proved to be successful, [7.1] [7.2], engineers did not hesitate to design and build more elaborate structures, thus satisfying the highway engineers' desire for improved highway alignment.

To date, thousands of curved bridges have been built in steel, in reinforced or prestressed concrete, as well as for composite action. They are being studied all over the world, and the extensive bibliography recently collected by McManus et al., [9.16], indicates the amount of literature that has been published in the last few decades. The bibliography in the Appendix of this dissertation was compiled independently and attempts to classify this large amount of information according to the main analytical methods and bridge types.

In this chapter, the most common methods proposed so far for the analysis of curved bridges will be reviewed shortly with special emphasis on their respective assumptions and the resulting limitations. It will be the objective of the next two chapters to describe in more detail different approaches which are believed to be more accurate than the traditional methods. The purpose of the development of these refined analysis techniques is not so much to replace the old methods but rather to test their accuracy and to establish limits of applicability.

3.2 Straight Bridge Approximation

It seems to be a paradox to open the discussion of curved bridge analyses with the straight bridge approximation. However, it is true that many bridges have only such small degrees of curve that the curvature effects are indeed negligible and straight bridge analyses sufficient. In fact, many curved bridges on the open highway - as has been shown in Chapter 2.3 - have such small curvatures that curved bridge analyses are not necessary.

For straight bridges, numerous methods of analysis have been proposed and are in use by practicing engineers, some of which are referenced in the Appendix. For box girder bridges, the methods developed by Scordelis, [10.1] [10.2], have been found to be very accurate and efficient in conjunction with the use of digital computers.

In the past it used to be up to the common sense of bridge engineers to decide the limiting values for curvatures and opening angles up to which straight bridge approximations would be permissible. It is one objective of this dissertation to employ refined analytical methods in order to rationally investigate these limits.

3.3 Curved Beam Theory

Curved beam theory has virtually been the only means so far by which engineers attempted to account for curvature effects in curved bridges. This theory is generally based on the following assumptions,

(1) cross sectional dimensions are small compared to the span length so that the elastic properties can be assumed to be concentrated along the beam centroidal axis;

(2) Cross sections do not distort transversely;

(3) Plane sections remain plane.

Assumptions (1) and (2) may in some practical cases be grossly violated thus raising some doubt about the validity of curved beam results. However, torque-resistant closed sections will generally keep cross-sectional distortions small, and closely spaced transverse diaphragms are the ultimate structural means to satisfy assumption (2). Then, if it can be shown that the maximum effects on individual bridge girders for design purposes as predicted by beam theory are close to values based on more refined analyses, then the violation of the above assumptions becomes less important. Finally, curvatures are often so small that even rough estimates of their effects introduce only small errors into the final results.

The circularly curved beam loaded normal to the plane of initial curvature can be analyzed using very elementary tools of structural analysis. It is therefore surprising how much literature has been published on this subject in the past 50 years. In fact, many of the references in the Appendix are virtually repetitive. Before presenting some curved beam formulas, it should be noted that the simply supported curved beam without torsional end constraints is unstable. In bridge practice, almost all supports are designed to offer at least partial fixity, for example single column supports, if not complete fixity as most end supports do.

For the analysis of continuous curved beams it is then logical to select the simply supported beam fixed against torsion as the primary structural element, Fig. 3.1, which is statically indeterminate

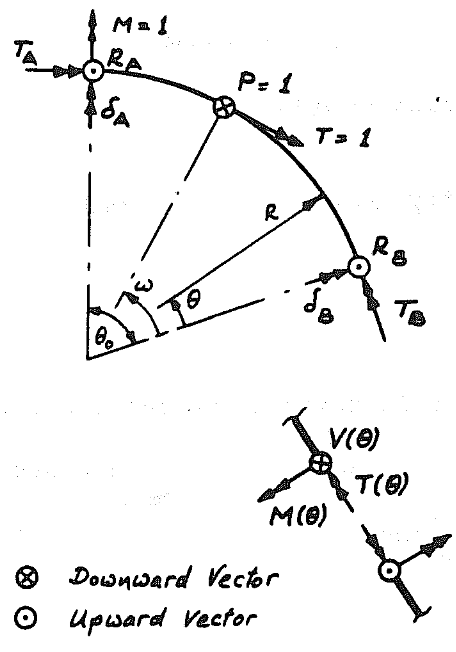

Fig. 3.1 Curved Beam Element

to the first degree. If the ends were only partially constrained against rotation, then the equations below would have to be slightly modified.

Treating the torsional end moment $T_A = X$ as redundant, one finds for a unit load $P = 1$ acting at some angle ω, that

$$X = T_A = -R\left(\frac{\omega}{\theta_o} - \frac{\sin\omega}{\sin\theta_o}\right) \qquad (3.1)$$

The other reactions are then

$$\begin{aligned} R_A &= \frac{\sin\omega}{\sin\theta_o} - \frac{X}{R} = \frac{\omega}{\theta_o} \\ R_B &= 1 - \frac{\sin\omega}{\sin\theta_o} + \frac{X}{R} = \frac{\theta_o - \omega}{\theta_o} \\ T_B &= R\left(1 - \frac{\sin\omega + \sin(\theta_o - \omega)}{\sin\theta_o}\right) + X = R\left(\frac{\theta_o - \omega}{\theta_o} - \frac{\sin(\theta_o - \omega)}{\sin\theta_o}\right) \end{aligned} \qquad (3.2)$$

and internal shears and moments are

$$\left.\begin{aligned} V(\theta) &= \frac{\sin\omega}{\sin\theta_o} - 1 - \frac{X}{R} = -\frac{\theta_o - \omega}{\theta_o} \\ M(\theta) &= \frac{\sin\theta\,\sin(\theta_o - \omega)}{\sin\theta_o} R \\ T(\theta) &= R\left(1 - \frac{\cos\theta\,\sin(\theta_o - \omega) + \sin\omega}{\sin\theta_o}\right) + X = R\left(\frac{\theta_o - \omega}{\theta_o} - \frac{\cos\theta\,\sin(\theta_o - \omega)}{\sin\theta_o}\right) \end{aligned}\right\} 0 \leq \theta \leq \omega$$

$$(3.3)$$

$$\left.\begin{aligned} V(\theta) &= \frac{\sin\omega}{\sin\theta_o} - \frac{X}{R} = \frac{\omega}{\theta_o} \\ M(\theta) &= \frac{\sin\omega\,\sin(\theta_o - \theta)}{\sin\theta_o} R \\ T(\theta) &= -\frac{\sin\omega\,(1 - \cos(\theta_o - \theta))}{\sin\theta_o} R + X = \left(-\frac{\omega}{\theta_o} + \frac{\sin\omega\,\cos(\theta_o - \theta)}{\sin\theta_o}\right) R \end{aligned}\right\} \omega \leq \theta \leq \theta_o$$

while the end rotations at the supports A and B become

$$\delta_A^{P=1} = \frac{R^2}{EI}\left[\frac{\omega\sin(\theta_0-\omega) - (\theta_0-\omega)\sin\omega\cos\theta_0}{2\sin^2\theta_0}(1+\kappa) + \kappa\left(\frac{\omega}{\theta_0} - \frac{\sin\omega}{\sin\theta_0}\right)\right]$$

$$\delta_B^{P=1} = \frac{R^2}{EI}\left[\frac{\omega\sin(\theta_0-\omega)\cos\theta_0 - (\theta_0-\omega)\sin\omega}{2\sin^2\theta_0}(1+\kappa) + \kappa\left(\frac{\theta_0-\omega}{\theta_0} - \frac{\sin(\theta_0-\omega)}{\sin\theta_0}\right)\right] \tag{3.4}$$

with

$$\kappa = \frac{EI}{GJ_x} \tag{3.5}$$

Similarly, if the beam is loaded with a unit twisting moment $T = 1$ at the angle ω, Fig. 3.1, then the redundant torque at point A becomes

$$X = T_A = -\frac{\sin\omega}{\sin\theta_0} \tag{3.6}$$

while the other reactions are

$$R_A = -\frac{\sin\omega}{R\sin\theta_0} - \frac{X}{R} = 0$$

$$R_B = \frac{\sin\omega}{R\sin\theta_0} + \frac{X}{R} = 0 \tag{3.7}$$

$$T_B = \frac{\sin\omega + \sin(\theta_0-\omega)}{\sin\theta_0} + X = \frac{\sin(\theta_0-\omega)}{\sin\theta_0}$$

and internal shears and moments,

$$V(\theta) = -\frac{\sin\omega}{R\sin\theta_0} - \frac{X}{R} \equiv 0$$

$$\left.\begin{aligned} M(\theta) &= -\frac{\sin(\theta_0-\omega)\sin\theta}{\sin\theta_0} \\ T(\theta) &= \frac{\cos\theta\sin(\theta_0-\omega) + \sin\omega}{\sin\theta_0} + X = \frac{\cos\theta\sin(\theta_0-\omega)}{\sin\theta_0} \end{aligned}\right\} 0 \le \theta \le \omega$$

$$\left.\begin{aligned} M(\theta) &= -\frac{\sin\omega\sin(\theta_0-\theta)}{\sin\theta_0} \\ T(\theta) &= \frac{\sin\omega(1-\cos(\theta_0-\theta))}{\sin\theta_0} + X = -\frac{\cos(\theta_0-\theta)\sin\omega}{\sin\theta_0} \end{aligned}\right\} \omega \le \theta \le \theta_0 \tag{3.8}$$

The end rotations for this load case are then

$$\delta_A^{T=1} = \frac{R^2}{EI}\,\frac{(\theta_0-\omega)\sin\omega\cos\theta_0 - \omega\sin(\theta_0-\omega)}{2\sin^2\theta_0}(1+\kappa)$$

$$\delta_B^{T=1} = \frac{R^2}{EI}\,\frac{(\theta_0-\omega)\sin\omega - \omega\sin(\theta_0-\omega)\cos\theta_0}{2\sin^2\theta_0}(1+\kappa) \tag{3.9}$$

Finally, the reactions, internal shears and moments, and end rotations due to a unit bending moment M = 1 at point A, Fig. 3.1, are as follows.

$$R_A = -R_B = -\frac{1}{R\theta_o}$$
$$T_A = \frac{1}{\theta_o} - \frac{\cos\theta_o}{\sin\theta_o} \tag{3.10}$$
$$T_B = \frac{1}{\theta_o} - \frac{1}{\sin\theta_o}$$

$$V(\theta) = -\frac{1}{R\theta_o}$$
$$M(\theta) = \frac{\sin\theta}{\sin\theta_o} \tag{3.11}$$
$$T(\theta) = \frac{1}{\theta_o} - \frac{\cos\theta}{\sin\theta_o}$$

$$\delta_A^{M=1} = \frac{R}{EI}\left[\frac{\theta_o - \sin\theta_o\cos\theta_o}{2\sin^2\theta_o}(1+\kappa) + \kappa\left(\frac{\cos\theta_o}{\sin\theta_o} - \frac{1}{\theta_o}\right)\right]$$
$$\delta_B^{M=1} = \frac{R}{EI}\left[\frac{\theta_o\cos\theta - \sin\theta_o}{2\sin^2\theta_o}(1+\kappa) + \kappa\left(\frac{1}{\sin\theta_o} - \frac{1}{\theta_o}\right)\right] \tag{3.12}$$

By proper integration of Eq. (3.1) - (3.9), most practical load cases can be treated. For example, for uniform load of intensity p, the reactions are

$$R_A = R_B = \frac{R\theta_o}{2}p$$
$$T_A = -T_B = pR^2\left(\frac{\theta_o}{2} - \frac{1-\cos\theta_o}{\sin\theta_o}\right) \tag{3.13}$$

and shears and moments,

$$V(\theta) = pR\left(\theta - \frac{\theta_o}{2}\right)$$
$$M(\theta) = pR^2\left(\frac{\sin(\theta_o-\theta) + \sin\theta}{\sin\theta_o} - 1\right) \tag{3.14}$$
$$T(\theta) = pR^2\left(\frac{\theta_o}{2} - \theta + \frac{\cos(\theta_o-\theta) - \cos\theta}{\sin\theta_o}\right)$$

These or similar formulas have been derived in the literature so often that reference to individual authors will not be made here.

On the basis of Eq. (3.1) - (3.14) or their equivalents for different torsional support conditions, the analysis of continuous curved beams poses no basic difficulties. Solution techniques developed for straight continuous beams can be readily applied to the curved case if modified properly. In relaxation methods such as moment distribution, for example, the numerical iteration scheme is complicated because bending and twisting moments are coupled, [3.4], [3.5], [3.7], [3.27], and in all stiffness methods, the stiffness coefficients for the straight beam element have to be replaced by appropriate curved beam stiffness coefficients. Stampf [3.11] [3.19] and Morris [3.36], for example, derived these coefficients in general form. Utilized in a direct stiffness approach in conjunction with a digital computer, this method is probably the most efficient and versatile one and superior over other solution techniques proposed in the literature, such as the conjugate structure [3.9], or the transfer matrix application [3.26], a numerical forward integration procedure [3.17], or the variety of flexibility methods and various stiffness techniques. For small curvatures, however, approximate methods may be appropriate. Bretthauer and Nötzold [3.20] and Tung and Fountain [4.42] show that it is accurate enough, for certain conditions, to determine the redundant bending moments over the supports from a corresponding straight continuous beam analysis.

Concluding, it may be stated that the curved bridge problem can be solved for most practical cases, provided the structure can adequately be approximated by a continuous beam curved in plan and having constant curvature in each field of discretization.

3.4 Refined Curved Beam Theories

The behavior of curved beams under transverse loadings depends largely on its resistance to torsion. The curved beam theory outlined above is fairly accurate for solid cross sections, provided their torsional rigidity constant J_x can be determined with sufficient accuracy. Thin-walled beams, on the other hand, will generally require a refined analysis, especially if cross sectional distortions must be expected under loading. Thin-walled beams of closed cross sections carry most of the torque by Saint-Venant torsion, while open sections have to develop torsion bending stresses as a consequence of restrained warping, which may carry an appreciable portion of the applied torque.

In reinforced or prestressed concrete bridge girders with fairly large plate thicknesses, warping stresses are generally low, so that ordinary beam theory will often give reliable results. Steel girders with thin plate thicknesses, however, develop much higher warping stresses, which can only be determined with refined torsion bending analyses, which are often very complex, involving the solution of systems of differential equations.

A considerable amount of literature has been published on the theory of torsion bending of thin-walled beams, but only those contributions dealing directly with curved beams are referenced in the Appendix. Much pioneering research has been done in the Soviet Union, originating from Vlassov [4.17], Umanskii [4.2] [4.3] [4.7], and Grigoriev [4.9] [4.10]. The most advanced work of more recent date has been published mainly in the German steel construction journal "Der Stahlbau," primarily by Dabrowski [4.18] [4.26] [4.30] [4.31] from

Poland, who summarized much of his work in a book [4.40]. In Japan, Konishi and Komatsu, [4.20] [4.22] [4.34], developed their own, less rigorous theory. For open sections, Becker [4.32] presented an extended theory in conjunction with a direct stiffness analysis procedure which he programmed for the digital computer.

For practical purposes, the above mentioned refined theories for curved steel girders are probably accurate enough. For concrete girders, these theoretical refinements are generally not necessary, although some findings might be also then of practical value. Thus, the idealization of a curved bridge as a thin-walled beam can often lead to satisfactory results.

3.5 Plate and Grid Analyses

A plate shaped as a circular ring sector, Fig. 3.2., can be analyzed without difficulties as long as the straight radial edges are simply supported. In this case, the plate equation

$$\left(\frac{\partial^2}{\partial r^2}+\frac{1}{r}\frac{\partial}{\partial r}+\frac{1}{r^2}\frac{\partial^2}{\partial \theta^2}\right)\left(\frac{\partial^2 w}{\partial r^2}+\frac{1}{r}\frac{\partial w}{\partial r}+\frac{1}{r^2}\frac{\partial^2 w}{\partial \theta^2}\right)=\frac{q}{D} \quad (3.15)$$

with

$$D=\frac{Et^3}{12(1-\nu^2)} \quad (3.16)$$

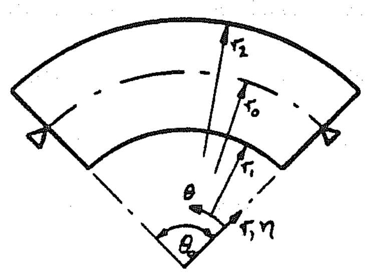

Fig. 3.2 Curved Plate

can be uncoupled by developing the external loads and the displacements into sine series,

$$q=\sum_{n=1}^{\infty} q_n \sin\frac{n\pi\theta}{\theta_0} \quad (3.17)$$

$$w=\sum_{n=1}^{\infty} w_n \sin\frac{n\pi\theta}{\theta_0} \quad (3.18)$$

because a solution to Eq. (3.15) in the form of Eq. (3.18) satisfies automatically the boundary conditions

$$w\big|_{\theta=0,\theta_0} = M_\theta\big|_{\theta=0,\theta_0} = 0 \tag{3.19}$$

Substitution of Eq. (3.17) and (3.18) into Eq. (3.15) leads to the ordinary differential equation

$$\frac{d^4W_n}{dr^4} + \frac{2}{r}\frac{d^3W_n}{dr^3} - (1+2m^2)\frac{1}{r^2}\frac{d^2W_n}{dr^2} + (1+2m^2)\frac{1}{r^3}\frac{dW_n}{dr} + m^2(m^2-4)\frac{W_n}{r^4} = \frac{q_n}{D} \tag{3.20}$$

with

$$m = \frac{n\pi}{\theta_0} \tag{3.21}$$

For numerical reasons, it is convenient to introduce the dimensionless radial coordinate

$$\eta = \frac{r}{r_0} \tag{3.22}$$

with

$$r_0 = \frac{r_1 + r_2}{2} \tag{3.23}$$

so that Eq. (3.20) reads now

$$\frac{d^4W_n}{d\eta^4} + \frac{2}{\eta}\frac{d^3W_n}{d\eta^3} - (1+2m^2)\frac{1}{\eta^2}\frac{d^2W_n}{d\eta^2} + (1+2m^2)\frac{1}{\eta^3}\frac{dW_n}{d\eta} + m^2(m^2-4)\frac{W_n}{\eta^4} = \frac{q_n r_0^4}{D} \tag{3.24}$$

for which the homogeneous solution is given by

$$W_n^h(\eta) = A_n\eta^{m} + B_n\eta^{-m} + C_n\eta^{m+2} + D_n\eta^{-m+2} \tag{3.25}$$

In order to find the particular integral of Eq. (3.24), this Euler equation with variable coefficients has to be transformed into an equation with constant coefficients, using the transformation $\eta = e^z$. The particular integral is then readily found to be

$$W_n^p(\eta) = \frac{\eta^4 r_0^4}{D(m^4-20m^2+64)}\cdot q_n \qquad m \neq 4 \tag{3.26a}$$

$$W_n^p(\eta) = -\frac{\eta^4 r_0^4 \ln\eta}{96D}\cdot q_n \qquad m = 4 \tag{3.26b}$$

where for uniform load of intensity q_o,

$$q_n = \frac{4q_o}{n\pi} = \frac{4q_o}{m\theta_0} \tag{3.27}$$

The complete solution of Eq. (3.15) becomes then

$$w(\eta,\theta) = \sum_{n=1}^{\infty} \left(A_n \eta^{m} + B_n \eta^{-m} + C_n \eta^{m+2} + D_n \eta^{-m+2} + \frac{\eta^4 r_o^4 q_n}{D(m^4-20m^2+64)} \right) \sin m\theta \quad (3.28)$$

The constants of integration, A_n, B_n, C_n, D_n, are free to adjust the general solution to any boundary conditions along the curved edges.

Moments and shears throughout the plate are then given by

$$M_r = -D\sum_{n=1}^{\infty} \Big[A_n(m^2-m)(1-\nu)\eta^{m-2} + B_n(m^2+m)(1-\nu)\eta^{-m-2} + C_n(m^2+3m+2-\nu m^2+\nu m+2\nu)\eta^{m} + D_n(m^2-3m+2-\nu m^2-\nu m+2\nu)\eta^{-m} + \frac{(12+4\nu-\nu m^2)\eta^2 r_o^4}{D(m^4-20m^2+64)} q_n \Big] \frac{\sin m\theta}{r_o^2} \quad (3.29)$$

$$M_\theta = -D\sum_{n=1}^{\infty} \Big[A_n(m-m^2)(1-\nu)\eta^{m-2} - B_n(m^2+m)(1-\nu)\eta^{-m-2} + C_n(-m^2+m+2+\nu m^2+3\nu m+2\nu)\eta^{m} + D_n(-m^2-m+2+\nu m^2-3\nu m+2\nu)\eta^{-m} + \frac{(-m^2+4+12\nu)\eta^2 r_o^4}{D(m^4-20m^2+64)} q_n \Big] \frac{\sin m\theta}{r_o^2} \quad (3.30)$$

$$M_{r\theta} = D(1-\nu)\sum_{n=1}^{\infty} \Big[A_n(m^2-m)\eta^{m-2} - B_n(m^2+m)\eta^{-m-2} + C_n(m^2+m)\eta^{m} - D_n(m^2-m)\eta^{-m} + \frac{3m\eta^2 r_o^4}{D(m^4-20m^2+64)} q_n \Big] \frac{\cos m\theta}{r_o^2} \quad (3.31)$$

$$Q_r = -D\sum_{n=1}^{\infty} \Big[4C_n(m^2+m)\eta^{m-1} + 4D_n(m^2-m)\eta^{-m-1} + \frac{(32-2m^2)\eta r_o^4}{D(m^4-20m^2+64)} q_n \Big] \frac{\sin m\theta}{r_o^3} \quad (3.32)$$

$$Q_\theta = -D\sum_{n=1}^{\infty} \Big[4C_n(m^2+m)\eta^{m-1} - 4D_n(m^2-m)\eta^{-m-1} + \frac{(16m-m^3)\eta r_o^4}{D(m^4-20m^2+64)} q_n \Big] \frac{\cos m\theta}{r_o^3} \quad (3.33)$$

while the Kirchhoff shear becomes

$$V_r = Q_r - \frac{1}{r}\frac{\partial M_{r\theta}}{\partial\theta}$$

$$= -D\sum_{n=1}^{\infty} \Big[A_n(m^2-m^3)(1-\nu)\eta^{m-3} + B_n(m^2+m^3)(1-\nu)\eta^{-m-3} + C_n(-m^3+3m^2+4m+\nu m^3+\nu m^2)\eta^{m-1} + D_n(m^3+3m^2-4m-\nu m^3+\nu m^2)\eta^{-m-1} + \frac{(-5m^2+32+3\nu m^2)\eta r_o^4}{D(m^4-20m^2+64)} q_n \Big] \frac{\sin m\theta}{r_o^3} \quad (3.34)$$

In the case that m = 4, the particular integral (3.26b) should replace (3.26a) in all equations (3.29) to (3.34).

Solutions such as given above have been known for a long time [5.1] [5.2] [5.6] and have recently been extended to include variable plate thickness [5.18] [5.19].

Rüdiger [5.15] went further and derived the flexibility matrix of the ring sector plate of Fig. 3.2 in plate bending as well as in-plane action, subjecting it to various harmonic edge loads. Deriving similar flexibility coefficients for the curved beam, and developing all external loads into Fourier series, he was then in the position to assure complete compatibility along the circumferential joints using the flexibility method of analysis in order to find the unknown interaction forces between the various structural elements, Fig. 3.3. Rüdiger's solution is then exact within the assumptions of the theory of elasticity except that vertical elements are approximated by beam theory. For practical application, however, it is advisable to convert this approach to a direct stiffness method and to program it for the computer, in a very similar way as his theory of straight folded plates [10.14] was converted by Goldberg and Leve [10.15] and later by Scordelis [10.16]. Although Rüdiger applied his theory only to open sections, Fig. 3.4a, the extension to closed sections, Fig. 3.4b, should not pose any difficulty if the direct stiffness method is used.

The main limitation of Rüdiger's approach is its restriction to horizontal and vertical structural elements. Although the extension to sloping elements which would be segments of conical frustra might be possible, the derivation of closed-form stiffness coefficients will be very involved, as has been demonstrated for a slightly different problem by Popov et al. [10.20], so that a suitable approximate method will in general be preferable. Such an approximate method will be described in detail in Chapter 5.

Gruber [5.13] developed a different approximate method which is the extension of the so-called ordinary folded plate theory to the

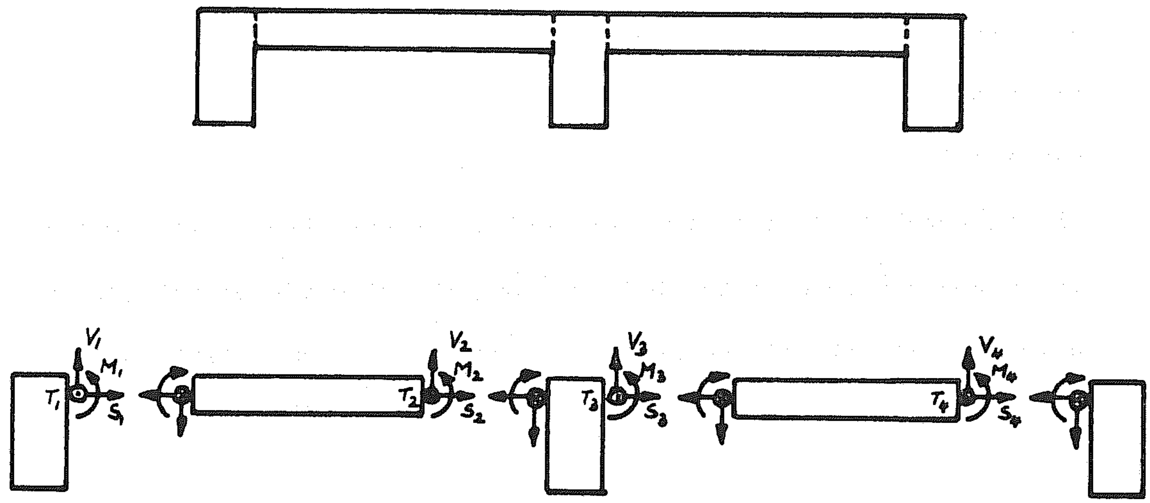

Fig. 3.3 Interaction Forces In Curved Slab And Girder Bridge After Rüdiger [5.15]

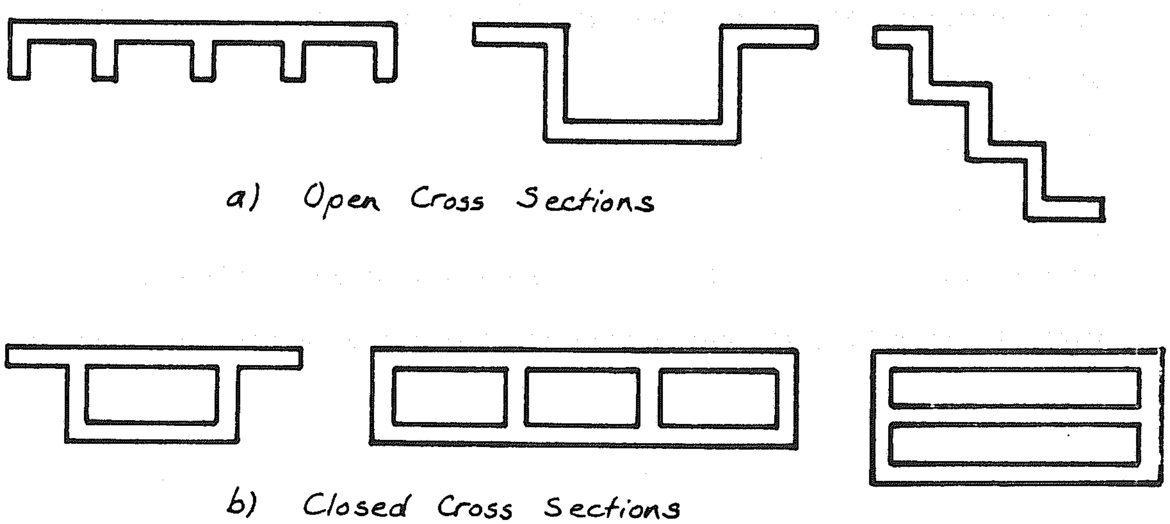

Fig. 3.4 Structure Types Which Can Be Solved By Rüdiger's Method [5.15]

curved case. In his derivation, the theory is restricted to open cross-sections, Fig. 3.4a, but is also extended to take continuity into account. Finally, Gruber gives also an estimate for the effect of skew end supports.

The finite difference technique is another method to solve curved plate problems, and its potential for the analysis of structures of simple geometry is largely recognized. Yüksel [5.31] applied this method to isotropic continuous curved plates, and Heins and Looney [5.32] used it to analyze curved orthotropic plates. Bell and Heins [5.32] studied also the interaction between an orthotropic bridge deck and curved girder supports, expressing the solution in terms of a Fourier series and deriving the necessary stiffness coefficients by a slope-deflection method.

The technique of analyzing interconnected bridge systems, associated with the names of Guyon [10.25] and Massonet [10.26], has been widely accepted for the analysis and design of straight bridges [10.27]. It is therefore surprising how little effort has been undertaken so far to apply this technique to the curved bridge problem [5.23]. For box girder bridges, however, this method may prove to be inappropriate, because even in the straight case, the problem of assigning appropriate equivalent torsional stiffnesses has not been successfully solved so far. Therefore, also the other approaches of approximating the bridge by a grid [5.17] [5.26] [5.28] [5.33] will be very difficult to apply to bridges with closed sections.

Steel bridges, on the other hand, in particular railroad bridges, are very often grids physically and offer themselves to grid analyses. Most of the references listed in the Appendix, which address themselves to the analysis of steel bridges, are based on various grid methods, and provided the individual member stiffnesses can be derived accurately enough, then the bridge analysis presents no basic difficulties.

4. FINITE ELEMENT ANALYSIS

4.1 General

The finite element method of analysis has been developed in recent years and has since found useful applications in a variety of problems of structural engineering and mechanics. An extensive amount of literature has been published on the various aspects of this powerful technique, and Zienkiewicz has published a text which gives a summary treatment of the subject with many references [10.12].

In this chapter, the application of the finite element method to bridge type structures will be briefly discussed, because its versatility lends itself to the analysis of structures with complex geometries such as curved box girder bridges. A general computer program called FINPLA2 has been developed by the writer which is capable of analyzing general non-prismatic folded plate structures with an arbitrarily integrated three-dimensional frame. The element models used in this program will be described, as will be the program itself and its usage. Some examples will illustrate its applicability to curved bridge structures.

4.2 Finite Element Models

Much research has already been directed towards the objective of obtaining finite element models with optimum properties for certain problems, both regarding accuracy of results and expenditure in computation. For the analysis of folded plate structures, it appears advantageous to assign six degrees of freedom to each nodal point, three translational, and three rotational. Although five degrees of freedom have often been used for general shell programs, special techniques are required to take account for the missing sixth degree of freedom, i.e., the rotation normal to the shell or plate surface. The addition of the sixth degree of freedom in FINPLA2 is particularly important since the finite element system is combined with a three-dimensional frame in which the member nodes also have six degrees of freedom. The elimination of the complications associated with the five degree of freedom system justifies the increase in computational effort involved in solving the larger number of equations.

Subdividing a general folded plate structure such as shown in Fig. 4.1a into a number of flat quadrilateral elements, interconnected at the corner nodal points, the problem of analyzing this system can be reduced to one of standard structural analysis, once proper stiffness matrices for each of the elements have been established.

For a small-deflection linear theory, the in-plane and plate bending actions are uncoupled. The associated stiffness coefficients may therefore be derived independent of each other.

The plane stress element model used in program FINPLA2, was derived in its original form by Abu Ghazaleh [10.7] for a rectangular shape and has also been described in detail in [10.2]. Willam [10.6] rederived the element stiffness in skew natural coordinates for a general quadrilateral shape. The special feature of this element is that in addition to the commonly used two translational degrees of freedom per node, each node is assigned a rotational degree of freedom, defined as the averaged rotation about the element z-axis, Fig. 4.1b, i.e., for a rectangular element,

$$\theta_{z_i} = \frac{1}{2}\left[\left(\frac{\partial v}{\partial x}\right)_i - \left(\frac{\partial u}{\partial y}\right)_i\right] \tag{4.1}$$

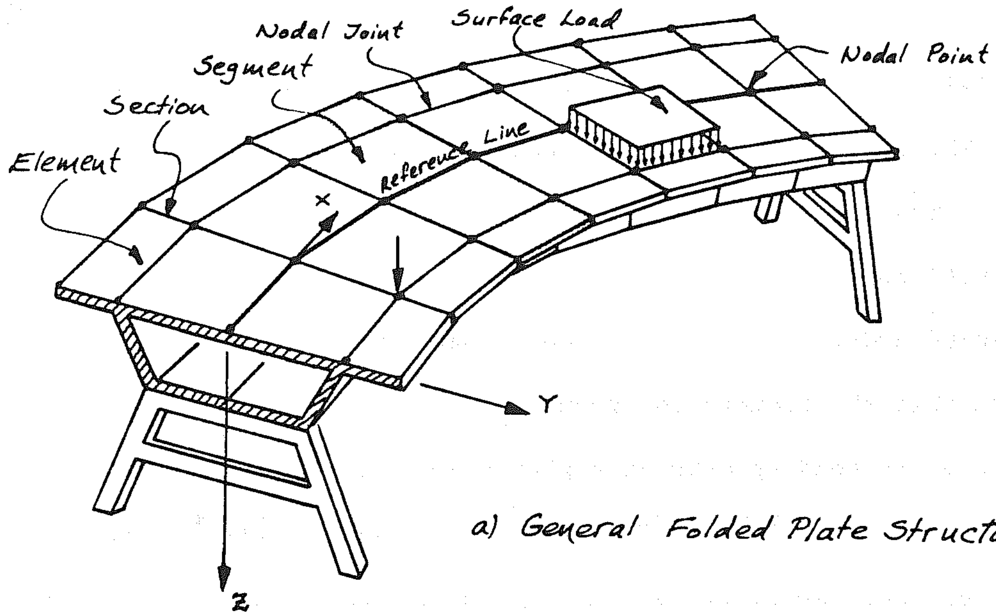

a) General Folded Plate Structure

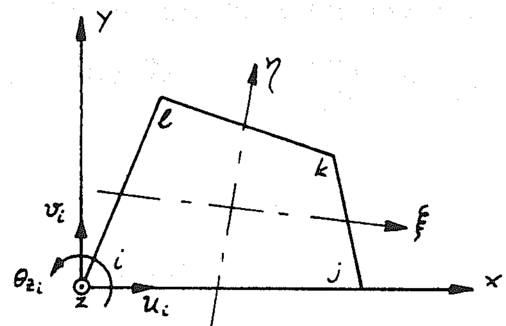

b) Plane Stress Element [10.6]

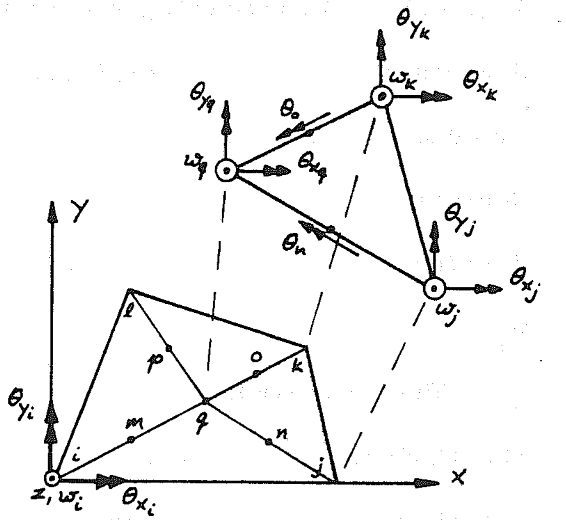

c) Plate Bending Element [10.9]

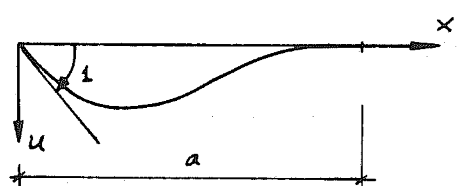

$$u = a\left[\left(\frac{x}{a}\right)^3 - 2\left(\frac{x}{a}\right)^2 + \left(\frac{x}{a}\right)\right]$$

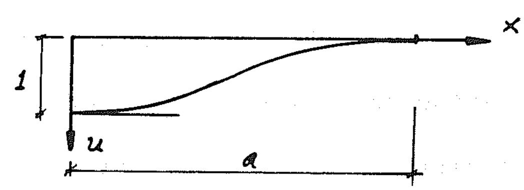

$$u = 2\left(\frac{x}{a}\right)^3 - 3\left(\frac{x}{a}\right)^2 + 1$$

d) Beam Displacement Functions for Rotational Degrees of Freedom of Plane Stress Element

Fig. 4.1 Finite Element Models

thus raising the total number of degrees of freedom for the element to 12. The actual element displacements u and v are assumed to vary linearly with the translational degrees of freedom u_i, v_i, and as beam functions with the rotational degrees of freedom θ_{z_i}, Fig. 4.1d. The assumed nodal rotations introduce angular discontinuities at the nodes so that the element is incompatible.

The plate bending element employed in program FINPLA2 has been derived by Felippa [10.9]. This compatible quadrilateral element is made up of four subtriangles, each of which has 11 degrees of freedom, Fig. 4.1c. In combining the four subelements, a quadrilateral with 19 degrees of freedom is obtained. However, the 7 internal degrees of freedom can be eliminated from the element stiffness by static condensation, reducing the stiffness to the essential 12 degrees of freedom, for each node the rotations θ_{x_i} and θ_{y_i} and the translation w_i.

The beam element used in the three-dimensional frame assembly has the 12 degrees of freedom shown in Fig. 4.2a. The stiffness matrix for this element can be found in the literature [10.28]. In order to allow for arbitrary eccentricities of the beam elements, rigid links are introduced to connect the beam nodes with those nodal points predefined by plate type finite elements, Fig. 4.2b. The transformation relating the joint displacement degrees of freedom r_i to the beam deformations v_i is given for either one of the two end points by

$$\begin{Bmatrix} v_1 \\ v_2 \\ v_3 \\ v_4 \\ v_5 \\ v_6 \end{Bmatrix} = \begin{bmatrix} a_{11} & a_{12} & a_{13} & (a_{13}e_y - a_{12}e_z) & (a_{11}e_z - a_{13}e_x) & (a_{12}e_x - a_{11}e_y) \\ a_{21} & a_{22} & a_{23} & (a_{23}e_y - a_{22}e_z) & (a_{21}e_z - a_{23}e_x) & (a_{22}e_x - a_{21}e_y) \\ a_{31} & a_{32} & a_{33} & (a_{33}e_y - a_{32}e_z) & (a_{31}e_z - a_{33}e_x) & (a_{32}e_x - a_{31}e_y) \\ 0 & 0 & 0 & a_{11} & a_{12} & a_{13} \\ 0 & 0 & 0 & a_{21} & a_{22} & a_{23} \\ 0 & 0 & 0 & a_{31} & a_{32} & a_{33} \end{bmatrix} \begin{Bmatrix} r_1 \\ r_2 \\ r_3 \\ r_4 \\ r_5 \\ r_6 \end{Bmatrix} \qquad (4.2)$$

where the a_{ij} quantities are the direction cosines of the element axes, and e_x, e_y, e_z constitute the components of eccentricity of the beam

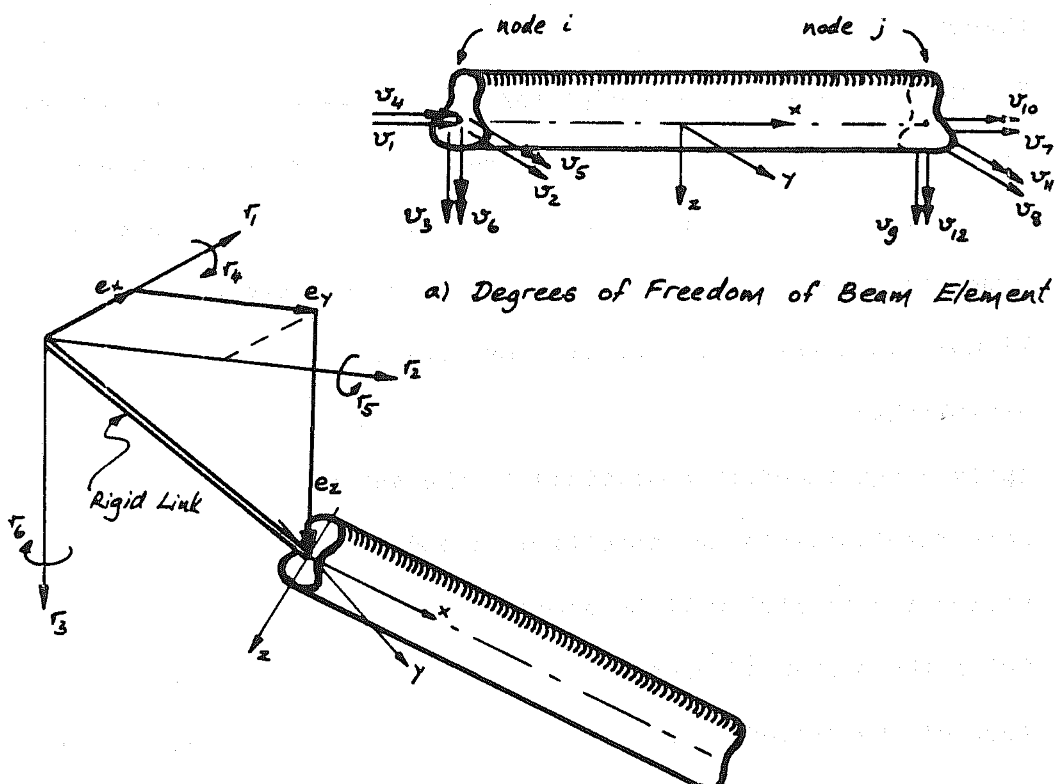

a) Degrees of Freedom of Beam Element

b) Eccentric Beam Connection

Fig. 4.2 Beam Element - Notations

node under consideration.

The solution process of the finite element method has been described so often, that only the main steps will be enumerated below.

1. Discretize the structure into a number of quadrilateral elements by dividing it longitudinally into a number of segments, and transversely into individual elements, Fig. 4.1a. Nodal points within a section have to be numbered such as to minimize the bandwidth of the system of equations.
2. Calculate all element stiffnesses and transform them to a common global coordinate frame.
3. Form the structure stiffness by assembling the element stiffnesses according to the standard direct stiffness method of structural theory.
4. Set up the load vector containing all specified external loads. For loads distributed over the area of an element, calculate equivalent nodal loads using the tributary area principle or some other appropriate technique such as consistent load theory. If more than one load case is considered, a load matrix has to be established.
5. Apply given boundary conditions to the set of equations. If non-zero displacements are specified, a modification of the load vector (or matrix) will be necessary.
6. Solve the system of equations by a technique which takes advantage of the banded nature of the structural stiffness. If also the variation of the bandwidth is taken into account, considerable reduction in computational effort may result.

7. Once the nodal joint displacements are known as the solution to the equations of step 6, reactions may be found by multiplying the original structure stiffness (i.e., not modified due to boundary conditions) with the displacement vector. A complete matrix multiplication will also yield the residual loads on the structure which are a measure for the accuracy with which the equations had been solved.
8. Transform nodal displacements from global to element coordinates for the computation of internal stresses and moments in plate and beam elements.

4.3 Description of Program FINPLA2

The purpose of a general computer program is that it provides for some given problem satisfactory results involving a minimum of the following items: a) required amount of input preparation, b) execution time and core storage requirements in the computer, and c) amount of output data reduction necessary for meaningful interpretation. Program FINPLA2, a generalization of a previously reported program [10.5], was conceived and written with due consideration of all three aspects above. Its objective was to provide rapid solutions to a large class of structures which are so far not amenable to other methods of analysis. The program was designed primarily for general non-prismatic folded plate structures of arbitrary horizontal alignment, which may or may not be integrated into a general three-dimensional frame, Fig.4.1a.

The structure is discretized by dividing it longitudinally into a certain number of structure segments by vertical sections, and by subdividing each such segment into finite elements. The approximate prismatic nature of the considered class of structures has the requirement that each section contains the same number of so-called primary nodal points, and maintains the same overall shape. The structure may have variable width and depth along its length. Secondary nodal points are introduced independently to allow the integration of arbitrary frame members with end points not predefined by plate type elements.

The structure alignment is described by a reference line which may be a straight line, a circular curve, or an arbitrary planar string polygon. Cross sections may vary from section to section within the above mentioned limitations and the material law for each plate element may be linear orthotropic. Loading on the structure may consist of any surface loads uniformly distributed over any finite element, and of concentrated loads which may be applied to any nodal point of the structure. Each structure can be analyzed for an arbitrary number of load cases. Boundary conditions, including specified non-zero displacements, may be applied to any point of the structure. The array dimensions are kept variable so that problems of practically any size and complexity can be solved.

The required input is kept to a minimum and consists of a description of the reference line and the configuration of the structure segments, with repeating segments being internally generated. Input further contains description of transverse diaphragms; nodal point configuration, connectivity and element properties of the three-dimensional frame; boundary conditions; loading data; and information on various output options such as coordinate transformations or averaging of internal stress resultants and moments.

Output consists of a complete echo check of the input data which may be supplemented by some internally generated information such as nodal point coordinates or element stiffnesses; displacements of all nodal points in the structure; reactions and residual loads at nodes for which displacements have or have not been specified; internal stresses and moments in all plate and beam elements. In skew structures, internal stresses in plate elements may be rotated as desired. A general option to average stress resultants and moments is very effective in reducing tedious manual computation for output interpretation purposes. Another option provides, for any section, the complete statical moment of the structure which is useful in particular for bridge structures for which it may be broken up into individual girder moments. Finally, the execution times for the various phases of the program are printed out.

It is intended to document this computer program elsewhere [10.29], so that reference for further details may be made to this publication.

4.4 Examples

The first example is the simply supported curved beam of Fig. 4.3, with the ends restrained against rotation about the beam axis, having an opening angle of $\theta_o = 30°$ and a developed span length of 20 ft. Figure 4.3a shows the moment diagram for uniform loading, and Fig. 4.3b for a concentrated midspan load. Results obtained from ordinary curved beam theory as outlined in Chapter 3 are compared with program FINPLA2 results, which are shown for a solid cross section (discretized by 2 elements transversely and 12 elements longitudinally for half the beam)

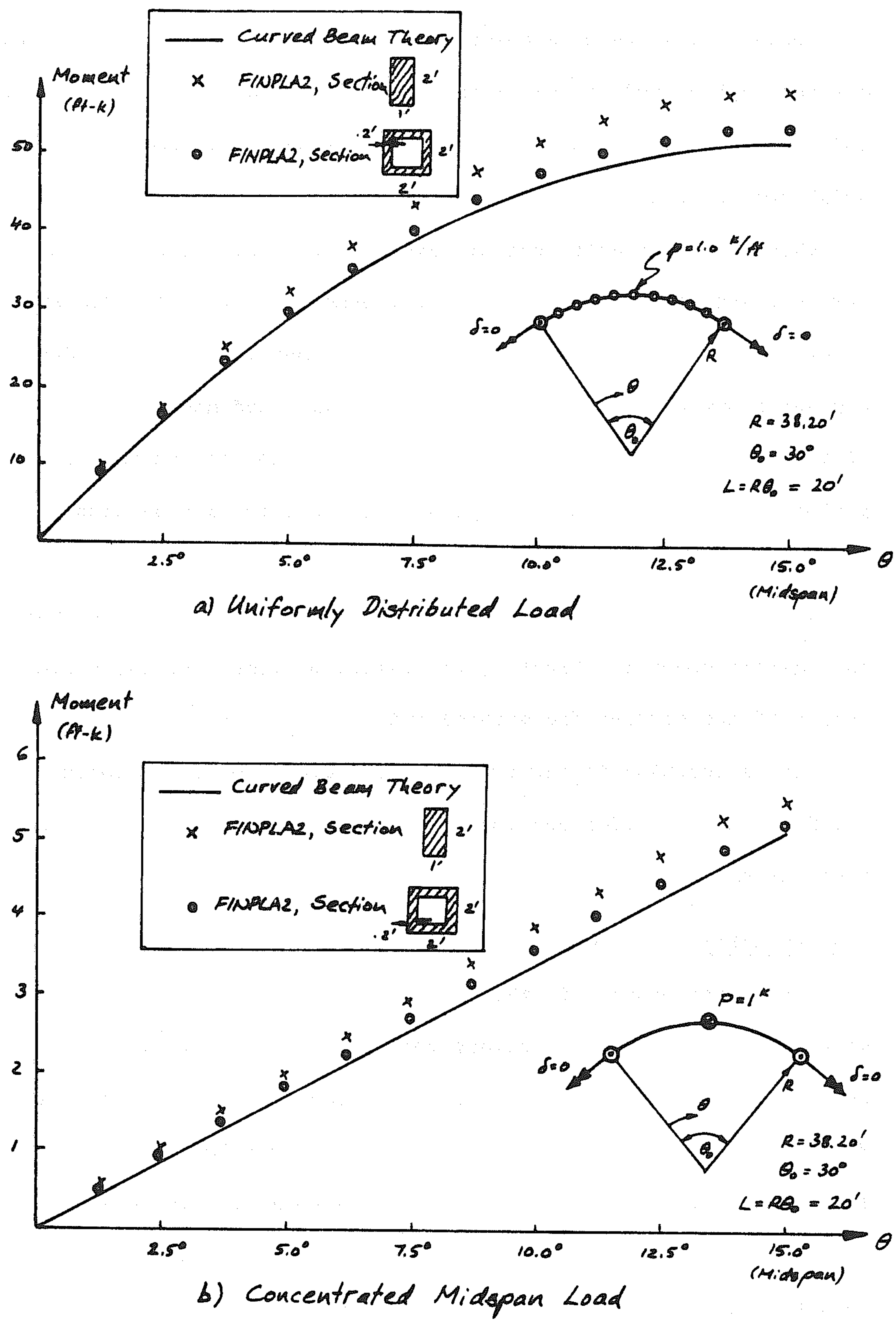

Fig. 4.3 Bending Moments in Curved Beam

and a square box section (represented by 8 elements transversely and 12 elements longitudinally). In view of the fairly coarse meshes used, agreement of the two theories appears to be very good, and can be expected to increase with further mesh refinement.

It may be interesting to note that the midspan nodal point reactions corresponding to the displacements which for symmetry reasons were set equal to zero, agree exactly with the theoretical bending moments.

The next example is the plate of Fig. 4.4, curved in plan with an opening angle of $\theta_o = 30°$ and a developed centerline span of $L = R\theta_o = 20$ ft. The straight radial edges are simply supported, and the curved edges are free, with a unit concentrated load placed at midspan of either the inner or the outer edge.

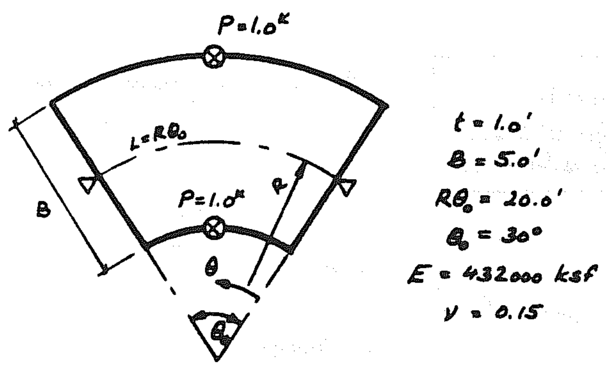

Fig. 4.4 Curved Plate Example

Figure 4.5 shows plate bending moments calculated according to the plate theory discussed in Chapter 3, based on 25 non-zero terms of the Fourier series, as well as results from program FINPLA2, based on a mesh representation of 4 X 12 = 48 elements for half the plate. The agreement between finite element theory and the closed form solution, as demonstrated in Fig. 4.5, is excellent and fully satisfactory for practical purposes.

Results for curved box girder bridges based on finite element theory will be presented in Chapter 6, and additional capabilities of program FINPLA2 will be described in [10.29].

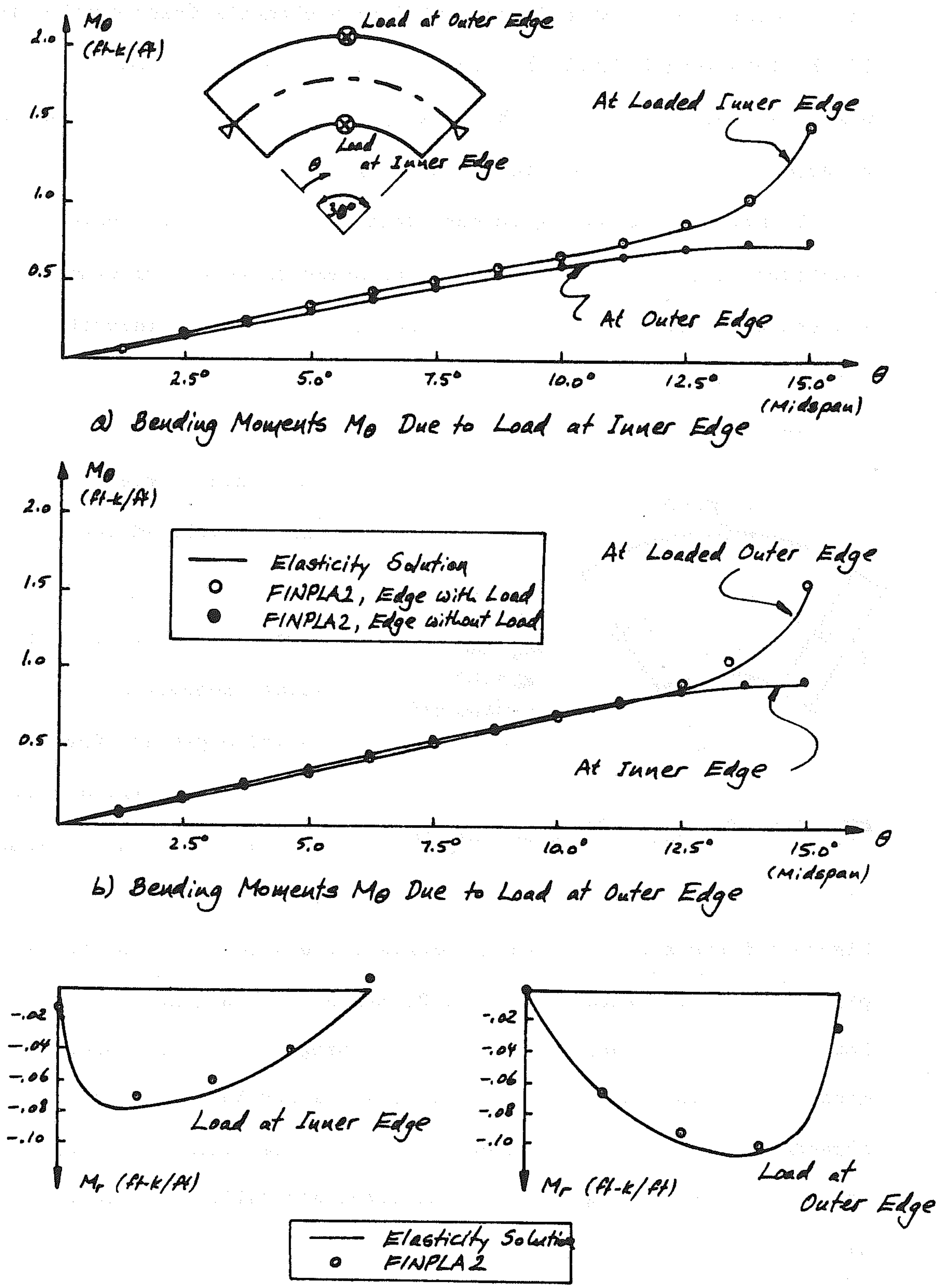

a) Bending Moments M_θ Due to Load at Inner Edge

b) Bending Moments M_θ Due to Load at Outer Edge

c) Bending Moments M_r

Fig. 4.5 Bending Moments in Curved Plate

5. FINITE STRIP ANALYSIS OF CURVED FOLDED PLATES

5.1 Introduction

5.1.1 General

In this chapter, the finite strip method of analysis will be described in detail, as it is applied to simply supported folded plate structures curved in plan and composed of elements which are in general segments of conical frustra, interconnected along their common circumferential edges, Fig. 5.1. This method, which will be designated as the curved strip method, is an approximate numerical technique capable of analyzing a variety of complex structural systems. All

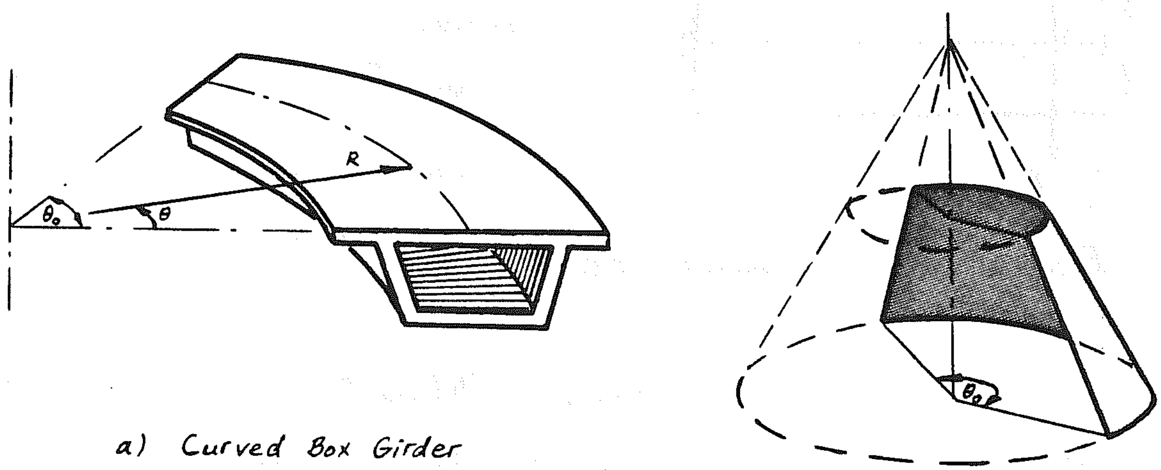

a) Curved Box Girder

b) Typical Structural Element

Fig. 5.1 Curved Folded Plate Structure

static and geometric quantities are to be developed into Fourier series along the hoop direction much in a similar way as is done to solve various other problems involving plate and shell theory. Some of the well-known techniques to which the curved strip method is closely related, will be briefly summarized below, before the method itself is presented and some of its features are discussed.

5.1.2 Leve's Solution for Simply Supported Plates

This well known special solution technique has been described in detail in the literature, for example by Timoshenko [5.8], and will therefore be only briefly mentioned here. For a rectangular plate which is simply supported along the two opposite sides, x = o and x = a, Fig. 5.2, the plate equation

$$\Delta\Delta w = \frac{p}{D} \tag{5.1}$$

is conveniently solved with the deflection w expanded into a sine series,

$$w = \sum_{n=1}^{\infty} w_n(y) \sin \frac{n\pi x}{a} \tag{5.2}$$

because a solution of this type satisfies automatically the boundary conditions

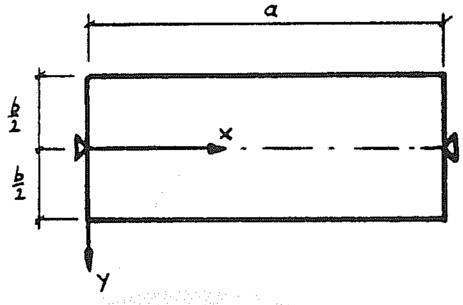

Fig. 5.2 Simply Supported Plate

$$w\big|_{x=0,a} = M_x\big|_{x=0,a} = M_y\big|_{x=0,a} = 0 \tag{5.3}$$

If the loading term is also expanded into a sine series,

$$p = \sum_{n=1}^{\infty} p_n \sin \frac{n\pi x}{a} \tag{5.4}$$

where, for example, for uniform loading,

$$p_n = \frac{4p}{n\pi} \tag{5.5}$$

then the substitution of Eqs. (5.2) and (5.4) into (5.1) leads to the ordinary differential equation

$$\frac{d^4 w_n}{dy^4} - 2\left(\frac{n\pi}{a}\right)^2 \frac{d^2 w_n}{dy^2} + \left(\frac{n\pi}{a}\right)^4 w_n = \frac{p_n}{D} \tag{5.6}$$

for which the homogeneous solution is given by

$$w_n^h(y) = A_n \sinh\frac{n\pi y}{a} + B_n \frac{n\pi y}{a}\cosh\frac{n\pi y}{a} + C_n \frac{n\pi y}{a}\sinh\frac{n\pi y}{a} + D_n \cosh\frac{n\pi y}{a} \tag{5.7}$$

and the particular solution,

$$w_n^p(y) = \left(\frac{a}{n\pi}\right)^4 \frac{p_n}{D} \tag{5.8}$$

The constants of integration, A_n, B_n, C_n, D_n, may then be determined such that the complete solution

$$w(x,y) = \sum_{n=1}^{\infty}\left(A_n \sinh\frac{n\pi y}{a} + B_n \frac{n\pi y}{a}\cosh\frac{n\pi y}{a} + C_n \frac{n\pi y}{a}\sinh\frac{n\pi y}{a} + D_n \cosh\frac{n\pi y}{a} + \left(\frac{a}{n\pi}\right)^4 \frac{p_n}{D}\right)\sin\frac{n\pi x}{a} \tag{5.9}$$

satisfies the boundary conditions along the edges $y = \pm\frac{b}{2}$.

5.1.3 Harmonic Analysis of Prismatic Folded Plate Structures

Adjusting the free constants of Eq. (5.9) successively to each one of the following four sets of boundary conditions,

$$\begin{array}{ll}
w|_{y=\pm\frac{b}{2}} = \frac{\partial w}{\partial y}\Big|_{y=-\frac{b}{2}} = 0 & \frac{\partial w}{\partial y}\Big|_{y=\frac{b}{2}} = 1\cdot\sin\frac{n\pi x}{a} \\
w|_{y=\pm\frac{b}{2}} = \frac{\partial w}{\partial y}\Big|_{y=\frac{b}{2}} = 0 & \frac{\partial w}{\partial y}\Big|_{y=-\frac{b}{2}} = 1\cdot\sin\frac{n\pi x}{a} \\
w|_{y=-\frac{b}{2}} = \frac{\partial w}{\partial y}\Big|_{y=\pm\frac{b}{2}} = 0 & w|_{y=\frac{b}{2}} = 1\cdot\sin\frac{n\pi x}{a} \\
w|_{y=\frac{b}{2}} = \frac{\partial w}{\partial y}\Big|_{y=\pm\frac{b}{2}} = 0 & w|_{y=-\frac{b}{2}} = 1\cdot\sin\frac{n\pi x}{a}
\end{array} \tag{5.10}$$

and evaluating the corresponding edge forces for each case, it is possible to derive a plate bending stiffness matrix $[k^B]_{4\times4}$ in which element k^B_{ij} is the force component required to enforce the boundary conditions associated with the unit edge displacement j in the n'th harmonic mode as specified in Eq. (5.10).

Proceeding in a similar manner to solve the corresponding plane stress problem

$$\Delta\Delta F = 0 \tag{5.11}$$

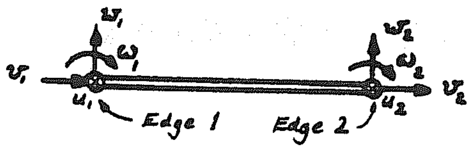

Fig. 5.3 Edge Displacements of Folded Plate Element

one can derive a plane stress stiffness matrix $[k^P]_{4\times4}$, thus establishing the complete element stiffness $[k]_{8\times8}$ associated with the 8 degrees of freedom shown in Fig. 5.3. Once this element stiffness is available, it is possible to perform a direct stiffness analysis of any plate assemblage for one term of the Fourier series at a time, and to accumulate the final results as the sum of all harmonic terms, provided all plates are simply supported at their ends which is equivalent to the assumption of idealized end diaphragms which do not permit any displacements within their plane but offer no resistance to displacements normal to their plane.

This approach towards the analysis of folded plate structures is closely associated with the names of Rüdiger [10.14], Goldberg and Leve [10.15], and DeFries-Skene and Scordelis [10.16]. Scordelis [10.1] extended this method to incorporate intermediate transverse rigid diaphragms which may or may not be externally supported, by defining redundant interaction forces between diaphragms and plate system, which are then determined using a force method. Current research at the University of California at Berkeley incorporates also flexible diaphragms and frame supports into the system.

5.1.4 Finite Strip Analysis of Prismatic Folded Plate Structures

Instead of deriving an element stiffness based on the closed-form solution of Eq. (5.6) and (5.11), one can find with slightly less numerical effort an approximate stiffness based on a numerical scheme called the "finite strip analysis," because of its close association with the finite element concept. In fact, the differential equations (5.1) and (5.11) are summary statements which combine compatibility conditions (strain-displacement relations), material properties (stress-strain law) and equilibrium requirements. Hence, assuming the displacements to vary in a certain fashion, as functions of some unknown nodal displacements, the strains and stresses can be obtained using the known strain-displacement and stress-strain relations, respectively, so that the potential energy can be formed as a function of the unknown nodal displacements, and from this energy expression the element stiffness is readily extracted.

With this approach the names of Cheung [10.17] [10.18] and Powell and Ogden [10.19] are closely associated. It will be presented in detail later in this chapter as it is applied to curved folded plate structures and will be shown in Section 5.6.2 to degenerate to the straight folded plate case. Willam and Scordelis [10.4] extended the theory to include orthotropic plates with eccentric stiffeners, and Cheung [5.40] recently applied this method to the orthotropic curved plate problem.

5.1.5 Finite Element Analysis of Shells of Revolution

If a shell of revolution is subjected to axisymmetric loads only, it may be approximated by a series of conical frustra, Fig. 5.4.

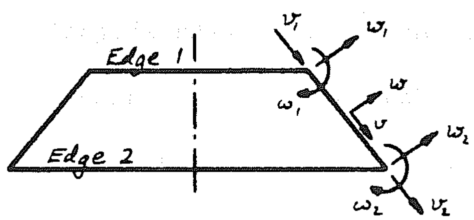

Fig. 5.4 Axisymmetric Shell Element

The derivation of the stiffness for such an element is in principle a one-dimensional problem because it is independent of the circumferential coordinate. Thus, one may assume the element displacements to vary along the meridian as

$$\begin{Bmatrix} v \\ w \end{Bmatrix} = \begin{bmatrix} \phi_v & 0 \\ 0 & \phi_w \end{bmatrix} \begin{Bmatrix} v_i \\ w_i \end{Bmatrix} \qquad (5.12)$$

where $\{v_i\}^T = \langle v_1 \ v_2 \rangle$ and $\{w_i\}^T = \langle w_1 \ w_2 \ \omega_1 \ \omega_2 \rangle$ are the nodal displacement values, Fig. 5.4, and $\langle \Phi_u \rangle$ and $\langle \Phi_w \rangle$ are vectors containing linear and cubic interpolation polynomials, respectively. The strains follow then from the appropriate strain-displacement equations and the stresses from Hooke's law so that the strain energy can be formed as a function of the nodal degrees of freedom, which in turn yields directly the element stiffness.

If the applied loads are not axisymmetric, they may be resolved into Fourier series, and then the displacements have to be developed as

$$\begin{Bmatrix} u \\ v \\ w \end{Bmatrix} = \sum_{n=1}^{\infty} \begin{bmatrix} \phi_u \cos n\theta & 0 & 0 \\ 0 & \phi_v \sin n\theta & 0 \\ 0 & 0 & \phi_w \sin n\theta \end{bmatrix} \begin{Bmatrix} u_i \\ v_i \\ w_i \end{Bmatrix}_n \qquad (5.13)$$

where $\{u_i\}^T = \langle u_1 \ u_2 \rangle$ are the circumferential joint displacements which raise the number of degrees of freedom per joint to 4. The structure is then assembled and solved for the generalized joint displacements for one harmonic at a time, in a very similar way to that used for the straight folded plate system.

Grafton and Strome [10.12] presented this theory for axisymmetric loads for the first time, and Percy et al. [10.13] extended it to non-axisymmetric loads.

5.2 Direct Stiffness Solution of Curved Folded Plate Structures

The curved strip method of analysis is a combination and extension of the techniques introduced in the previous paragraphs. It has been developed for the analysis of simply supported structures which are composed of segments of conical frustra in general, Fig. 5.5b, and cylindrical shells, Fig. 5.5d, and circular ring plate segments, Fig. 5.5e, in particular. These curved elements are joined together along their common circumferential edges.

Provided a stiffness matrix can be derived for a typical curved strip element, which relates the generalized joint displacements and forces, it will be possible to apply the same techniques developed for straight folded plates to perform the structural assembly process and to solve the system for the generalized joint displacements. All loads, displacements, and forces are for this purpose developed into Fourier series such that the advantage of the simple end support conditions is taken.

For the analysis, the following assumptions are made.

a) The thickness of each curved strip element is constant and small compared with the other strip dimensions;

b) Straight lines which are perpendicular to the middle surface of the undeformed element remain straight and perpendicular to the deformed middle surface;

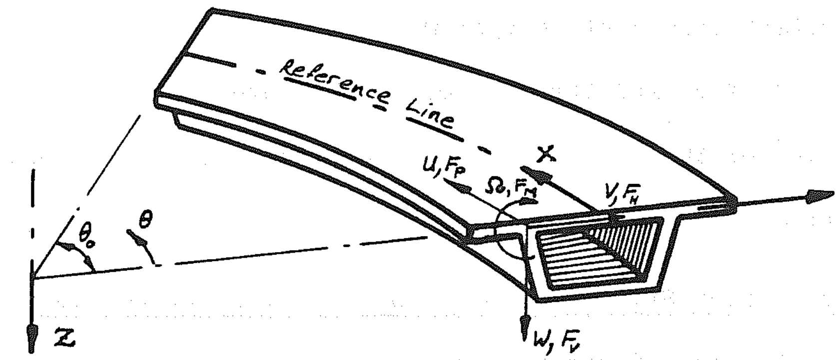

a) Global Joint Displacements U, V, W, Ω, And Joint Loads F_H, F_V, F_P, F_M

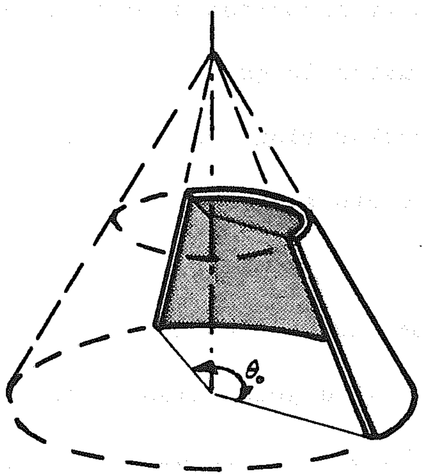

b) General Cone Segment, $0 < \varphi < 90°$

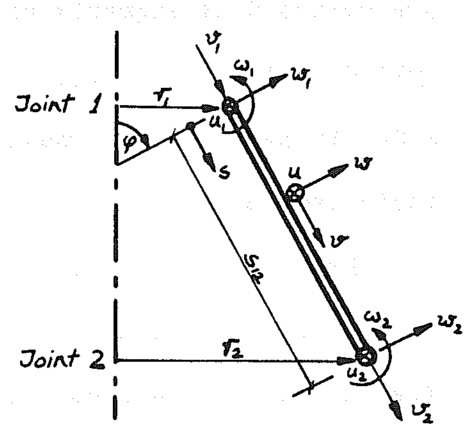

c) Nodal Joint Degrees of Freedom

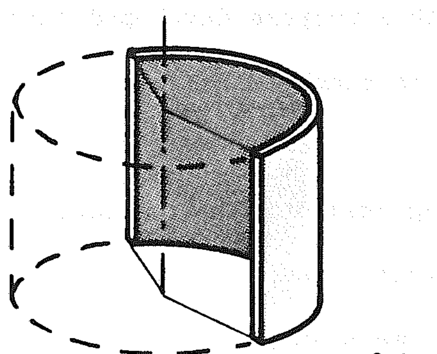

d) Cylindrical Shell Segment

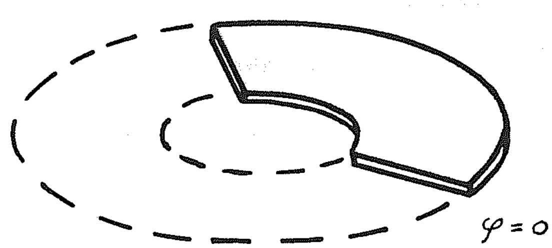

e) Circular Ring Plate Segment

Fig. 5.5 Curved Folded Plate Structure - Notations

c) The material is homogeneous and linear elastic, with orthotropic properties which are constant throughout any one element.

However, material property variations in the radial direction may be approximated by further subdividing each plate into curved strips and assigning different properties to each of them such as to simulate the true variation of the element properties.

The actual steps in the analysis procedure can be summarized as follows.

1. Replace all surface or line loads distributed across the width of a curved strip element by a set of equivalent nodal joint loads and transform their components to the global system, F_H, F_V, F_M, F_P, shown in Fig. 5.5a.
2. Resolve all loads to which the structure is subjected, into Fourier series and form the loading vector by adding all load contributions for one typical term of the series. The dimension m of this vector equals four times the number of joints in the structure.
3. Calculate the 8X8 stiffness matrix of each curved strip element for a typical term of the Fourier series.
4. Transform each element stiffness to the global coordinates U,V,W,Ω of Fig. 5.5a, so that the structure stiffness matrix may be assembled according to the principles of the well-known direct stiffness procedure. This mXm matrix, in conjunction with the loading vector, constitutes the set of equilibrium equations for a typical term of the Fourier series expansion.
5. Solve the system of equations for the unknown joint displacements which actually are the amplitudes of the displacement functions for the respective harmonic term.

6. Transform the joint displacements back to the element coordinates in order to determine the edge displacements to which each curved strip element is subjected.
7. Calculate for the edge displacements of this particular harmonic the internal forces in each curved strip element.
8. Repeat all of the above steps for each harmonic of the Fourier series and sum up the contributions of each term in order to obtain the final displacements and internal stress resultants throughout the structure.

The key step in this analysis is the derivation of the 8X8 stiffness matrix for a general conical shell segment in the n'th mode of the harmonic series, and will be described in detail in the next section. The consistent load theory used to convert distributed loadings to joint loads will be explained in Section 5.4, together with the determination of internal forces.

A computer program called CURSTR has been written so that the tedious numerical calculations can be performed very efficiently by a digital computer. This program has been described in detail in [5.41], and Section 5.5 will therefore give only a brief summary of its capabilities.

5.3 Stiffness Matrix of Curved Strip Element

For a closed shell of revolution, the period of the Fourier series expansion is π, Eq. (5.13). For a segment of a conical shell, Fig. 5.5b, it is logical to change this period accordingly, i.e. displacements are described in the following form

$$\begin{Bmatrix} u(\eta,\theta) \\ v(\eta,\theta) \\ w(\eta,\theta) \end{Bmatrix} = \sum_{n=1}^{\infty} \begin{Bmatrix} u_n(\eta)\cos\frac{n\pi\theta}{\theta_0} \\ v_n(\eta)\sin\frac{n\pi\theta}{\theta_0} \\ w_n(\eta)\sin\frac{n\pi\theta}{\theta_0} \end{Bmatrix} = \sum_{n=1}^{\infty} \begin{bmatrix} \phi_u(\eta)\cos\frac{n\pi\theta}{\theta_0} & 0 & 0 \\ 0 & \phi_v(\eta)\sin\frac{n\pi\theta}{\theta_0} & 0 \\ 0 & 0 & \phi_w(\eta)\sin\frac{n\pi\theta}{\theta_0} \end{bmatrix} \begin{Bmatrix} u_i \\ v_i \\ w_i \end{Bmatrix}_n \tag{5.14a}$$

where

$$\langle \phi_u(\eta) \rangle = \langle \phi_v(\eta) \rangle = \tfrac{1}{2} \langle (1-\eta) \;\; (1+\eta) \rangle \tag{5.14b}$$

and $\quad \langle \phi_w(\eta) \rangle = \frac{1}{4} \left\langle (2-3\eta+\eta^3),\ (2+3\eta-\eta^3),\ \frac{s_{12}}{2}(1-\eta-\eta^2+\eta^3),\ \frac{s_{12}}{2}(-1-\eta+\eta^2+\eta^3) \right\rangle$

are the polynomials interpolating the respective displacement quantities between their nodal values, Fig. 5.5c,

$$\{u_i\}_n = \begin{Bmatrix} u_1 \\ u_2 \end{Bmatrix}_n \qquad \{v_i\}_n = \begin{Bmatrix} v_1 \\ v_2 \end{Bmatrix}_n \qquad \{w_i\}_n = \begin{Bmatrix} w_1 \\ w_2 \\ \omega_1 \\ \omega_2 \end{Bmatrix}_n \tag{5.14c}$$

η is the transverse natural coordinate, Fig. 5.6, defined to assume the values -1 and +1 at the joints 1 and 2, respectively. The transverse rotations are then defined as

$$\omega = \frac{\partial w}{\partial s} = \frac{\partial w}{\partial \eta}\frac{\partial \eta}{\partial s} = \frac{2}{s_{12}}\frac{\partial w}{\partial \eta} \tag{5.15}$$

where s_{12} is the meridional distance between joints 1 and 2, and s the ordinary transverse coordinate, Fig. 5.6a.

In Eq. (5.14), a linear variation of the in-plane displacement components u and v, Fig. 5.6b, and a cubic variation of the normal displacement component w, Fig. 5.6c, has been chosen. One could equally well replace Eq. (5.14b) by any order polynomials while

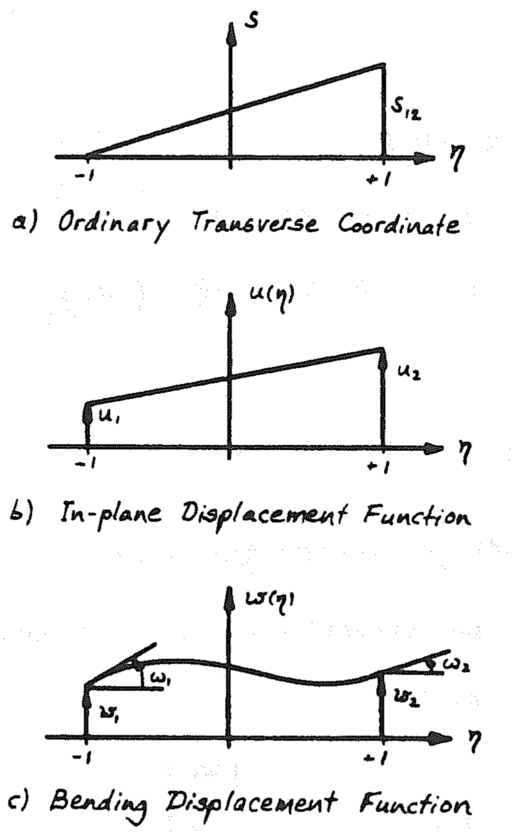

Fig. 5.6 Displacement Functions

adding degrees of freedom to the element, resulting in an increase in accuracy and computational effort. In Section 5.8, a stiffness based on quadratic in-plane displacements will be presented, together with a brief discussion of its advantages and disadvantages.

Most investigators studying shells of revolution by the Finite Element Method use the strain-displacement relations derived by Novozlilov [10.22]

$$\begin{Bmatrix} \varepsilon_s \\ \varepsilon_\theta \\ 2\varepsilon_{s\theta} \\ \kappa_s \\ \kappa_\theta \\ 2\kappa_{s\theta} \end{Bmatrix} = \begin{Bmatrix} \dfrac{\partial v}{\partial s} \\ \dfrac{\partial u}{r\partial\theta} + \dfrac{\cos\varphi}{r} v + \dfrac{\sin\varphi}{r} w \\ \dfrac{\partial u}{\partial s} - \dfrac{\cos\varphi}{r} u + \dfrac{\partial v}{r\partial\theta} \\ -\dfrac{\partial^2 w}{\partial s^2} \\ \dfrac{\sin\varphi}{r^2}\dfrac{\partial u}{\partial\theta} - \dfrac{\partial^2 w}{r^2\partial\theta^2} - \dfrac{\cos\varphi}{r}\dfrac{\partial w}{\partial s} \\ \dfrac{2\sin\varphi}{r}\dfrac{\partial u}{\partial s} - \dfrac{2\sin\varphi\cos\varphi}{r^2} u - \dfrac{2}{r}\dfrac{\partial^2 w}{\partial s\partial\theta} + \dfrac{2\cos\varphi}{r^2}\dfrac{\partial w}{\partial\theta} \end{Bmatrix} \tag{5.16}$$

In order to express the strain vector in terms of the generalized nodal displacements, substitution of Eq. (5.14a) into (5.16) leads for harmonic number n to

$$\begin{Bmatrix} \varepsilon_s \\ \varepsilon_\theta \\ 2\varepsilon_{s\theta} \\ \kappa_s \\ \kappa_\theta \\ 2\kappa_{s\theta} \end{Bmatrix}_n = \begin{bmatrix} 0 & \frac{\partial \phi_v}{\partial s} \sin\frac{n\pi\theta}{\theta_0} & 0 \\ -\frac{n\pi}{r\theta_0}\phi_u \sin\frac{n\pi\theta}{\theta_0} & \frac{\cos\varphi}{r}\phi_v \sin\frac{n\pi\theta}{\theta_0} & \frac{\sin\varphi}{r}\phi_w \sin\frac{n\pi\theta}{\theta_0} \\ \left(\frac{\partial\phi_u}{\partial s} - \frac{\cos\varphi}{r}\phi_u\right)\cos\frac{n\pi\theta}{\theta_0} & \left(\frac{n\pi}{r\theta_0}\right)\phi_v \cos\frac{n\pi\theta}{\theta_0} & 0 \\ 0 & 0 & -\frac{\partial^2\phi_w}{\partial s^2}\sin\frac{n\pi\theta}{\theta_0} \\ -\frac{\sin\varphi}{r^2}\left(\frac{n\pi}{\theta_0}\right)\phi_u \sin\frac{n\pi\theta}{\theta_0} & 0 & \left[\left(\frac{n\pi}{r\theta_0}\right)^2\phi_w - \frac{\cos\varphi}{r}\frac{\partial\phi_w}{\partial s}\right]\sin\frac{n\pi\theta}{\theta_0} \\ 2\left(\frac{\sin\varphi}{r}\frac{\partial\phi_u}{\partial s} - \frac{\sin\varphi\cos\varphi}{r^2}\right)\cos\frac{n\pi\theta}{\theta_0} & 0 & 2\left(\frac{n\pi}{r\theta_0}\right)\left(\frac{\cos\varphi}{r}\phi_w - \frac{\partial\phi_w}{\partial s}\right)\cos\frac{n\pi\theta}{\theta_0} \end{bmatrix} \begin{Bmatrix} u_i \\ v_i \\ w_i \end{Bmatrix}_n \qquad (5.17a)$$

or for short

$$\{\varepsilon\}_n = [T_n]\{u_i\}_n \qquad (5.17b)$$

The general orthogonal anisotropic material law reads

$$\begin{Bmatrix} N_s \\ N_\theta \\ N_{s\theta} \\ M_s \\ M_\theta \\ M_{s\theta} \end{Bmatrix}_n = \begin{bmatrix} \frac{t^m E_s^m}{1-\nu_{s\theta}^m\nu_{\theta s}^m} & \nu_{\theta s}^m \frac{t^m E_\theta^m}{1-\nu_{s\theta}^m\nu_{\theta s}^m} & 0 & 0 & 0 & 0 \\ \nu_{s\theta}^m \frac{t^m E_s^m}{1-\nu_{s\theta}^m\nu_{\theta s}^m} & \frac{t^m E_\theta^m}{1-\nu_{s\theta}^m\nu_{\theta s}^m} & 0 & 0 & 0 & 0 \\ 0 & 0 & t^m G^m & 0 & 0 & 0 \\ 0 & 0 & 0 & \frac{(t^b)^3 E_s^b}{12(1-\nu_{s\theta}^b\nu_{\theta s}^b)} & \nu_{\theta s}^b \frac{(t^b)^3 E_\theta^b}{12(1-\nu_{s\theta}^b\nu_{\theta s}^b)} & 0 \\ 0 & 0 & 0 & \nu_{s\theta}^b \frac{(t^b)^3 E_s^b}{12(1-\nu_{s\theta}^b\nu_{\theta s}^b)} & \frac{(t^b)^3 E_\theta^b}{12(1-\nu_{s\theta}^b\nu_{\theta s}^b)} & 0 \\ 0 & 0 & 0 & 0 & 0 & \frac{(t^b)^3 G^b}{12} \end{bmatrix} \begin{Bmatrix} \varepsilon_s \\ \varepsilon_\theta \\ 2\varepsilon_{s\theta} \\ \kappa_s \\ \kappa_\theta \\ 2\kappa_{s\theta} \end{Bmatrix}_n \qquad (5.18a)$$

or symbolically

$$\{\sigma\}_n = [D]\{\varepsilon\}_n \qquad (5.18b)$$

where superscript "m" denotes membrane or in-plane characteristics and superscript "b" stands for bending properties. Later, the elements of the $[D]_{6\times6}$ matrix will be referred to by d_{ij}.

The commonly used, isotropic homogeneous material law follows from Eq. (5.18) by setting

$$
\begin{aligned}
E_s^m = E_s^b = E_\theta^m &= E_\theta^b = E \\
\nu_{s\theta}^m = \nu_{\theta s}^m = \nu_{s\theta}^b &= \nu_{\theta s}^b = \nu \\
G^m = G^b = G &= \frac{E}{2(1+\nu)} \\
t^m = t^b &= t
\end{aligned}
\tag{5.19}
$$

Using Eqs. (5.17) and (5.18), the potential energy stored in a conical shell element can be expressed as

$$
\begin{aligned}
E_{Pot} &= \frac{1}{2}\int_A \{\varepsilon\}^T\{\sigma\}\, dA \\
&= \frac{1}{2}\sum_{n=1}^{\infty}\sum_{m=1}^{\infty}\{u_i\}_n^T\left(\int_{s=0}^{s_{12}}\int_{\theta=0}^{\theta_o}[T_n]^T[D][T_m]\, r\, ds\, d\theta\right)\{u_i\}_m
\end{aligned}
\tag{5.20}
$$

Because of the orthogonality of the displacement functions, the triple product vanishes for $n \neq m$, and for $n = m$,

$$
\int_0^{\theta_o}\sin^2\frac{n\pi\theta}{\theta_o}\, d\theta = \int_0^{\theta_o}\cos^2\frac{n\pi\theta}{\theta_o}\, d\theta = \frac{\theta_o}{2}
\tag{5.20a}
$$

so that Eq. (5.20) simplifies to

$$
E_{Pot} = \frac{1}{2}\sum_{n=1}^{\infty}\{u_i\}_n^T\left(\frac{\theta_o}{2}\int_{s=0}^{s_{12}}[\hat{T}_n]^T[D][\hat{T}_n]\, r\, ds\right)\{u_i\}_n
\tag{5.21}
$$

where $[\hat{T}_n]$ is equal to $[T_n]$ with all $\sin\frac{n\pi\theta}{\theta_o}$ and $\cos\frac{n\pi\theta}{\theta_o}$ multipliers deleted.

The element stiffness for a typical harmonic n follows from Eq. (5.21) as

$$
\begin{aligned}
[k]_n &= \frac{\theta_o}{2}\int_0^{s_{12}}[\hat{T}_n]^T[D][\hat{T}_n]\, r\, ds \\
&= \frac{\theta_o s_{12}}{4}\int_{-1}^{1}[\hat{T}_n]^T[D][\hat{T}_n]\, r\, d\eta
\end{aligned}
\tag{5.22}
$$

Partitioning $[k]_n$ with respect to the displacement components u, v, w, one obtains

$$[k]_n = \frac{\theta_o s_{12}}{4}\begin{bmatrix} k_{uu} & k_{uv} & k_{uw} \\ & k_{vv} & k_{vw} \\ (\text{symm.}) & & k_{ww} \end{bmatrix} = \frac{\theta_o s_{12}}{4}\int_{-1}^{1}\begin{bmatrix} \bar{k}_{uu} & \bar{k}_{uv} & \bar{k}_{uw} \\ & \bar{k}_{vv} & \bar{k}_{vw} \\ (\text{symm.}) & & \bar{k}_{ww} \end{bmatrix} r\,d\eta \tag{5.23}$$

with

$$\begin{aligned}
[k_{uu}]_n = {} & [d_{22}(\tfrac{n\pi}{\theta_o})^2 + d_{33}\cos^2\varphi]\int_{-1}^{1}\frac{\phi_u^T\phi_u}{r}\,d\eta + \sin^2\varphi\,[d_{55}(\tfrac{n\pi}{\theta_o})^2 + 4d_{66}\cos^2]\int_{-1}^{1}\frac{\phi_u^T\phi_u}{r^3}\,d\eta \\
& - d_{33}\cos\varphi\int_{-1}^{1}(\phi_u'^T\phi_u + \phi_u^T\phi_u')\,d\eta - 4d_{66}\sin^2\varphi\cos\varphi\int_{-1}^{1}\frac{(\phi_u'^T\phi_u + \phi_u^T\phi_u')}{r^2}\,d\eta \\
& + d_{33}\int_{-1}^{1}\phi_u'^T\phi_u'\,r\,d\eta + 4d_{66}\sin^2\varphi\int_{-1}^{1}\frac{\phi_u'^T\phi_u'}{r}\,d\eta
\end{aligned}$$

$$[k_{uv}]_n = -(\tfrac{n\pi}{\theta_o})\cos\varphi\,(d_{22}+d_{33})\int_{-1}^{1}\frac{\phi_u^T\phi_v}{r}\,d\eta + (\tfrac{n\pi}{\theta_o})d_{33}\int_{-1}^{1}\phi_u'^T\phi_v\,d\eta - (\tfrac{n\pi}{\theta_o})d_{12}\int_{-1}^{1}\phi_u^T\phi_v'\,d\eta$$

$$\begin{aligned}
[k_{uw}]_n = {} & -(\tfrac{n\pi}{\theta_o})d_{22}\sin\varphi\int_{-1}^{1}\frac{\phi_u^T\phi_w}{r}\,d\eta - \sin\varphi(\tfrac{n\pi}{\theta_o})[d_{55}(\tfrac{n\pi}{\theta_o})^2 + 4d_{66}\cos^2\varphi]\int_{-1}^{1}\frac{\phi_u^T\phi_w}{r^3}\,d\eta \\
& + \sin\varphi\cos\varphi(\tfrac{n\pi}{\theta_o})(d_{55}+4d_{66})\int_{-1}^{1}\frac{\phi_u^T\phi_w'}{r^2}\,d\eta + \sin\varphi(\tfrac{n\pi}{\theta_o})d_{45}\int_{-1}^{1}\frac{\phi_u^T\phi_w''}{r}\,d\eta \\
& + 4d_{66}\sin\cos\varphi(\tfrac{n\pi}{\theta_o})\int_{-1}^{1}\frac{\phi_u'^T\phi_w}{r^2}\,d\eta - 4d_{66}\sin\varphi(\tfrac{n\pi}{\theta_o})\int_{-1}^{1}\frac{\phi_u'^T\phi_w'}{r}\,d\eta
\end{aligned} \tag{5.23 (a-f)}$$

$$[k_{vv}]_n = [d_{22}\cos^2\varphi + d_{33}(\tfrac{n\pi}{\theta_o})^2]\int_{-1}^{1}\frac{\phi_v^T\phi_v}{r}\,d\eta + d_{12}\cos\varphi\int_{-1}^{1}(\phi_v'^T\phi_v + \phi_v^T\phi_v')\,d\eta + d_{11}\int_{-1}^{1}\phi_v'^T\phi_v'\,r\,d\eta$$

$$[k_{vw}]_n = d_{22}\sin\varphi\cos\varphi\int_{-1}^{1}\frac{\phi_v^T\phi_w}{r}\,d\eta + d_{12}\sin\varphi\int_{-1}^{1}\phi_v'^T\phi_w\,d\eta$$

$$\begin{aligned}
[k_{ww}]_n = {} & d_{22}\sin^2\varphi\int_{-1}^{1}\frac{\phi_w^T\phi_w}{r}\,d\eta + (\tfrac{n\pi}{\theta_o})^2[d_{55}(\tfrac{n\pi}{\theta_o})^2 + 4d_{66}\cos^2\varphi]\int_{-1}^{1}\frac{\phi_w^T\phi_w}{r^3}\,d\eta \\
& - (d_{55}+4d_{66})\cos\varphi(\tfrac{n\pi}{\theta_o})^2\int_{-1}^{1}\frac{(\phi_w'^T\phi_w + \phi_w^T\phi_w')}{r^2}\,d\eta - d_{45}(\tfrac{n\pi}{\theta_o})^2\int_{-1}^{1}\frac{(\phi_w^T\phi_w'' + \phi_w''^T\phi_w)}{r}\,d\eta \\
& + [d_{55}\cos^2\varphi + 4d_{66}(\tfrac{n\pi}{\theta_o})^2]\int_{-1}^{1}\frac{\phi_w'^T\phi_w'}{r}\,d\eta + d_{45}\cos\varphi\int_{-1}^{1}(\phi_w'^T\phi_w'' + \phi_w''^T\phi_w')\,d\eta + d_{44}\int_{-1}^{1}\phi_w''^T\phi_w''\,r\,d\eta
\end{aligned}$$

and

$$r = \frac{r_2 + r_1}{2} + \frac{r_2 - r_1}{2}\,\eta \tag{5.24}$$

A prime denotes differentiation with respect to s, i.e.

$$\phi' = \frac{\partial\phi}{\partial s} = \frac{2}{s_{12}}\frac{\partial\phi}{\partial\eta} \tag{5.25}$$

All integral expressions in Eqs. (5.23a-f) are of the form

$$I_{ij} = \int_{-1}^{1}\frac{\eta^i d\eta}{(a\eta+b)^j} \qquad \begin{matrix} i = 0,1,\ldots,6 \\ j = 0,1,2,3 \end{matrix} \tag{5.26}$$

with

$$a = \frac{r_2 - r_1}{2}\ , \qquad b = \frac{r_2 + r_1}{2}$$

Substituting $r = a\eta+b$, $\eta = (r-b)/a$, $d\eta = dr/a$, one obtains

$$I_{ij} = \frac{1}{a^{i+1}}\left[\int_{-1}^{1} r^{i-j}dr + c_1 b\int_{-1}^{1} r^{i-1-j}dr + \ldots + c_{i-1}b^{i-1}\int_{-1}^{1} r^{-j+1}dr + b^i\int_{-1}^{1} r^{-j}dr\right] \tag{5.27}$$

where c_k are the binomial coefficients. With this expansion, the integrals Eq. (5.26) are easily evaluated explicitly. However, after an extensive numerical investigation it was found that for large radii, which are likely to occur in the analysis of curved bridges, the explicitly integrated expressions are extremely sensitive to numerical calculation because they are formed as differences of very large numbers of almost equal magnitude. For example, the computed integral $I_{6,3}$ was already of opposite sign to the correct value for a mean radius $b = 500$ and $a = 5$. Therefore, this procedure is replaced by numerical integration, the accuracy of which increases even for large radii, as can be easily shown by a limiting process with Eq. (5.26). It was found that an 8'th order Gaussian quadrature formula gave results which were sufficiently accurate for all practical values of a and b.

Before assembling the element stiffness matrices to form the structure stiffness, Eq. (5.23) has to be transformed into global coordinates,

$$[\bar{k}]_n = [A]^T[k]_n[A] \tag{5.28}$$

where the transformation matrix $[A]$ is defined by

$$\begin{Bmatrix} u_1 \\ u_2 \\ v_1 \\ v_2 \\ w_1 \\ w_2 \\ \omega_1 \\ \omega_2 \end{Bmatrix} = \begin{bmatrix} 0 & 0 & 0 & 1 & 0 & 0 & 0 & 0 \\ 0 & 0 & 0 & 0 & 0 & 0 & 0 & 1 \\ \cos\varphi & \sin\varphi & 0 & 0 & 0 & 0 & 0 & 0 \\ 0 & 0 & 0 & 0 & \cos\varphi & \sin\varphi & 0 & 0 \\ \sin\varphi & -\cos\varphi & 0 & 0 & 0 & 0 & 0 & 0 \\ 0 & 0 & 0 & 0 & \sin\varphi & -\cos\varphi & 0 & 0 \\ 0 & 0 & -1 & 0 & 0 & 0 & 0 & 0 \\ 0 & 0 & 0 & 0 & 0 & 0 & -1 & 0 \end{bmatrix} \begin{Bmatrix} V_1 \\ W_1 \\ \Omega_1 \\ U_1 \\ V_2 \\ W_2 \\ \Omega_2 \\ U_2 \end{Bmatrix} \tag{5.29}$$

Finally, it shall now be verified that the curved strip formulation converges toward the straight finite strip theory if the limits $r \to \infty$ and $\theta_o \to 0$ are approached such that $L = r\theta_o$ = const., i.e. as each conical element loses more and more curvature until it approaches the shape of a rectangular plate. Thus, substituting $L = r\theta_o$ into Eq. (5.23) and going to the limit, one obtains

$$[k]_n = \frac{L s_{12}}{4} \begin{bmatrix} k_{uu} & k_{uv} & k_{uw} \\ & k_{vv} & k_{vw} \\ (\text{symm.}) & & k_{ww} \end{bmatrix}_n = \frac{L s_{12}}{4} \int_{-1}^{1} \begin{bmatrix} \bar{k}_{uu} & \bar{k}_{uv} & \bar{k}_{uw} \\ & \bar{k}_{vv} & \bar{k}_{vw} \\ (\text{symm.}) & & \bar{k}_{ww} \end{bmatrix}_n d\eta \tag{5.30}$$

where

$$[k_{uu}]_n = d_{22}\left(\frac{n\pi}{L}\right)^2 \int_{-1}^{1} \phi_u^T \phi_u \, d\eta + d_{33} \int_{-1}^{1} \phi_u'^T \phi_u' \, d\eta$$

$$= \begin{bmatrix} \left(\frac{2}{3} d_{22}\alpha_n^2 + \frac{2 d_{33}}{s_{12}^2}\right) & \left(\frac{d_{22}\alpha_n^2}{3} - \frac{2 d_{33}}{s_{12}^2}\right) \\ \left(\frac{d_{22}\alpha_n^2}{3} - \frac{2 d_{33}}{s_{12}^2}\right) & \left(\frac{2}{3} d_{22}\alpha_n^2 + \frac{2 d_{33}}{s_{12}^2}\right) \end{bmatrix} \tag{5.30a}$$

$$[k_{uv}]_n = \left(\frac{n\pi}{L}\right) d_{33} \int_{-1}^{1} \phi_u'^T \phi_v \, d\eta - \left(\frac{n\pi}{L}\right) d_{12} \int_{-1}^{1} \phi_u^T \phi_v' \, d\eta$$

$$= \frac{\alpha_n}{S_{12}} \begin{bmatrix} (d_{12} - d_{33}) & -(d_{12} + d_{33}) \\ (d_{12} + d_{33}) & -(d_{12} - d_{33}) \end{bmatrix}$$

$$[k_{uw}] \equiv 0$$

(5.30 b-f)

$$[k_{vv}] = d_{33} \left(\frac{n\pi}{L}\right)^2 \int_{-1}^{1} \phi_v^T \phi_v \, d\eta + d_{11} \int_{-1}^{1} \phi_v'^T \phi_v' \, d\eta$$

$$= \begin{bmatrix} \left(\frac{2}{3} d_{33} \alpha_n^2 + \frac{2 d_{11}}{S_{12}^2}\right) & \left(\frac{1}{3} d_{33} \alpha_n^2 + \frac{2 d_{11}}{S_{12}^2}\right) \\ \left(\frac{1}{3} d_{33} \alpha_n^2 + \frac{2 d_{11}}{S_{12}^2}\right) & \left(\frac{2}{3} d_{33} \alpha_n^2 + \frac{2 d_{11}}{S_{12}^2}\right) \end{bmatrix}$$

$$[k_{vw}] \equiv 0$$

$$[k_{ww}]_n = d_{55} \left(\frac{n\pi}{L}\right)^4 \int_{-1}^{1} \phi_w^T \phi_w \, d\eta - d_{45} \left(\frac{n\pi}{L}\right)^2 \int_{-1}^{1} (\phi_w''^T \phi_w + \phi_w^T \phi_w'') \, d\eta + 4 d_{66} \left(\frac{n\pi}{L}\right)^2 \int_{-1}^{1} \phi_w'^T \phi_w' \, d\eta + d_{44} \int_{-1}^{1} \phi_w''^T \phi_w'' \, d\eta$$

$$\begin{bmatrix} \left(\frac{26}{35} d_{55} \alpha_n^4 + \beta_1 + \beta_2\right) & \left(\frac{9}{35} d_{55} \alpha_n^4 - \beta_1 - \beta_2\right) & \left(\frac{11}{105} d_{55} S_{12} \alpha_n^4 + \frac{S_{12}}{2} \beta_1 + \beta_3\right) & \left(-\frac{13}{210} d_{55} S_{12} \alpha_n^4 + \frac{S_{12}}{2} \beta_1 + \frac{S_{12}}{12} \beta_2\right) \\ & \left(\frac{26}{35} d_{55} \alpha_n^4 + \beta_1 + \beta_2\right) & \left(\frac{13}{210} d_{55} S_{12} \alpha_n^4 - \frac{S_{12}}{2} \beta_1 - \frac{S_{12}}{12} \beta_2\right) & \left(-\frac{11}{105} d_{55} S_{12} \alpha_n^4 - \frac{S_{12}}{2} \beta_1 - \beta_3\right) \\ & & \left(\frac{2}{105} d_{55} S_{12}^2 \alpha_n^4 + \frac{8 d_{44}}{S_{12}^2} + \frac{S_{12}^2}{9} \beta_2\right) & \left(-\frac{d_{55}}{70} S_{12}^2 \alpha_n^4 + \frac{4 d_{44}}{S_{12}^2} - \frac{S_{12}^2}{36} \beta_2\right) \\ & \text{(symmetric)} & & \left(\frac{2}{105} d_{55} S_{12}^2 \alpha_n^4 + \frac{8 d_{44}}{S_{12}^2} + \frac{S_{12}^2}{9} \beta_2\right) \end{bmatrix}$$

with $\alpha_n = \frac{n\pi}{L}$ $\quad \beta_1 = \frac{24 d_{44}}{S_{12}^4}$ $\quad \beta_2 = \frac{12 \alpha_n^2}{5 S_{12}^2} (2 d_{45} + 4 d_{66})$ $\quad \beta_3 = \frac{\alpha_n^2}{5 S_{12}} (12 d_{45} + 4 d_{66})$

These stiffness coefficients are identical to those derived by Willam and Scordelis [10.4]. Note that because of $[k_{uw}]_n \equiv [k_{vw}]_n \equiv 0$, bending and membrane actions are no longer coupled, and, of course, the angle φ does not appear anymore, because the element stiffness of a rectangular plate must be independent of its orientation, while for a conical shell, the inclination angle has an important influence on the element stiffness.

5.4 Consistent Load Analysis and Determination of Internal Forces

If loads are distributed over the whole width of a plate element with an arbitrary variation in the circumferential direction, their components in the u, v, w directions, Fig. 5.5c, can be written as

$$\begin{Bmatrix} p_u(\eta,\theta) \\ p_v(\eta,\theta) \\ p_w(\eta,\theta) \end{Bmatrix} = \begin{bmatrix} \phi_p(\eta) & 0 & 0 \\ 0 & \phi_p(\eta) & 0 \\ 0 & 0 & \phi_p(\eta) \end{bmatrix} \begin{Bmatrix} \bar{p}_u(\theta) \\ \bar{p}_v(\theta) \\ \bar{p}_w(\theta) \end{Bmatrix} \tag{5.31a}$$

or symbolically,

$$\{p_i(\eta,\theta)\} = [\phi_p(\eta)]\{\bar{p}_i(\theta)\} \tag{5.31b}$$

where $\bar{p}_i(\theta)$ are the intensities of the distributed load components at the nodal joints and $\Phi_p(\eta)$ is an appropriate interpolation polynomial which for this discussion is chosen to be linear, (compare Fig. 5.6b),

$$\phi_p(\eta) = \tfrac{1}{2}\langle (1-\eta) \quad (1+\eta)\rangle \tag{5.32}$$

Because the $[\Phi_p(\eta)]$-matrix is a function of η only, the Fourier representation of the load vector $\{p_i(\eta,\theta)\}$ may be applied to its nodal values only, which are then developed as

$$\{\bar{p}_i(\theta)\} = \sum_{n=1}^{\infty}\{\bar{p}_i\}_n \sin\frac{n\pi\theta}{\theta_o} \tag{5.33}$$

where the vector

$$\{\bar{p}_i\}_n = \frac{2}{\theta_o}\int_0^{\theta_o}\{\bar{p}_i(\theta)\}\sin\frac{n\pi\theta}{\theta_o}\,d\theta \tag{5.34}$$

contains the amplitudes of the Fourier series of Eq. (5.33) which can be found explicitly for various load cases. If the load is distributed uniformly with respect to θ, one obtains

$$\bar{p}^j_{i_n} = \frac{4 \bar{p}^j_i}{n\pi} \tag{5.35}$$

where $\bar{p}^j_i$ is the load intensity at joint j. For a transverse line load at $\theta = \theta_p$ of intensity $\bar{P}^j_i$ at joint j, one gets

$$\bar{p}^j_{i_n} = \frac{2}{r_j \theta_o} \sin \frac{n\pi\theta_p}{\theta_o} \cdot \bar{P}^j_i \tag{5.36}$$

and for a load of intensity $\bar{p}^j_i$ at joint j between $\theta_p - \frac{\delta}{2}$ and $\theta_p + \frac{\delta}{2}$ and zero outside this range, the result is

$$\bar{p}^j_{i_n} = \frac{4}{n\pi} \sin \frac{n\pi\theta_p}{\theta_o} \sin \frac{n\pi\delta}{2\theta_o} \cdot \bar{p}^j_i \tag{5.37}$$

In consistent load analysis, the distributed loads of Eq. (5.31) are replaced by consistent nodal loads

$$\{R_i(\theta)\} = \sum_{n=1}^{\infty} \{R_i\}_n \sin \frac{n\pi\theta}{\theta_o} \tag{5.38}$$

such that the work done by their amplitudes $\{R_i\}_n$, while going through the corresponding nodal displacement amplitudes $\{\bar{u}_i\}_n$ equals the work done by the distributed loads $\{p_i(\eta,\theta)\}$ while going through their associated displacement field $\{u_i(\eta,\theta)\}$, i.e.

$$\{\bar{u}_i\}_n^T \{R_i\}_n = \frac{s_{12}}{2} \iint_{\eta\,\theta} \{u_i(\eta,\theta)\}^T \{p_i(\eta,\theta)\}\, r\, d\eta\, d\theta \tag{5.39}$$

Substituting Eqs. (5.14a) and (5.31b) into (5.39) and making use of the orthogonality relations of Eq. (5.20a) and the virtual work principle, one obtains

$$\{R_i\}_n = \frac{s_{12}\theta_o}{4} \int_{\eta} [\phi(\eta)]^T [\phi_p(\eta)] \{\bar{p}_i\}_n\, r\, d\eta \tag{5.40}$$

which becomes explicitly, for the interpolation polynomials of Eq. (5.14b) and (5.32) used,

$$\begin{Bmatrix} R_{u_1} \\ R_{u_2} \\ R_{v_1} \\ R_{v_2} \\ R_{w_1} \\ R_{w_2} \\ R_{\omega_1} \\ R_{\omega_2} \end{Bmatrix}_n = \frac{s_{12}\theta_o}{120} \begin{bmatrix} 10(2b-a) & 10b & 0 & 0 & 0 & 0 \\ 10b & 10(2b+a) & 0 & 0 & 0 & 0 \\ 0 & 0 & 10(2b-a) & 10b & 0 & 0 \\ 0 & 0 & 10b & 10(2b+a) & 0 & 0 \\ 0 & 0 & 0 & 0 & (21b-11a) & (9b-a) \\ 0 & 0 & 0 & 0 & (9b+a) & (21b+11a) \\ 0 & 0 & 0 & 0 & s_{12}(3b-a) & 2bs_{12} \\ 0 & 0 & 0 & 0 & -2bs_{12} & -s_{12}(3b+a) \end{bmatrix} \begin{Bmatrix} \bar{p}_{u_1} \\ \bar{p}_{u_2} \\ \bar{p}_{v_1} \\ \bar{p}_{v_2} \\ \bar{p}_{w_1} \\ \bar{p}_{w_2} \end{Bmatrix}_n \qquad (5.41)$$

with

$$a = \frac{r_2 - r_1}{2}, \qquad b = \frac{r_2 + r_1}{2}$$

The $\{\bar{p}_i\}_n$ vector depends on the type of loading and has been given for some cases, Eqs. (5.35), (5.36), (5.37). For the equation of equilibrium of the structural assembly, the consistent nodal load vector $\{R_i\}_n$ has to be transformed into the global coordinate system of the structure, Fig. 5.5,

$$\{F_i\}_n = [A]^T \{R_i\}_n \qquad (5.42)$$

where $[A]^T$ is the transpose of the displacement transformation matrix of Eq. (5.29).

Line loads or concentrated loads acting directly on the joints, are treated like distributed surface loads, except that the integration extends only over the respective joint rather than over the whole element area.

Once the equations of equilibrium have been solved, and the final joint displacements determined as the sum of the various harmonic contributions, then internal forces throughout the curved plate are calculated as follows. Substituting Eq. (5.17b) into (5.18b) leads to

$$\{\sigma\}_n = [D][T_n]\{u_i\}_n \tag{5.43a}$$

or explicitly,

$$\begin{Bmatrix} N_s \\ N_\theta \\ N_{s\theta} \\ M_s \\ M_\theta \\ M_{s\theta} \end{Bmatrix}_n = \begin{bmatrix} -\left(\frac{n\pi}{r\theta_o}\right) d_{12}\phi_u \sin\frac{n\pi\theta}{\theta_o} & \left(d_{11}\frac{\partial\phi_v}{\partial s} + d_{12}\frac{\cos\varphi}{r}\phi_v\right)\sin\frac{n\pi\theta}{\theta_o} & \frac{\sin\varphi}{r} d_{12}\phi_w \sin\frac{n\pi\theta}{\theta_o} \\ -\left(\frac{n\pi}{r\theta_o}\right) d_{22}\phi_u \sin\frac{n\pi\theta}{\theta_o} & \left(d_{12}\frac{\partial\phi_v}{\partial s} + d_{22}\frac{\cos\varphi}{r}\phi_v\right)\sin\frac{n\pi\theta}{\theta_o} & \frac{\sin\varphi}{r} d_{22}\phi_w \sin\frac{n\pi\theta}{\theta_o} \\ d_{33}\left(\frac{\partial\phi_u}{\partial s} - \frac{\cos\varphi}{r}\phi_u\right)\cos\frac{n\pi\theta}{\theta_o} & \left(\frac{n\pi}{r\theta_o}\right) d_{33}\phi_v \cos\frac{n\pi\theta}{\theta_o} & 0 \\ -\left(\frac{n\pi}{r\theta_o}\right)\frac{\sin\varphi}{r} d_{45}\phi_u \sin\frac{n\pi\theta}{\theta_o} & 0 & \left[\left(\frac{n\pi}{r\theta_o}\right)^2 d_{45}\phi_w - d_{44}\frac{\partial^2\phi_w}{\partial s^2} - \frac{\cos\varphi}{r} d_{45}\frac{\partial\phi_w}{\partial s}\right]\sin\frac{n\pi\theta}{\theta_o} \\ -\left(\frac{n\pi}{r\theta_o}\right)\frac{\sin\varphi}{r} d_{55}\phi_u \sin\frac{n\pi\theta}{\theta_o} & 0 & \left[\left(\frac{n\pi}{r\theta_o}\right)^2 d_{55}\phi_w - d_{45}\frac{\partial^2\phi_w}{\partial s^2} - \frac{\cos\varphi}{r} d_{55}\frac{\partial\phi_w}{\partial s}\right]\sin\frac{n\pi\theta}{\theta_o} \\ \frac{\sin^2\varphi}{r} d_{66}\left(\frac{\partial\phi_u}{\partial s} - \frac{\cos\varphi}{r}\phi_u\right)\cos\frac{n\pi\theta}{\theta_o} & 0 & 2d_{66}\left(\frac{n\pi}{r\theta_o}\right)\left(\frac{\cos\varphi}{r}\phi_w - \frac{\partial\phi_w}{\partial s}\right)\cos\frac{n\pi\theta}{\theta_o} \end{bmatrix} \begin{Bmatrix} u_i \\ v_i \\ w_i \end{Bmatrix}_n \tag{5.43b}$$

where $\langle\Phi_u\rangle = \langle\Phi_v\rangle$ and $\langle\Phi_w\rangle$ are given by Eq. (5.14b), and $d_{ij} = d_{ji}$ are the elements of the constitutive matrix [D] of Eq. (5.18). The edge displacements have to be calculated from the global joint displacements by applying the simple transformation

$$\{u_i\}_n = [A]\{U_i\}_n \tag{5.44}$$

to be substituted into Eq. (5.43). The final internal forces are then accumulated as the sum of the harmonic contributions,

$$\{\sigma\} = \sum_{n=1}^{\infty}\{\sigma\}_n \tag{5.45}$$

Figure 5.7 defines the sign convention for internal forces and moments.

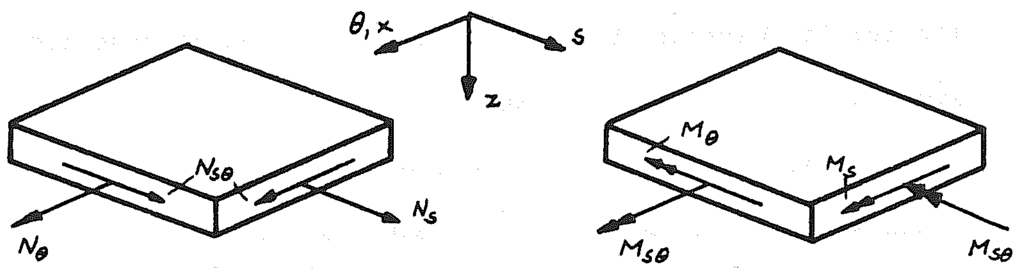

Fig. 5.7 Sign Convention For Internal Forces And Moments

5.5 Description of Program CURSTR

A computer program called CURSTR has been written in FORTRAN IV language by means of which it is possible to analyze very efficiently prismatic folded plate structures curved in plan and simply supported along their straight radial edges. A detailed program description is given in Ref. [5.41].

The dimensioning of the arrays has been kept variable so that structures of almost any practical size may be analyzed. Each plate may have material properties described by the general law, Eq. (5.18). The loading may consist of surface loads which vary linearly across the width of an element and are constant over a specified portion of the circumferential length of the element, as well as joint loads which may also extend uniformly over the whole length of a joint or over a specified fraction of it.

If all applied loads are symmetric about the midspan section, a program option may suppress all even terms of the Fourier series. Similarly, for antisymmetric loadings, all odd harmonics may be suppressed. For a complete axisymmetric shell subjected to axisymmetric loading, the Fourier analysis degenerates such that only the zero'th harmonic term survives. This special case has also been incorporated into the program.

Another option enables the user to print out not only the final results after all harmonic contributions have been summed but also results after any partial sum of harmonics has been accumulated. This option is useful to study the convergence of various output quantities.

For most structures, in particular bridge structures, it is often very useful to compare the known statical moment at some section due to the applied loads with the gross internal resisting moment as a check. This gross moment may be calculated as the sum of individual girder moments which in turn are calculated by multiplying the longitudinal stress resultants with the respective distance to the neutral axis and then integrating these differential moments over the girder areas. Wherever longitudinal plate bending moments also contribute to these moments, they are taken into account.

Output, then, consists of the final displacements of all joints in the structure; internal stress resultants, moments and element displacements for each curved strip element at as many transverse sections and intermediate harmonics as specified by the user; gross resisting moment of each individual girder as well as the percentage of this moment compared to the statical moment contributed by all girders at any specified section; and finally, computer execution time for each completed problem.

Computing times for the execution of small structures amount to only a few seconds on the CDC 6400 of the Berkeley Computer Center of the University of California, and all of the examples studied so far required far less than one minute of central processing time.

5.6 Examples

5.6.1 Straight Beam and Square Plate

The simply supported straight beam of Fig. 5.8 has been analyzed by program CURSTR for uniformly distributed load and a concentrated midspan load, using a radius of curvature R = 10 000' and θ_o = 0.01 Rad. Table 5.1 lists the results together with those from elementary beam theory as well as the closed form elasticity solution [10.1] (program MULTPL)

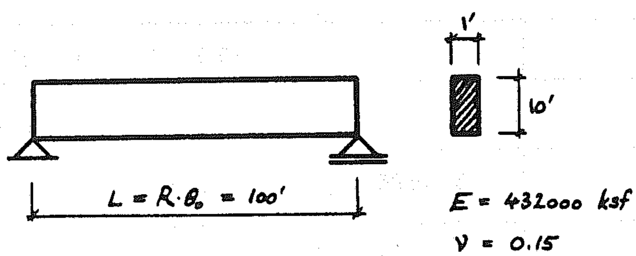

Fig. 5.8 Example 1 - Simply Supported Straight Beam

and the straight finite strip theory [10.4] (program MULSTR). In studying the effect of mesh refinement on the curved strip results, one recognizes the convergence towards the elasticity solution. In particular, the stress concentration under the concentrated load is approached rapidly, but the gross internal moment does not change with mesh refinement. Elementary beam theory, of course, does not include the stress concentration, but the deflection check is in fair agreement.

Figure 5.9 shows the midspan moments of a square plate due to a concentrated load placed at the plate center and expressed by 50 non-zero terms of the respective Fourier series. The plate is in all cases simply supported along two opposite edges, and the boundary conditions

TABLE 5.1. RESULTS FOR SIMPLY SUPPORTED STRAIGHT BEAM

LOADING	METHOD	NO. OF STRIPS	MIDSPAN DEFLECTION ($ft \times 10^{-2}$)	MAX. STRESS RESULTANT N_x (lb/ft)	MIDSPAN MOMENT (ft-lb)
Uniform Load q=1.0 (5 non-zero harm.)	Beam Theory		3.6169	-75.00	1250.0
	MULTPL	2	3.6928	-75.27	1250.9
	MULSTR	2	3.6626	-75.46	1250.6
	CURSTR	1	3.6043	-75.04	1250.6
		2	3.6648	-75.46	1250.6
		5	3.6895	-75.50	1250.6
Conc. Midspan Load P=1 (50 non-zero harmonics)	Beam Theory		.05787	-1.500	25.00
	MULTPL	2	.05943	-1.876	25.23
	MULSTR	2	.05881	-1.556	24.90
	CURSTR	1	.05793	-1.494	24.90
		2	.05884	-1.577	24.90
		5	.05928	-1.820	24.90

for the other two edges are a) free, b) simply supported, and c) fixed. Radius of curvature is taken as R = 10 000', and θ_o = .001 Rad. As can be seen, CURSTR results based on an idealization with 10 strips agree very well with the closed form solution of program MULTPL, except right under the load. However, M_x- values agree surprisingly well even there, in spite of the large stress gradients. The disagreement between the MULTPL results for M_x and M_y under the load in case b) where they should be equal, stems from the fact that even 50 non-zero harmonics are not sufficient to describe the sharp peak of the moment curve more accurately.

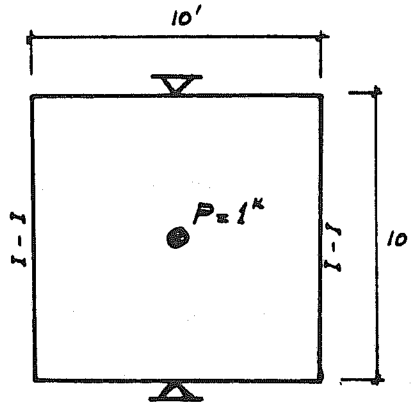

Case	Boundary Conditions for Edges I - I	
a	Free	(FR)
b	Simply Supported	(SS)
c	Fixed	(FX)

$E = 432000$ ksf
$\nu = 0.15$
$t = 0.5$ ft

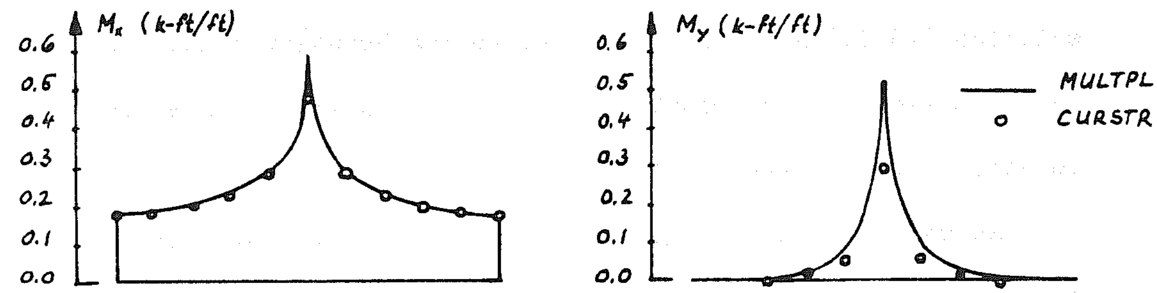

a) SS - SS - FR - FR Plate

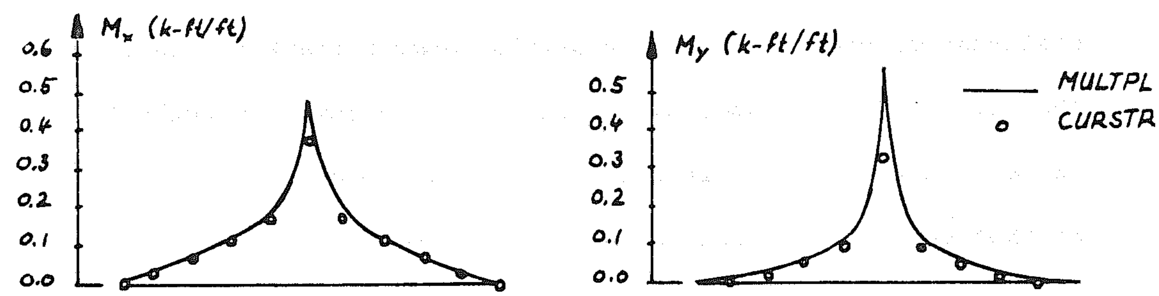

b) SS - SS - SS - SS Plate

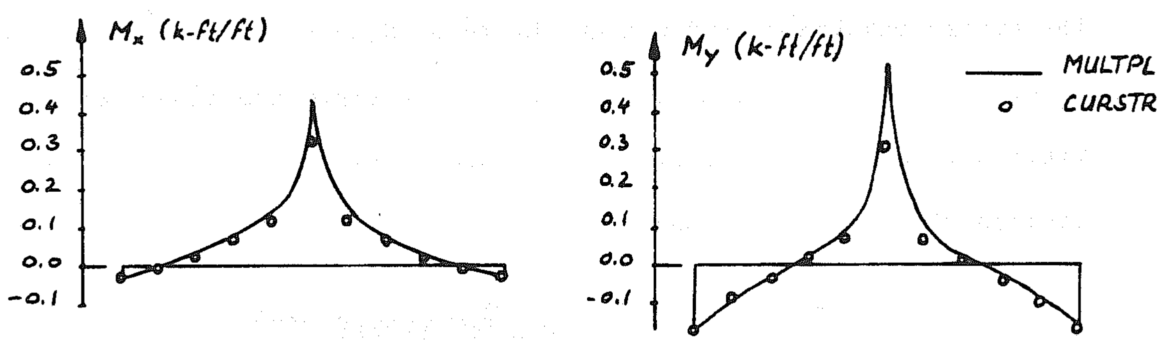

c) SS - SS - FX - FX Plate

Fig. 5.9 Example 2 - Midspan Moments of Square Plate

5.6.2 Axisymmetric Shells

The following two examples illustrate the degeneration of the curved strip theory for a shell of revolution under axisymmetric loading. The cylinder of Fig. 5.10a is fixed at the bottom and subjected to a uniform radial load at the free top edge. It was analyzed with program CURSTR using the four mesh representations indicated in Fig. 5.10a. For comparison, the free constants of Flügge's closed form solution [10.21] have been adjusted to the boundary conditions of this problem, and the resulting displacements and moments are shown in Fig. 5.10 as "exact" solution.

As can be seen in Fig. 5.10, CURSTR displacements agree very well with the closed form solution, even for the coarse mesh A. Also the bending moment check is excellent throughout the region of the edge disturbance, except for the unbalanced moment right at the free edge. The curved strip method, of course, is an approximate analysis technique. In particular, it does not satisfy force boundary conditions so that unbalanced force quantities at free edges as well as inter-element stress discontinuities exist. While these inter-element stress discontinuities can to a large extent be easily overcome by averaging the stress resultants and moments between adjacent elements, unbalanced forces at free edges can be reduced only by employing finer meshes. Table 5.2 shows how rapidly the unbalanced moment of example 3 decreases with mesh refinement.

TABLE 5.2. UNBALANCED MOMENT (IN-LB/IN.) AT FREE EDGE OF CYLINDER

Mesh	A	B	C	D	Theoretical
Unbalanced Moment	.053814	.022330	.007458	.002126	.000000

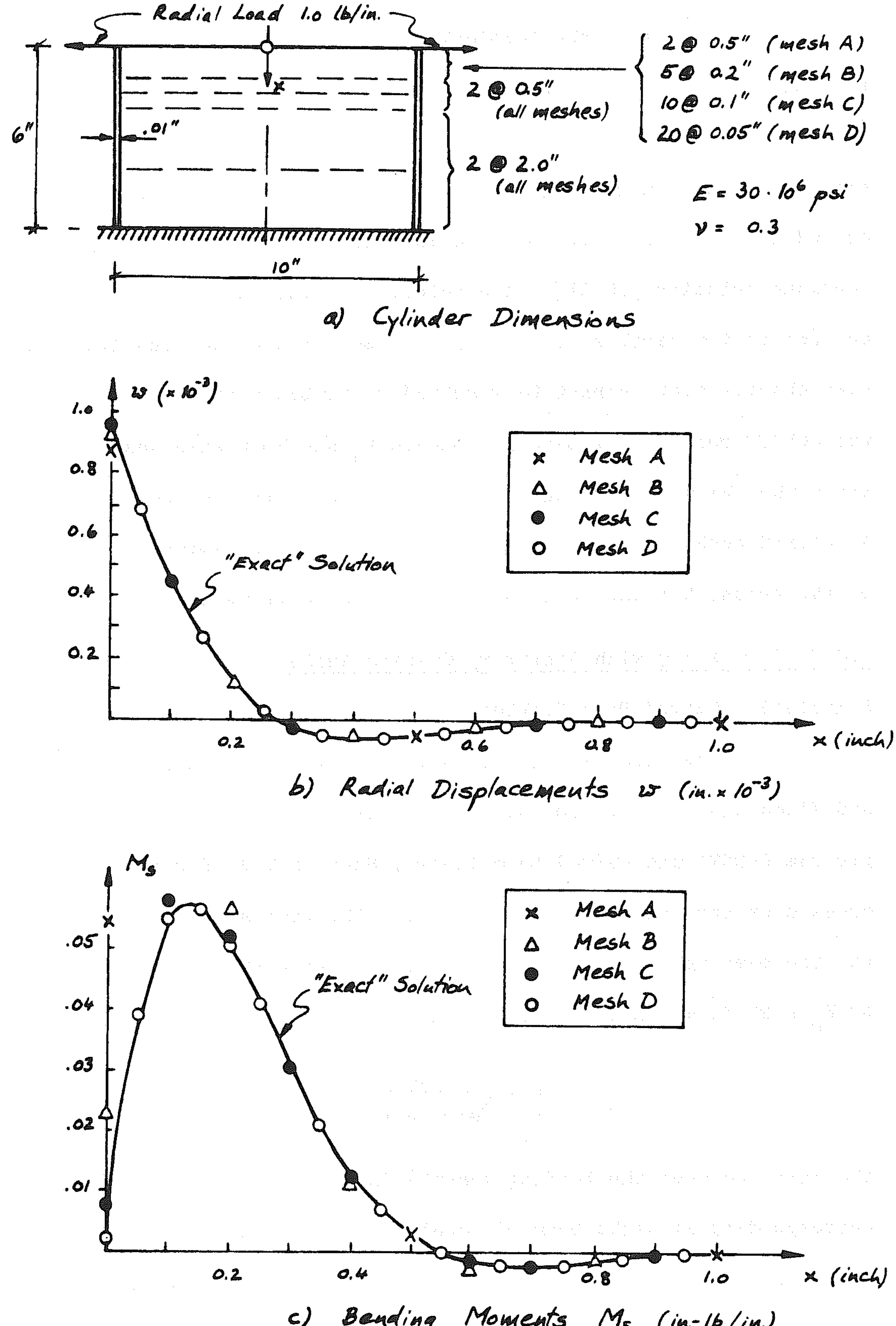

Fig. 5.10 Example 3 - Bending of a Cylinder

Example No. 4 is the toroidal shell of Fig. 5.11, subjected to internal pressure, and analyzed by program CURSTR, using 18 elements to represent half of the torus. Because it is very difficult to obtain a closed form bending solution for this problem [10.23], the curved strip results are compared in Fig. 5.11 only with Flügge's membrane solution [10.21]. The deformation incompatibilities at the top and bottom circles, $\beta = 0$ and $\beta = 180°$, where the Gaussian curvature changes sign, cannot be resolved by membrane stresses alone, and the CURSTR results for bending moments M_s and hoop stresses N_θ illustrate what kind of bending action is necessary to restore continuity. A refined mesh was also studied, with 72 elements representing half of the torus, but the results shown in Fig. 5.11 were hardly changed.

5.6.3 Structures with Arbitrary Opening Angle

Example 5 - Curved Beam Problem

The curved beam of Fig. 5.12a is at both ends simply supported and fixed against rotation about its axis and has been analyzed by program CURSTR and curved beam theory, Section 5.3, for the four cross sections depicted in Fig. 5.12a. The radius of curvature R and the opening angle θ_o are variable such that the span remains $R \cdot \theta_o = 20$ ft = const. Denoting with

$$\rho = \frac{M_{curved}}{M_{straight}} \tag{5.46}$$

the ratio between the bending moments in a curved beam and in the corresponding straight beam of equal span length $L = R \cdot \theta_o$, curved beam theory predicts an increase of this ratio with growing curvature. This increase is illustrated in Fig. 5.12b for the midspan

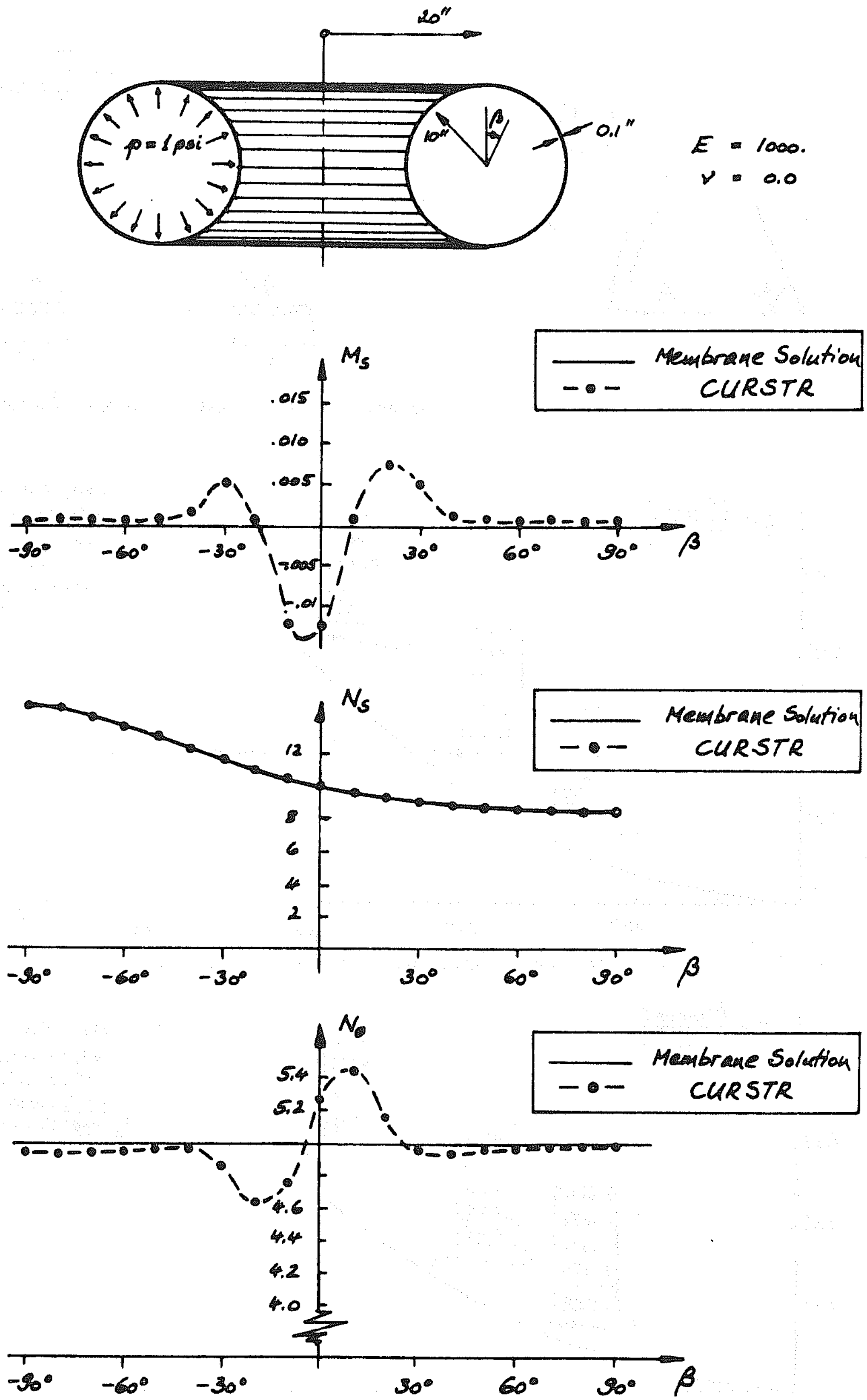

Fig. 5.11 Example 4 - Torus With Internal Pressure

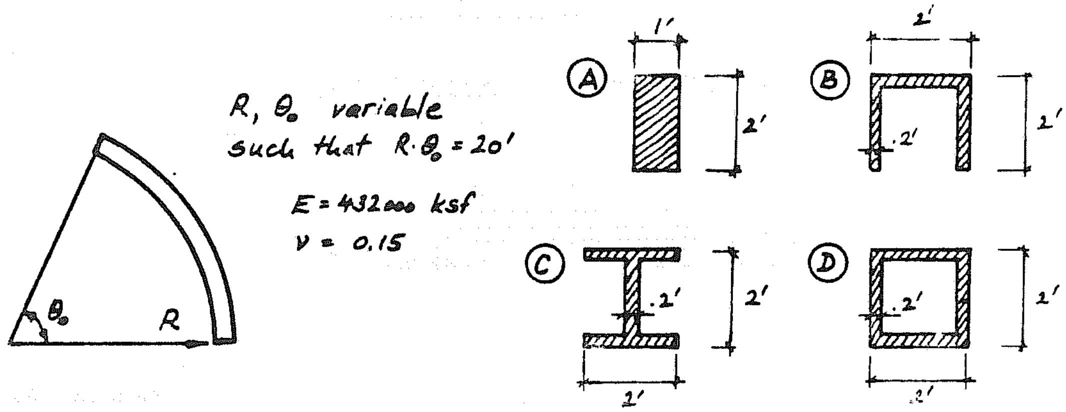

a) Curved Beam Dimensions and Cross Section Types

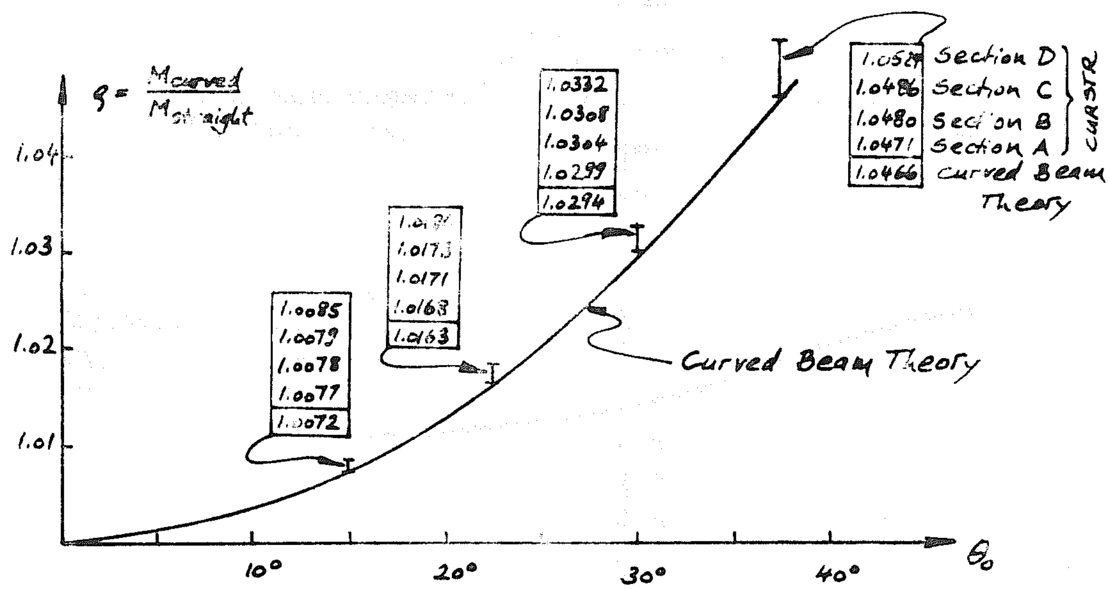

b) Moment Variation for Uniform Load

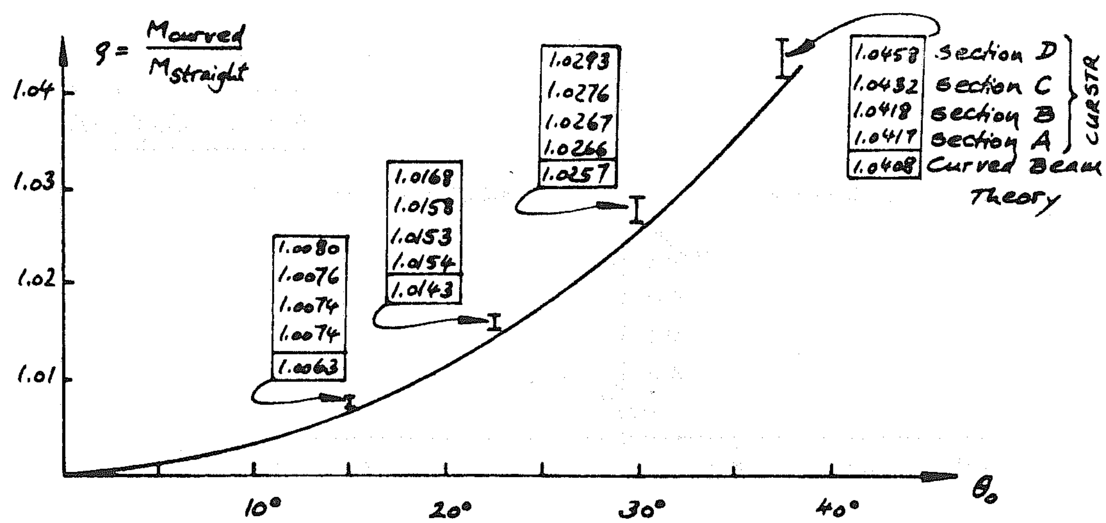

c) Moment Variation for Concentrated Load

Fig. 5.12 Example 5 - Curved Beam Problem moment due to uniform load, and in Fig. 5.12c for the moment one foot away from a concentrated midspan load, because right under a concentrated load, the moment curve is discontinuous, and too many Fourier series terms would be required to adequately represent that value.

The main importance of Fig. 5.12 is that it shows that even an opening angle of 30° increases the midspan moment by at most only 3%. In the light of this observation, the differences between the CURSTR results for the four cross sections are clearly negligible, although it is interesting to note the consistent moment increase for channel, I-beam and box sections, in that order, while results for the solid beam, section A, are almost identical with curved beam results.

Example 6 - Curved Plate Problem

The curved plate of Fig. 5.13a is simply supported along the straight edges and free at the curved boundaries. It has been analyzed for various opening angles θ_o (such that the span length $L = R\theta_o$ remained constant) using program CURSTR. The results are compared with those obtained from the closed form solution of the plate equation for this special boundary value problem, Section 3.5.

Figure 5.14 illustrates the effect of curvature on the statical midspan moment as well as on the longitudinal plate bending moments M_θ at midspan of the two edges. Defining the ρ-ratio as in the previous example, Eq. (5.46), its variation with θ_o plotted in Fig. 5.14 reveals several interesting facts. For a unit load placed at point A, the statical moment decreases with increasing θ_o because the actual length of the loaded interior edge is reduced with increasing θ_o.

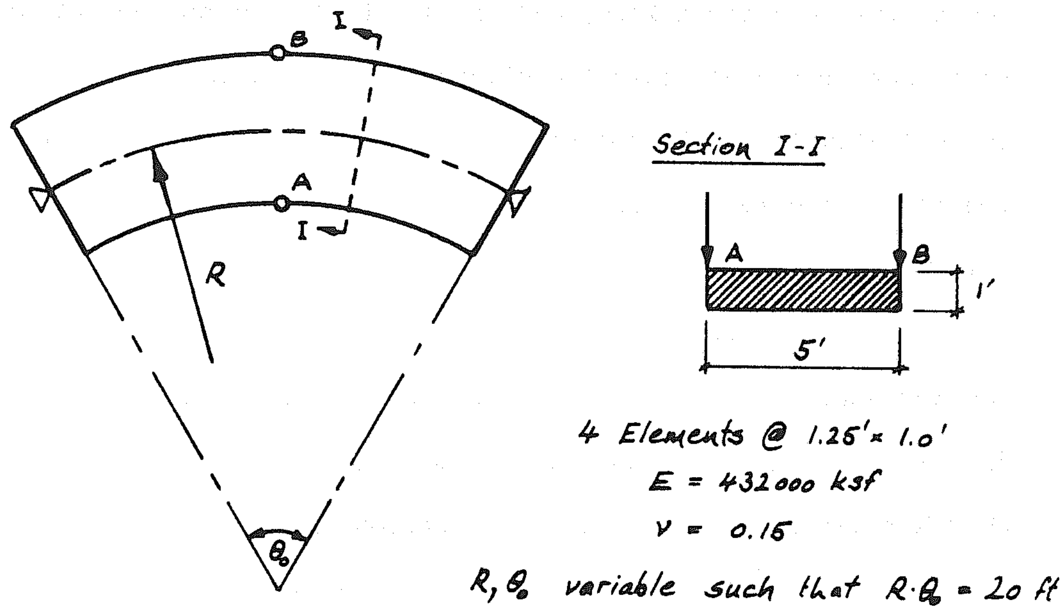

a) Notations for Simply Supported Curved Plate

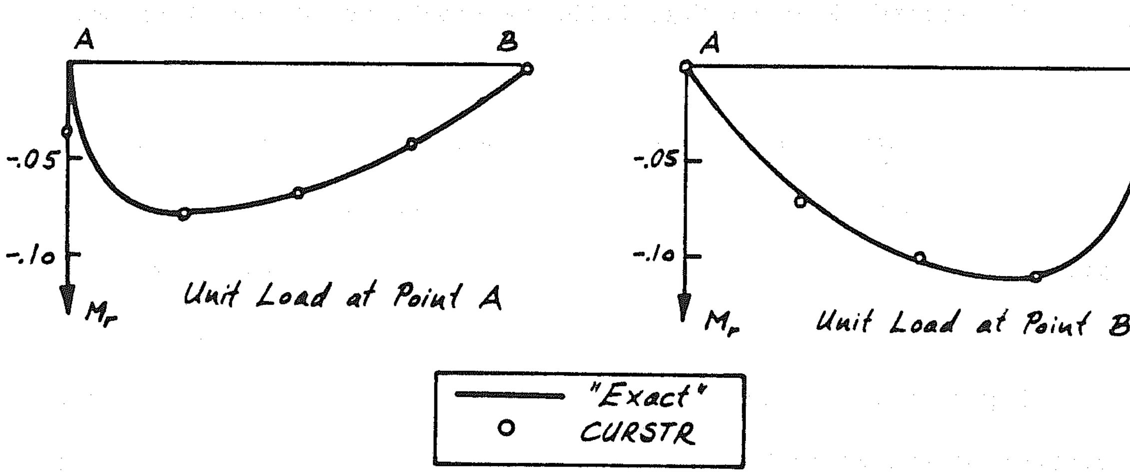

b) Transverse Bending Moments M_r (ft-k/ft) at Midspan
(for θ_o = 30°)

Fig. 5.13 Example 6 - Curved Plate Problem

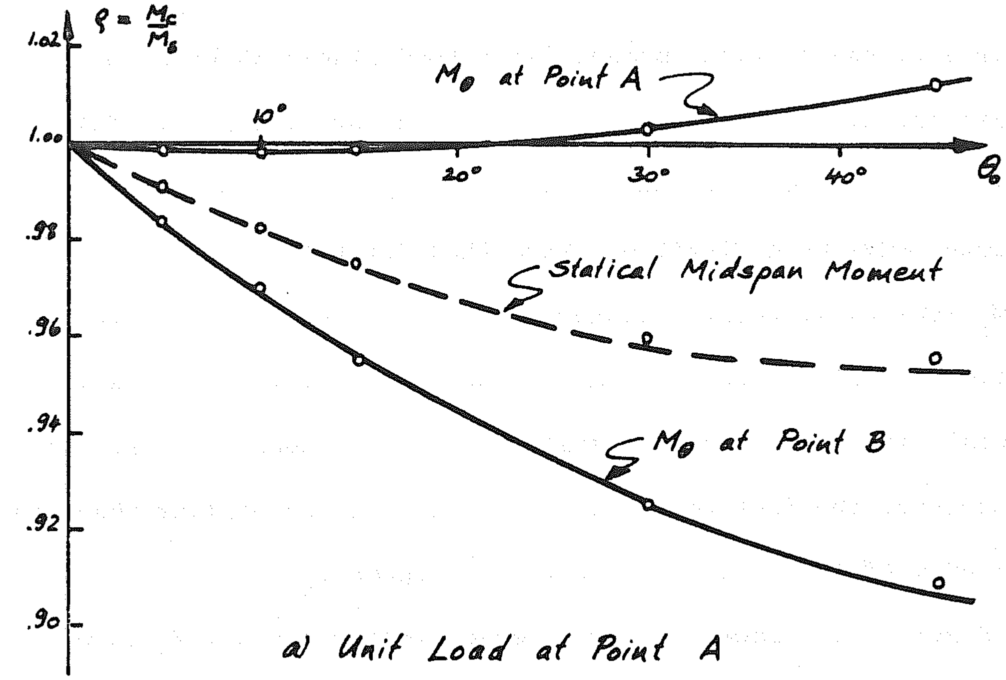

a) Unit Load at Point A

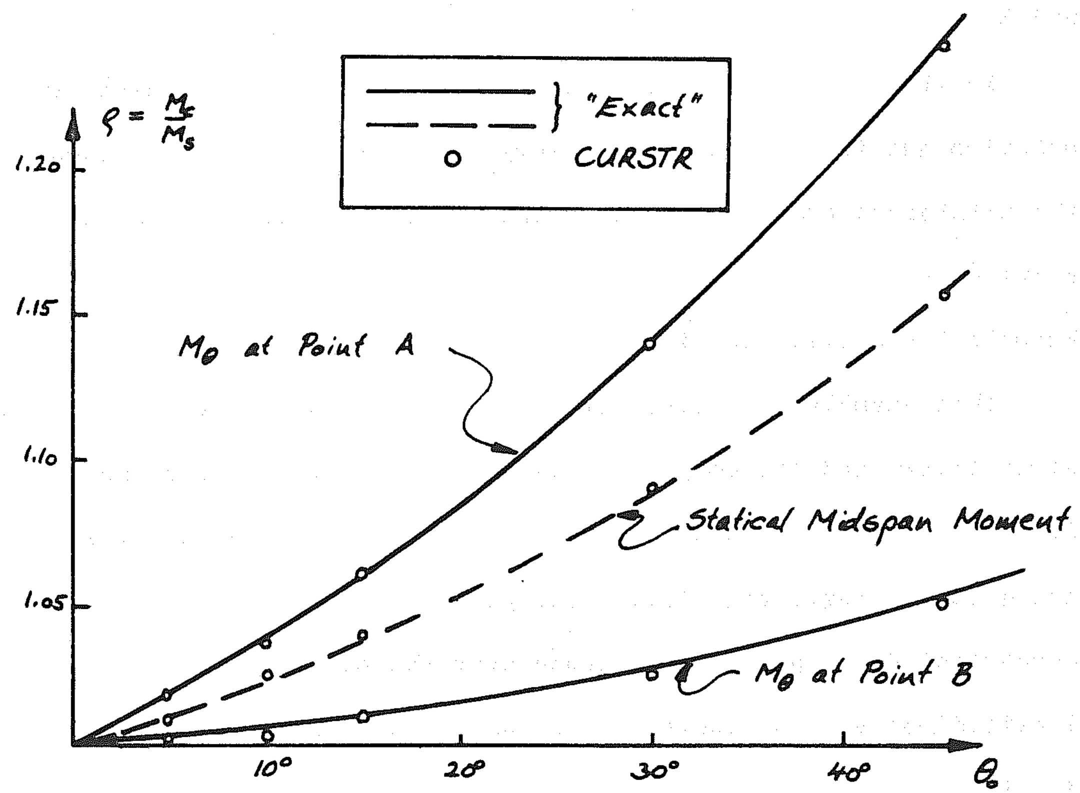

b) Unit Load at Point B

Fig. 5.14 Effect of Curvature on Longitudinal Moments M_θ of Plate

Conversely, the statical moment for a load placed at point B increases because the outer edge becomes longer with increasing θ_o. With increasing curvature, the inner edge of the plate becomes stiffer and the outer edge more flexible. Note that for both load positions the M_θ moments at point A (inner edge) and B (outer edge) are respectively greater than and smaller than the average moment across the width represented by the statical midspan moment curves. This corroborates the fact that the inner edge becomes stiffer than the outer edge of the plate for increasing angles θ_o.

Figure 5.13b shows the transverse bending moments M_r at midspan for an opening angle of $\theta_o = 30°$, with unit loads placed at point A and B.

In all cases, the excellent agreement between the elasticity solution and the curved strip theory is to be noted. The reason for the unbalanced moment M_r at the loaded edge has been discussed previously.

Example 7 - Curved Box Girder

This example, finally, illustrates the versatility of the curved strip theory and the computer program CURSTR, by studying the influence of superelevation on the state of stress in a curved single-box girder bridge, Fig. 5.15. The girder is subjected to a single concentrated 1 kip load at midspan over the outer web. The change in longitudinal stress resultants N_θ and transverse bending moments M_r is almost entirely due to the horizontal component of the unit load which is assumed to act normal to the deck of the superelevated box. As a consequence, the box is subjected to a small bending moment about its vertical axis so that compression stresses are superimposed

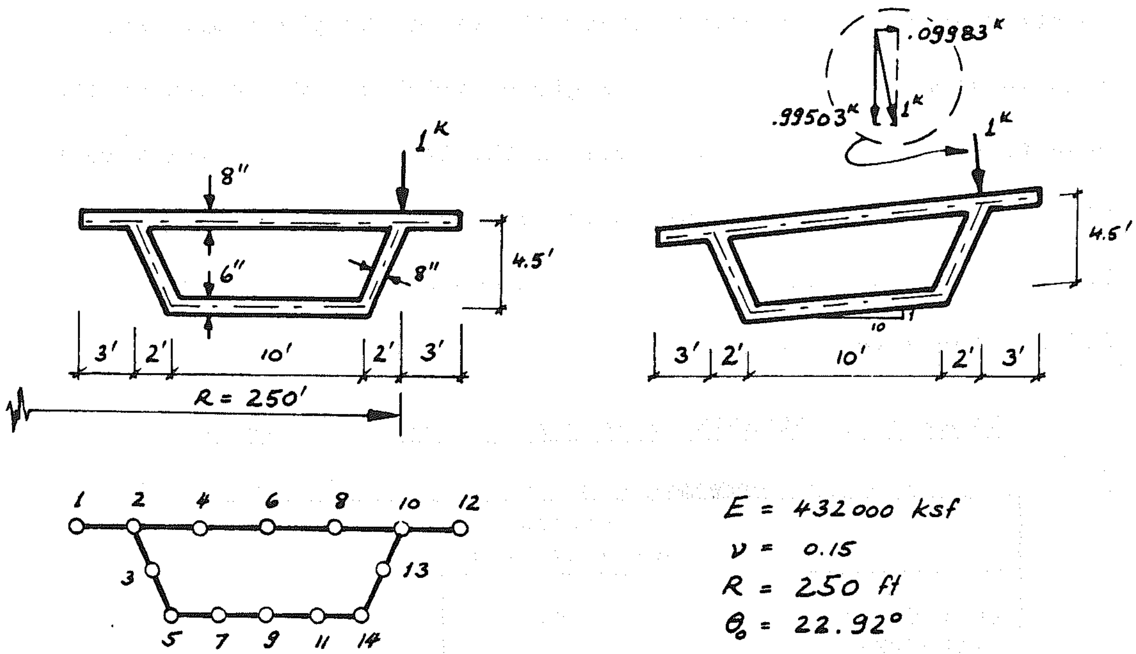

a) Dimensions and Mesh Layout for Plane and Superelevated Box Girder

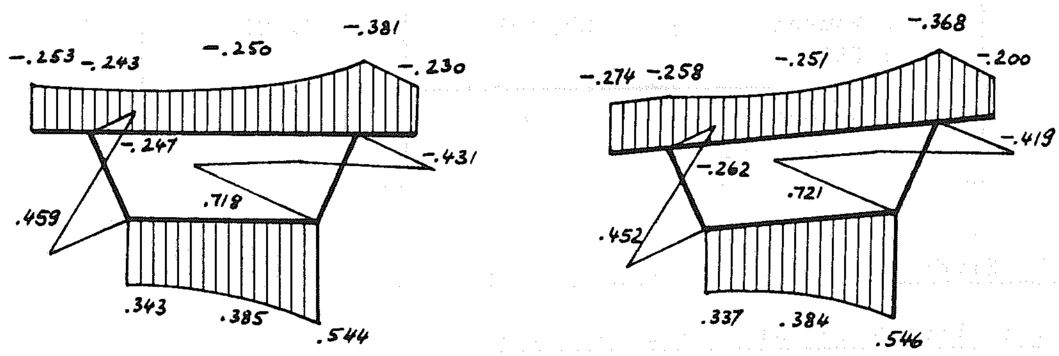

b) N_θ - Stress Resultants at Midspan (k/ft)

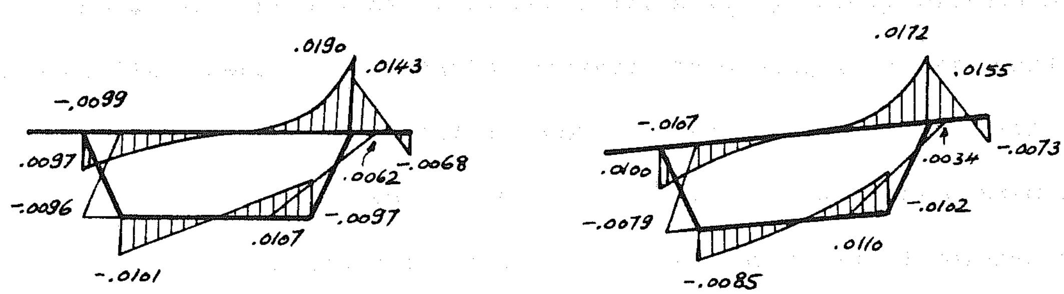

c) M_r - Transverse Bending Moments at Midspan (k-ft/ft)

Fig. 5.15 Example 7 - Curved Box Girder

to stresses in the interior girder (left) of the plane box, and tensile stresses in the exterior girder (right). One check on the results can be obtained by comparing the internal resisting moment with the statical moment due to the applied load, calculated on the basis of curved beam theory. These moments are summarized in Table 5.3 and the agreement is excellent.

TABLE 5.3. MOMENTS (FT-KIPS) IN CURVED BOX GIRDER

	Box Without Superelevation	Box With Superelevation
Left Girder (CURSTR)	10.894	11.013
Right Girder (CURSTR)	14.186	14.198
Total Moment (CURSTR)	25.080	25.211
Total Moment (Curved Beam Th.)	25.081	25.189

5.7 Study of Strain-Displacement Relations

5.7.1 Remark on Thin Shell Theories

The strain-displacement relations, Eq. (5.16) are due to Novozhilov [10.22]. If a different shell theory had been used, other strain-displacement equations might replace them. All so-called thin-shell theories have in common is that they approximate the three-dimensional elastic continuum (which the shell actually is) by a two-dimensional system because this is more amenable to analytical treatment. However, this approximation usually involves assumptions which will in most cases lead to certain inconsistencies or inaccuracies. The consideration of higher-order theories will often have some advantages but is seldom justified for ordinary shell problems.

It is the objective of this subchapter to compare the results based on Flügge's theory [10.21] with those obtained using Novozhilov's thin shell theory [10.22]. In fact, most authors studying shells of revolution by the finite element method [10.10] [10.11] [10.13] have used Novozhilov's equations. It therefore seemed to be of interest to investigate if there was any rationale behind this seemingly tacit agreement.

In his discussion of shells of revolution, Flügge derived two sets of strain-displacement equations. Simplifying these for the conical shell, one has

$$\begin{aligned}
\varepsilon_s &= \frac{\partial v}{\partial s} - \frac{\partial^2 w}{\partial s^2} z \\
\varepsilon_\theta &= \frac{\partial u}{r\partial\theta} + \frac{\cot\varphi}{r_2 + z} v - \frac{1}{r\sin\varphi}\frac{\partial^2 w}{\partial\theta^2}\frac{z}{r_2+z} - \cot\varphi\frac{\partial w}{\partial s}\frac{z}{r_2+z} + \frac{w}{r_2+z} \\
2\varepsilon_{s\theta} &= \frac{r_2+z}{r_2}\frac{\partial u}{\partial s} - \frac{r_2+z}{r_2^2}\cot\varphi\cdot u + \frac{1}{\sin\varphi}\frac{1}{r_2+z}\frac{\partial v}{\partial\theta} - \frac{z}{\sin\varphi}\left(\frac{1}{r_2+z} + \frac{1}{r_2}\right)\frac{\partial^2 w}{\partial s\,\partial\theta} + \cot\varphi\left(\frac{z}{r_2+z} + \frac{z}{r_2}\right)\frac{\partial w}{r\partial\theta}
\end{aligned} \tag{5.47}$$

and

$$\begin{aligned}
\varepsilon_s &= \frac{\partial v}{\partial s} - \frac{\partial^2 w}{\partial s^2} z \\
\varepsilon_\theta &= \frac{\partial u}{r\partial\theta} + \frac{\cos\varphi}{r} v - \frac{\partial^2 w}{r^2\partial\theta^2} z - \frac{\cos\varphi}{r}\frac{\partial w}{\partial s} z + \frac{\sin\varphi}{r} w \\
2\varepsilon_{s\theta} &= \frac{\partial u}{\partial s} - \frac{\cos\varphi}{r} u + \frac{\partial v}{r\partial\theta} - 2\frac{\partial^2 w}{r\partial s\partial\theta} z + \frac{2\cos\varphi}{r^2}\frac{\partial w}{\partial\theta} z
\end{aligned} \tag{5.48}$$

All differences between Eqs. (5.47) and (5.48) are due to the one assumption that z (or thickness t) is negligibly small compared to $r_2 = r/\sin\varphi$, Fig. 5.16.

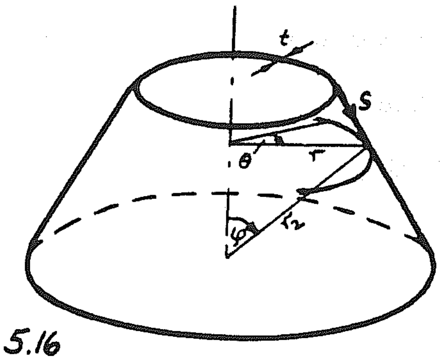

Fig. 5.16
Notations for Conical Shell

The force-displacement equations resulting from these two sets of equations are as follows.

$$
\begin{array}{rcl|l}
N_s &=& D\left[\frac{\partial v}{\partial s} + \nu\left(\frac{\partial u}{r\partial\theta} + \frac{\cos\varphi}{r}v + \frac{\sin\varphi}{r}w\right)\right] & - K\frac{\sin\varphi}{r}\frac{\partial^2 w}{\partial s^2} \\
N_\theta &=& D\left[\left(\frac{\partial u}{r\partial\theta} + \frac{\cos\varphi}{r}v + \frac{\sin\varphi}{r}w\right) + \nu\frac{\partial v}{\partial s}\right] & - K\frac{\sin\varphi}{r}\left[\frac{\sin\varphi\cos\varphi}{r^2}v + \frac{\sin^2\varphi}{r^2}w + \frac{\partial^2 w}{r^2\partial\theta^2} + \frac{\partial w}{\partial s}\frac{\cos\varphi}{r}\right] \\
N_{s\theta} &=& D\frac{1-\nu}{2}\left[\frac{\partial u}{\partial s} + \frac{\partial v}{r\partial\theta} - \frac{\cos\varphi}{r}u\right] & + K\frac{1-\nu}{2}\frac{\sin\varphi}{r}\left[\frac{\sin\varphi}{r}\frac{\partial u}{\partial s} + \frac{\sin\varphi\cos\varphi}{r^2}u - \frac{\partial^2 w}{r\partial s\partial\theta} + \frac{\cos\varphi}{r^2}\frac{\partial w}{\partial\theta}\right] \\
N_{\theta s} &=& D\frac{1-\nu}{2}\left[\frac{\partial u}{\partial s} + \frac{\partial v}{r\partial\theta} - \frac{\cos\varphi}{r}u\right] & + K\frac{1-\nu}{2}\frac{\sin\varphi}{r}\left[\frac{\sin\varphi}{r^2}\frac{\partial v}{\partial\theta} + \frac{\partial^2 w}{r\partial s\partial\theta} - \frac{\cos\varphi}{r^2}\frac{\partial w}{\partial\theta}\right] \\
M_s &=& K\left[\frac{\partial^2 w}{\partial s^2} + \nu\left(\frac{\partial^2 w}{r^2\partial\theta^2} + \frac{\cos\varphi}{r}\frac{\partial w}{\partial s}\right)\right] & + K\frac{\sin\varphi}{r}\left[-\frac{\partial v}{\partial s} - \nu\frac{\partial u}{r\partial\theta}\right] \\
M_\theta &=& K\left[\left(\frac{\partial^2 w}{r^2\partial\theta^2} + \frac{\cos\varphi}{r}\frac{\partial w}{\partial s}\right) + \nu\frac{\partial^2 w}{\partial s^2}\right] & + K\frac{\sin\varphi}{r}\left[-\frac{\sin\varphi}{r}w - \frac{\cos\varphi}{r}v\right] \\
M_{s\theta} &=& K\frac{1-\nu}{2}\left[2\frac{\partial^2 w}{r\partial s\partial\theta} - 2\frac{\cos\varphi}{r^2}\frac{\partial w}{\partial\theta}\right] & + K\frac{1-\nu}{2}\frac{\sin\varphi}{r}\left[-2\frac{\partial u}{\partial s} + 2\frac{\cos\varphi}{r}u\right] \\
M_{\theta s} &=& K\frac{1-\nu}{2}\left[2\frac{\partial^2 w}{r\partial s\partial\theta} - 2\frac{\cos\varphi}{r^2}\frac{\partial w}{\partial\theta}\right] & + K\frac{1-\nu}{2}\frac{\sin\varphi}{r}\left[-\frac{\partial v}{r\partial\theta} - \frac{\partial u}{\partial s} + \frac{\cos\varphi}{r}u\right]
\end{array}
\tag{5.49}
$$

with

$$D = \frac{Et}{1-\nu^2}\,, \qquad K = \frac{Et^3}{12(1-\nu^2)} = D\frac{t^2}{12}$$

All contributions to the right of the dashed line are due to the higher order terms of Eq. (5.47). With the simplifying assumptions

$$\nu = 0\,, \qquad N_{s\theta} = N_{\theta s}\,, \qquad M_{s\theta} = M_{\theta s}$$

it is possible to write Eq. (5.49) in the form

$$\{\sigma\} = [D]\{\varepsilon\}$$

where [D] is given by Eq. (5.18a) with $\nu = 0$, and the strain vector is

$$\begin{Bmatrix} \varepsilon_s \\ \varepsilon_\theta \\ 2\varepsilon_{s\theta} \\ \kappa_s \\ \kappa_\theta \\ 2\kappa_{s\theta} \end{Bmatrix} = \left\{ \begin{array}{c|l} \dfrac{\partial v}{\partial s} & -\dfrac{\sin\varphi}{r}\dfrac{t^2}{12}\dfrac{\partial^2 w}{\partial s^2} \\ \dfrac{\partial u}{r\partial\theta} + \dfrac{\cos\varphi}{r}v + \dfrac{\sin\varphi}{r}w & -\dfrac{\sin\varphi}{r}\dfrac{t^2}{12}\left(\dfrac{\sin\varphi\cos\varphi}{r^2}v + \dfrac{\sin^2\varphi}{r^2}w + \dfrac{\partial^2 w}{r^2\partial\theta^2} + \dfrac{\cos\varphi}{r}\dfrac{\partial w}{\partial s}\right) \\ \dfrac{\partial u}{\partial s} + \dfrac{\partial v}{r\partial\theta} - \dfrac{\cos\varphi}{r}u & +\dfrac{\sin\varphi}{r}\dfrac{t^2}{12}\left(\dfrac{\sin\varphi}{r}\dfrac{\partial u}{\partial s} + \dfrac{\sin\varphi\cos\varphi}{r^2}u - \dfrac{\partial^2 w}{r\partial s\partial\theta} + \dfrac{\cos\varphi}{r^2}\dfrac{\partial w}{\partial\theta}\right) \\ \dfrac{\partial^2 w}{\partial s^2} & -\dfrac{\sin\varphi}{r}\dfrac{\partial v}{\partial s} \\ \dfrac{\partial^2 w}{r^2\partial\theta^2} + \dfrac{\cos\varphi}{r}\dfrac{\partial w}{\partial s} & -\dfrac{\sin\varphi}{r}\left(\dfrac{\sin\varphi}{r}w + \dfrac{\cos\varphi}{r}v\right) \\ 2\dfrac{\partial^2 w}{r\partial s\partial\theta} - 2\dfrac{\cos\varphi}{r^2}\dfrac{\partial w}{\partial\theta} & -2\dfrac{\sin\varphi}{r}\left(\dfrac{\partial u}{\partial s} - \dfrac{\cos\varphi}{r}u\right) \end{array} \right\} \tag{5.50}$$

where the terms on the left of the dashed line form the strain vector of the simplified theory based on Eq. (5.48) while the higher-order theory of Eq. (5.47) requires in addition the terms on the right of the dashed line.

Substituting the displacement functions (5.14a) into Eq. (5.50) and carrying out the triple product under the integral of Eq. (5.22), lengthy expressions for the stiffness coefficients are obtained which can be simplified by suppressing terms whenever at^2/r^2 appears beside 1, with constant "a" usually involving the angle φ. The expressions obtained are as follows.

$$[k]_n = D\,\frac{\theta_0 s_{12}}{4}\int_{-1}^{1}\begin{bmatrix} \bar{k}_{uu} & \bar{k}_{uv} & \bar{k}_{uw} \\ & \bar{k}_{vv} & \bar{k}_{vw} \\ (\text{symm.}) & & \bar{k}_{ww} \end{bmatrix} r\,d\eta \tag{5.51}$$

with

$$\bar{k}_{uu} = \left[\left(\frac{n\pi}{\theta_0}\right)^2 + \frac{\cos^2\varphi}{2}\right]\frac{\phi_u^T\phi_u}{r^2} + \frac{1}{2}\phi_u'^T\phi_u' - \frac{1}{2}\frac{\cos\varphi}{r}\left(\phi_u'^T\phi_u + \phi_u^T\phi_u'\right)$$

$$\bar{k}_{uv} = -\frac{3}{2}\cos\varphi\left(\frac{n\pi}{\theta_0}\right)\frac{\phi_u^T\phi_u}{r^2} + \frac{1}{2}\left(\frac{n\pi}{\theta_0}\right)\frac{\phi_u'^T\phi_u}{r} \tag{5.51a-c}$$

$$\bar{k}_{uw} = -\left(\frac{n\pi}{\theta_0}\right)\frac{\sin\varphi}{r}\left[1 + \left(\frac{n\pi}{\theta_0}\right)^2\frac{t^2}{12r^2}\right]\frac{\phi_u^T\phi_w}{r} + \underline{\left(\frac{n\pi}{\theta_0}\right)\frac{\sin\varphi}{12}\frac{t^2}{r^2}\left[\frac{\cos\varphi}{r}\left(\frac{7}{2}\phi_u^T\phi_w' + \frac{5}{2}\phi_u'^T\phi_w\right) - \frac{5}{2}\phi_u'^T\phi_w'\right]}$$

$$\bar{k}_{vv} = \phi_u'^T\phi_u' + [\cos^2\varphi + \tfrac{1}{2}(\tfrac{n\pi}{\theta_0})^2]\,\frac{\phi_u^T\phi_u}{r^2}$$

$$\bar{k}_{vw} = \frac{\sin\varphi\cos\varphi}{r^2}\phi_u^T\phi_w + \underline{\frac{\sin\varphi\cos\varphi}{r^2}\cdot\frac{5}{2}\frac{t^2}{12r^2}(\tfrac{n\pi}{\theta_0})^2\phi_u^T\phi_w - \frac{\sin\varphi}{r}\frac{t^2}{12r^2}[2\cos^2\varphi + \tfrac{1}{2}(\tfrac{n\pi}{\theta_0})^2]\phi_u^T\phi_w' - \frac{\sin\varphi}{6}\frac{t^2}{r}\phi_u'^T\phi_w''}$$

$$\begin{aligned}\bar{k}_{ww} = {} & [\frac{\sin^2\varphi}{r^2} + \frac{t^2}{12r^4}(\tfrac{n\pi}{\theta_0})^2(4\sin^2\varphi + (\tfrac{n\pi}{\theta_0})^2 + 2\cos^2\varphi)]\phi_w^T\phi_w - 3\cos\varphi\frac{t^2}{12r^3}(\tfrac{n\pi}{\theta_0})^2(\phi_w'^T\phi_w + \phi_w^T\phi_w') \\ & + [\cos^2\varphi + 2(\tfrac{n\pi}{\theta_0})^2]\frac{t^2}{12r^2}\phi_w'^T\phi_w' + \frac{t^2}{12}\phi_w''^T\phi_w'' - \underline{2\frac{\sin^2\varphi\cos\varphi}{r}\frac{t^2}{12r^2}(\phi_w'^T\phi_w + \phi_w^T\phi_w')}\end{aligned} \tag{5.51d-f}$$

The underlined contributions are due to the higher order terms of Eq. (5.50).

By comparing Eq. (5.50) with (5.16), one recognizes that Novozhilov's and Flügge's simplified theory lead to almost identical strain-displacement equations, except for three terms. It is the objective of this section to study qualitatively the importance of Flügge's higher-order terms as well as to investigate the effect of the three terms in Novozhilov's theory which are not included in Flügge's simplified theory. However, it will be helpful to discuss briefly the significance of eigenvalues and rigid body modes of a conical shell element, before proceeding to numerical studies on the element level, and on the structural level thereafter.

3.7.2 Eigenvalues and Rigid Body Modes

Physically, an eigenvalue of an element stiffness matrix can be interpreted as the energy stored in the element while it is deformed in the associated mode shape. A mode of deformation in which no energy is stored, is called a rigid body mode.

For a complete conical shell element, there are four rigid body displacement configurations possible, Fig. 5.17. In order to obtain all four of them, the complete expansion of displacements has to be

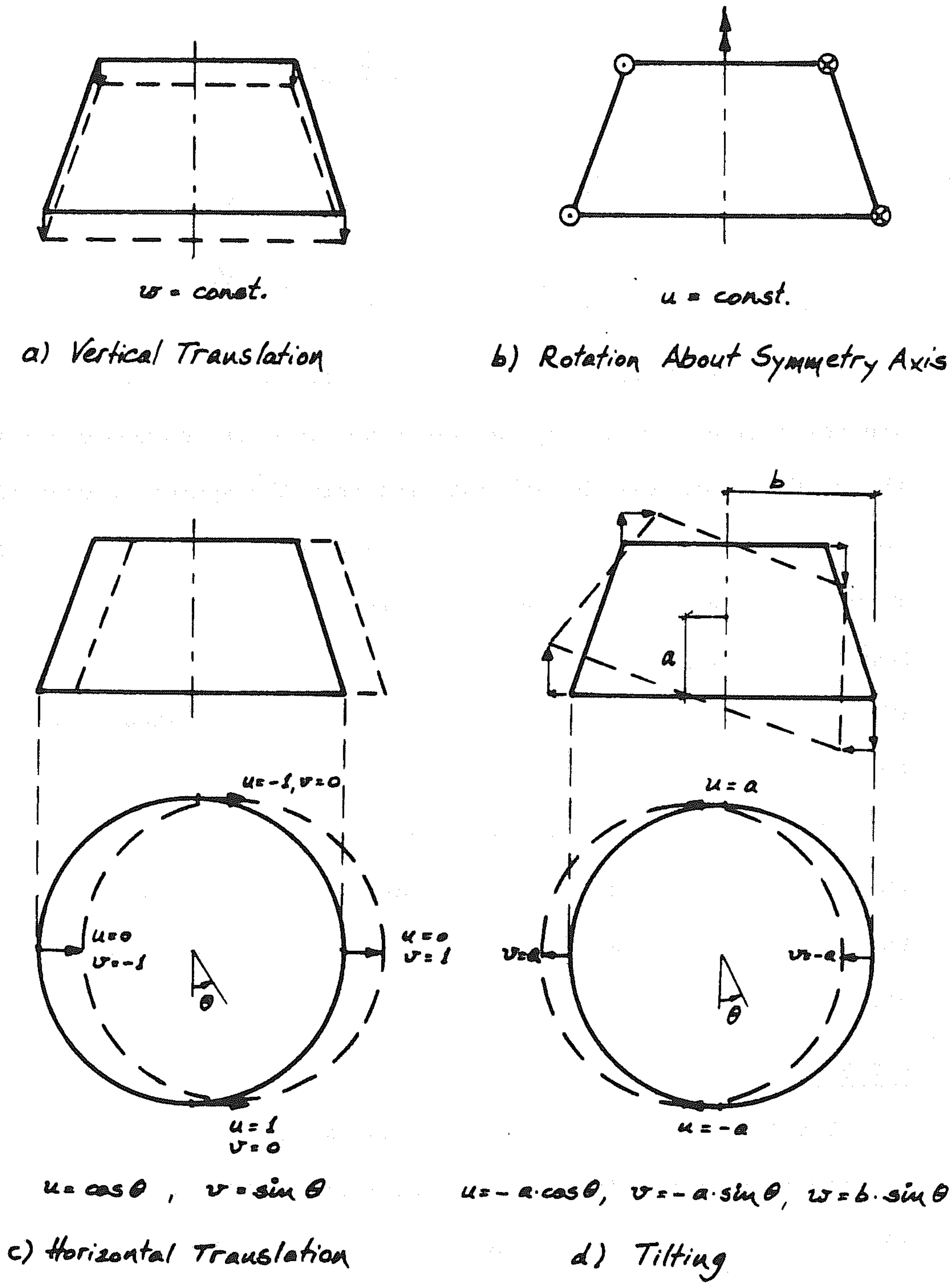

Fig. 5.17 Rigid Body Modes of Conical Shell Element

used,

$$\begin{aligned} u &= \sum_{n=0}^{\infty} u_n' \cos\frac{n\pi\theta}{\theta_o} + \sum_{n=1}^{\infty} u_n'' \sin\frac{n\pi\theta}{\theta_o} \\ v &= \sum_{n=1}^{\infty} v_n' \sin\frac{n\pi\theta}{\theta_o} + \sum_{n=0}^{\infty} v_n'' \cos\frac{n\pi\theta}{\theta_o} \\ w &= \sum_{n=1}^{\infty} w_n' \sin\frac{n\pi\theta}{\theta_o} + \sum_{n=0}^{\infty} w_n'' \cos\frac{n\pi\theta}{\theta_o} \end{aligned} \tag{5.52}$$

This expansion shows that the first two rigid body modes of Fig. 5.17 are associated with n = 0, and the other two with harmonic n = 1. Although the expansion (5.14a) contains only the symmetric part of Eq. (5.52), all four rigid body modes should be present in our stiffness formulation because the constant terms of the w-expansion which leads to the only rigid body mode contained in the antisymmetric part of Eq. (5.52) is automatically absorbed in the stiffness formulation of Eq. (5.23).

Finally, the ratio between the absolute values of the largest and smallest non-zero eigenvalue of a matrix, which is called the condition number, is of interest because it provides information about the stability properties of a matrix, [10.24].

5.7.3 Studies on Element Level

The first objective of these studies was a numerical comparison between element stiffnesses based on Flügge's higher-order theory, Eq. (5.47), and his simplified theory, Eq. (5.48). In analyzing a conical shell element with an r/t-ratio of order 10, it was found that many higher-order terms contributed almost nothing to the final stiffness coefficients. For an r/t-ratio of about 40, the contributions of the remaining higher-order terms were also found to be small. But the final stiffness coefficients were often formed as differences of large numbers, thus upgrading the importance of small additional contributions. Based on this finding it was decided to study in some detail the effect of the three terms in Novozhilov's equations, see Eq. (5.16),

$$
\begin{Bmatrix} \varepsilon_s \\ \varepsilon_\theta \\ 2\varepsilon_{s\theta} \\ \kappa_s \\ \kappa_\theta \\ 2\kappa_{s\theta} \end{Bmatrix}
=
\begin{Bmatrix}
\dfrac{\partial v}{\partial s} \\[2mm]
\dfrac{\partial u}{r\partial\theta} + \dfrac{\cos\varphi}{r} v + \dfrac{\sin\varphi}{r} w \\[2mm]
\dfrac{\partial u}{\partial s} - \dfrac{\cos\varphi}{r} u + \dfrac{\partial v}{r\partial\theta} \\[2mm]
-\dfrac{\partial^2 w}{\partial s^2} \\[2mm]
\overbrace{\dfrac{\sin\varphi}{r^2}\dfrac{\partial u}{\partial\theta}}^{1} - \dfrac{\partial^2 w}{r^2\partial\theta^2} - \dfrac{\cos\varphi}{r}\dfrac{\partial w}{\partial s} \\[2mm]
\overbrace{2\dfrac{\sin\varphi}{r}\dfrac{\partial u}{\partial s}}^{2} - \underbrace{2\dfrac{\sin\varphi\cos\varphi}{r^2} u}_{3} - \dfrac{2}{r}\dfrac{\partial^2 w}{\partial s\partial\theta} + 2\dfrac{\cos\varphi}{r^2}\dfrac{\partial w}{\partial\theta}
\end{Bmatrix}
\tag{5.53}
$$

which are not present in Flügge's first-order strain vector (5.50), and which have been labelled in Eq. (5.53) for identification. In the final element stiffness of Eq. (5.23), only submatrices $\bar{k}_{uu}$ and $\bar{k}_{uw}$ are affected by these terms, namely

$$
\begin{aligned}
\bar{k}_{uu} = {} & \left[d_{22}\left(\frac{n\pi}{\theta_0}\right)^2 + d_{33}\cos^2\varphi\right]\frac{\phi_u^T\phi_u}{r^2} + \underline{\sin^2\varphi\Big[\overbrace{d_{55}\left(\frac{n\pi}{\theta_0}\right)^2}^{1} + \overbrace{4d_{66}\cos^2\varphi}^{3}\Big]\frac{\phi_u^T\phi_u}{r^4}} - d_{33}\frac{\cos\varphi}{r}(\phi_u'^T\phi_u + \phi_u^T\phi_u') \\
& \underbrace{-4d_{66}\frac{\sin^2\varphi\cos\varphi}{r^3}(\phi_u'^T\phi_u + \phi_u^T\phi_u')}_{2\,3} + d_{33}\phi_u'^T\phi_u' + \underbrace{4d_{66}\frac{\sin^2\varphi}{r^2}\phi_u'^T\phi_u'}_{2}
\end{aligned}
\tag{5.54}
$$

$$
\begin{aligned}
\bar{k}_{uw} = {} & -\sin\varphi\left(\frac{n\pi}{\theta_0}\right)\frac{d_{22}}{r^2}\phi_u^T\phi_w - \underline{\sin\varphi\left(\frac{n\pi}{\theta_0}\right)\Big[\overbrace{d_{55}\left(\frac{n\pi}{\theta_0}\right)^2}^{1} + \overbrace{4d_{66}\cos^2\varphi}^{3}\Big]\frac{\phi_u^T\phi_w}{r^4}} + \underline{\frac{\sin\varphi\cos\varphi}{r^3}\left(\frac{n\pi}{\theta_0}\right)(\overbrace{d_{55}}^{1} + \overbrace{4d_{66}}^{3})\phi_u^T\phi_w'} \\
& + \underbrace{\sin\varphi\left(\frac{n\pi}{\theta_0}\right)\frac{d_{45}}{r^2}\phi_u^T\phi_w''}_{1} + \underbrace{4d_{66}\frac{\sin\varphi\cos\varphi}{r^3}\left(\frac{n\pi}{\theta_0}\right)\phi_u'^T\phi_w}_{2} - \underbrace{\frac{\sin\varphi}{r^2}\left(\frac{n\pi}{\theta_0}\right)4d_{66}\phi_u'^T\phi_w'}_{2}
\end{aligned}
$$

where the underlined contributions are due to the term with the corresponding number label.

In selecting elements for comparison it should be noted that all three terms under consideration have the multiplier $\sin\varphi$ and would drop out automatically for a circular plate element, Fig. 5.18a.

The actual effect which the suppression of any one of those terms on the element stiffness matrix has, can be studied by comparing the eigenvalues of the respective stiffness matrices. These have been summarized in Table 5.4 for the cylinder and cone of Fig. 5.18. In studying Table 5.4, the following observations can be made.

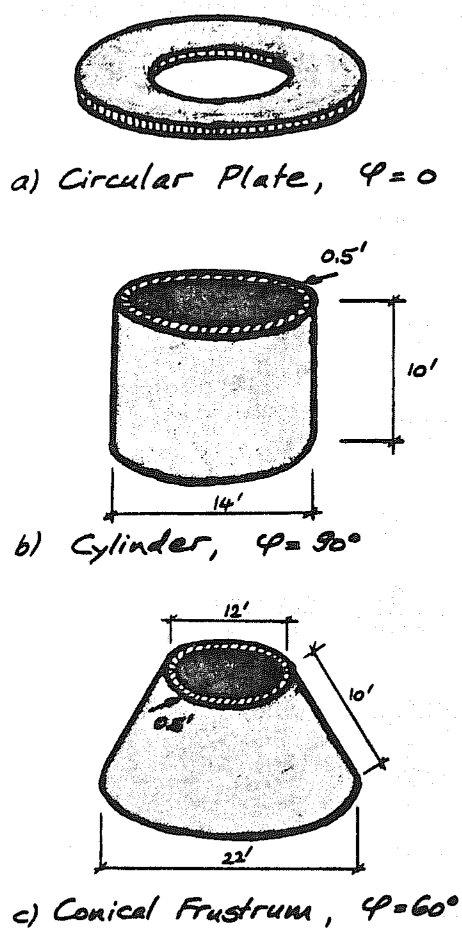

Fig. 5.18 Shell Elements

1. The third term in Eq. (5.53) has no influence on the cylinder stiffness because of its multiplier $\cos\varphi$.
2. The first six eigenvalues are only slightly affected by suppressing any one of the three terms. But this influence will increase for higher harmonics because of the multipliers n, n^2, and n^4, Eq. (5.54).
3. In retaining all three terms of Eq. (5.53), all four rigid body modes mentioned earlier are preserved. However, the suppression of any one of the three terms may lead to the loss of at least

TABLE 5.4 EIGENVALUES OF SHELL ELEMENTS

	Harmonic Number n	Term Dropped	$1/10^{10}$	$2/10^{10}$	$3/10^{9}$	$4/10^{9}$	$5/10^{8}$	$6/10^{8}$	7	8
Cylinder, Fig. 5.18b	0	None	.239429	.090540	.533139	.366013	.741506	.470693	$.2659 \cdot 10^{-6}$	$-.5749 \cdot 10^{-5}$
		1	.239429	.090540	.533139	.366013	.741506	.470693	$.2659 \cdot 10^{-6}$	$-.5749 \cdot 10^{-5}$
		2	.239429	.090540	.533139	.365391	.741506	.470693	$-.1459 \cdot 10^{-5}$	$-.4526 \cdot 10^{-5}$
		3	.239429	.090540	.533139	.366013	.741506	.470693	$.2659 \cdot 10^{-6}$	$-.5749 \cdot 10^{-5}$
	1	None	.288006	.097282	.871913	.386907	1.24347	.571699	$-.3061 \cdot 10^{-5}$	$-.1583 \cdot 10^{-4}$
		1	.287928	.097277	.871255	.387333	1.24833	.573078	$.1121 \cdot 10^{6}$	$.1805 \cdot 10^{5}$
		2	.288006	.097282	.871175	.387033	1.24347	.570048	$.1547 \cdot 10^{6}$	$-.9943 \cdot 10^{-5}$
		3	.288006	.097282	.871913	.386907	1.24347	.571699	$-.4198 \cdot 10^{-5}$	$-.1434 \cdot 10^{-4}$
	2	None	.441233	.165589	1.16871	.661836	2.16535	1.08736	$.1577 \cdot 10^{7}$	$.1447 \cdot 10^{7}$
		1	.440741	.165440	1.16852	.661505	2.19549	1.09902	$.2769 \cdot 10^{7}$	$.1797 \cdot 10^{7}$
		2	.441233	.165492	1.16871	.661696	2.16535	1.08463	$.2212 \cdot 10^{7}$	$.1577 \cdot 10^{7}$
		3	.441233	.165589	1.16871	.661836	2.16535	1.08736	$.1577 \cdot 10^{7}$	$.1447 \cdot 10^{7}$
Cone Frustrum, Fig. 5.18c	0	None	.179546	.106026	.497241	.350319	.643625	.377502	$.1431 \cdot 10^{-4}$	$-.3602 \cdot 10^{-5}$
		1	.179546	.106026	.497241	.350319	.643625	.377502	$.1431 \cdot 10^{-4}$	$-.3602 \cdot 10^{-5}$
		2	.179546	.106026	.496764	.350319	.643625	.377502	$.3149 \cdot 10^{5}$	$.1512 \cdot 10^{-4}$
		3	.179546	.106026	.497105	.350319	.643625	.377502	$.3147 \cdot 10^{5}$	$.8604 \cdot 10^{-5}$
	1	None	.219880	.126860	.716889	.313907	.910735	.463385	$-.4370 \cdot 10^{-5}$	$-.1943 \cdot 10^{-4}$
		1	.219840	.126845	.716611	.314147	.914076	.463778	$.5798 \cdot 10^{5}$	$.4903 \cdot 10^{4}$
		2	.219878	.126846	.716513	.313988	.911151	.462536	$.6287 \cdot 10^{5}$	$-.1218 \cdot 10^{-4}$
		3	.219884	.126860	.716718	.313899	.911157	.463158	$.2025 \cdot 10^{5}$	$.1780 \cdot 10^{4}$
	2	None	.356935	.176147	1.07798	.470403	1.55682	.976404	$.2288 \cdot 10^{7}$	$.5958 \cdot 10^{6}$
		1	.356678	.176103	1.07748	.470048	1.57300	.983263	$.3028 \cdot 10^{7}$	$.7910 \cdot 10^{6}$
		2	.356926	.176111	1.07780	.470228	1.55722	.974283	$.2691 \cdot 10^{7}$	$.7182 \cdot 10^{6}$
		3	.356942	.176140	1.07786	.470430	1.55624	.975483	$.2455 \cdot 10^{7}$	$.5616 \cdot 10^{6}$

Shaded numbers are zero eigenvalues.

one rigid body mode. The third term, for example, suppresses three rigid body modes of the cone.

4. As for the condition number which is to be understood as the ratio of the largest to the smallest non-zero eigenvalue, the orders of magnitude are small, and the suppression of none of the three terms changes this ratio considerably.
5. As can be seen from Eq. (5.54) or (5.23), all contributions due to the three terms under consideration decrease more or less rapidly with increasing radius. In fact, in rerunning the above examples with mean radii increased by factor 100, it was found that the influence of the three terms on the first six eigenvalues was seldom felt in the sixth significant figure, while "zero" eigenvalues were by order 10^4 or more smaller than given in Table 5.4.

The above observations lead to the conclusion that the two different shell theories discussed may eventually lead to different results. It will be the objective of the studies on the structural level to investigate the actual degree of the discrepancy.

5.7.4 Studies on Structural Level

In order to assess the actual importance of the three additional terms in Novozhilov's strain-displacement relations of Eq. (5.53), a variety of test examples have been studied, some results of which are summarized in Table 5.5. The example is the curved beam of Fig. 5.12a with variable curvature such that the actual span length along the arc remains constant 20 feet. In addition to the four cross-section types of Fig. 5.12a, the sections of Fig. 5.19 have been analyzed also. The internal resisting moments listed in Table 5.5 have been obtained by integrating longitudinal stress resultants N_θ

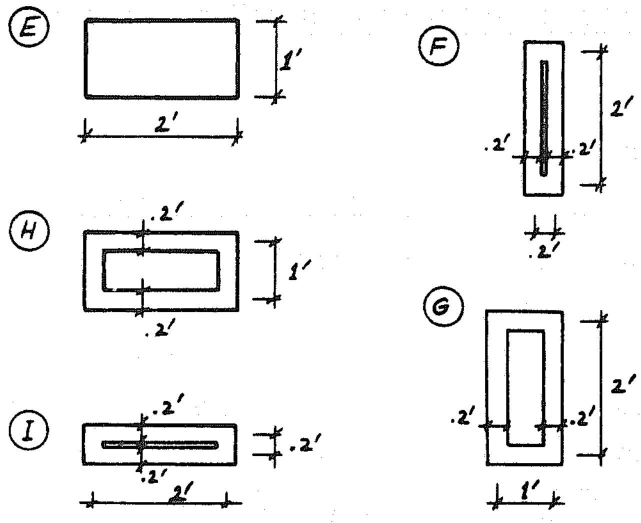

(Cross Sections A,B,C,D see Fig. 5.12a)

Fig. 5.19 Additional Curved Beam Sections for Comparison of Shell Theories

as described in Section 5.5.

In studying the results of Table 5.5, the following observations can be made.

1. Since all terms under consideration decrease with growing curvature radius, Eq. (5.54), both shell theories converge towards each other as well as towards the straight finite strip formulation, as has been shown in Section 5.3. For R = 20,000 ft. and $\theta_o = .0573° \approx 0$, therefore, the results based on Novozhilov's and Flügge's simplified theory are practically identical.

2. As the curved beam theory indicates, the statical midspan moment increases with curvature. While this behavior is very well represented by the curved strip analysis based on Novozhilov's theory for the solid beam section A, Fig. 5.12a, the results of Flügge's theory virtually remain constant at the midspan moment of the equivalent straight beam. For large curvatures, the discrepancy might be appreciable. Although deflections according to Flügge's theory do increase with curvature, the rate of this increase is far too low.

TABLE 5.5 COMPARISON BETWEEN NOVOZHILOV'S AND FLÜGGE'S THEORY

Cross Section Type	θ_o	No. of Strips	Midspan Moment			Midspan Deflection X ft/10^{-2}	
			Beam Theory	Novozhilov	Flügge	Novozhilov	Flügge
A	≈ 0°	2	50.000	50.024	50.024	.73252	.73252
A	15°	2	50.359	50.384	50.024	.75435	.74406
A	30°	2	51.469	51.493	50.024	.82319	.77868
A	45°	2	53.428	53.452	50.025	.95014	.83639
A	90°	2	67.150	67.175	50.025	2.03266	1.14799
E	90°	1	67.150	67.318	67.318	5.91987	5.91987
B	≈ 0°	3	50.000	50.024	50.024	.92726	.92726
B	45°	3	53.428	53.518	51.981	4.17679	3.94468
B	90°	3	67.150	67.555	56.120	26.22461	18.68155
B	90°	12	67.150	67.587	56.118	26.30997	18.73175
C	≈ 0°	5	50.000	50.024	50.024	.58652	.58652
C	45°	5	53.428	53.562	52.887	3.20511	3.13114
C	90°	5	67.150	67.722	62.938	16.85551	14.84996
C	90°	12	67.150	67.260	62.521	16.91540	14.89676
F	90°	4	67.150	67.593	60.593	14.71497	12.16201
F	90°	10	67.150	67.206	60.256	14.79501	12.22125
G	90°	4	67.150	67.740	66.755	2.49613	2.44067
G	90°	12	67.150	67.309	66.335	2.51123	2.45528
D	90°	4	67.150	68.043	67.477	1.47193	1.45352
D	90°	16	67.150	68.045	67.477	1.48365	1.46506
H	90°	4	67.150	67.626	66.945	4.88982	4.82237
H	90°	12	67.150	67.596	66.914	4.93291	4.86484
I	90°	4	67.150	67.595	65.559	92.01084	88.52158
I	90°	10	67.150	67.589	65.549	92.69715	89.18390

3. Because all three terms establishing the difference between Flügge's and Novozhilov's theories have the multiplier $\sin\varphi$, both theories yield identical results for the curved plate, section E.

4. It follows from the last two observations that the behavior of beams composed of horizontal and vertical plates will fall somewhere in between the two extremes just considered. Because the vertical webs of the channel, section B, carry an appreciable amount of the load, Flügge's theory compares poorly with curved beam theory. But in the I-beam section C, the horizontal flanges constitute the essential load-carrying components, and therefore the comparison is much more favorable.

5. The response of a box beam is largely governed by its high torsional stiffness for which a general estimate is given by Bredt's formula,

$$J = \frac{4A^2}{\oint \frac{ds}{t}} \tag{5.55}$$

while open sections can resist torsional moments only by non-uniform shearing stress distribution within each plate making up the cross section, as well as by torsion bending. The excellent agreement between the two shell theories for the square box, section D, suggests that the three terms do not affect the torsional rigidity of a closed section.

6. If the box section becomes narrower, sections G and F, then Bredt's stiffness of Eq. (5.55) decreases rapidly, and the behavior of the box will approach that of a vertical plate element, with Flügge's theory worsening. If the box becomes flatter, sections H and I, Bredt's stiffness also decreases, but the box behavior will approach

that of a horizontal plate, with Flügge's theory comparing very well.

7. Refinements of the mesh representation of the beam sections have very little influence on the results, and the discrepancies between the two shell theories are hardly affected.

From the preceding comparative studies the following conclusions may be drawn.

1. Basing the curved strip theory on Flügge's simplified strain-displacement equations (5.48) leads to some reduction in storage requirements and execution time for the computer program, because various contributions to the curved strip stiffness matrix do not have to be calculated. However, compared with the overall computational effort, the element stiffness calculations do not require much time anyway.

2. The three terms not present in Flügge's simplified theory are essential in describing the torsional rigidity of a vertical curved plate element. Although the associated error decreases in built-up cross sections, in particular for cellular sections, no general statement can be made regarding the accuracy of Flügge's theory for open and closed sections.

3. Concluding this discussion, it is recommended that the three terms in Novozhilov's strain-displacement equations (5.53) be retained for curved strip analyses, as most investigators working in the field of finite element analysis of rotational shells in fact do.

5.8 Study of Quadratic In-Plane Displacement Functions

5.8.1 Element Stiffness and Consistent Load Vector

The accuracy of results based on an approximate theory such as the curved strip method of analysis, can be improved in two ways. Firstly, the structural idealization may be refined by discretizing the structure using a larger number of curved strip elements, i.e., increasing the number of joints. Secondly, one may refine the element model itself, i.e., increasing the number of degrees of freedom of each element so that the accuracy of the results is improved without increasing the number of elements or joints.

In this section, the second approach will be illustrated by improving the relatively crude approximation of in-plane displacements, Eq. (5.14). In order to obtain a quadratic variation, a new joint o is introduced halfway between joints 1 and 2, having two degrees of freedom as shown in Fig. 5.20. These additional degrees of freedom are easily added into the previously derived element stiffness, if they are understood as deviations from linearity, Fig. 5.20b. Accordingly, the displacement functions (5.14) will now be written as

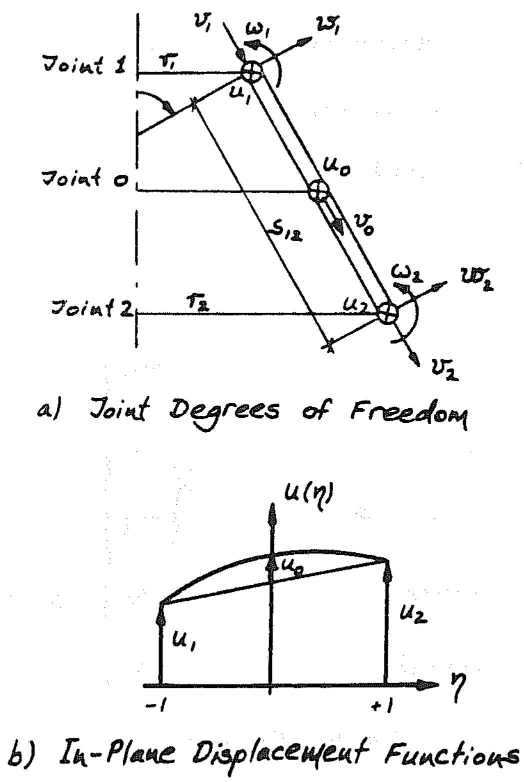

Fig. 5.20 Curved Strip Element with Quadratic In-Plane Displacement Functions

$$\begin{Bmatrix} u(\eta,\theta) \\ v(\eta,\theta) \\ w(\eta,\theta) \end{Bmatrix} = \sum_{n=1}^{\infty} \begin{bmatrix} \phi_u(\eta)\cos\frac{n\pi\theta}{\theta_0} & 0 & 0 \\ 0 & \phi_v(\eta)\sin\frac{n\pi\theta}{\theta_0} & 0 \\ 0 & 0 & \phi_w(\eta)\sin\frac{n\pi\theta}{\theta_0} \end{bmatrix} \begin{Bmatrix} u_i \\ v_i \\ w_i \end{Bmatrix}_n \tag{5.56}$$

where

$$\langle\phi_u(\eta)\rangle = \langle\phi_v(\eta)\rangle = \frac{1}{2}\langle (1-\eta) \quad (1+\eta) \quad 2(1-\eta^2)\rangle$$

and

$$\langle\phi_w(\eta)\rangle = \frac{1}{4}\langle(2-3\eta+\eta^3) \quad (2+3\eta-\eta^3) \quad \frac{s_{12}}{2}(1-\eta-\eta^2+\eta^3) \quad \frac{s_{12}}{2}(-1-\eta+\eta^2+\eta^3)\rangle \tag{5.56a}$$

$$\{u_i\}_n = \begin{Bmatrix} u_1 \\ u_2 \\ u_0 \end{Bmatrix}_n \qquad \{v_i\}_n = \begin{Bmatrix} v_1 \\ v_2 \\ v_0 \end{Bmatrix}_n \qquad \{w_i\}_n = \begin{Bmatrix} w_1 \\ w_2 \\ \omega_1 \\ \omega_2 \end{Bmatrix}_n \tag{5.56b}$$

The final element stiffness is again calculated according to Eq. (5.23), except that the new vectors Φ_u and Φ_u' have to be substituted, so that the stiffness will be a 10X10 matrix.

Similarly, by restricting again the transverse load variation across an element to linearity, substitution of (5.56a) into (5.40) leads to a consistent load vector, to be calculated from

$$\begin{Bmatrix} R_{u_1} \\ R_{u_2} \\ R_{u_0} \\ R_{v_1} \\ R_{v_2} \\ R_{v_0} \\ R_{w_1} \\ R_{w_2} \\ R_{\omega_1} \\ R_{\omega_2} \end{Bmatrix} = \frac{s_{12}\theta_0}{120} \begin{bmatrix} 10(2b-a) & 10b & 0 & 0 & 0 & 0 \\ 10b & 10(2b+a) & 0 & 0 & 0 & 0 \\ (20b-4a) & (20b+4a) & 0 & 0 & 0 & 0 \\ 0 & 0 & 10(2b-a) & 10b & 0 & 0 \\ 0 & 0 & 10b & 10(2b+a) & 0 & 0 \\ 0 & 0 & (20b-4a) & (20b+4a) & 0 & 0 \\ 0 & 0 & 0 & 0 & (21b-11a) & (9b-a) \\ 0 & 0 & 0 & 0 & (9b+a) & (21b+11a) \\ 0 & 0 & 0 & 0 & s_{12}(3b-a) & 2bs_{12} \\ 0 & 0 & 0 & 0 & -2bs_{12} & -s_{12}(3b+a) \end{bmatrix} \begin{Bmatrix} p_{u_1} \\ p_{u_2} \\ p_{v_1} \\ p_{v_2} \\ p_{w_1} \\ p_{w_2} \end{Bmatrix} \tag{5.57}$$

Before assembling the structure stiffness for solution of the equations of equilibrium, it is advantageous to eliminate the interior degrees of freedom on the element level by the standard technique of static condensation, thus resulting again in an 8X8 element stiffness and an 8X1 consistent load vector.

In order to study the effect of the additional degrees of freedom, some comparative studies on the element level are presented below, followed by selected studies on the structural level.

5.8.2 Studies on Element Level

Because the displacement functions used for the stiffness derivation satisfy completeness and inter-element continuity requirements, convergence of the results will be expected to be monotonic, and the refined element discussed in this section will always yield more flexible results than the previously discussed element.

For the closed conical frustrum and curved beam shown in Fig. 5.21, eigenvalues have been calculated from the element stiffness matrix based first on linear in-plane displacement functions (referred to as CONE(1)), as well as on quadratic in-plane displacement functions, with interior degrees of freedom condensed out (referred to as CONE(2)), and are summarized in Table 5.6. In addition, Table 5.6 shows the eigenvalues calculated from the difference matrix $K_{Diff} = K_{CONE(1)} - K_{CONE(2)}$.

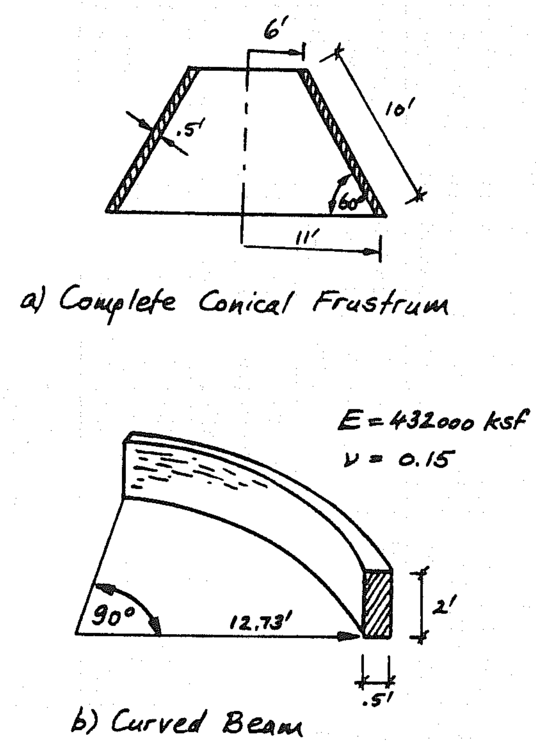

Fig. 5.21 Example Elements

In studying the results shown in Table 5.6, the following observations can be made.

TABLE 5.6. EIGENVALUES OF ELEMENT STIFFNESS BASED ON LINEAR AND QUADRATIC IN-PLANE DISPLACEMENTS

	Case No.	Har-monic No. n		1	2	3	4	5	6	7	8
Complete Conical Frustrum	1	0	a	$.75229\cdot10^{6}$	$.57462\cdot10^{6}$	$.32321\cdot10^{6}$	$.16512\cdot10^{6}$	$.30199\cdot10^{5}$	$.17628\cdot10^{5}$	$.27183\cdot10^{-8}$	$-.24819\cdot10^{-8}$
			b	$.74775\cdot10^{6}$	$.53620\cdot10^{6}$	$.31419\cdot10^{6}$	$.16417\cdot10^{6}$	$.30190\cdot10^{5}$	$.17560\cdot10^{5}$	$.32617\cdot10^{-8}$	$-.50313\cdot10^{-9}$
			c	$.43983\cdot10^{5}$	$.90213\cdot10^{4}$	$.17446\cdot10^{-8}$	$.92440\cdot10^{-9}$	$-.28471\cdot10^{-9}$	$-.36399\cdot10^{-9}$	$-.58588\cdot10^{-9}$	$-.22426\cdot10^{-8}$
	2	1	a	$.97700\cdot10^{6}$	$.66546\cdot10^{6}$	$.42331\cdot10^{6}$	$.15826\cdot10^{6}$	$.43041\cdot10^{5}$	$.22260\cdot10^{5}$	$-.12565\cdot10^{-8}$	$-.30963\cdot10^{-8}$
			b	$.71277\cdot10^{6}$	$.60163\cdot10^{6}$	$.41682\cdot10^{6}$	$.15825\cdot10^{6}$	$.42495\cdot10^{5}$	$.22240\cdot10^{5}$	$.11427\cdot10^{-8}$	$-.45469\cdot10^{-8}$
			c	$.27252\cdot10^{6}$	$.62615\cdot10^{5}$	$.23165\cdot10^{-8}$	$.10086\cdot10^{-8}$	$.79589\cdot10^{-10}$	$-.19969\cdot10^{-9}$	$-.40546\cdot10^{-9}$	$-.21421\cdot10^{-8}$
	3	2	a	$.16740\cdot10^{7}$	$.91030\cdot10^{6}$	$.62100\cdot10^{6}$	$.24452\cdot10^{6}$	$.74241\cdot10^{5}$	$.46777\cdot10^{5}$	$.12596\cdot10^{4}$	$.31092\cdot10^{3}$
			b	$.95996\cdot10^{6}$	$.63011\cdot10^{6}$	$.53471\cdot10^{6}$	$.23840\cdot10^{6}$	$.68788\cdot10^{5}$	$.46711\cdot10^{5}$	$.12591\cdot10^{4}$	$.30923\cdot10^{3}$
			c	$.90550\cdot10^{6}$	$.18663\cdot10^{6}$	$.53533\cdot10^{-8}$	$.44002\cdot10^{-8}$	$.15570\cdot10^{-8}$	$.98140\cdot10^{-9}$	$-.18376\cdot10^{-8}$	$-.56727\cdot10^{-8}$
	4	10	a	$.22423\cdot10^{8}$	$.10971\cdot10^{8}$	$.65922\cdot10^{7}$	$.39063\cdot10^{7}$	$.30134\cdot10^{7}$	$.78413\cdot10^{6}$	$.22989\cdot10^{6}$	$.73136\cdot10^{5}$
			b	$.78563\cdot10^{7}$	$.49653\cdot10^{7}$	$.30429\cdot10^{7}$	$.28622\cdot10^{7}$	$.25465\cdot10^{7}$	$.78122\cdot10^{6}$	$.21748\cdot10^{6}$	$.68533\cdot10^{5}$
			c	$.17940\cdot10^{8}$	$.77134\cdot10^{7}$	$.11312\cdot10^{-6}$	$.29256\cdot10^{-7}$	$.10774\cdot10^{-7}$	$.32257\cdot10^{-8}$	$-.15827\cdot10^{-7}$	$-.11102\cdot10^{-6}$
	5	100	a	$.28227\cdot10^{11}$	$.58683\cdot10^{10}$	$.21355\cdot10^{10}$	$.10874\cdot10^{10}$	$.10442\cdot10^{10}$	$.68618\cdot10^{9}$	$.33621\cdot10^{9}$	$.26337\cdot10^{9}$
			b	$.28216\cdot10^{11}$	$.58682\cdot10^{10}$	$.10877\cdot10^{10}$	$.74200\cdot10^{9}$	$.36745\cdot10^{9}$	$.32882\cdot10^{9}$	$.26327\cdot10^{9}$	$.16389\cdot10^{9}$
			c	$.17586\cdot10^{10}$	$.85303\cdot10^{9}$	$.14475\cdot10^{-3}$	$.33859\cdot10^{-4}$	$.42424\cdot10^{-5}$	$-.43717\cdot10^{-5}$	$-.24922\cdot10^{-4}$	$-.37579\cdot10^{-4}$
Curved Beam	6	0	a	$.22101\cdot10^{7}$	$.10806\cdot10^{7}$	$.28086\cdot10^{6}$	$.48380\cdot10^{5}$	$.12760\cdot10^{5}$	$.22355\cdot10^{4}$	$.11132\cdot10^{-7}$	$-.10460\cdot10^{-7}$
			b	$.22101\cdot10^{7}$	$.10806\cdot10^{7}$	$.28076\cdot10^{6}$	$.48380\cdot10^{5}$	$.12760\cdot10^{5}$	$.21860\cdot10^{4}$	$.32557\cdot10^{-8}$	$-.13552\cdot10^{-9}$
			c	$.15130\cdot10^{3}$	$.93033\cdot10^{-9}$	$.47551\cdot10^{-12}$	$.17482\cdot10^{-13}$	$.39380\cdot10^{-26}$	$.11479\cdot10^{-40}$	$0\cdot0$	$-.22909\cdot10^{-14}$
	7	1	a	$.22202\cdot10^{7}$	$.11251\cdot10^{7}$	$.28327\cdot10$	$.71128\cdot10^{5}$	$.44147\cdot10^{5}$	$.36349\cdot10^{4}$	$.72727\cdot10^{2}$	$.12312\cdot10^{2}$
			b	$.22051\cdot10^{7}$	$.11176\cdot10^{7}$	$.28319\cdot10^{6}$	$.70218\cdot10^{5}$	$.44100\cdot10^{5}$	$.35854\cdot10^{4}$	$.72288\cdot10^{2}$	$.12312\cdot10^{2}$
			c	$.16032\cdot10^{5}$	$.76367\cdot10^{4}$	$.20956\cdot10^{-8}$	$.13702\cdot10^{-8}$	$.55239\cdot10^{-9}$	$.27685\cdot10^{-9}$	$-.10340\cdot10^{-9}$	$-.74489\cdot10^{-8}$
	8	2	a	$.22510\cdot10^{7}$	$.12542\cdot10^{7}$	$.29085\cdot10^{6}$	$.22809\cdot10^{6}$	$.49329\cdot10^{5}$	$.10191\cdot10^{5}$	$.23197\cdot10^{4}$	$.35970\cdot10^{3}$
			b	$.21923\cdot10^{7}$	$.12234\cdot10^{7}$	$.29080\cdot10^{6}$	$.21607\cdot10^{6}$	$.49329\cdot10^{5}$	$.10094\cdot10^{5}$	$.23104\cdot10^{4}$	$.35969\cdot10^{3}$
			c	$.70723\cdot10^{5}$	$.30929\cdot10^{5}$	$.14537\cdot10^{-7}$	$.12540\cdot10^{-8}$	$.64632\cdot10^{-9}$	$.25435\cdot10^{-9}$	$-.13496\cdot10^{-9}$	$-.68164\cdot10^{-9}$

a) Eigenvalues of stiffness matrix $K_{CONE(1)}$
b) Eigenvalues of stiffness matrix $K_{CONE(2)}$
c) Eigenvalues of difference matrix $K_{Diff.} = K_{CONE(1)} - K_{CONE(2)}$
Shaded numbers are "zero" eigenvalues.

(1) CONE(2) results are always more flexible than the corresponding CONE(1) results. Therefore the difference matrix has only positive non-zero eigenvalues. The numerical reduction of eigenvalues due to the additional degrees of freedom may be appreciable. In case 4, for instance, the largest eigenvalue is reduced by 71.4%.

(2) Rigid body modes are not affected by the added degrees of freedom. In the closed conical shell element, all four zero eigenvalues are retained, and two in the curved beam, the other two being contaminated with the loss of axisymmetry.

(3) The difference matrix has only two non-zero eigenvalues, as one would expect as a consequence of the static condensation process, because thus the 8X8 CONE(2) stiffness contains a linear combination of the two interior degrees of freedom, and this is not present in the 8X8 CONE(1) stiffness. In the curved beam example, for n=0, only one non-zero eigenvalue appears because, with $\cos\varphi = 0$, no energy is stored in the second eigenmode associated with the interior degrees of freedom.

The above results show that the CONE(2) stiffness is indeed more flexible than the CONE(1) stiffness, while still being an upper bound to the true stiffness, so that better results can be expected on the structural level.

5.8.3 Studies on Structural Level

The curved beam of Fig. 5.12a has been analyzed for an angle of curvature, $\theta_o = 90°$ and the cross sections B (channel), C (I-Beam), and D (square box), Fig. 5.12a, as well as the narrow box section F, Fig. 5.19, using the two different element stiffnesses discussed above, and the results are summarized in Table 5.7. In studying these results, the following observations can be made.

1. Deflections increase in all cases only slightly with mesh refinement. While for CONE(1) results, this change might amount to almost 1%, the changes of CONE(2) results are much smaller.
2. The effect of mesh refinement on internal forces is slightly bigger but still hardly noteworthy. But it is interesting to note that the internal resisting moment, which is calculated as described in Section 5.5, is virtually unaffected by mesh refinement. A similar observation has already been made in Table 5.5.
3. The fact that both, CONE(1) and CONE(2) results hardly change with mesh refinements, together with the observation that the results of both theories agree to several figures, leads to the conclusion that these results are very accurate.

Regarding the actual distribution of internal forces, the quadratic in-plane displacement formulation may have some advantage. Figure 5.22 illustrates the shearing stress distribution at the end of a simply supported straight beam with a concentrated midspan load and discretized by various numbers of elements. As can be seen, the results based on the quadratic variation of in-plane displacements approximate the true stress distribution much better than the results stemming from linear in-plane displacement functions. However, at mid-element, the two formulations are almost identical, so that the stress distribution from CONE(1) can be considerably improved if mid-element values are interpolated. But still, the large stress discontinuities between adjacent elements are not present in the CONE(2) results, so that these seem to be still more reliable, because in other cases it is more

TABLE 5.7 COMPARISON BETWEEN CONE(1) AND CONE(2) ON STRUCTURAL LEVEL

Cross Section No.*	Case No.	No. of Strips	Midspan Deflection X 10^{-2}				Maximum N_x		Maximum M_y		Midspan Moment	
			Left Web		Right Web							
			CONE(1)	CONE(2)	CONE(1)	(CONE(2)	CONE(1)	CONE(2)	CONE(1)	CONE(2)	CONE(1)	CONE(2)
B (channel)	1	3	18.857	18.902	33.592	33.662	59.083	59.112	3.1976	3.1882	67.555	67.582
	2	6	18.911	18.927	33.670	33.697	60.074	60.005	3.3055	3.3013	67.583	67.594
	3	12	18.926	18.930	33.694	33.701	60.224	60.100	3.2753	3.2741	67.587	67.590
C (I-Beam)	4	5	16.856	16.935			99.986	99.339	.9475	.9512	67.722	67.762
	5	12	16.916	16.938			99.825	99.249	.9111	.9122	67.260	67.270
	6	24	16.932	16.938			99.577	99.215	.9018	.9021	67.515	67.577
F (narrow box)	7	4	14.321	14.395	15.109	15.185	44.684	44.466	.6051	.6034	67.593	67.593
	8	10	14.400	14.406	15.190	15.197	44.836	44.638	.5392	.5392	67.206	67.209
D (square box)	9	4	1.3569	1.3675	1.5870	1.5988	15.702	15.679	.6581	.6588	68.043	68.089
	10	16	1.3680	1.3689	1.5993	1.6004	15.741	15.677	.6478	.6479	68.045	68.109

*See Figs. 5.12a and 5.19.

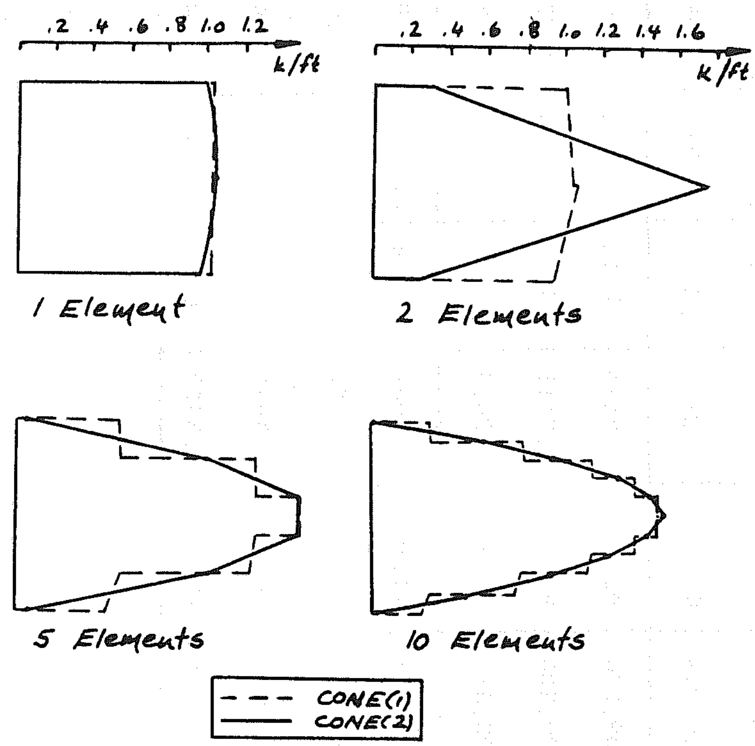

Fig. 5.22 Shearing Stress Distribution at End of Simply Supported Beam

advantageous to average stresses between adjacent elements rather than choosing mid-element values, and this confusion regarding stress interpretation is greatly reduced in the CONE(2) theory.

Finally, Fig. 5.23 shows that for a straight box beam, the stress concentration under an eccentrically applied midspan concentrated load is much better represented by the CONE(2) results than by CONE(1) theory. The CONE(2) result for the coarse mesh (6 elements) represents the critical N_x-value even better than the CONE(1) theory with the fine mesh (12 elements). Accurate reference values for comparison were obtained by program MULTPL [10.1].

Concluding, it may be stated that the slightly increased computational effort and additional computer core storage requirement of about 1300 words justifies the employment of quadratic in-plane displacement functions only if stress concentrations are expected or if difficulties in interpreting internal stress output arise, i.e., if no general rationale is available to determine if mid-element stresses or stress averages of adjacent elements should be used. Improvement of deflections and overall structural response is so small that it alone

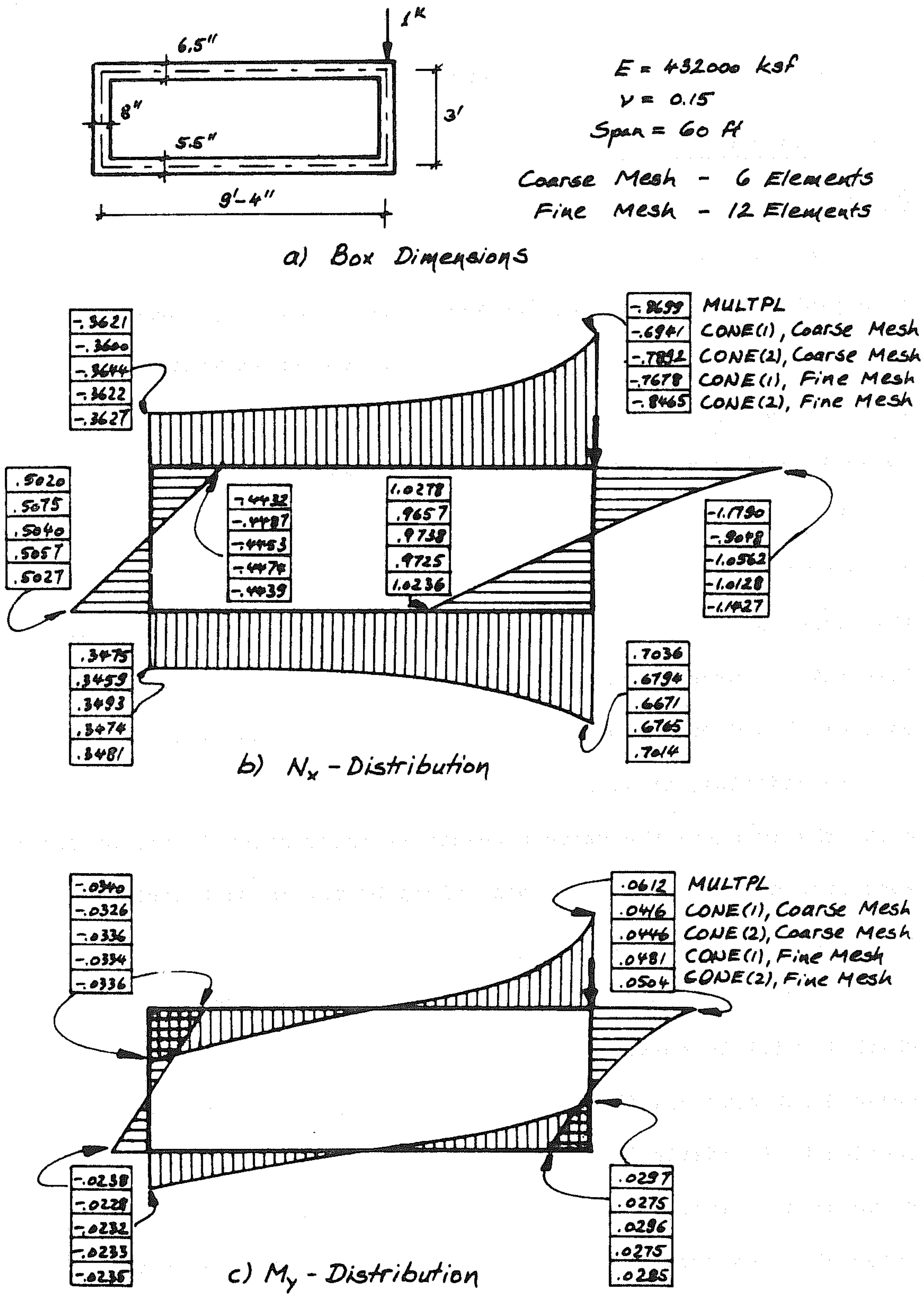

Fig. 5.23 Comparison Between CONE(1) And CONE(2) For Straight Box Beam

makes the use of the refined element unnecessary.

5.9 Continuous Curved Folded Plate Theory

5.9.1 Introduction

As versatile and accurate as the curved strip theory in its form just discussed may be, its restriction to simply supported single-span structures is a severe limitation which weighs even heavier if curved bridges are to be analyzed, because many of them, in particular interchange structures, are continuous.

Likewise, many reinforced concrete bridges have intermediate diaphragms which prevent cross sectional distortions under loading. In this case, however, the bridge structure is forced to behave more or less like a curved beam, and some of the curved beam theories mentioned earlier should be capable of producing reliable results.

In addition, it will often be difficult to describe with a folded plate theory alone the structure-support interaction if the bridge is supported by single- or multiple-column bents, as most continuous reinforced concrete bridges are.

In this section, a force method will be described by means of which it will be possible to account for continuity as well as transverse diaphragms and flexible frame supports. This method has been applied by Scordelis [10.1] and Lo [10.8] to straight folded plate structures to incorporate rigid diaphragms which may or may not be externally supported. The computer program MUPDI which was written on the basis of this theory, gave excellent results for a variety of structures [10.1] [10.2], although there are problems inherent in the theory, which will be briefly discussed later.

5.9.2 Continuous Curved Strip Theory

This theory is based on the standard force method of structural analysis. All unknown intermediate reactions and generally continuous interaction forces and moments are approximated by an appropriate set of discrete forces which are taken as redundants so that the simply supported single-span structure serves as the primary structure. Let $\{\delta_o\}$ be the vector containing all displacements of the structure due to external loads acting alone, with all redundants removed, Fig. 5.24a. Each element of this $\{\delta_o\}$-vector is to correspond to one element of the redundant force vector $\{X\}$. In successively applying unit redundant loads to the system and solving for the displacements, the individual columns $\{f_i\}$ of the structure flexibility matrix $[F] = [f_1\ f_2 \ldots f_n]$ will be established, with n being the number of unknown redundants which are found from the compatibility requirement

$$\{\delta_o\} + [F]\{X\} = \{o\} \tag{5.58}$$

from which

$$\{X\} = - [F]^{-1}\{\delta_o\} \tag{5.59}$$

The actual steps for solving a continuous curved folded plate structure can then be summarized as follows.

1. Identify all intermediate reactions and interaction forces and moments as redundants and remove them from the structure. Plate interaction forces may be assumed to vary linearly across a plate element, while joint interaction forces are considered concentrated or uniformly distributed longitudinally over the width of the diaphragm or frame support.

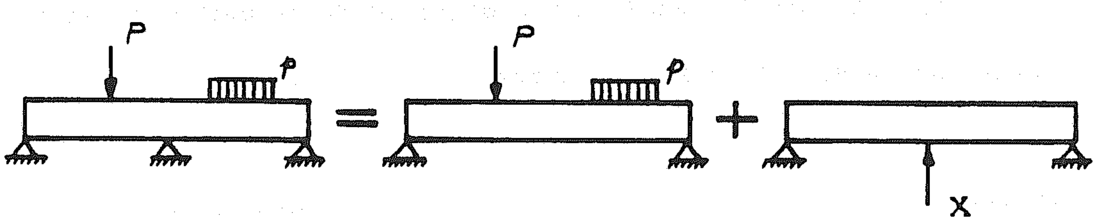

a) Primary Structure for Continuous Curved Box Girder

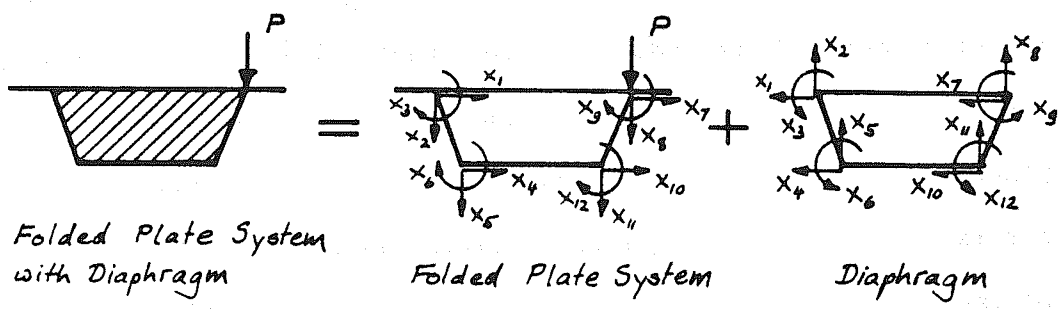

b) Interaction Forces in Box Girder with Diaphragm

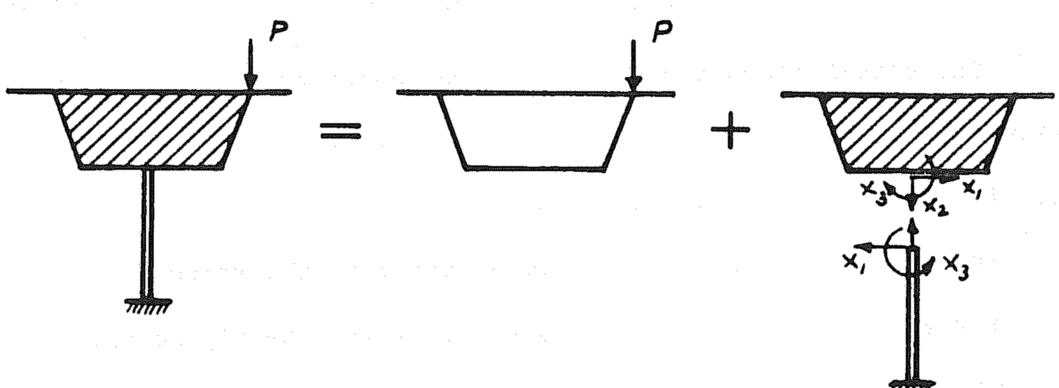

c) Single-Column Supported Box Girder

Fig. 5.24 Continuous Curved Folded Plates

2. Analyze the primary structure for the given external loads only and solve for the displacements $\{\delta_o\}$ corresponding to the redundant forces.
3. Analyze the primary structure for one redundant force X_i of unit value, with all other external actions removed, and solve for the same displacement quantities as in step 2 to obtain column $\{f_i\}$ of the structural flexibility matrix $[F]$.
4. Repeat step 3 for $i = 1, 2, \ldots, n$ so that the $[F]$- matrix is complete, and solve Eq. (5.59) to find all unknown redundant forces.
5. Final results are found by superposition of all actions imposed on the structure, i.e., for some output quantity s,

$$s = s_o + \sum_{i=1}^{n} s_i X_i \tag{5.60}$$

where s_o is the result due to external loads alone, and s_i is the result due to the unit redundant X_i.

If a curved folded plate structure has an intermediate transverse diaphragm which is not externally supported, then the compatibility condition, Eq. (5.58) has to be modified because now only the relative displacements of the various joints have to be zero, provided the diaphragm is considered rigid. For example, the 12 redundant interaction forces shown in Fig. 5.24b are not independent if the diaphragm can undergo three rigid body displacements so that only 9 interaction force patterns and the corresponding displacements enter the compatibility condition Eq. (5.58). The modified flexibility matrix can then be obtained by

$$\underset{9\times 9}{[\bar{F}]} = \underset{9\times 12}{[B]^T}\underset{12\times 12}{[F]}\underset{12\times 9}{[B]} \tag{5.61}$$

where [B] is a 12X9 force transformation matrix relating the original

12 redundants of Fig. 5.24b to a new set of 9 linearly independent self-equilibrating interaction force patterns.

In the case that the diaphragm is not rigid or that some flexible frame is built into the plate system, such as shown in Fig. 5.24c, Eq. (5.58) has to be modified as

$$\{\delta_o\} + [F]\{X\} = \{\delta\} \tag{5.62}$$

where

$$\{\delta\} = [f]\{-X\} \tag{5.63}$$

is the actual displacement vector for the points where the interaction forces are acting, so that the redundants are found to be

$$\{X\} = -([F] + [f])^{-1}\{\delta_o\} \tag{5.64}$$

provided the flexibility [f] of the supporting frame is known. For a general computer program, it is generally advantageous to find [f] as the inverse of the frame assembly stiffness.

5.9.3 Examples

The curved box girder of Fig. 5.25a is continuous over two spans of 50 ft. and subjected to dead load only. The interior support can be thought of as an externally supported diaphragm which may be simulated by enforcing the conditions $\delta_{5V} = \delta_{14V} = \delta_{10H} = 0$, Fig. 5.25b, requiring the solution of three simultaneous equations.

Considering that the same curved box girder has a single simply supported span of 100 ft., but a rigid movable diaphragm at midspan, then the 8 selected interaction forces shown in Fig. 5.25c are not independent, and the original 8X8 flexibility matrix has to be reduced to order 5 using the transformation, Eq. (5.61). Choosing the interaction forces X_3, X_4, X_8 as dependent quantities, the required force

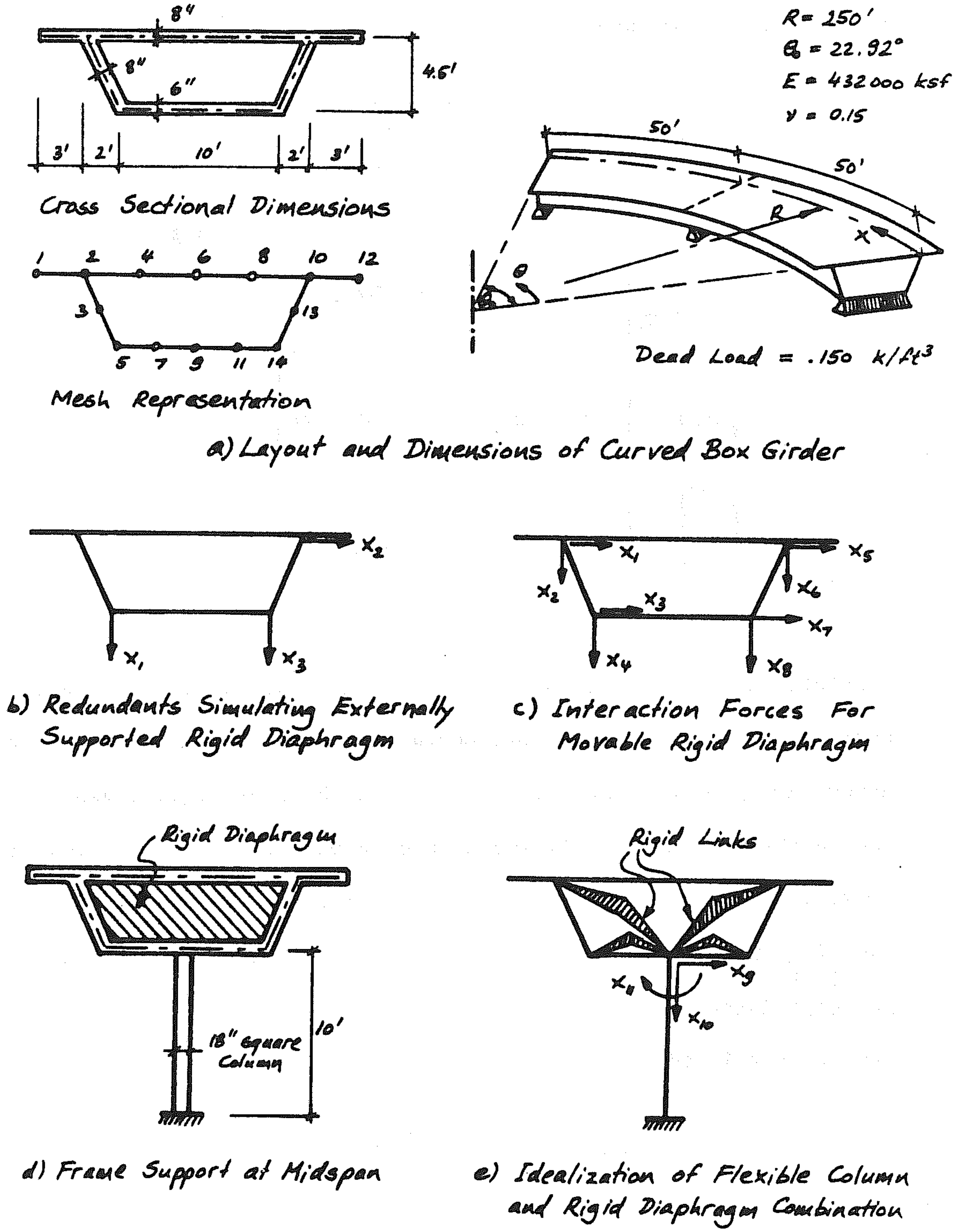

a) Layout and Dimensions of Curved Box Girder

b) Redundants Simulating Externally Supported Rigid Diaphragm

c) Interaction Forces For Movable Rigid Diaphragm

d) Frame Support at Midspan

e) Idealization of Flexible Column and Rigid Diaphragm Combination

Fig. 5.25 Curved Box Girder With Intermediate Support and Diaphragm transformation becomes

$$\begin{Bmatrix} X_1 \\ X_2 \\ X_3 \\ X_4 \\ X_5 \\ X_6 \\ X_7 \\ X_8 \end{Bmatrix} = \begin{bmatrix} 1.0 & 0 & 0 & 0 & 0 \\ 0 & 1.0 & 0 & 0 & 0 \\ -1.0 & 0 & -1.0 & 0 & -1.0 \\ 0.45 & -1.2 & 0.45 & 0.2 & 0 \\ 0 & 0 & 1.0 & 0 & 0 \\ 0 & 0 & 0 & 1.0 & 0 \\ 0 & 0 & 0 & 0 & 1.0 \\ -0.45 & 0.2 & -0.45 & -1.2 & 0 \end{bmatrix} \begin{Bmatrix} \bar{X}_1 \\ \bar{X}_2 \\ \bar{X}_3 \\ \bar{X}_4 \\ \bar{X}_5 \end{Bmatrix}$$

In the case where the rigid midspan diaphragm is connected to a flexible single column, as shown in Fig. 5.25d, three additional degrees of freedom may be introduced, Fig. 5.25e. The four corner nodes can then be connected to the column head by rigid links. Although the system has only three independent degrees of freedom, it is convenient to solve Eq. (5.64) directly for all 11 interaction forces. The $[F]_{11 \times 11}$- matrix for the curved box without column and diaphragm can be established from unit-load analyses, while the bent flexibility may be calculated according to

$$\underset{11\times 11}{[\bar{f}]} = \underset{11\times 3}{[B]^T}\underset{3\times 3}{[f]}\underset{3\times 11}{[B]}$$

where

$$[f] = \begin{bmatrix} \frac{L^3}{3EI} & 0 & \frac{L^2}{2EI} \\ 0 & \frac{L}{EA} & 0 \\ \frac{L^2}{2EI} & 0 & \frac{L}{EI} \end{bmatrix}$$

represents the flexibility of the single column fixed at its base, and [B] is the force transformation matrix, in expanded form

$$\begin{Bmatrix} X_9 \\ X_{10} \\ X_{11} \end{Bmatrix} = \begin{bmatrix} 1.0 & 0 & 1.0 & 0 & 1.0 & 0 & 1.0 & 0 & 1.0 & 0 & 0 \\ 0 & 1.0 & 0 & 1.0 & 0 & 1.0 & 0 & 1.0 & 0 & 1.0 & 0 \\ 4.5 & -7.0 & 0 & -5.0 & 4.5 & 7.0 & 0 & 5.0 & 0 & 0 & 1.0 \end{bmatrix} \begin{Bmatrix} X_1 \\ X_2 \\ X_3 \\ X_4 \\ X_5 \\ X_6 \\ X_7 \\ X_8 \\ X_9 \\ X_{10} \\ X_{11} \end{Bmatrix}$$

In Fig. 5.26, longitudinal stress distributions at the midspan section x = 50 ft. ($\theta = 11.46°$) are plotted for the single simply supported span and the three other cases for which it serves as primary structure. As can be seen, the influence of the movable diaphragm appears to be small, but the load transfer from the interior (left) to the exterior girder (right) is clearly noticeable, Fig. 5.26c. Actual load distributing effects will be more pronounced under the action of concentrated loads and should be studied using more redundant interaction forces. The high stress concentrations over the points of unyielding support, Fig. 5.26b, would be reduced if more interaction forces had been selected, as the stress distribution over the flexible support already demonstrates, Fig. 5.26d.

Figure 5.27 illustrates the variation of transverse bending moments at the quarterspan section x = 25 ft. ($\theta = 5.73°$) for all four cases. While the movable diaphragm reduces these moments slightly, Fig. 5.27a and c, the moments are almost identical in the two continuous cases, Fig. 5.27b and d.

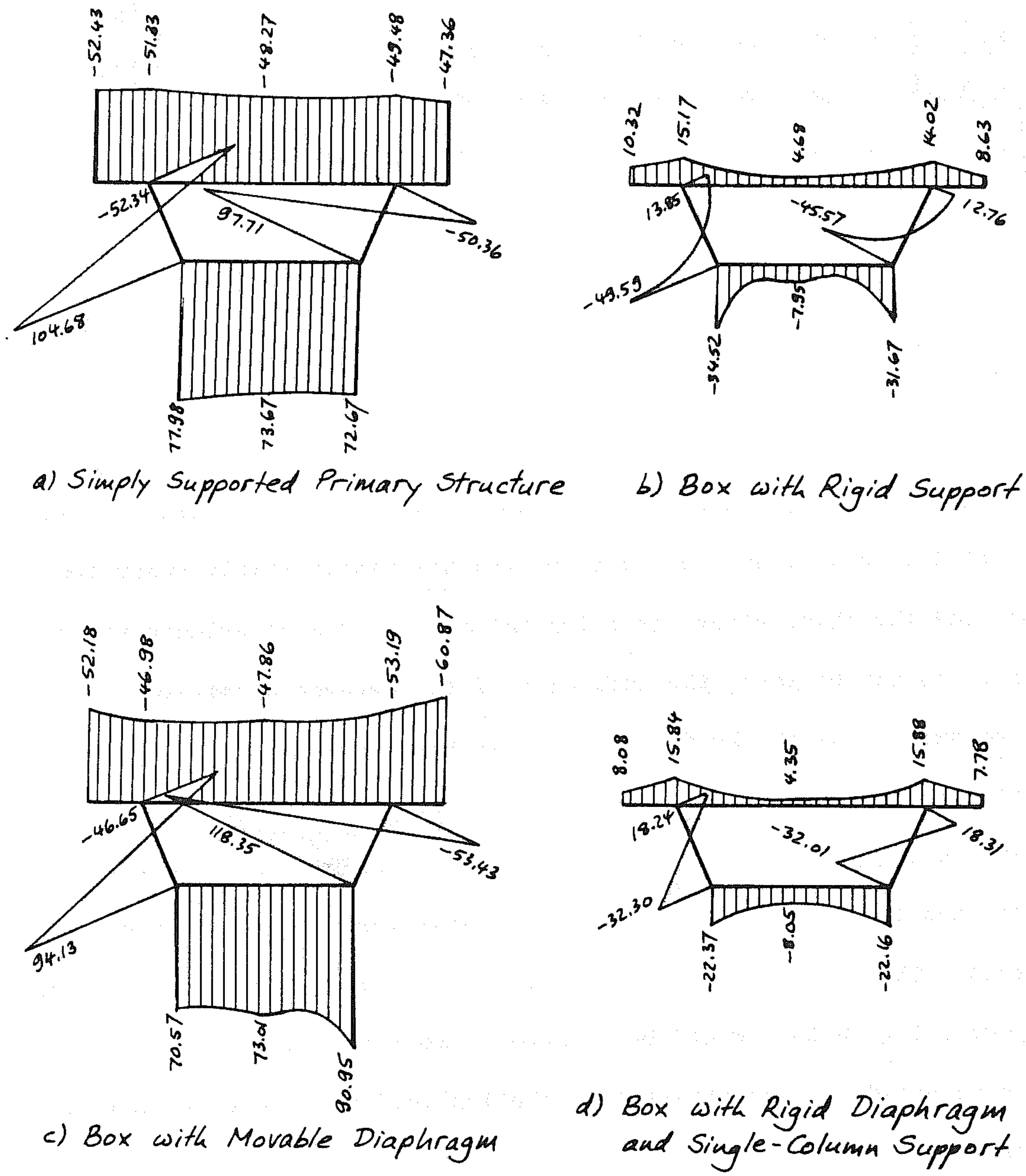

a) Simply Supported Primary Structure

b) Box with Rigid Support

c) Box with Movable Diaphragm

d) Box with Rigid Diaphragm and Single-Column Support

Fig. 5.26 Longitudinal Stress Resultants N_θ (k/ft) At Midspan (x=50 ft) of Curved Box Girder Bridge Due to Dead Load

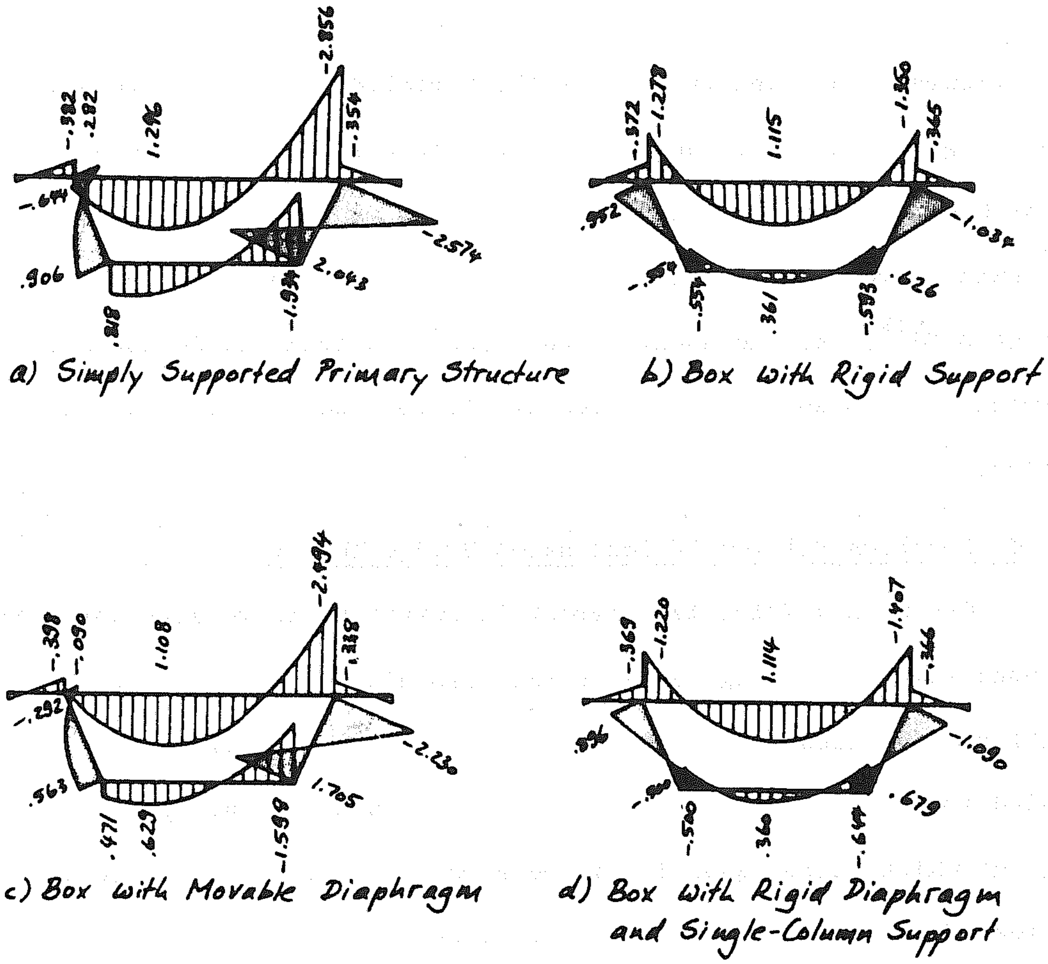

Fig. 5.27 Transverse Bending Moments M_s (ft-k/ft) At Quarterspan (X=25 ft) Due to Dead Load

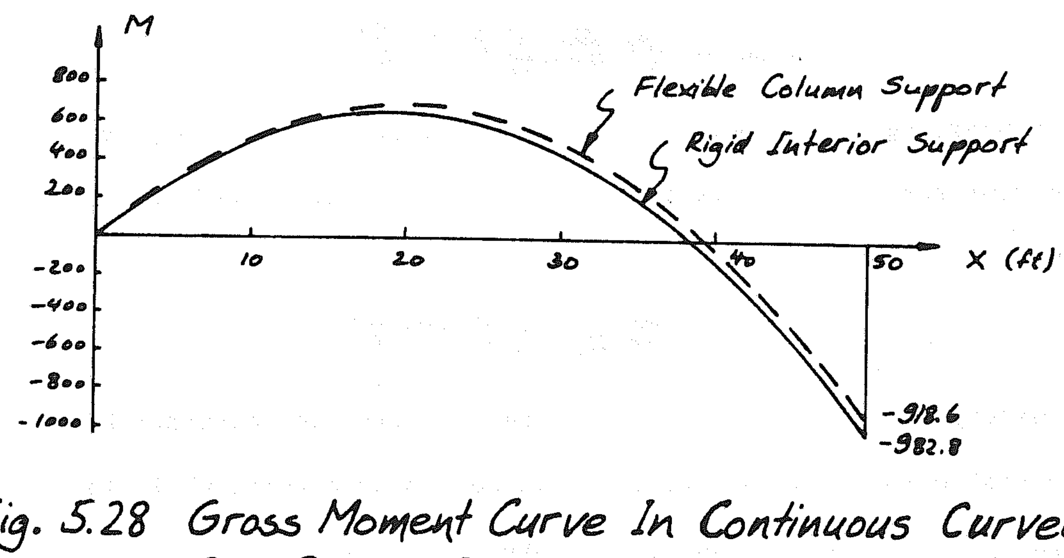

Fig. 5.28 Gross Moment Curve In Continuous Curved Box Girder Bridge Due to Dead Load

Figure 5.28, finally depicts the variation of gross internal resisting moment along the span. The column stiffness in this example is so high that the maximum negative moment is reduced by only 6.5%. The axial force in the column was found to be 220.5^{k}, the bending moment $3.26^{'k}$, and the shear force, 0.53^{k}. A total of 50 non-zero harmonics has been used to represent all loadings and interaction forces.

5.9.4 Problems Related to Continuous Bridge Theory

One main difficulty inherent in curved strip results for continuous structures originates in the harmonic idealization of the problem. The question of how many terms of the Fourier series are needed to yield satisfactory results depends on a) the type of loading, b) which output quantity is referred to, and c) what specific degree of accuracy is called satisfactory.

Regarding the loading type, it should be noted that the Fourier representation of a uniform load,

$$p(x) = \frac{4p_o}{\pi} \lim_{N\to\infty} \sum_{n=1}^{N} \frac{1}{n} \sin\frac{n\pi x}{L} \tag{5.65}$$

is converging slowly but in a monotonic manner, Fig. 5.29a, while the representation of the Dirac-delta for a concentrated load P at $x = \xi$,

$$p(x) = \frac{2P}{L} \lim_{N\to\infty} \sum_{n=1}^{N} \sin\frac{n\pi\xi}{L} \sin\frac{n\pi x}{L} \tag{5.66}$$

is divergent, Fig. 5.29c, or more specifically, the distance between successive roots of Eq. (5.66) converges towards zero, while the amplitudes remain bounded by the envelope indicated in Fig. 5.29c by the dotted line. The series

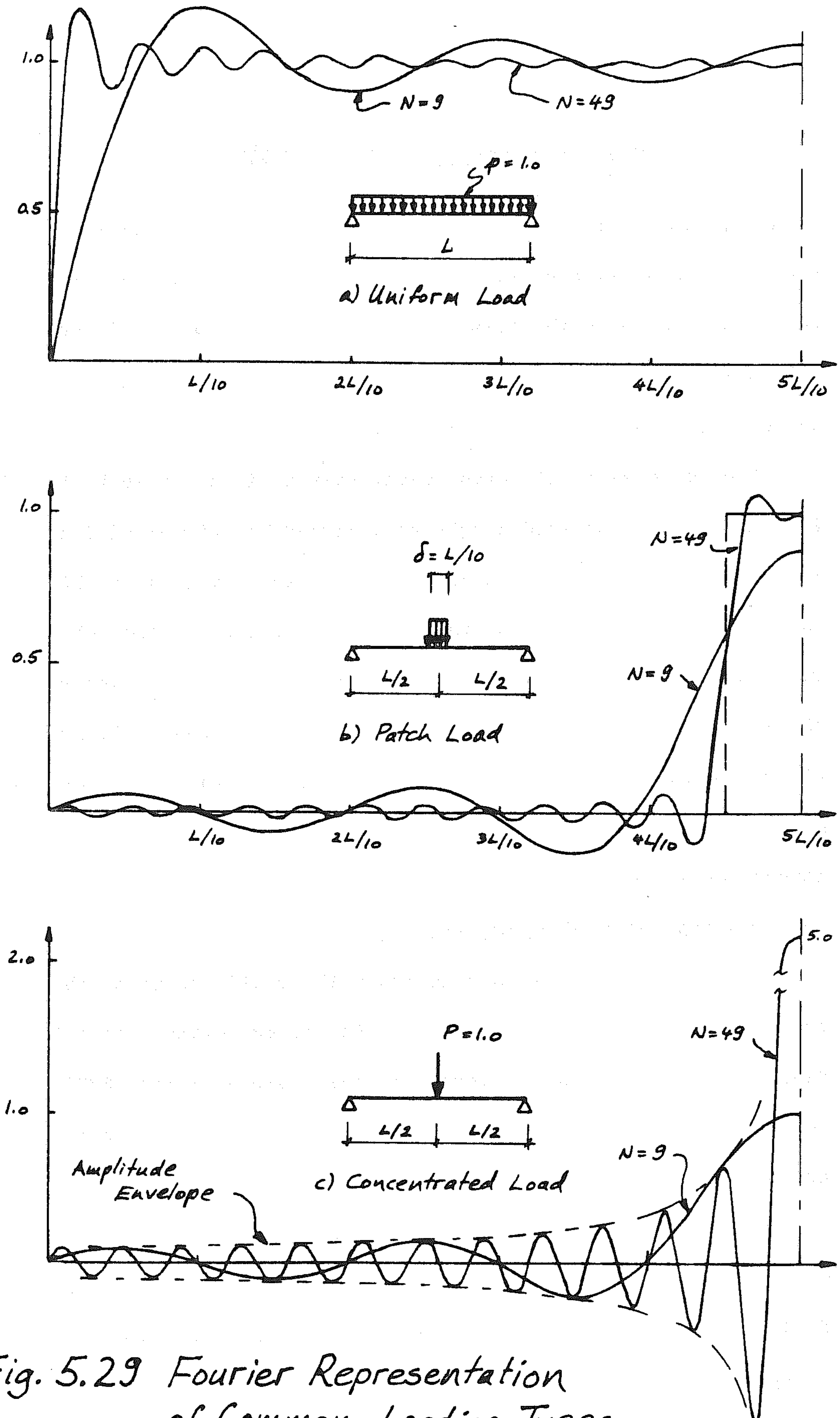

Fig. 5.29 Fourier Representation of Common Loading Types

$$p(x) = \frac{4p_o}{\pi} \lim_{N \to \infty} \sum_{n=1}^{N} \frac{1}{n} \sin \frac{n\pi\xi}{L} \sin \frac{n\pi\delta}{2L} \sin \frac{n\pi x}{L} \tag{5.67}$$

finally, represents a load of intensity p_o, uniformly distributed over a width δ, with centroid at ξ, Fig. 5.29b. For $\xi = \delta = \frac{L}{2}$, Eq. (5.67) takes on the form of Eq. (5.65), and for $\delta = 0$ such that $p_o \cdot \delta = P$, it reduces to Eq. (5.66). The rate of convergence of the series Eq. (5.67) depends on the ratio δ/L.

The convergence of output quantities is illustrated by Fig. 5.30 for the simply supported single-span curved box girder of Fig. 5.25a, subjected to a vertical concentrated midspan load at joint 10. All output quantities shown in Fig. 5.30 are measured in the web element right under the load, only the values given for u, $N_{s\theta}$, and $M_{s\theta}$ are those at the support because they are zero at midspan. Figure 5.30 clearly demonstrates the different convergence behavior of displacements, in-plane forces, and bending moments. It is of particular importance to realize how slow the convergence of moment quantities for this type of loading may be.

The required degree of accuracy will usually be up to the designer for whom slide-rule accuracy used to be one guideline. In this light, displacements and membrane forces in the example of Fig. 5.30 are accurate enough for $N \geq 80$, i.e. if at least 40 nonzero terms are used.

There are cases, however, for which a very high degree of accuracy may be necessary. The flexibility matrix [F] of certain continuous folded plates may be highly unstable in a numerical sense. For example, even the set of equations for the redundants of Fig. 5.25b is not very well-conditioned. Using 25 non-zero harmonics, one obtains

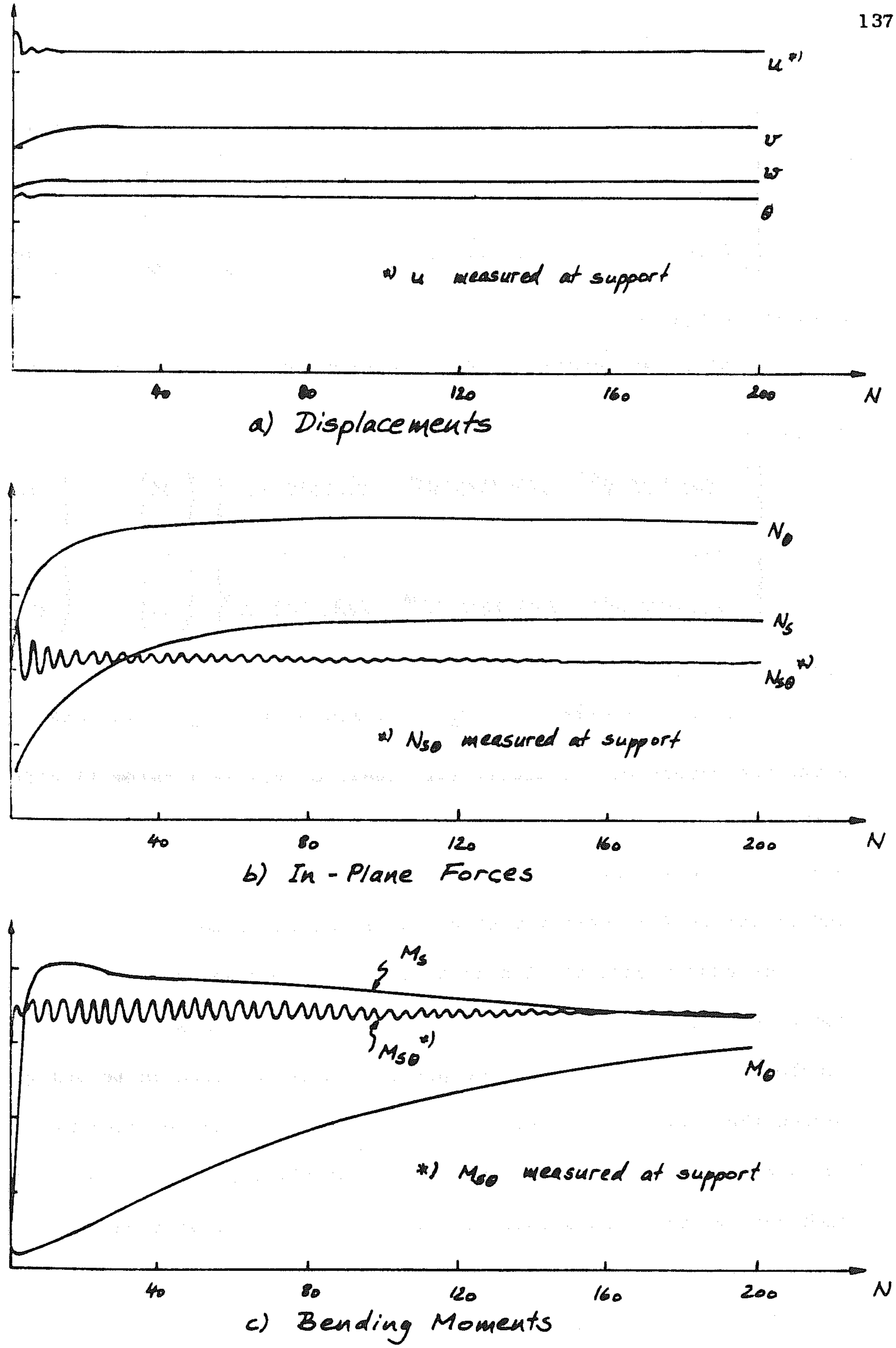

Fig. 5.30 Convergence of Curved Strip Results Under a Concentrated Load

$$\begin{bmatrix} .58397721 \cdot 10^{-3} & .6076\,8063 \cdot 10^{-5} & .5023\,6991 \cdot 10^{-3} \\ .6076\,8063 \cdot 10^{-5} & .7643\,6405 \cdot 10^{-4} & .1103\,7092 \cdot 10^{-4} \\ .5023\,6991 \cdot 10^{-3} & .1103\,7092 \cdot 10^{-4} & .6222\,9154 \cdot 10^{-3} \end{bmatrix} \begin{Bmatrix} X_1 \\ X_2 \\ X_3 \end{Bmatrix} = - \begin{Bmatrix} .12162987 \cdot 10^{0} \\ .1932\,8022 \cdot 10^{-2} \\ .1263\,3674 \cdot 10^{0} \end{Bmatrix}$$

with the solution

$$X_1 = -110.07577 \qquad X_2 = -0.0517\,9151 \qquad X_3 = -114.15455$$

If 50 non-zero terms are accumulated, the equations become

$$\begin{bmatrix} .5846\,9417 \cdot 10^{-3} & .6076\,8454 \cdot 10^{-5} & .50236992 \cdot 10^{-3} \\ .6076\,8454 \cdot 10^{-5} & .7672\,5983 \cdot 10^{-4} & .1103\,7218 \cdot 10^{-4} \\ .50236992 \cdot 10^{-3} & .1103\,7218 \cdot 10^{-4} & .6230\,4286 \cdot 10^{-3} \end{bmatrix} \begin{Bmatrix} X_1 \\ X_2 \\ X_3 \end{Bmatrix} = - \begin{Bmatrix} .1216\,2987 \cdot 10^{0} \\ .1932\,8009 \cdot 10^{-2} \\ .1263\,3673 \cdot 10^{0} \end{Bmatrix}$$

with the solution

$$X_1 = -114.42848 \qquad X_2 = -0.4586\,5520 \qquad X_3 = -108.92654$$

A maximum change of the flexibility coefficients well below 1% effects a change of the vertical reactions by 5%. The flexibility matrices of other structures may be so ill-conditioned that small changes of the individual coefficients may alter the reactions completely.

The consequence of this fact is that either an extremely large number of Fourier terms has to be used in the analysis, or less coupled sets of redundant force patterns must be selected in order to reduce the magnitude of the off-diagonal flexibility coefficients. But for a general computer program, it will be difficult to establish for each case a well-conditioned set of redundant force patterns automatically.

Finally, the choice of the primary structure itself is generally poor, because large correction forces are required to restore compatibility. However, this deficiency may be partially overcome by estimating the magnitude of certain interaction forces and analyzing the structure subjected to these estimated forces in addition to the given external loads. The correction forces required to restore complete continuity can be reduced considerably by this procedure.

6. BEHAVIOR OF CURVED BOX GIRDER BRIDGES

6.1 Objective

In this chapter, curved box girder bridges are analyzed using the methods presented in the last two chapters. After a comparison between the results of the finite element and curved strip theory, selected parameter studies will be described with the objective of providing an insight into the behavior of curved box girder bridges. Only once their main structural action is basically understood and the influence of the various geometric parameters recognized, will it be possible to derive some generally applicable design recommendations.

In Chapter 2 it has been shown that the designer is generally confronted with two basic types of highway bridges -- those supporting through traffic lanes (open highway), and those supporting turning roads. While the open highway is usually designed for higher speeds (therefore small curvatures), it is mainly the ramps with lower design speeds and sharp curvatures that are of interest for refined analytical studies. These ramp structures, moreover, very seldom carry more than two traffic lanes, so that cross sections with 1 to 5 cells may constitute economical designs. In this chapter, therefore, the one- and two-cell bridge will be studied in some detail, and the findings will be extrapolated to 3- and 4-cell bridges.

6.2 Comparison Between Finite Element and Curved Strip Theory

In order to study the relative agreement between the two methods of analysis described in chapters 4 and 5, the box girder bridge of Fig. 6.1, subjected to a standard AASHO truck in either position A or B, has been analyzed by programs FINPLA2 and CURSTR with the mesh layout depicted in Fig. 6.1c. Resulting longitudinal stresses N_θ and transverse bending moments M_r due to the truck placed at position A are shown in Fig. 6.2, and for truck B in Fig. 6.3, all results referring to the midspan section.

As can be seen in Figs. 6.2 and 6.3, disagreement between N_θ-values may be as high as 10%. However, this high discrepancy is mainly restricted to web elements, while agreement in the top and bottom deck plates is much better, so that the total statical moment by the two methods differ by only a few percent. There are several possible sources to explain the difference between the two theories. Firstly, a fairly coarse mesh layout was used so that it is difficult for both theories to capture the severe stress concentrations in the vicinity of the concentrated wheel loads. Secondly, only 50 harmonic terms were used in program CURSTR to describe the wheel loads. As was shown earlier, this is clearly not enough to obtain convergence of any internal forces or moments in the vicinity of the load. Additional harmonic terms will increase the critical stresses, and better agreement with finite element results which are consistently higher, can be expected.

Agreement between the two theories for transverse bending moments, on the other hand, is excellent. In fact, the differences are almost negligible, which seems to indicate that the plate bending element model of program FINPLA2 behaves much more like the curved strip element than the in-plane element model does.

Concluding, it may be stated that the agreement between finite element and curved strip theory is satisfactory for practical purposes,

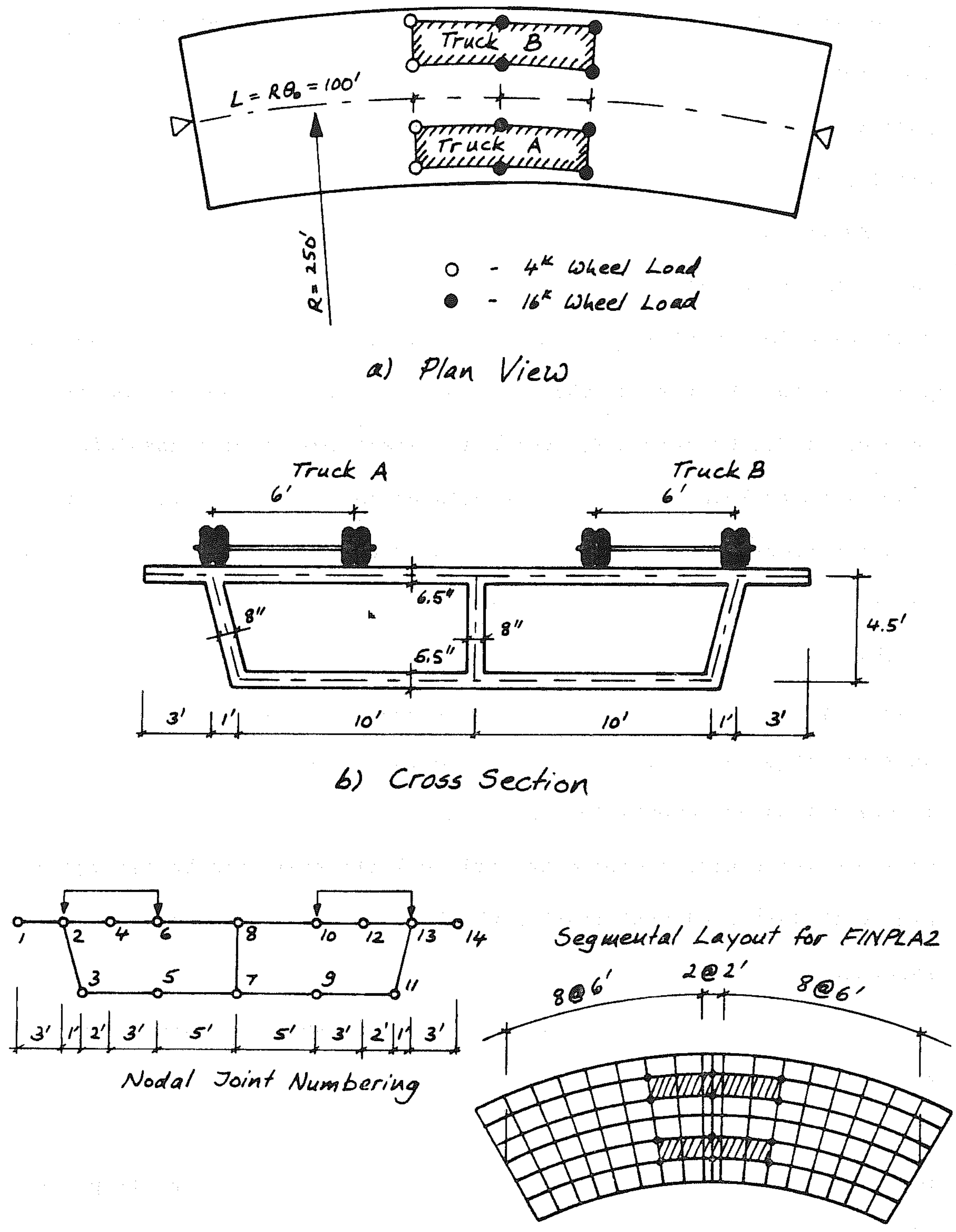

Fig. 6.1 Curved Box Girder Bridge Comparison Example

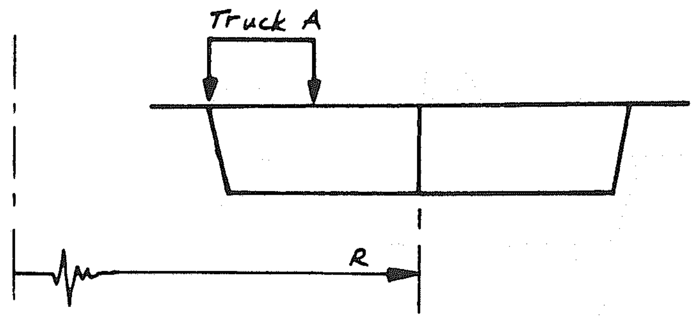

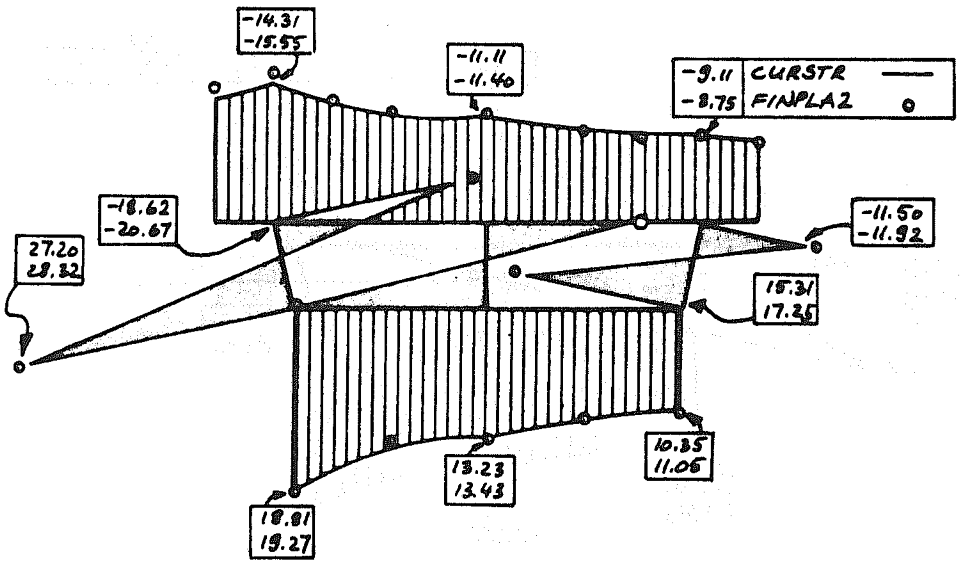

a) Longitudinal Stress Resultant N_θ (k/ft)

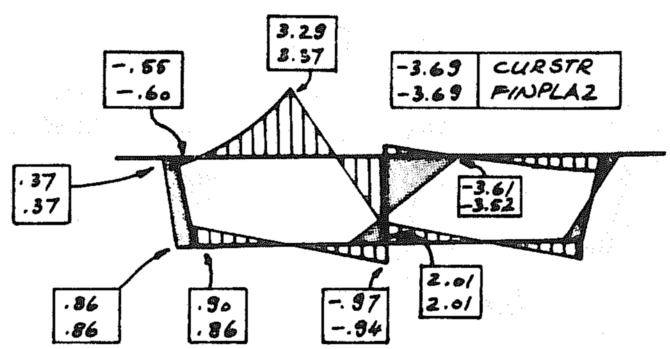

b) Transverse Bending Moments M_s (ft-k/ft)

Fig. 6.2 Midspan Stresses and Moments In Curved Box Girder Bridge Due to Truck A

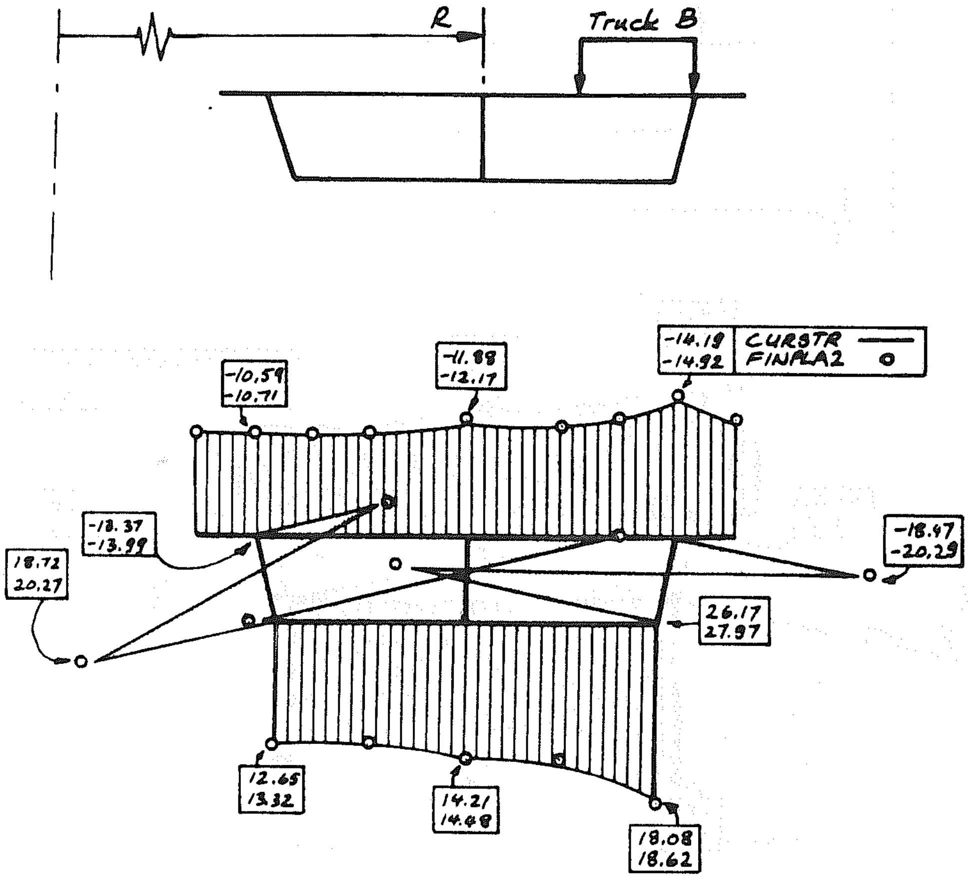

a) Longitudinal Stress Resultants N_θ (k/ft)

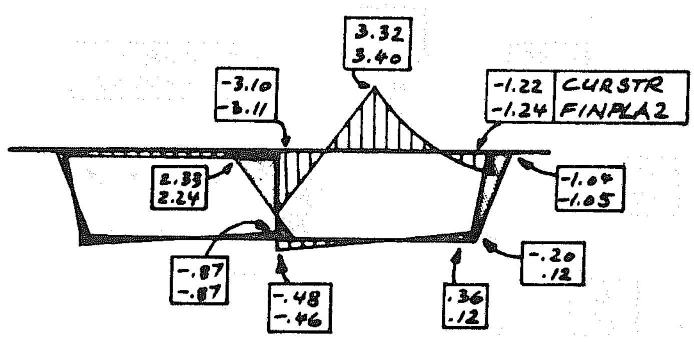

b) Transverse Bending Moments M_s (ft-k/ft)

Fig. 6.3 Midspan Stresses and Moments In Curved Box Girder Bridge Due to Truck B and it can be expected to improve with further mesh refinement. This check is invaluable for the analysis of curved box girder bridges for which no other general refined methods of analysis are available. Since both theories are completely independent, it can be assumed if they lead to very similar results, that these results are good approximations to the true solution.

6.3 Concept of Wheel Load Distribution

Before studying the effect of the various influence parameters on the behavior of curved box girder bridges, it is necessary to define the concepts of the design philosophy in which the subsequent findings will be evaluated. The final design question in the context of this chapter will be the determination of the amount of reinforcing steel required for sufficient strength under design loadings. One direct approach to the solution of this problem is to analyze the bridge by an appropriate method for all possible loading conditions, to determine for each point the maximum or minimum stress, and to assign the corresponding quantity of reinforcement to cover these stresses. For practical purposes, however, this approach will be justified only for very unusual structures, and for more ordinary bridges, a simplified method of design will be desirable.

One such simplified approach can be obtained by defining discrete girders in the bridge. For box girder bridges, interior girders will in general be of I-beam shape with top and bottom flanges equal in width to the web spacing while exterior girders consist of an exterior web with a top flange extending from the midpoint between girder webs to the edge of the cantilever overhang and the bottom flange being equal in width to half of the web spacing, Fig. 6.4. Once these

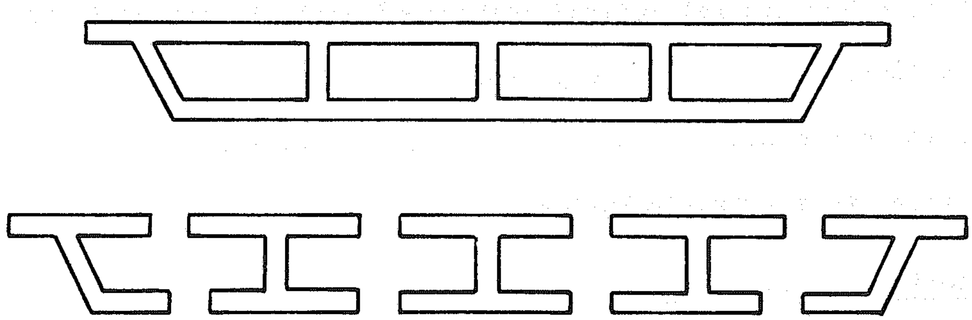

Fig. 6.4 Design Model for Box Girder Bridge

discrete girders have been defined, the problem of obtaining the required amount of reinforcement is much easier, because the question to be answered becomes now: How much reinforcement does any one of the individual girders require for sufficient strength under some given design loading or loading envelope?

This problem can be solved by introducing the concept of load distribution, as long as it can be determined what the maximum share of the load is that any one girder may take. In [10.3] the distribution of wheel loads in straight box girder bridges had been studied extensively. In particular, the useful concept of two extreme cases had been introduced: a so-called "rigid" bridge with perfect load distribution, in which each girder takes the load proportional to its bending rigidity; and the so-called "flexible" bridge without any load distribution, in which each girder has to carry alone all loads directly applied to it. Any realistic bridge will fall somewhere in between these two extremes.

In Chapter 7, the application of this design concept will be exemplified. The definitions introduced so far shall be sufficient to explain the emphasis put on load distribution in the following sections. The discussion shall be restricted to distribution of wheel loads, because for spans usually encountered in highly curved bridges, these will be the most important design live loads.

6.4 The Single-Cell Curved Box Girder

Notation for the prototype box girder to be studied in this section is given in Fig. 6.5. The large number of influence parameters

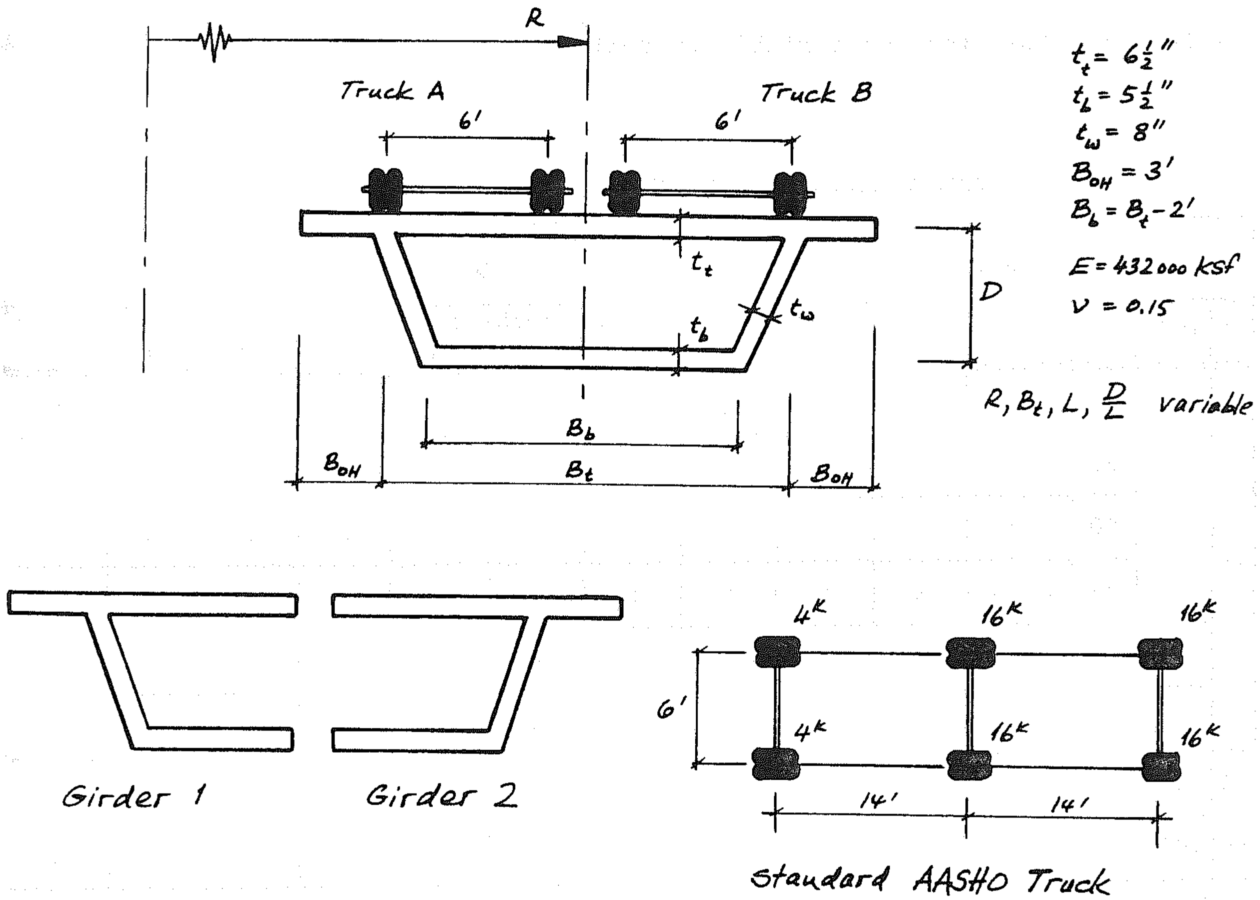

Fig. 6.5 Notations for Single-Cell Box Girder

makes the problem prohibitive, therefore it has to be restricted to those considered to be the most important. Besides the span L and curvature radius R, also the cell width at the top, B_t, and depth, D, or depth-span ratio will be taken into account, whereas other factors such as plate thicknesses, web inclination angle, top slab overhang, and material properties will be kept constant at the values indicated in Fig. 6.5. The box girder is considered to be simply supported at both ends. Loading consists of a standard AASHO truck [10.29], placed transversely in either position A or B, and longitudinally such that the second axle is acting on the midspan section.

Table 6.1 summarizes the cases that were studied, indicating the selected values for the variable parameters. As for the cell width,

TABLE 6.1 CASE STUDY LIST FOR SINGLE BOX

Radius R			10 000*	1 000		400		300		200		100	
B	D/L	L	Truck A	Truck A	Truck B	Truck A	Truck B	Truck A	Truck B	Truck A	Truck B	Truck A	Truck B
12		40	x							x	x	x	x
		60	x					x	x	x	x	x	x
		80	x			x	x	x	x	x	x	x	x
		100	x	x	x	x	x	x	x	x	x		
	.04	60	x					x	x	x	x	x	x
	.07	60	x					x	x	x	x	x	x
14	.055	60	x							x	x	x	x
16	.055	60	x							x	x	x	x

*Considered to be a "straight" bridge.

it must be admitted that the listed values are unusual for one-cell box girders in the United States, although they are fairly common in European practice. But then, the plate thicknesses usually taper towards the webs, and the values given in Fig. 6.5 are probably inadequate. For studies of load distribution, however, the values indicated are believed to be informative. The cases with R = 10,000 ft. are considered as limiting cases of essentially straight bridges.

All 54 cases listed in Table 6.1 have been analyzed by program CURSTR, using a mesh of 10 elements for B = 12' and 11 elements for B > 12', with 50 terms of the Fourier series representing each wheel load assumed to be distributed longitudinally over one foot. Resulting midspan girder moments are listed in Tables 6.2a and 6.2b. The amount of wheel load distribution may be represented by the moment percentage which is the fraction of the total moment carried by any one girder. These moment percentages are also listed in Tables 6.2a and 6.2b.

Some small inconsistencies may be discovered in comparing cases which should theoretically have the same total moment from the analysis. The disagreement is mostly due to the coarse mesh and small number of harmonic terms used in the analysis. These differences, however, are of influence only in comparing the absolute girder moments, but the moment percentages are hardly affected. For verification, one case (Table 6.2a, R = 100 ft., L = 60 ft., Truck A) was also analyzed using 18 elements and 100 harmonic terms. As a consequence, the girder moments are changed from 415.8 to 440.1 and from 333.3 to 350.5 ft-kips, respectively, while the percentages change only from .555 to .557 and from .445 to .443, respectively. This case reinforces the contention that the approximate analyses gave accurate

TABLE 6.2a GIRDER MOMENTS FOR SINGLE-CELL BOX GIRDER (B_t = 12 FT., D/L = .055)

Radius R (ft)			10 000		1 000		400		300		200		100	
Span			Truck A	Truck B	Truck A	Truck B	Truck A	Truck B	Truck A	Truck B	Truck A	Truck B	Truck A	Truck B
40	Girder 1	Moment	214.3	174.4							212.6	182.9	212.3	194.2
		%	.551	.449							.560	.455	.569	.465
	Girder 2	Moment	174.4	214.3							167.0	218.7	161.1	223.0
		%	.449	.551							.440	.545	.431	.535
	Total	Moment	388.7	388.7							379.6	401.6	373.4	417.2
60	Girder 1	Moment	401.8	353.2					403.5	365.6	405.4	373.3	415.8	402.2
		%	.532	.468					.540	.475	.544	.480	.555	.493
	Girder 2	Moment	353.2	401.8					343.9	403.6	340.1	405.1	333.3	114.0
		%	.468	.532					.460	.525	.456	.520	.445	.507
	Total	Moment	755.0	755.0					747.4	769.2	745.5	778.4	749.2	816.2
80	Girder 1	Moment	589.6	529.2			594.0	544.9	596.5	551.2	603.0	565.5	635.8	624.6
		%	.527	.473			.534	.480	.536	.483	.541	.488	.555	.504
	Girder 2	Moment	529.2	589.6			518.5	589.5	515.7	590.2	511.5	593.0	510.5	613.4
		%	.473	.527			.466	.520	.464	.517	.459	.512	.445	.496
	Total	Moment	1118.8	1118.8			1112.5	1134.4	1112.2	1141.4	1114.5	1158.5	1146.3	1238.0
100	Girder 1	Moment	777.5	703.8	780.2	712.6	787.4	728.2	792.8	738.5	806.8	762.5		
		%	.525	.475	.528	.479	.533	.484	.536	.487	.542	.493		
	Girder 2	Moment	703.8	777.5	697.4	775.9	689.4	775.9	686.3	777.1	683.0	782.6		
		%	.475	.525	.472	.521	.467	.516	.464	.513	.458	.507		
	Total	Moment	1481.3	1481.3	1477.6	1488.5	1476.8	1504.1	1479.2	1515.6	1492.8	1545.1		

TABLE 6.2b GIRDER MOMENTS FOR SINGLE-CELL BOX GIRDER (L = 60 FT)

B_t	D/L	Radius		10,000		300		200		100	
				Truck A	Truck B	Truck A	Truck B	Truck A	Truck B	Truck A	Truck B
12	.04	Girder 1	Moment	419.4	374.2	419.5	386.5	420.7	393.3	429.0	419.7
			%	.528	.472	.534	.479	.536	.482	.544	.491
		Girder 2	Moment	374.2	419.4	366.6	420.7	363.8	423.2	360.1	435.6
			%	.472	.528	.466	.521	.464	.518	.456	.509
		Total Moment		793.6	793.6	786.1	807.3	784.5	816.5	789.1	855.3
	.07	Girder 1	Moment	431.6	362.6	436.7	379.8	440.4	389.3	456.5	424.6
			%	.543	.457	.555	.470	.561	.476	.578	.496
		Girder 2	Moment	362.6	431.6	350.1	428.4	344.8	428.2	333.3	431.7
			%	.457	.543	.445	.530	.439	.524	.422	.504
		Total Moment		794.2	794.2	786.8	808.2	785.2	817.5	789.8	856.3
14	.055	Girder 1	Moment	444.4	349.8			448.6	376.7	459.4	412.3
			%	.559	.441			.575	.458	.589	.477
		Girder 2	Moment	349.8	444.4			331.9	444.9	320.5	452.4
			%	.441	.559			.425	.542	.411	.523
		Total Moment		794.2	794.2			780.5	821.6	779.9	864.7
16	.055	Girder 1	Moment	468.8	325.4			472.3	357.0	481.1	398.1
			%	.590	.410			.609	.432	.626	.456
		Girder 2	Moment	325.4	468.8			303.4	468.7	288.0	474.4
			%	.410	.590			.391	.568	.374	.544
		Total Moment		794.2	794.2			775.7	825.7	769.1	872.5

girder moment percentages.

In studying the results of Tables 6.2a and 6.2b, the following observations can be made.

1. Load distribution is always better under truck B, i.e., when the truck is placed on the outside girder. This phenomenon is similar to the one discussed with the curved plate problem in Section 5.6.3. The interior girder is stiffer than the exterior girder and therefore attempts to carry a larger portion of the load. If directly loaded with the truck, it is not willing to transfer much of this load. But if the more flexible exterior girder is loaded, the interior girder is very successful in attracting an appreciable amount of the load.
2. If curvature increases, the outside girder becomes more flexible and the inside girder stiffer. Consequently, load distribution improves with curvature increase, as long as the outside girder is loaded, otherwise load distribution gets worse. This behavior is independent of span, cell width, and depth-span ratio.
3. A truck placed on the outside girder produces a bigger total statical moment than if placed on the inside girder, because the spans of the two girders are different.
4. The two phenomena just discussed have a cancelling effect. While the span increase tends to increase the moment carried by the outside girder, the reduction in stiffness tends to decrease it again. The converse is true for the inside girder. The very interesting consequence of this fact is that the design moments for both girders are very similar. In that respect it can be said that curvature has only a small effect on the relative girder

moments, although the absolute moments do increase with curvature.

5. In one case of Table 6.2a (R = 100 ft., L = 80 ft.), the interior girder takes more moment than the exterior girder, even if the truck is placed over the outside girder. This case, however, involves an opening angle of 45.8° which is highly unlikely to occur in bridge practice.
6. The influence of span is similar to the one found for straight bridges [10.3]. Short spans are stiff longitudinally, and wheel loads cannot easily be distributed onto unloaded girders. As the span becomes longer, the transverse bridge stiffness increases relative to it, so that load distribution improves.
7. The depth-span ratio has a similar effect. If the girders become shallower, the longitudinal bridge stiffness decreases, and load distribution will improve. For high depth-span ratios, on the other hand, load distribution will worsen.
8. Also the influence of the cell width can be interpreted in this manner, except that now the transverse bridge stiffness is affected. An increase of this stiffness relative to the longitudinal bridge stiffness will improve load distribution (decreasing B_t). But an increasing cell width B_t weakens the transverse stiffness, and the loaded girder will have less chance to transfer load to the other girder. The influence of plate thicknesses can be predicted with the same reasoning.
9. Since the selected box dimensions permit only one traffic lane to be carried, the moments listed in Tables 6.2a and 6.2b would be design moments.

6.5 The Two-Cell Curved Box Girder

The cross section of the prototype bridge to be studied in this section, is shown in Fig. 6.6. As variable parameters, again the radius of curvature, R, and the cell width B_t deserve most attention, but also two different spans were considered. Table 6.3 lists all cases studied.

TABLE 6.3 CASE STUDY LIST FOR TWO-CELL BOX

Cell Width B	Span L	Critical Loading for Girder	Radius					
			10 000	1000	400	300	200	100
7	60	1	x			x	x	x
		2	x				x	
		3				x	x	x
	100	1	x	x	x	x	x	
		2	x	x	x	x		
		3		x	x	x	x	
8	60	1	x			x	x	x
		2	x					x
		3				x	x	x
10	60	1	x			x	x	x
		2	x			x	x	x
		3				x	x	x

In an investigation of this bridge with the three girders as shown in Fig. 6.6, the question of critical truck positions arises. While these positions are obvious for both exterior girders 1 and 3, the loading for the center girder 2 can only be found by trial and error,

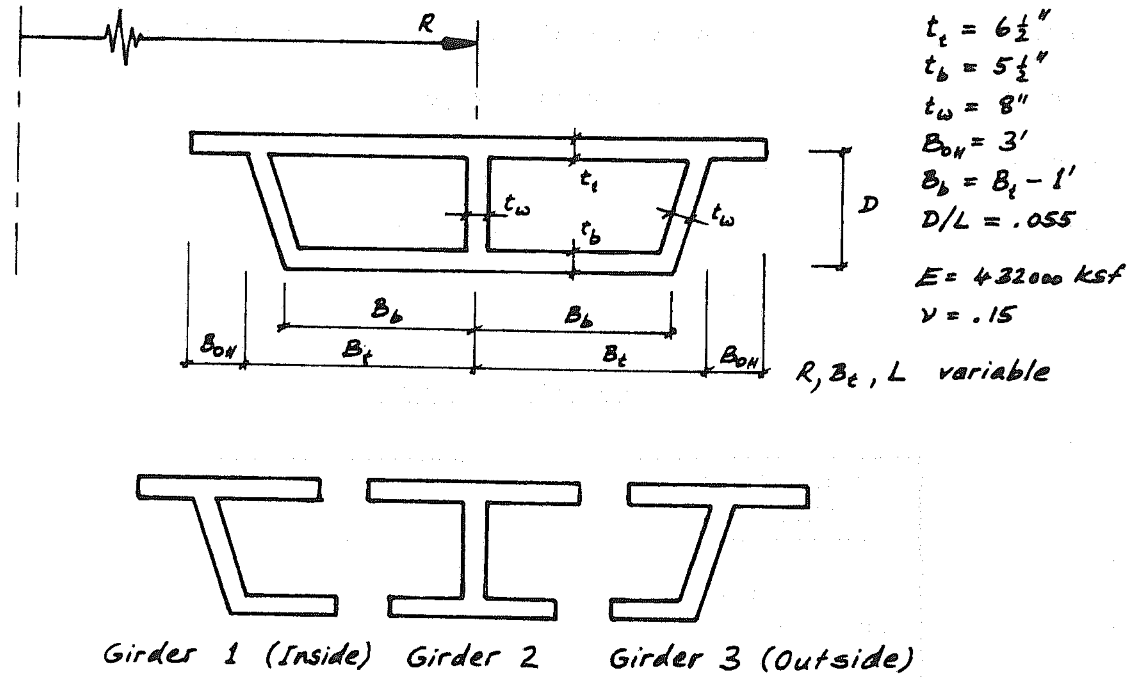

Fig. 6.6 Notation for Two-Cell Curved Box Girder

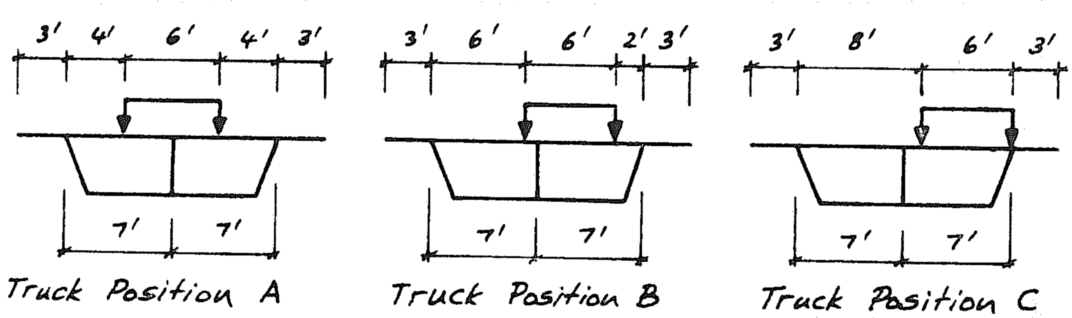

Fig. 6.7 Trial Truck Positions to Find Critical Case for Interior Girder (Cell Width B_t=7')

because shifting a truck from the central position towards the outside girder increases its total statical moment, and provided there is enough curvature, then the share that girder 2 gets from this added moment may very well be larger than the loss due to the shift of the truck away from center. Table 6.4 illustrates this phenomenon for two cases. The trial truck positions are shown in Fig. 6.7.

TABLE 6.4 MOMENTS OF GIRDER 2

Truck Position (Fig. 6.7)	A	B	C
Case 1 - R = 200', L = 60'	343.4	345.7	346.0
Case 2 - R = 1000', L = 100'	627.4	626.6	622.9

In case 1, the curvature is large enough so that truck position C is the critical case, while in case 2, truck position A produces the maximum moment as in a straight bridge situation.

For a cell width of B_t = 7 ft., only one truck may be placed on the bridge, because the AASHO specifications [10.29] require a clearance of 4 ft. between standard trucks. For B_t = 8 ft, however, two trucks can fit onto the 16 ft. roadway, with their transverse position fixed, Fig. 6.8. This loading will be

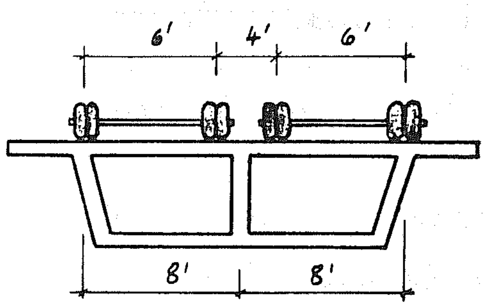

Fig. 6.8 Critical Loading for Two-Cell Box with B_t=8 ft.

critical for all three girders. The cases listed in Table 6.3 for $B_t = 8$ ft., were therefore analyzed for up to three single truck loadings, two of which give the loading of Fig. 6.8 if combined. For $B_t = 10$ ft., finally, two trucks may be shifted transversely across the bridge to produce the maximum moments for any girder. In practice, the 20 ft. roadway might correspond to a 12 ft. lane plus an 8 ft. shoulder.

In analyzing with program CURSTR each of the cases listed in Table 6.3 for maximum girder moments, the results summarized in Table 6.5 were obtained, again with 50 terms of the Fourier series representing the loads, and now 14 elements approximating the bridge cross section. The moment values listed in Table 6.5 are actual design moments, i.e., in each case produced by the most critical truck positions. The moment percentages indicate what fraction these design moments constitute, compared with the total statical moments produced by these critical loading conditions. Because moments for different girders may be caused by different load patterns, the percentages do not necessarily add up to 1.0.

In studying Table 6.5, the following observations may be made.

1. The moments of girder 1 and 2 always increase with curvature, although this increase is worth mentioning only for strong curvatures--reflecting the increase of statical moment with curvature as it was already observed in the curved beam problem, Fig. 5.12.
2. The moment of girder 3 initially decreases slightly with increasing curvature and starts increasing for larger curvatures. This behavior clearly demonstrates the two opposing effects mentioned in the previous section. A similar phenomenon was observed in the

TABLE 6.5 GIRDER MOMENTS IN TWO-CELL BOX GIRDER

Cell Width B_t	Span L	Radius R		10 000	1 000	400	300	200	100
7	60	Girder 1	Moment	252.6			252.9	253.7	258.8
			%	.318			.323	.325	.332
		Girder 2	Moment	340.7			341.4	346.0	364.2
			%	.429			.420	.421	.420
		Girder 3	Moment	252.6			253.4	254.7	261.5
			%	.318			.312	.309	.301
	100	Girder 1	Moment	477.6	478.8	482.5	485.4	493.1	
			%	.316	.318	.321	.323	.326	
		Girder 2	Moment	627.0	627.4	630.5	636.0	649.0	
			%	.414	.414	.414	.413	.409	
		Girder 3	Moment	477.6	476.7	477.3	478.4	482.6	
			%	.316	.313	.310	.308	.304	
8	60	Girder 1	Moment	457.2			467.6	474.1	500.4
			%	.288			.294	.297	.306
		Girder 2	Moment	674.4			677.2	680.2	697.3
			%	.424			.424	.424	.424
		Girder 3	Moment	457.2			450.5	448.7	448.6
			%	.288			.282	.279	.270
10	60	Girder 1	Moment	470.3			478.1	480.5	506.3
			%	.296			.302	.303	.316
		Girder 2	Moment	701.5			703.9	706.9	723.6
			%	.442			.441	.441	.440
		Girder 3	Moment	470.3			464.6	463.6	465.4
			%	.296			.289	.285	.275

discussion of the curved plate problem, compare Fig. 5.14.

3. The fraction of the total moment which any girder of a straight bridge carries is approximately proportional to its bending rigidity. For example, the interior girder of the two-cell bridge of Fig. 6.6 accounts for about 42% of the total bridge moment of inertia, while each exterior girder contributes about 29%. These values are very close to the moment percentages taken by the three girders in the case R = 10,000 ft., B_t = 8 ft., for which the loading of Fig. 6.8 happened to be the critical one for all three girders.

4. In the curved case, the girders change their relative stiffness. While the central girder maintains its original length, the outside girder becomes longer and more flexible, while the inside girder becomes shorter and stiffer. Correspondingly, the percentages of girder 2 hardly change at all with curvature, but for girder 3 it decreases steadily, and for girder 1 it increases with increasing curvature.

5. The influence of span on load distribution is small, but the same "distribution" effect of longer spans can be observed like in the preceding section. For L = 60 ft., R = 10,000 ft., girder 1 and 2 take 31.8 and 42.9% of the design load, respectively. For L = 100 ft., these values become 31.6 and 41.4%.

6. The cell width is important in two respects. First, it determines the number of trucks that may be placed on the bridge. Secondly, it accelerates the curvature effects. The wider the bridge is, the faster the stiffness of girder 1 increases and the stiffness of girder 3 decreases with growing curvature. This acceleration can

be seen in comparing the cases of B_t = 8 ft. with those of B_t = 10 ft.

6.6 Additional Studies of Curved Box Girders

In the last two sections, the one- and two-cell box girders have been studied in some detail. In this section, the first objective will be to investigate if the findings and observations of these studies also apply to three- and four-cell bridges.

Figure 6.9 shows the selected bridge cross sections and the load cases for which they were analyzed. Table 6.6 summarizes the cases studied.

TABLE 6.6 CASE STUDY LIST FOR 3- AND 4-CELL BRIDGES

	3-Cell Bridge		4-Cell Bridge			
Load Case	A	B	A	B	C	D
Radius						
10,000	x		x	x	x	x
400	x	x				
300	x	x				
200	x	x	x	x	x	x

Again, program CURSTR was used to analyze these bridges, using 50 harmonic terms to represent the wheel loads, and discretizing the bridge cross section with the mesh layouts shown in Fig. 6.9. The resulting girder moments at midspan and their percentages with respect to the total midspan moment are listed in Table 6.7 for the three-cell bridge, and in Table 6.8 for the four-cell bridge.

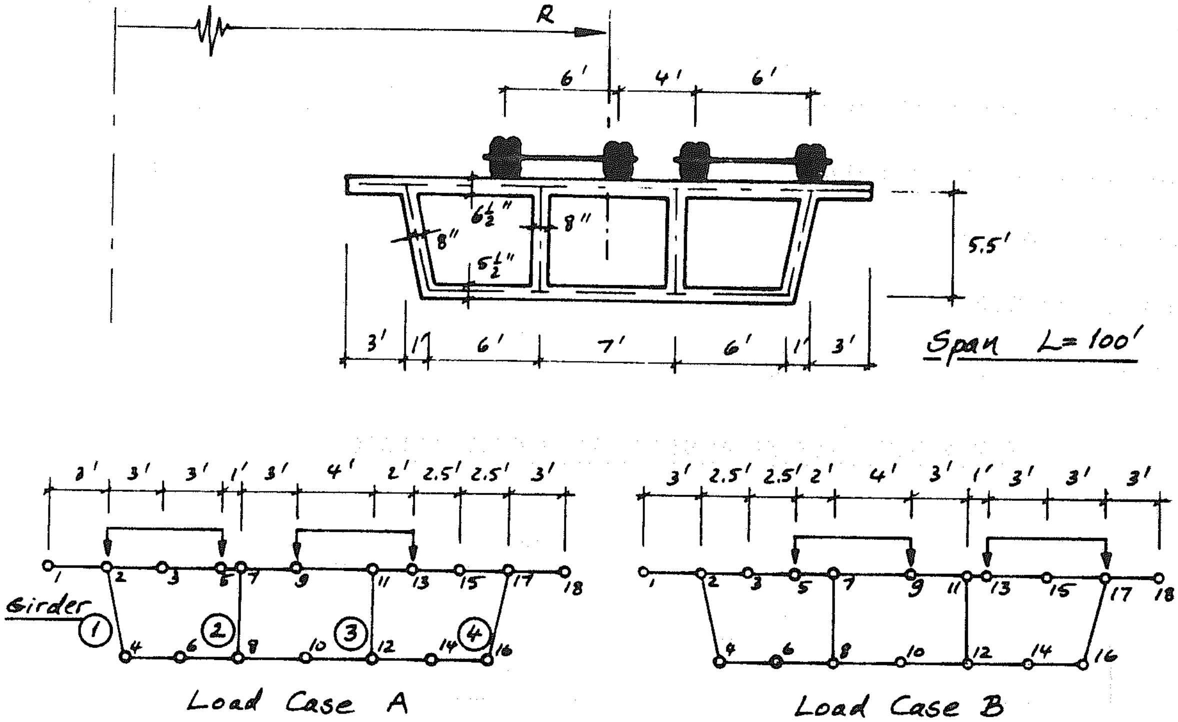

a) Three-Cell Bridge with Load Cases and Joint Idealization

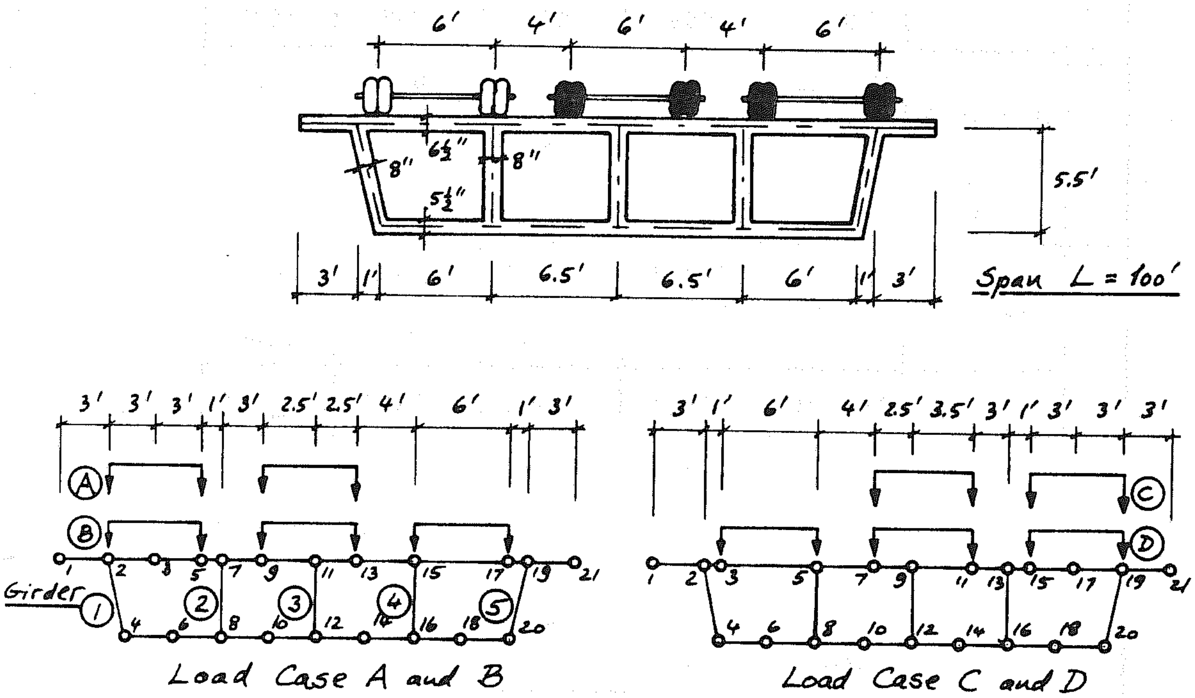

b) Four-Cell Bridge with Load Cases and Joint Idealization

Fig. 6.9 Three- and Four-Cell Box Girder Bridges

Because of the small probability that many lanes are loaded simultaneously to the maximum, the AASHO specifications permit a reduction factor of 0.9 for three loaded lanes, and 0.75 for 4 or more loaded lanes. In Table 6.8, therefore, the moment values due to load cases B and D are already reduced by 10%.

TABLE 6.7 GIRDER MOMENTS IN 3-CELL BRIDGE

Radius R			10,000	400	300	200
Load Case A	Girder 1	Moment	657.6	671.0	677.5	693.4
		%	.217	.222	.224	.227
	Girder 2	Moment	911.9	916.7	920.6	932.0
		%	.302	.303	.304	.305
	Girder 3	Moment	870.8	862.7	862.1	864.1
		%	.288	.286	.285	.283
	Girder 4	Moment	584.6	570.3	567.0	562.9
		%	.193	.189	.187	.185
	Total Moment		3024.9	3020.7	3027.2	3052.4
Load Case B	Girder 1	Moment	584.6	608.7	618.4	641.1
		%	.193	.199	.200	.204
	Girder 2	Moment	870.8	890.1	898.7	919.9
		%	.288	.290	.291	.293
	Girder 3	Moment	911.9	916.6	920.4	931.6
		%	.302	.299	.298	.296
	Girder 4	Moment	657.6	650.5	650.0	651.5
		%	.217	.212	.211	.207
	Total Moment		3024.9	3065.9	3087.5	3144.1

TABLE 6.8 GIRDER MOMENTS IN 4-CELL BRIDGE

Radius R			10 000	400	300	200
Load Case A	Girder 1	Moment	558.1			580.8
		%	.184			.194
	Girder 2	Moment	737.7			745.7
		%	.244			.249
	Girder 3	Moment	688.6			679.7
		%	.228			.226
	Girder 4	Moment	614.8			592.8
		%	.203			.198
	Girder 5	Moment	425.1			398.7
		%	.141			.133
	Total Moment		3024.3			2997.7
Load Case B	Girder 1	Moment	680.8			730.7
		%	.167			.175
	Girder 2	Moment	918.5			957.4
		%	.225			.230
	Girder 3	Moment	909.6			927.1
		%	.223			.222
	Girder 4	Moment	908.7			906.5
		%	.222			.217
	Girder 5	Moment	666.4			648.4
		%	.163			.156
	Total Moment		4084.0			4170.1
Load Case C	Girder 1	Moment	426.7			482.1
		%	.141			.151
	Girder 2	Moment	616.2			671.3
		%	.203			.210
	Girder 3	Moment	689.3			728.3
		%	.228			.228
	Girder 4	Moment	737.6			759.0
		%	.244			.237
	Girder 5	Moment	557.0			558.4
		%	.184			.174
	Total Moment		3026.8			3199.1
Load Case D	Girder 1	Moment	668.6			722.6
		%	.164			.172
	Girder 2	Moment	909.8			954.4
		%	.223			.228
	Girder 3	Moment	909.7			932.9
		%	.223			.222
	Girder 4	Moment	917.6			920.7
		%	.224			.220
	Girder 5	Moment	679.0			664.4
		%	.166			.158
	Total Moment		4084.7			4195.0

Tables 6.7 and 6.8 exhibit very similar characteristics as were observed for one- and two-cell bridges. As before, the total moment at midspan goes initially down with increasing curvature, if the standard AASHO trucks are shifted towards the center of curvature. But if the curvature grows further, then the total statical moment increases also from some specific curvature on. The critical load case for girder 1 and 2 of the three-cell bridge is case A, while case B produces the higher moments in girders 3 and 4, as one would expect. Likewise, in the four-cell bridge, the load cases A and B are critical for girders 1 and 2, while load cases C and D produce maximum moments in girders 3, 4, and 5.

In comparing the girder design moments for the three-cell bridge, it is interesting to note that the two interior girders 2 and 3 are subjected to about the same maximum moment for all considered curvature radii, while the design moment for girder 1 is always higher than for girder 4. However, the average of the moment percentages for girder 1 and 4 remains almost constant at the value .205, while the average of moment percentages for girders 2 and 3 is approximately .295, independent of the curvature. These values are again the relative girder stiffness factors, i.e., the ratio of the individual girder moment of inertia to the total bridge moment of inertia. The same observation can be made also with the four-cell bridge, where the stiffness factors are .163 for girders 1 and 5, .224 for girders 2 and 4, and .226 for girder 3.

Finally, it is desired to obtain a general idea of the effect of end boundary conditions on the load distribution of curved box girder bridges. So far, only simply supported bridges have been analyzed.

Below, the results for the two-cell box girder of Fig. 6.6 with one or both ends fixed against any displacements, will be presented for the two different truck positions of Fig. 6.8. The radius of curvature was chosen to be R = 200 ft., the span L = 100 ft., cell width B_t = 8 ft., and depth D = 5.5 ft. For the analysis, program FINPLA2 was used, and the results are summarized in Table 6.9. The following conclusions may be drawn from these results.

1. Comparing the girder moment percentages at midspan and at a fixed support, a redistribution of moments can be observed similar to the one previously found for straight bridges [10.3]. While girder 2 takes at both sections a comparable fraction of the total moment, girder 1 is released of much of the load due to truck A, while gaining only little additional load from truck B, so that as a net result, at a fixed end support, girders 1 and 2 receive moments of similar magnitude so that all three girders may be assigned moments proportional to their moment of inertia.
2. In comparing the results of Table 6.9 with the corresponding ones in Table 6.5 (L = 60 ft., B_t = 8 ft., R = 200 ft.), it is found that at the midspan section, girder 1 takes a fraction of the total moment which is almost independent of the end conditions (.297 for both ends simply supported, .292 for one end fixed, .296 for both ends fixed), while the share of girder 3 tends to decrease (.279, .262, .259 for the three cases).
3. Although the results of Table 6.9 are too few to permit any general conclusions, similar continuity effects can be observed as were reported on straight bridges [10.3]. Fixing either one or both end supports reduces the effective span, and a general

TABLE 6.9 MOMENTS IN CURVED BOX GIRDER WITH ONE OR BOTH ENDS FIXED

Moment at			Midspan		Support	
			Moment	%	Moment	%
One End Fixed	Truck A*	Girder 1	279.9	.334	-314.2	.302
		Girder 2	372.9	.445	-457.7	.440
		Girder 3	185.2	.221	-267.7	.258
		Total	838.0	1.000	-1039.6	1.000
	Truck B*	Girder 1	215.0	.251	-289.8	.259
		Girder 2	382.0	.447	-495.2	.442
		Girder 3	258.0	.302	-335.5	.299
		Total	855.0	1.000	-1120.5	1.000
	Truck A+B	Girder 1	494.9	.292	-604.0	.280
		Girder 2	754.9	.446	-952.9	.441
		Girder 3	443.2	.262	-603.2	.279
		Total	1693.0	1.000	-2160.1	1.000
Both Ends Fixed	Truck A*	Girder 1	210.4	.356	-203.4	.317
		Girder 2	261.9	.444	-281.6	.439
		Girder 3	117.7	.200	-156.7	.244
		Total	590.0	1.000	-641.7	1.000
	Truck B*	Girder 1	143.4	.236	-170.7	.250
		Girder 2	270.2	.446	-301.4	.442
		Girder 3	192.8	.318	-210.1	.308
		Total	606.4	1.000	-682.2	1.000
	Truck A+B	Girder 1	353.8	.296	-374.1	.283
		Girder 2	532.1	.445	-583.0	.440
		Girder 3	310.5	.259	-366.8	.277
		Total	1196.4	1.000	-1323.9	1.000

*See Fig. 6.8.

worsening of load distribution will result. As a consequence, girder moment distribution factors will increase, although the actual design moment might decrease because the total statical moment due to the truck loading is divided into positive midspan and negative support moments.

7. DESIGN OF CURVED BOX GIRDER BRIDGES

7.1 General

In Chapter 2, design had been defined in a very broad sense. It may be described as a process in the course of which by successive decisions the most important parameters are to be determined, followed by assigning values to the less important variables. As was seen in Chapter 2, the general alignment and geometrical layout of bridges are not likely to be determined by structural considerations. In most cases, in fact, they will be chosen in order to satisfy highway engineering or other requirements.

In the context of this chapter, design will be defined as follows. Given the major dimensions of individual bridge components, what strength has to be assigned to these components such that the bridge behaves satisfactorily under given loadings at optimum cost? For this purpose it will be necessary to determine the maximum shears and moments in all bridge girders under the most critical combination of loads.

Various approaches are possible to achieve this goal. As mentioned in Section 6.3, an accurate method would require many complete bridge analyses in order to construct maximum moment envelopes for each girder. Approximate design methods, however, will in most cases be justified and even preferable, as long as it can be shown that the resulting designs are on the safe side and not overconservative. Such a simplified design method will necessarily take all major influence parameters into account. For straight bridges, the concept of number of lines of wheel loads was very useful. Because the actual moment associated with one such wheel load line can be calculated fairly easily, any girder design moment may be determined as soon as it is known what the maximum possible number of wheel load lines falling on the considered girder is.

For curved bridges, this wheel load line concept cannot be applied without modification because the girder design moment due to one wheel load line is a function of the transverse position of the line of wheel loads. In Section 7.3, therefore, such a modification will be introduced into a simplified design method.

The emphasis in this chapter is put on global design of the bridge superstructure. Local design problems and substructure considerations are of different nature, but may be equally important. They will briefly be mentioned in Section 7.4.

7.2 Accurate Method of Design

The accurate determination of internal stresses in curved box girder bridges requires the availability of computer programs such as have been described in this dissertation, to give all important internal forces at any point of the structure, due to wheel loads, placed anywhere on the structure. Since both programs, CURSTR and FINPLA2, have been shown to converge towards results which are exact within the limitations of linear theory of elasticity, any degree of accuracy may be achieved with mesh refinement. An accurate design procedure would then involve the following steps.

1. Select for each bridge girder a set of points for construction of the maximum moment envelope--for continuous bridges also for minimum moments.
2. Using any appropriate refined method of analysis, establish the influence surface for the moment at some point A out of the set of

points selected in step 1. The ordinate at some point B of this surface would indicate the girder moment at point A due to a unit load at point B.

3. Find for this influence surface the most critical loading, by forming any possible combination of standard AASHO trucks and applying reduction factors if more than two lanes are loaded simultaneously. For the critical truck combination, add up the influence surface ordinates to obtain the maximum (or minimum) design moment for the girder under consideration at point A.
4. Repeat steps 2 and 3 for all the points selected in step 1.

The design method outlined above leads directly to the critical design moments, circumventing the determination of maximum numbers of wheel lines from which the critical moments would have to be determined in additional steps.

This refined design method is recommended mostly for unusual structures for which approximate design methods are not reliable. It may also lead to substantial savings whenever applied to repetitive standard structures. The disadvantage of this method lies in the large number of required complete bridge analyses and the considerable amount of data reduction. However, a multiple load case option in the computer program may permit the execution of all necessary load cases in one run, for little extra cost. A standard subroutine for plotting contour lines of influence surfaces will help reduce manual data reduction considerably.

7.3 Simplified Method of Design

Although the accurate design method outlined above may be used with advantage for many structures, engineers generally prefer to determine girder design moments by a much simpler procedure, preferably by a set of some simple equations, arguing that in most cases, the savings through a refined design method are so small that they hardly justify the computational effort involved in it.

The results from the parameter studies of Chapter 6 are not complete enough to base a very general design formula on them. However, these results do permit a general prediction of curved box girder behavior.

The proposed simplified design method would consist of the following steps.

1. Calculate the moment M_o due to one line of wheel loads applied to a straight beam of the same span as the developed length of the curved bridge reference line. For the simply supported beam of Fig. 7.1, this moment is given by

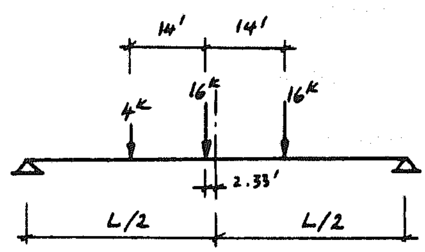

Fig. 7.1 Simply Supported Beam with One Wheel Line

$$M_o = 0.09\ L^2 - .8398L - 54.041 \quad (7.1)$$

where L is the span length.

2. Determine the number of wheel lines acting on the bridge, N_{WL}. For one traffic lane, $N_{WL} = 2$, for two traffic lanes, $N_{WL} = 4$, for three lanes, $N_{WL} = (6)(0.9) = 5.4$, and for four or more traffic lanes, $N_{WL} = (2N_L)(0.75) = 1.5\ N_L$, where N_L is the number of lanes.

3. Calculate for each girder the relative stiffness factor ρ, according to the formula

$$\rho = \frac{I_{Girder}}{I_{Bridge}} \tag{7.2}$$

where I_{Girder} is the moment of inertia of the girder under consideration, and I_{Bridge} is the moment of inertia of the total bridge cross section about the neutral axis. Because most box girder bridges have regular web spacings, Eq. (7.2) will have to be calculated usually only once for a typical interior girder, and once for a typical exterior girder.

4. Calculate girder moment distribution factors according to the formula

$$\alpha = 1 + \frac{B}{R}\left[2.1 - \frac{L'}{600}\right] \tag{7.3}$$

where

B is the average cell width

R is the radius of the bridge center line

L' is the effective space between inflection points

5. The final girder design moment is then found to be

$$M = \alpha \cdot \rho \cdot N_{WL} \cdot M_o \tag{7.4}$$

This design procedure is very approximate because a formula such as Eq. (7.3) usually will not fit all available data, unless it becomes unduly complicated and difficult to use. In particular, it will be very involved to capture the coupling effects of some of the parameters involved such as the relative magnitude between load concentration factors of girders on the inside and on the outside of the bridge. This parameter is completely ignored in Eq. (7.3). Besides, this formula should be restricted to radii $R \geq 100$ ft., effective spans $L' \leq 100$ ft., and cell widths $B \leq 16$ ft. The maximum value for α should be set at 1.20.

Additional parameter studies and further research might produce a formula equivalent to Eq. (7.3) which takes more of the important parameters into account. However, the form of Eq. (7.3) already indicates that curvature radii larger than 1000 ft. change the α-factors such a small amount that bridges with such small curvatures may be considered straight for analysis purposes.

7.4 Miscellaneous Design Considerations

Until now, only the global design of the bridge superstructure has been considered. It should be emphasized, however, that local design is of equal importance. In fact, tests and experienced bridge failures have shown, that if reinforced concrete bridges fail, they do so usually locally. But local design problems have not been discussed in this investigation, because it is the author's belief that the effect of curvature on local design is almost negligible, so that methods developed for straight bridges, may very well be applied also to curved bridges.

The substructure design, finally, also deserves special attention and careful engineering design, because the substructure often comprises a very important cost factor. In addition, curved bridges and in particular multi-span structures, pose a series of interesting and challenging problems, which are considered outside the scope of this dissertation. However, an excellent treatise on this subject matter has been presented by Leonhardt and Andrä [7.8]. Although this paper was published 10 years ago, most of their design recommendations are still valid today, with the exception of some complex bearing designs to which American bridge designers usually prefer much simpler solutions.

8. CONCLUSIONS

Due to the increased usage of curved bridges in modern highway systems it appears to be desirable to replace or reinspect the approximate design methods which are presently in use. In this dissertation, two refined methods of analysis have been developed which are capable of describing the complex structural behavior of curved bridges in a more accurate way than existing methods do. One method is based on the finite element method, and the other is the finite strip method as applied to curved folded plate structures.

Based on these new methods of analysis, curved box girder bridges were studied with special emphasis on their load distribution characteristics. Finally, design recommendations were developed. A so-called accurate method may be used to determine girder design moment with any desired degree of accuracy. This involves considerable computational effort. A simplified design method may help to determine the design moments only approximately but very rapidly. Additional parameter studies of curved box girder bridges may permit the refinement of the proposed design equations, so that these bridges may be designed in the future such that safety and also economy requirements are satisfied.

APPENDIX

BIBLIOGRAPHY

1. Selected References on Highway and Traffic Engineering

1.1 "A Policy on Geometric Design of Rural Highways," American Association of State Highway Officials, Washington, D.C., 1965.

1.2 "A Policy on Arterial Highways in Urban Areas," American Association of State Highway Officials, Washington, D.C., 1957.

1.3 "Geometric Design Standards for Highways Other Than Freeways," American Association of State Highway Officials, Washington, D.C., 1965.

1.4 "Highway Design and Operational Practices Related to Highway Safety," A Report of the Special AASHO Traffic Safety Committee, American Association of State Highway Officials, Washington, D.C., February, 1967.

1.5 "Road User Benefit Analyses For Highway Improvements," Informational Report by the Committee on Planning and Design Policies, American Association of State Highway Officials, Washington, D.C., 1960.

1.6 Oglesby, C. H. and L. I. Hewes, "Highway Engineering," Second Edition, John Wiley and Sons, Inc., New York, 1963.

1.7 Barnett, J., "Transition Curves for Highways," Bureau of Public Roads, U.S. Government Printing Office, Washington, D.C., 1940.

1.8 Leisch, J. E., "Adaptability of Interchanges to Interstate Highways," ASCE-Transactions, vol. 124, 1959, p. 588.

1.9 "The Freeway in the City," A Report to the Secretary, Department of Transportation, by the Urban Advisors to the Federal Highway Administrator, U.S. Government Printing Office, Washington, D.C., 1968.

1.10 Mumford, L., "The Highway and the City," A Mentor Book, 1964.

Bibliographical Notes

The references [1.1] through [1.5] contain a selected set of design standards, specifications, and recommendations for highways. The book by Oglesby and Hewes [1.6] is a basic and elementary, but also comprehensive introduction into highway engineering. References [1.7] and [1.8] are listed as selected in-depth treatment of transition curves and interchange design. The report [1.9] is a very valuable contribution in that the purely engineering and economic points of view are transcended, and aspects of cultural, sociologic, aesthetic, and similarly important considerations are treated with the weight they deserve. In [1.10], finally, a well known cultural critic publishes his ideas about the highway problem in today's cities.

2. Elementary Curved Beam Theory

2.1 de Saint-Venant, B., "Mémoire sur le calcul de la résistance et de la flexion des pièces solides à simple ou à double courbure," etc., (Analysis of solid beams of simple or double curvature, etc.), Comptes-Rendus, l'Académie des Sciences de Paris, Vol. 17, 1843, pp. 942-954, and pp. 1020-1031.

2.2 Resal, H., "De la déformation qu'éprouve une pièce à simple ou à double courbure sous L'action de forces qui lui font subir en même temps une flexion et une torsion," (On the deformation of a simply or doubly curved beam subjected to forces which produce bending and torsion), Journal de Mathématique pures et appliquées, Société Mathématique Francaise, Vol. 3, 1877, pp. 307-322.

2.3 Grashof, F. and R. Gärtner, "Theorie der Elastizität und Festigkeit," (Theory of elasticity and strength of materials), Berlin, 2nd Ed., p. 294.

2.4 Koenen, M., "Theorie gekrümmter Erker- und Balkonträger," (Theory of curved bow- and balcony girders), Deutsche Bauzeitung, 1885, p. 607.

2.5 Starkweather, G. P., "Bending Moments in Circular Girders," Engineering News, Vol. 42, 1900, p. 335.

2.6 Stutz, J., "Zur Theorie der halbringförmigen Balkonträger," (On the theory of semi-circular balcony girders), Zeitschrift des Österr. Ing. und Arch.-Ver., Dec. 2, 1904.

2.7 Ramisch, G., "Der halbringförmige und symmetrisch belastete Balkonträger," (The semicircular symmetrically loaded balcony girder), Zeitschrift des Österr. Ing. und Arch.-Ver., April 7, 1905.

2.8 Slocum, S. E., "A Simple Method for the Calculation of the Bending Strength of Curved Pieces," Engineering News, Vol. 55, 1906, p. 604.

2.9 Pfleiderer, C., "Die Beanspruchung stabförmiger Träger mit gekrümmter Mittellinie," (Stresses in prismatic curved beams), Zeitschrift des Vereins Deutscher Ingenieure, No. 82923D, Feb. 9, and No. 87652D, Sept. 21, 1907.

2.10 Andrews, E. S., "The Stresses in Curved Beams," Engineer, London, No. 32464A, April 19, 1912.

2.11 Müller-Breslau, H. "Die neueren Methoden der Festigkeitslehre," (New methods in the theory of strength of materials), 4th Ed., Leipzig, 1913, p. 265.

2.12 Kannenberg, B. G., "Zur Theorie torsionsfester Ringe," (On the theory of torque-resistant rings), Der Eisenbau, 1913, p. 329.

2.13 Gibson, A. H. and E. G. Ritchie, "A Study of the Circular-Arc Bow-Girder," Constable and Co., London, 1914.

2.14 Federhofer, K., "Berechnung des senkrecht zu seiner Ebene belasteten Bogenträgers," (Analysis of bow girders loaded normal to their plane), Zeitschrift für Mathematik und Physik, Vol. 62, 1914, pp. 40-63.

2.15 Marcus, H., "Abriss einer allgemeinen Theorie des eingespannten Trägers mit räumlich gewundener Mittellinie," (General theory of fixed girders curved in space), Zeitschrift für Bauwesen, 1914, pp. 198-223.

2.16 Marcus, H., "Die elastische Linie als räumliches Gebilde," (The elastica as spacial curve), Zentralblatt der Bauverwaltung, Vol. 36, 1916, p. 501.

2.17 Guest, J. J., "Curved Beams," Proceedings, Royal Society, London, Vol. 95, No. A665, Sept. 2, 1918, pp. 1-21.

2.18 Andrec, W. L., "Zur Berechnung gekrümmter Träger," (On the analysis of curved girders), Der Eisenbau, Vol. 9, 1918, pp. 184-190.

2.19 Beran, A., "Zur Berechnung von Balkonträgern," (On the analysis of balcony girders), Prager Technische Blätter, Vol. 3 and 4, 1919.

2.20 Marcus, H., "Die elastische Linie des doppelt gekrümmten Trägers," (The elastica of the doubly curved girder), Zeitschrift für Bauwesen, 1919, pp. 163-180.

2.21 Düsterbehn, F., "Ringförmige Träger," (Ring beams), Der Eisenbau, Vol. 11, No 3, Feb. 17, 1920, pp. 73-80.

2.22 Düsterbehn, F., "Biegungslinien ringförmiger Träger," (Bending lines of curved beams), Der Eisenbau, Vol. 12, No. 10, Oct. 11, 1921, pp. 249-264.

2.23 Unold, G., "Der Kreisträger," (The circularly curved girder), Forschungsarbeiten auf dem Gebiete des Ingenieurwesens, No. 255, Verein Deutscher Ingenieure, Berlin, 1922.

2.24 Heymans, P., "Torsion Problems of Curved Beams," Proceedings, National Academy of Science, Vol. 2, No. 2, Feb. 1925, pp. 161-166.

2.25 Winslow, A. M. and H. G. Edmonds, "Tests and Theory of Curved Beams," American Society of Mechanical Engineers, Advance Paper for Meeting Dec. 6-9, 1926.

2.26 Pippard, A. J. S., and F. L. Barrow, "The Stress Analysis of Bow Girders," Building Research Technical Paper No. 1, Dept. of Scientific and Industrial Research, His Majesty's Stationary Office, London, 1926, pp. 1-27.

2.27 Hessler, S., "Der nach einem Kreisbogen gekrümmte, beiderseits eingespannte Eisenbetonträger mit rechteckigem Querschnitt," (The circular curved reinforced concrete girder of rectangular cross section, fixed at both ends), Beton und Eisen, Vol. 26, No. 23, Dec. 5, 1927, pp. 429-433.

2.28 Biezeno, C. B., "Über die quasi-statische Berechnung geschlossener kreisförmiger Ringe konstanten Querschnittes," (On the quasi-static analysis of closed circular rings of constant cross section), Zeitschrift für angewandte Mathematik und Mechanik, Vol. 8, 1928, p. 237.

2.29 Hailer, J., "Beitrag zur Berechnung gekrümmter Träger," (Contribution to the analysis of curved girders), Bautechnik, Vol. 10, No. 28, June 24, 1932, p. 372; Corrections, No. 48, Nov. 4, 1932, p. 638.

2.30 Wilson, B. J., "A Simple Method of Determining Stress in Curved Flexural Members," University of Illinois, Engr. Exper. Station, Bulletin No. 20, Vol. xxv, 1932.

2.31 Oesterblom, I., "Bending and Torsion in Horizontally Curved Beams," ACI-Journal, Vol. 3, No. 9, May 1932, pp. 597-606; Discussion in Vol. 4, No. 3, Nov. 1932, pp. 153-160.

2.32 Keast, S. A., "Design of Curved Beams," Amerikanskaya Technika i Promyshlennost, Vol. 11, No. 3, March 1934, pp. 121-124.

2.33 Marquardsen, R. P. V., "Comparison of Curved and Straight Beams of Rectangular Cross-Section," Concrete, Vol. 43, No. 4, April 1935, pp. 11-12.

2.34 Fabbri, G., "Il Caicolo delle Travi ad Asse Curvo," (Analysis of curved beams), Annali del R. Instituto Superiore d'Ingegneria di Padova, Supplement to Vol. 4, No. 2, June 1935, pp. 75-85.

2.35 Kratochwilla, H., "Erkerträger aus Eisenbeton," (Reinforced concrete bow girders), Bauingenieur, Vol. 17, No. 21 22, May 29, 1936, pp. 211-214.

2.36 Hogan, M. B., "Circular Beams Loaded Normal to the Plane of Curvature," ASME Transactions, Journal of Applied Mechanics, Vol. 5, No. 2, June 1938, pp. A81-A85.

2.37 Moorman, R. B. B., "Semigraphical Method of Analysis for Horizontally Curved Beams," University of Missouri, Engr. Exper. Station, Bulletin No. 29, Vol. 39, No. 20, Oct. 15, 1938.

2.38 Moorman, R. B. B., "Stresses in Curved Beams Under Loads Normal to the Plane of its Axis," Iowa State College of Agriculture and Mechanical Arts, Engr. Exper. Station, Bulletin, Vol. 145, No. 38 and No. 41, March 1940.

2.39 Hogan, M. B., "The Solution of Closed Rings with Equally Spaced Supports,"Utah University, Engr. Exper. Station, Bulletin, Vol. 34, Nov. 1943.

2.40 Hogan, M. B., "Circular Beams Loaded Normal to the Plane of Curvature," ASME Transactions, Journal of Applied Mechanics, Vol. 11, No. 1, March 1944, pp. A51-A56.

2.41 Best, C. G., "Theory of Curved Beams," ASME Transactions, Journal of Applied Mechanics, Vol. 13, No. 4, Dec. 1946, pp. A294-A296.

2.42 Hogan, M. B., "The Deflection of Circular Arcs Subjected to Combined Flexure and Torsion," Utah University, Engr. Exper. Station, Bulletin No. 27, Vol. 35, No. 19, April 1947.

2.43 Moorman, R. B. B. and M. B. Tate, "Influence Lines for Horizontally Curved Fixed-End Beams of Circular-Arc Plan," Missouri University, Bulletin, Engr. Series, No. 35, 1947.

2.44 Beyer, K., "Die Statik im Stahlbetonbau," (Structural analysis for reinforced concrete structures), 2nd Ed., Springer-Verlag, Berlin, 1948.

2.45 Panayotounakos, E. D., "Transversely Loaded Circular Beams," Technika Chronika, Athens, Vol. 26, No. 298, April 1949, pp. 117-134.

2.46 Erlik, S., "Semi-Circular Bow Girders," Concrete and Constructional Engineering," Vol. 44, No. 6, June 1949, pp. 169-174.

2.47 Prudon, G., "Poutres circulaires chargées normalement à leur plan," (Circular beams loaded normal to their plan), Techniques des Travaux, Vol. 25, No. 9-10, Sept.-Oct., 1949, pp. 316-320.

2.48 Yu, T. M., "Shearing Stresses in Curved Beams," Scientific Record, Shanghai, Vol. 2, No. 4, Nov. 1949, pp. 401-408.

2.49 Panayotounakos, E. D., "Circular Helicoidal Beams," Technika Chronika (Athens), Vol. 27, No. 310, April 1950, pp. 216-220.

2.50 Langhaar, H. L., "Torsion of Curved Beams of Rectangular Cross Section," ASME Transactions, Journal of Applied Mechanics, Vol. 19, No. 1, March 1952, pp. 49-53.

2.51 Ratzersdorfer, J., "Solutions of Problems on Slightly Curved Beam," Aircraft Engineering, Vol. 24, No. 284, Oct. 1952, pp. 288-293, 319.

2.52 Volterra, E., "Bending of a Circular Beam Resting on an Elastic Foundation," ASME Transactions, Journal of Applied Mechanics, Vol. 19, No. 1, March 1952, pp. 1-4.

2.53 Swida, W., "Zur Statik des Kreisringträgers," (On the analysis of circular ring beams), Beton- und Stahlbetonbau, Vol. 48, No. 1, Jan. 1953, pp. 5-11.

2.54 Lazaro, A., Jr., "Design of Horizontal Circular Beams with Vertical Loads," Philippine Engr. Record, Vol. 13, No. 3-4, Jan. 1953, pp. 8-12.

2.55 Odqvist, F. K. G., "Theorie der elastischen Ringe starker Krümmung," (Theory of strongly curved elastic rings), Ingenieur-Archiv, Vol. 22, No. 2, 1953, pp. 98-107.

2.56 Volterra, E., "Deflection of Circular Beams Resting on Elastic Foundations Obtained by Methods of Harmonic Analysis," ASME, Journal of Applied Mechanics, Vol. 20, June 1953, pp. 227-232.

2.57 Volterra, E. and R. Chung, "Bending of Constrained Circular Beam Resting on Elastic Foundation," Proceedings, ASCE, Vol. 79, Separate No. 205, July 1953.

2.58 Federhofer, K., "Der senkrecht zu seiner Ebene belastete, elastisch gebettete Kreisringträger," (Circular ring beam on elastic foundation loaded normal to its plane), Zeitschrift für angewandte Mathematik und Mechanik, Vol. 33, No. 819, Aug/Sept 1953, pp. 292-293.

2.59 Johnson, W., "Expression for Circular Section Bow Girders Carrying a Concentrated Load," Engineer, Vol. 200, No. 5192, July 29, 1955, pp. 145-146.

2.60 Volterra, E., "Deflection of a Circular Beam Out of Its Initial Plane," ASCE-Transactions, Vol. 120, 1955, pp. 65-86.

2.61 Volterra, E., "Deflections of Bow Girders of Non-Circular Shapes," Journal of the Engineering Mechanics Division, ASCE, Vol. 82, No. EM1, Jan. 1956, paper 870.

2.62 Layrangues, P., "Calcul des pièces courbes à fibre moyenne plane et symétrique," (Analysis of curved beams with plane and symmetric axes), Travaux, Vol. 40, No. 262, Aug. 1956, pp. 465-472.

2.63 Abbassi, M. M., "Mathematical Analysis of Bow Girders of Any Shape," ASME Transactions, Journal of Applied Mechanics, Vol. 23, No. 4, December 1956, pp. 522-526.

2.64 Schulz, M. and M. Chedraui, "Tables for Circularly Curved Horizontal Beams with Symmetrical Uniform Loads," ACI-Journal, Vol. 28, No. 11, May 1957, pp. 1033-1040.

2.65 Holmes, A. M. C., "Analysis of Helical Beams Under Symmetrical Loading," Journal of the Structural Division, ASCE, Vol. 83, No. ST6, Nov. 1957, Proc. Paper 1437.

2.66 Trostel, R., "Beitrag zur Berechnung räumlich gekrümmter Stäbe nach der Theorie erster Ordnung," (Contribution to the first order theory of bars curved in space), Ingenieur-Archiv, 1957.

2.67 Mellor, P. B. and W. Johnson, "Approximate Deflections in Cantilevers Curved in Plan," Journal of the Royal Aeronautical Society, Vol. 62, No. 565, Jan. 1958, pp. 64-66.

2.68 Fursov, M. K., "K raschetu protchnosti krugovykh kolets," (On the strength analysis of circular rings), in Raschet Prostranstvennykh Konstruktsii (Analysis of three-dimensional structures), Vol. 4, Moscow, 1958, pp. 183-201.

2.69 Chatterji, P. P., "Torsion of Curved Beams of Rectangular Cross Section Having Transverse Isotropy," Zeitschrift für angewandte Mathematik und Mechanik, Vol. 38, March/April 1958, pp. 157-159.

2.70 Hansen, E., "Kreisringträger mit Rechteck-Querschnitt," (Circular ring beam with rectangular cross section), Bautechnik, Vol. 36, No. 8, August 1958, pp. 313-318.

2.71 Young, Y. F. and A. C. Scordelis, "An Analytical and Experimental Study of Helicoidal Girders," Journal of the Structural Division, ASCE, Vol. 84, No. ST5, Sept. 1958, Part 1, Proc. Paper 1756.

2.72 Fickel, H. H., "Analysis of Curved Girders," Journal of the Structural Division, ASCE, Vol. 85, No. ST7, Sept. 1959, Part 1, pp. 113-141.

2.73 Kämmel, G., "Zur Theorie des räumlich gekrümmten Stabes," (On the theory of bars curved in space), Ingenieur-Archiv, Vol. 27, No. 4, 1959, pp. 255-267.

2.74 Abbassi, M. M., "Stresses in Curved Beams of Non-Circular Center Line," ASME Transactions, Journal of Applied Mechanics, Vol. 27, Series E, No. 3, Sept. 1960, pp. 445-454.

2.75 Kyrklund, H., "Über die Einschätzung von Biegespannungen in gekrümmten Balken," (On the estimate of flexural stresses in curved beams), Acta Polytechnica Scandinavica, No. 274, Civil Engr. and Building Constr. Series, No. 6, 1960.

2.76 Roth, W., "Die tordierte, einfach gekrümmte Welle mit konstanter Krümmung," (Twisted, curved axle with constant curvature), Ingenieur-Archiv, Vol. 27, 1960, pp. 326-349.

2.77 Collins, W. H. and C. J. Gaylord, "Structural Analysis of Horizontally Curved Girders," AASHO Committee on Electronics, Regional Conf. on Improved Highway Engr. Productivity, San Francisco, Mar. 2-3, 1962, pt. 2, pp. 63-84.

2.78 Vreden, W., "Zur Berechnung des Kreisringträgers mit einseitig tangential anschliessendem geraden Trägerstück," (Analysis of circular beam attached to a straight beam segment), Beton- und Stahlbetonbau, Vol. 57, No. 9, Sept. 1962, pp. 212-215.

2.79 Mitchell, C. G. B., "Curved Beams," Journal of the Aeronautical Society, Vol. 68, No. 638, Feb. 1962, pp. 134-137.

2.80 Levy, R., "Displacements of Circular Rings with Normal Loads," Journal of the Structural Division, ASCE, Vol. 88, No. ST1, Feb. 1962, pp. 23-54.

2.81 Spyropoulos, P. J., "Circularly Curved Beams Transversely Loaded," ACI-Journal, Vol. 60, No. 10, Oct. 1963, pp. 1457-1470.

2.82 Dyrbye, C., "Beams Curved in Space," Bygnstat. Medd., Vol. 35, No. 1, July 1964, pp. 1-10.

2.83 Krahula, J. L., "Out of Plane Bending of a Uniform Circular Ring," IABSE, Publications, Vol. 25, 1965, pp. 205-215.

2.84 Stampf, W., "Der im Grundriss kreisförmige, totaleingespannte und symmetrische Balken," (Circular curved symmetric girder, fixed at both ends), Bautechnik, Vol. 42, No. 12, Dec. 1965, pp. 404-408.

2.85 Schlaich, J., "Der kontinuierlich gelagerte Kreisring unter antimetrischer Belastung," (Circular ring beam on continuous support and loaded antisymmetrically), Beton- und Stahlbetonbau, Vol. 62, No. 1, Jan. 1967, pp. 21-23.

2.86 Heimeshoff, B., "Praktische Spannungsberechnung für den gekrümmten Träger mit Rechteckquerschnitt," (Practical stress analysis for the curved rectangular beam), Bautechnik, Vol. 44, No. 4, April 1967, pp. 135-140.

2.87 Griffel, W., "Computer Simplifies Finding Reactions to Curved Beams," Engineering Materials and Design, Vol. 10, No. 5, May 1967, pp. 683-686.

2.88 Posthauer, R. J. and A. P. Cole, "Development of Charts for the Analysis of Curved Girders," Presented at the ASCE National Meeting on Transportation Engineering, Feb. 1968.

3. Theory of Continuous Curved Beams and Frames with Curved Members

3.1 Kaufmann, H., "Beitrag zur Berechnung kreisförmig gekrümmter Träger auf drei und mehr Stützen," (On the analysis of circular curved beams on three or more supports), Zeitschrift für Bauwesen, Vol. 69, Nos. 10-12, 1919, pp. 667-683.

3.2 Worch, G., "Beitrag zur Ermittlung der Formänderungen ebener Stabzüge mit rämlicher Stützung, etc.," (Determination of deformations of plane curved continuous beams), Beto und Eisen, Vol. 29, No. 9, May 5, 1930, pp. 167-173; No. 10, May 20, 1930, pp. 183-189; and No. 11, June 5, 1930, pp. 200-205.

3.3 Schmidt, A., "Beitrag zur Festigkeit der Systeme mit gebogenen Balken," (On the strength of systems with curved beams), Werft Reederei Hafen, Vol. 13, No. 23, Dec. 1, 1932, pp. 347-351.

3.4 Curiel-Benfield, E., "Moment Distribution in Bow-Girders," M.S. Thesis, Massachusetts Institute of Technology, Cambridge, Mass., 1942.

3.5 Hogan, M. B., "Moment Distribution Applied to Combined Flexure and Torsion," Utah University, Engin. Exper. Station, Bulletin No. 26, Vol. 35, No. 16, Feb. 1945.

3.6 Hogan, M. B., "Derivation of Two 5-Moment Theorems for Continuous Plane Curved Beams," Utah University, Engin. Exper. Station, Bulletin No. 31, April 1947.

3.7 Velutini, B., "Analysis of Continuous Curved Beams," ACI-Journal, Vol. 22, No. 3, Nov. 1950, pp. 217-228.

3.8 Saravanos, S., "Analysis of Structures Consisting of Curved Members of Variable Section," Aircraft Engineering, Vol. 22, No. 251, Jan. 1950, pp. 24-25.

3.9 Baron, F. and J. P. Michalos, "Laterally Loaded Plane Structures and Structures Curved in Space," ASCE Transactions, Vol. 117, 1952, pp. 279-311.

3.10 Michalos, J. P., "Numerical Analysis of Frames with Curved Girders," ASCE Transactions, Vol. 121, 1956, pp. 521-543.

3.11 Stampf, W., "Der durchlaufende Bogenträger auf elastischen Stützen mit und ohne Versteifungsträger," (Curved continuous girder on elastic supports with and without stiffening beams), Springer-Verlag, Berlin, 1960.

3.12 Baron, F., "Matrix Analysis of Structures Curved in Space," Journal of the Structural Division, ASCE, Vol. 87, No. ST3, March 1961, pp. 17-38.

3.13 Childress, W. H., "Analysis of Continuous Bent Beams Loaded Out of Plane by the Carry-Over Joint Method," M.S. Thesis, Oklahoma State University, Stillwater, Okla., 1962.

3.14 Patel, J. A., "Analysis of Continuous Circular Beams Loaded Out of Plane," M.S. Thesis, Oklahoma State University, Stillwater, Okla., 1962.

3.15 Patel, P. D., "Analysis of Continuous Bent Beams Loaded Out of Plane by the Six Moment Equations," M.S. Thesis, Oklahoma State University, Stillwater, Okla., 1962.

3.16 Kamel, M. E., "Influence Areas for Continuous Beams in Space," Ph.D. Thesis, Oklahoma State University, Stillwater, Okla., 1963.

3.17 Donald, P.T.A. and W. G. Godden, "Numerical Solution to Curved Beam Problem," Structural Engineer, Vol. 41, No. 6, June 1963, pp. 179-186.

3.18 Yamazaki, T. and T. Ota, "Three Dimensional Analysis of Frames with Curved Girders," Japan Society of Civil Engineers-Transactions, No. 107, July 1964, pp. 1-14.

3.19 Stampf, W., "Zur Berechnung des im Grundriss gebogenen durchlaufenden Balkens belastet durch Vertikalkräfte und Torsionsmomente," (Analysis of plane curved continuous beam subjected to vertical loads and torsional moments), Bautechnik, Vol. 41, No. 8, Aug. 1964, pp. 253-261.

3.20 Bretthauer, G. and F. Nötzold, "Ein Beitrag zur Berechnung von gekrümmten Durchlaufträgern mit starrer und torsionsweicher Einspannung über den Stützen," (On the analysis of curved continuous beams with rigid and flexible support fixity), Bauingenieur, Vol. 39, No. 10, Oct. 1964, pp. 402-406.

3.21 Vreden, W., "Die Berechnung des gekrümmten Durchlaufträgers," (Analysis of curved continuous beam), Verlag Wilh.Ernst und Sohn, Berlin-München, 1964.

3.22 Wittfoht, H., "Kreisförmig gekrümmte Träger," (Circular curved girders), Springer-Verlag, Berlin-Heidelberg-Göttingen-New York, 1964.

3.23 Teczan, S. S. and B. Ovunc, "Analysis of Plane and Space Frameworks with Curved Members," IABSE, Publications, Vol. 25, 1965, pp. 339-352.

3.24 Yamamoto, H., "On Slope-Deflection Equation and Moment Distribution Method of Circular-Arc Bow Beams," Japan Society of Civil Engineers-Transactions, No. 114, Feb. 1965, pp. 1-7.

3.25 Goto, S., "On Analysis for Three-Dimensional Frames with Circular Beams," Japan Society of Civil Engineers-Transactions, No. 126, Feb. 1966, pp. 108.

3.26 Petersen, C., "Das Verfahren der Übertragungsmatrizen für gekrümmte Träger," (Transfer matrix method for curved girders), Bauingenieur, Vol. 41, No. 3, March 1966, pp. 98-102.

3.27 Schulz, M. and D. Huber, "Zur Berechnung kreisförmig gekrümmter Durchlaufträger nach dem Momentenausgleichsverfahren," (Analysis of circular curved continuous beams by moment distribution), Beton- und Stahlbetonbau, Vol. 61, No. 3, March 1966, pp. 54-61.

3.28 Vreden, W., "Neues allgemeines Berechnungsverfahren beliebig gelagerter gekrümmter Träger," (New general analytical method for arbitrarily supported curved girders), Verlag Wilh. Ernst und Sohn, Berlin-München, 1966.

3.29 Michalos, J., "Matrix Formulation of the Force Method for a Structure Curved in Space," IABSE, Publications, Vol. 26, 1966, pp. 327-336.

3.30 Reddy, M. N., "Influence Lines for Continuous Curved Members Loaded Laterally," M.S. Thesis, Oklahoma State University, Stillwater, Okla., 1966.

3.31 Bazant, Z. P., "Conjugate Analogy of Space Structures," Journal of the Structural Division, ASCE, Vol. 92, No. ST3, June 1966, pp. 137-160.

3.32 Engel, S., "Structural Analysis of Circular Curved Beams," Journal of the Structural Division, ASCE, Vol. 93, No. ST1, Feb. 1967, pp. 221-234.

3.33 Reddy, M. N. and J. J. Tuma, "Analysis of Laterally Loaded Continuous Curved Beams," Journal of the Structural Division, ASCE, Vol. 93, No. ST1, Feb. 1967, pp. 495-513.

3.34 Petersen, C., "Die Übertragungsmatrix des kreisförmig gekrümmten Trägers auf elastischer Unterlage," (Transfer matrix for circular curved beam on elastic foundation), Bautechnik, Vol. 44, No. 8, Aug. 1967, pp. 289-294.

3.35 Wittfoht, H., "Kreisförmig gekrümmte Träger mit exzentrischer Belastung," (Eccentrically loaded circular curved beams), Bauingenieur, Vol. 43, No. 1, Jan. 1968, pp. 15-19.

3.36 Morris, D. L., "Curved Beam Stiffness Coefficients," Journal of the Structural Division, ASCE, Vol. 94, No. ST5, May 1968, pp. 1165-1174.

3.37 Toppler, J. F., B. K. Chaudhuri, I. J. van den Berg, and F. R. Harris, "Horizontally-Curved Members: An Approximate Method of Design," Concrete, Vol. 2, No. 10, Oct. 1968, pp. 418-425.

3.38 Young, M. C., "Flexibility Influence Functions for Curved Beams," Journal of the Structural Division, ASCE, Vol. 95, No. ST7, July 1969, pp. 1407-1429.

4. Theory of Curved Thin-Walled Beams and Box Beams

4.1 Stüssi, F., "Der Kreisträger mit I-Querschnitt," (Circular curved I-beam), Schweizerische Bauzeitung, Vol. 111, April 1938, p. 166.

4.2 Umanskii, A. A., "Raschet tonkostennykh krivolineinykh balok," (Analysis of thin-walled curved beams), Proceedings of the Scientific-Technical Conference of the VVA, Zhukovskovo, Vol. 2, No. 2, 1944.

4.3 Umanskii, A. A., "O raschete ploskikh krivykh tonkostennykh sterzhnei s konechnoi zhestkostyu svobodnovo krucheniya," (On the analysis of plane curved, thin-walled beams of finite rigidity in free torsion), Proceedings of the Scientific-Technical Conference of the VVA, Zhukovskovo, Vol. 2, No. 2, 1944.

4.4 Dzhanelidze, G. Y., "Teoriya tonkikh krivolineinykh sterzhnei obladayushchikh v poperechnom sechenii nedeformiruemym konturom," (Theory of thin-walled curved beams having a non-deformable cross section), Prikladnaya Mathematika i Mekhanika, Vol. 8, No. 1, 1944.

4.5 Rzhanitsyn, A. R., "Raschet metallicheskich dvutavrovykh balok, poluchivskikh nachalnoye iskrivlennye v gorizontalnoi ploskosti," (Analysis of metal I-beams with initial curvature in the horizontal plane), Moscow, Gosstroiizdat, 1946.

4.6 Moorman, R.B.B., "Stresses in Uniformly Loaded Circular-Arc I-Beam," Missouri University, Bulletin-Engineering Series, No. 36, Oct., 1947.

4.7 Umanskii, A. A., "Prostranstvennye sistemy," (Three-dimensional structural systems), Stroiizdat, Moscow, 1948.

4.8 Griunberg, N. I., "Izgib i kruchenie tonkostennykh krivolineinykh sterzhnei," (Bending and torsion of curved thin-walled beams), Trudy Lab. Stroit. Mekh. Tsentr. Nauch., Stroiizdat, Moscow, 1949.

4.9 Grigorev, Y. P., "K raschetu krivykh tonkostennykh brusjev," (On the analysis of curved thin-walled beams), in Raschet prostranstvennykh konstruktsii, (Analysis of three-dimensional structures), Moscow, Vol. 1, 1950, pp. 175-218.

4.10 Grigorev, Y. P., "Formulas and Tables for the Analysis of Thin-Walled Circular Rings," Mashtroiizdat, Moscow, No. 11, 1950.

4.11 Anderson, C. G., "Flexural Stresses in Curved Beams of I- and Box-Section," Institution of Mechanical Engineers, Proceedings, Vol. 163, War Emergency Proc. No. 62, 1950, pp. 295-306 (discussion, pp. 316-327).

4.12 Malkina, R. L., "On the Theory of Curved Thin-Walled Members," Inzh. Sb., Moscow, Izd. Akad. Nauk, USSR, Vol. 9, 1951.

4.13 Esslinger, M., "Torsion des poutres en I courbes," (Torsion of curved I-beams), Annales des Ponts et Chaussées, Vol. 122, No. 2, March/April, 1952, pp. 131-149.

4.14 Cutts, C. E., "Horizontally Curved Box Beams," ASCE-Proceedings, Vol. 78, Separate No. 128, May 1952.

4.15 Bechert, H. G., "Zur Statik räumlich gekrümmter Träger," (On the static analysis of beams curved in space), Dissertation, T. H. Karlsruhe, 1954.

4.16 Björklund, A., "Beitrag zur Theorie der elastischen Ringe mit Berücksichtigung der Wölbbehinderung," (On the theory of elastic ring with warping restraint), Ingenieur-Archiv, Vol. 23, 1955, pp. 421-435.

4.17 Vlasov, V. Z., "Thin-Walled Elastic Beams," 2nd Ed., Moscow, 1959, Israel Program for Scientific Translations, Jerusalem, 1961.

4.18 Dabrowski, R., "Equations of Bending and Torsion of Curved Thin-Walled Bar with Axisymmetric Cross Section," Archiwum Mechaniki Stosowanej, Vol. 12, No. 5-6, 1960, pp. 789-799.

4.19 Courbon, J., "Théorie des Ponts Courbes," (Theory of curved bridges), Annales des Ponts et Chaussées, Vol. 131, No. 5, Sept./Oct. 1961, pp. 611-648.

4.20 Konishi, I. and S. Komatsu, "Fundamental Theory of Thin-Walled Curved Girders," Japan Society of Civil Engineers-Transactions, No. 87, Nov. 1962, pp. 35-48.

4.21 Kreisel, M., "Zur Berechnung drehfester, konstant gekrümmter Träger mit beliebig räumlicher Belastung," (On the analysis of torque-resistant girders of constant curvature with arbitrary loading), Stahlbau, Vol. 31, No. 5, May 1962, pp. 153-156; corrections, Vol. 32, No. 12, Dec. 1963, p. 384.

4.22 Konishi, I. and S. Komatsu, "On the Fundamental Theory of Thin-Walled Curved Girder," Japan Society of Civil Engineers-Transactions, No. 87, Nov. 1962, pp. 35-48.

4.23 Close, R. A., "Deflection of Circular Curved I-Beams," Journal of the Structural Division, ASCE, Vol. 90, No. ST1, Feb. 1964, pp. 203-207.

4.24 Kuranishi, S., "Analysis of Thin-Walled Curved Beams," Japan Society of Civil Engineers-Transactions, No. 108, August 1964, pp. 7-12.

4.25 Fukasawa, Y., "Fundamental Theory of Thin-Walled Curved Bars in Static Analysis," Japan Society of Civil Engineers-Transactions, No. 110, October 1964, pp. 30-51.

4.26. Dabrowski, R., "Zur Berechnung von gekrümmten dünnwandigen Trägern mit offenem Profil," (On the analysis of curved thin-walled beams with open cross sections), Stahlbau, Vol. 33, No. 12, December 1964, pp. 364-372.

4.27 Dziewolski, R., "Flexion des tubes rectangulairés courbés," (Bending of curved box beams with small curvature radius), Construction Métallique, Vol. 4, Dec. 1964, pp. 20-24.

4.28 Anheuser, L., "Beitrag zur Berechnung des Kreisträgers mit offenem dünnwandigem Profil," (Contribution to the analysis of circular girder with open thin-walled profile), Dissertation, Technische Hochschule Stuttgart, 1964.

4.29 Dabrowski, R., "Näherungsberechnung der gekrümmten Kastenträger mit verformbarem Querschnitt," (Approximate analysis of curved box girders with deformable cross section), IABSE, Seventh Congress, Rio de Janeiro, Prelim. Publ. VI, 1964, pp. 299-306.

4.30 Dabrowski, R., "Wölbkrafttorsion von gekrümmten Kastenträgern mit nichtverformbarem Profil," (Torsion bending of curved box girders with nondistorting cross section), Stahlbau, Vol. 34, No. 5, May 1965, pp. 135-141.

4.31 Dabrowski, R., "Einflusslinien der Biege- und Wölbkraftmomente in gekrümmten dünnwandigen Trägern," (Influence lines for bending moments and bimoments in curved thin-walled girders), Stahlbau, Vol. 34, No. 7, July 1965, pp. 214-222.

4.32 Becker, G., "Ein Beitrag zur statischen Berechnung beliebig gelagerter ebener gekrümmter Stäbe," etc., (On the static analysis of arbitrarily supported plane curved beams, etc.), Stahlbau, Vol. 34, No. 11, Nov. 1965, pp. 334-346, and No. 12, Dec. 1965, pp. 368-377.

4.33 Bazant. Z. P., "Non-Uniform Torsion of Thin-Walled Bars of Variable Section," IABSE, Publications, Vol. 25, 1965, pp. 17-39.

4.34 Konishi, I. and S. Komatsu, "Three Dimensional Analysis of Curved Girders with Thin-Walled Cross Section," IABSE, Publications, Vol. 25, 1965, pp. 143-204.

4.35 Blake, A., "Design of Curved Members for Machines," Industrial Press, Inc., New York, 1966.

4.36 Brookhart, G. C., "Circular Arc I-Type Girders," Journal of the Structural Division, ASCE, Vol. 93, No. ST6, December 1967, pp. 133-159.

4.37 Leninger, W. J., "Analytical and Experimental Study of Girders Curved in Plan," M.S. Thesis, Pennsylvania State University, University Park, Pa., 1968.

4.38 McManus, P. F., "Non-Uniform Torsion of Beams of Composite, Open, Thin-Walled Cross Section," M.S. Thesis, Carnegie-Mellon University, Pittsburgh, Pa., 1968.

4.39 Spates, K. R. and C. P. Heins, "The Analysis of Single Curved Girders with Various Loadings and Boundary Conditions," Civil Engineering Department, University of Maryland, College Park, Md., June 1968.

4.40 Dabrowski, R., "Gekrümmte dünnwandige Träger," (Curved thin-walled girders), Springer-Verlag, Berlin-Göttingen-Heidelberg-New York, 1968.

4.41 Siminou, J. and C. P. Heins, "Proposed Equations for Preliminary Design of Curved Girders," Civil Engineering Department, University of Maryland, College Park, Md., June 1969.

4.42 Tung, D.H.H. and R. S. Fountain," Approximate Torsional Analysis of Curved Box Girders by the M/R-Method," Unpublished Paper, 1970.

4.43 Heins, C. P. and K. R. Spates, "Behavior of Single Horizontally Curved Girder," Journal of the Structural Division, ASCE, Vol. 96, No. ST7, July 1970, pp. 1511-1524.

5. Curved Plate and Grid Theory

5.1 Clebsch, A., "Theorie der Elastizität fester Körper," (Theory of elastic solids), Leipzig, 1862, p. 319.

5.2 Föppl, A., "Die Biegung einer kreisförmigen Platte," (Bending of a circular plate), Sitzungs-Bericht der Bayrischen Akademie der Wissenschaften, 1912, p. 155.

5.3 Melan, E., "Die Berechnung einer exzentrisch durch eine Einzellast belasteten Kreisplatte," (Analysis of a circular plate with eccentric concentrated load), Der Eisenbau, Vol. 17, 1926, p. 190.

5.4 Flügge, W., "Die strenge Berechnung von Kreisplatten unter Einzellasten," (Rigorous analysis of circular plates with concentrated loads), Springer-Verlag, Berlin, 1928.

5.5 Flügge, W., "Kreisplatten mit linear veränderlichen Belastungen," (Circular plates with linearly varying loadings), Bauingenieur, Vol. 10, 1929, p. 221.

5.6 Reissner, H., "Über die unsymmetrische Biegung dünner Kreisringplatten," (On the unsymmetrical bending of circular ring plates), Ingenieur-Archiv, Vol. 1, 1929, p. 72.

5.7 Reissner, E., "Über die Biegung der Kreisplatte mit exzentrischer Einzellast," (On the bending of the circular plate with eccentric concentrated load), Mathematische Annalen, Vol. 111, 1935, p. 777.

5.8 Timoshenko, S. P. and S. Woinowsky-Krieger, "Theory of Plates and Shells," McGraw-Hill Book Co., 1st Ed., 1940, 2nd Ed., 1959.

5.9 Carrier, G. F., "The Bending of the Clamped Sectorial Plate," ASME Transactions, Journal of Applied Mechanics, Vol. 11, No. 3, Sept. 1944.

5.10 Müller, W., "Die Durchbiegung einer Kreisplatte unter exzentrisch angeordneten Lasten," (Deflection of a circular plate under eccentrically applied loads), Ingenieur-Archiv, Vol. 13, 1943, p. 355.

5.11 Girkmann, K., "Flächentragwerke," (Two-dimensional structures), Springer-Verlag, Wien, 1st Ed., 1946, 6th Ed., 1963.

5.12 Persen, L. N., "Influence Fields for Circular and Infinite Cantilever Plates," Tekniske Skrifter, Nr. 1N, Oslo, 1951.

5.13 Gruber, E., "Gekrümmte Faltwerke," (Curved folded plates), Bautechnik-Archiv, No. 7, 1953, pp. 62-102.

5.14 Nowacki, W. and J. Mossakowski, "Influence Surfaces of Plates Shaped as Sectors of a Circular Ring," Académie Polonaise des Sciences - Bulletin, Vol. 1, No. 3, 1953 (see also Archiwum Mechaniki Stosowanej, Vol. 5, No. 2, 1953).

5.15 Rüdiger, D., "Die strenge Theorie der Faltwerke konstanter Krümmung," (Rigorous theory for folded plates of constant curvature), Österreichisches Ingenieur-Archiv, Vol. 11, No. 1, Jan. 1957, pp. 5-20.

5.16 Heinisch, K., "Einflussflächen für eine schiefwinklige, gekrümmte Dreifeldplatte mit veränderlicher Plattendicke," (Influence surfaces for a skew and curved plate of variable thickness, continuous over three fields), Beton- und Stahlbetonbau, Vol. 55, No. 3, March 1960, pp. 58-64.

5.17 Kaczkowski, Z. and M. Zyburtowicz, "Rozwiazywanie rusztow plaskich o pretach zakrywionych," (Solution of plane gridwork with curved bars), Archiwum Inzynierii Ladowej, Vol. 8, No. 3, 1962, pp. 283-310.

5.18 Yoshimura, J., "The Bending of a Curvilinear Orthotropic Circular Ring Sector Plate," Japan Society of Civil Engineers-Transactions, No. 82, May 1962, pp. 1-10.

5.19 Yoshimura, J., "The Bending of a Curvilinear Orthotropic Circular Ring Sector Plate with Varying Thickness," Japan Society of Civil Engineers-Transactions, No. 86, Sept. 1962, pp. 20-28, and No. 89, Jan. 1963, pp. 31-40.

5.20 Komatsu, S., "Structural Analysis for Continuous S-Shaped Curved Girder Bridge," Proceedings, 13th Japan National Congress for Applied Mechanics, 1963.

5.21 Coull, A. and A. S. Ergin, "Analysis of Bridge Slabs Curved in Plan," Civil Engineering and Public Works Review, Vol. 60, No. 713, Dec. 1963, pp. 1745-1749.

5.22 Gavarini, C., "Teoria della piastra ad ortotropia polare con rigidezze variabili secondo il raggio," (Theory of orthotropic polar plates of varying rigidity), Giornale del Genio Civile, No. 10 and 11, 1965.

5.23 Ceradini, G., "Teoria dei ponti in curva a travi multiple," (Theory of curved multiple-girder bridges), Construzioni Metalliche, No. 2, 1965, and No. 4, 1965.

5.24 Ceradini, G., "Theory of Multi-Girder Curved Bridges," IABSE, Publications, Vol. 25, 1965, pp. 51-63.

5.25 Gavarini, C., "Indagini sperimentali su modelli di ponte in curva a travi multiple," (Experimental investigation of a multiple girder curved bridge model), Bollettino Ingegneri di Firenze, No. 12, 1965.

5.26 Hass, B., "Über die Lastverteilung bei kreisförmig gekrümmten Trägerrosten," (On the load distribution of circular curved grids), Bautechnik, Vol. 42, No. 12, Dec. 1965, pp. 415-418.

5.27 Gavarini, C., "Teoria dei ponte in curva a travi multiple," (Theory of curved multiple-girder bridges), Construzioni Metalliche, No. 3, 1965, No. 6, 1965, and No. 4, 1966.

5.28 Komatsu, S. and M. Oyama, "The Analytical Method for Arbitrarily Shaped Grillage with Consideration of the Torsional Rigidity of its Main Girders," Japan Society of Civil Engineers - Transactions, No. 134, Oct. 1966, pp. 33-42.

5.29 Yonezawa, H. and I. Mikami, "On the Limit Analysis of Curved Grillage Girders," Japan Society of Civil Engineers - Transactions, No. 132, Aug. 1966, pp. 18-26.

5.30 Gravina, P., "Beitrag zur Theorie und Berechnung der zellenförmig und drehsymmetrisch ausgesteiften Kreisplatten," (Contribution to the theory and analysis of cellular circular plates with symmetrically provided stiffeners), IABSE, Publications, Vol. 26, 1966, pp. 169-191.

5.31 Yüksel, F., "Berechnung gekrümmter Durchlaufplatten," (Analysis of curved continuous plates), Beton- und Stahlbetonbau, Vol. 61, No. 2, Feb. 1966, pp. 39-46.

5.32 Heins, C. P. and C. T. G. Looney, "The Analysis of Curved Orthotropic Highway Bridges by Finite Difference Technique," University of Maryland, College Park, Md., Jan. 1967.

5.33 Sawko, F., "Computer Analysis of Grillages Curved in Plan," IABSE, Publications, Vol. 27, 1967, pp. 151-170.

5.34 Coull, A. and P. C. Das, "Analysis of Curved Bridge Decks," Proceedings, Institution of Civil Engineers, London, Vol. 37, May 1967, pp. 75-85.

5.35 Heins, C. P., "The Presentation of the Slope-Deflection Fourier Series Method for the Analysis of Curved Orthotropic Highway Bridges," University of Maryland, College Park, Md., June 1967.

5.36 Bell, L. C. and C. P. Heins, "The Solution of Curved Bridge Systems Using the Slope-Deflection Fourier Series Method," University of Maryland, College Park, Md., June 1968.

5.37 Hails, R. L. and C. P. Heins, "The Study of a Stiffened Curved Plate Model Using the Finite Difference Technique," University of Maryland, College Park, Md., June 1968.

5.38 Komatsu, S. and M. Hayashi, "Analysis of Curved Grillage Girder Bridge with Skewed Supports," Japan Society of Civil Engineers - Transactions, No. 156, Sept. 1968, pp. 11-24.

5.39 Heins, C. P. and R. L. Hails, "Behavior of Stiffened Curved Plate Model," Journal of the Structural Division, ASCE, Vol. 95, No. ST11, Nov. 1969, pp. 2353-2370.

5.40 Cheung, Y. K., "The Analysis of Cylindrical Orthotropic Curved Bridge Decks," IABSE, Publications, Vol. 29, Part 2, 1969, pp. 41-52.

5.41 Meyer, C. and A. C. Scordelis, "Analysis of Curved Folded Plate Structures," Structural Engineering and Structural Mechanics Report No. SESM 70-8, University of California, Berkeley, Calif., June 1970.

6. Analysis and Design of Curved Steel Bridges

6.1 Resal, M., "Calcul des ponts courbés," (Analysis of curved bridges), Annales des Ponts et Chaussées, 4e Trimestre, 1905.

6.2 Kapsch, "Die Eisenkonstruktionen der Viadukte und Brücken der Hamburger Hochbahn," (The steel structures of the viaducts and bridges for Hamburg's elevated rapid transit railway), Deutsche Bauzeitung, 1914, p. 591.

6.3 Gottfeld, H., "Die Berechnung räumlich gekrümmter Stahlbrücken," (Analysis of curved steel bridges), Bautechnik, Vol. 10, 1932, p. 715.

6.4 Gottfeld, H., "Einflusslinien für räumlich gekrümmte Stahlbrücken," (Influence lines for curved steel bridges), Stahlbau, Vol. 6, No. 8, April 1933, pp. 57-64.

6.5 Melan, J., "Zur Berechnung räumlich gekrümmter Stahlbrücken," (On the analysis of curved steel bridges), Bauingenieur, Vol. 14, 1933, p. 463.

6.6 Fuchs, G. A., "Kinematische Ermittlung der Einflusslinien gekrümmter Brücken," (Kinematic determination of influence lines for curved bridges), Stahlbau, Vol. 10, 1937, p. 37.

6.7 Kühl, E., "Über die Berechnung räumlich gekrümmter Stahlbrücken," (On the analysis of curved steel bridges), Bauingenieur, Vol. 18, 1937, p. 160.

6.8 Stüssi, F., "Zur Berechnung von Stahlbrücken mit gekrümmten Hauptträgern," (On the analysis of steel bridges with curved main girders), Denkschrift der ETH zum 100 jährigen Bestehen des SIA, Zürich, 1937, p. 138.

6.9 Melan, E., "Die Berechnung gekrümmter Blechträgerbrücken," (Analysis of curved plate girder bridges), Stahlbau, Vol. 13, 1940, p. 121.

6.10 Wanke, J., "Zur Berechnung Stählerner Brücken mit gekrümmten auf konzentrischen Kreisen liegenden Hauptträgern," (Analysis of steel bridges with curved main girders lying on concentric circles), Forschungshefte aus dem Gebiete des Stahlbaues, No. 3, 1941, Berlin.

6.11 Wansleben, F., "Die Berechnung drehfester gekrümmter Stahlbrücken," (Analysis of torque-resistant curved steel bridges), Stahlbau, Vol. 21, No. 4, April 1952, pp. 53-56.

6.12 Black, W. and R. Kao, "Curved Girders Please Eye and Budget," Engineering News-Record, Vol. 166, No. 5, Feb. 2, 1961, p. 32.

6.13 Kuranishi, S., "Analysis of the Curved Bridge with Multiple Main Plate Girders," Japan Society of Civil Engineers - Transactions, No. 76, Oct. 1961, pp. 13-20.

6.14 Bezzone, A. P., and J. J. Kozak, "The Curved Steel Girder," American Road Builder, Jan. 1962.

6.15 Kopetz, J., "Aesthetics and Design of Expressway Bridges," Proceedings of the Third Annual Bridge Engineering Conference, Colorado State University, March 1962.

6.16 Reimers, K., "Gekrümmte Hohlkastenbrücke über die Stresemann-strasse in Hamburg," (Curved box girder bridge overcrossing the Stresemann Street in Hamburg), Stahlbau, Vol. 31, No. 4, April 1962.

6.17 Fasullo, E. J., "Curving a Box Girder," Modern Steel Construction, AISC, Vol. 2, No. 4, Oct. 1962.

6.18 Konishi, I. and S. Komatsu, "Three Dimensional Analysis of Simply Supported Curved Girder Bridges," Japan Society of Civil Engineers - Transactions, No. 90, Feb. 1963, pp. 11-26.

6.19 Konishi, I. and S. Komatsu, "Three Dimensional Stress Analysis for Continuous Curved Girder Bridges," Japan Society of Civil Engineers - Transactions, No. 91, March 1963, pp. 13-23.

6.20 Komatsu, S., "Practical Formulas for Curved Bridges with Multiple Plate Girders," Japan Society of Civil Engineers - Transactions, No. 93, May 1963, pp. 1-9.

6.21 Richardson, Gordon, and Associates, "Analysis and Design of Horizontally Curved Steel Bridge Girders," United States Steel Corporation, Structural Report No. ADUCO 91063, Sept. 1963.

6.22 Komatsu, S. et al., "Practical Calculation Formula for Adjusting the Stress Acting in the Cross Section of Cross Beam of Box-Shape Girders on Curve," Journal of the Japan Society of Civil Engineers, Vol. 50, No. 5, May 1965, pp. 33-37.

6.23 Lavelle, F. H. and J. S. Boick, "A Program to Analyze Curved Girder Bridges," Engineering Bulletin No. 8, University of Rhode Island, Division of Research and Development, Dec. 1965.

6.24 "Highway Structures Design Handbook," Vol. 1, United States Steel Corporation, ADUSS 88-2222, 1965.

6.25 Robertson, W. T., "Design and Erection of Curved Girder Bridges," ASCE Environmental Engineering Conference, Oct. 18-22, 1965, Preprint 263.

6.26 Soto, M. H., "Analysis of Suspended Curved Girder," Journal of the Structural Division, ASCE, Vol. 92, No. ST1, Feb. 1966, pp. 21-38.

6.27 Lavelle, F. H., "Analysis of Curved Steel Girder Bridges," AISC- Engineering Journal, Vol. 3, No. 3, July 1966, pp. 101-105.

6.28 Jaeger, E. and J. O. McCutcheon, "The Elastic Analysis of Interconnected Bridge Girders," Eleventh International Congress on Applied Mechanics, Berlin, Proceedings, 1966, pp. 612-620.

6.29 Clarke, C. B., "Testing of a Model Curved Steel Girder Bridge," AISC-Engineering Journal, Vol. 3, No. 3, July 1966, pp. 106-112.

6.30 Schmitt, W., "Interchange Utilizes Arc Welded Horizontally Curved Girder Spans," Unpublished paper submitted to Lincoln Arc Welding Foundation, 1966.

6.31 Marks, N. G., "Experimental Transit Expressway in Pittsburgh - Design of the Elevated Roadway," ASCE Transportation Engineering Conference, Philadelphia, Pa., Oct. 17-21, 1966, Preprint 402.

6.32 Tung, D. H. H., "Analysis of Curved Twin Box Girder Bridges," ASCE Structural Engineering Conference, Seattle, May 8-12, 1967, Preprint 484.

6.33 Tachibana, Y., S. Kakumizu, S. Yamano, and T. Mekato, "Model Experiment of Continuous Curved Girder Bridge," Journal of the Japan Society of Civil Engineers, Vol. 52, No. 6, June 1967, pp. 50-55.

6.34 Thatcher, W. M., "Horizontally Curved Steel Girders - Fabrication and Design," AISC-Engineering Journal, Vol. 4, No. 3, July 1967, pp. 107-112.

6.35 Naruse, T. and I. Aihara, "Curved Gracing Structure Whose Outer End is Strengthened by Box Girder," Journal of the Japan Society of Civil Engineers, Vol. 53, No. 3, March 1968, pp. 31-38.

6.36 Komatsu, S. and M. Hayashi, "Practical Formulas for Curved Box Girder Bridge," Japan Society of Civil Engineers - Transactions, No. 152, April 1968, pp. 46-46.

6.37 Gillespie, J. W., "Analysis of Horizontally Curved Bridges," AISC-Engineering Journal, Vol. 5, No. 4, October 1968, pp. 137-143.

6.38 Young, R. W., "Analytical Study of Horizontally Curved Single-Span Bridges," M.S. Thesis, Pennsylvania State University, University Park, Pa., 1968.

6.39 Tayjasanant, A., "Analysis of Horizontally Curved Twin Box Girder Bridges," M.S. Thesis, Carnegie-Mellon University, Pittsburgh, Pa., 1968.

6.40 Brockenbrough, R. L., "Investigation of Heat-Curved Girders," Paper presented at Annual AASHO Meeting, Minneapolis, Minn., Dec. 5, 1968.

6.41 Culver, C. G. and P. P. Christiano, "Static Model Tests of Curved Girder Bridge," Journal of the Structural Division, ASCE, Vol. 95, No. ST8, August 1969, pp. 1599-1614.

7. Analysis and Design of Curved Concrete Beams and Bridges

7.1 Miller, H. D., "Mountain Pass Highway Bridge Built on Sharp Curve," Engineering News-Record, Vol. 94, No. 7, Feb. 12, 1925, pp. 278-279.

7.2 "Concrete Arch Bridge at Donner Summit, Calif.," Engineering News-Record, Vol. 96, No. 9, March 4, 1926, pp. 357-358.

7.3 Hessler, S., "Der kontinuierliche, halbkreisförmig gebogene und gleichmässig belastete Eisenbetonträger, etc.," (Continuous, semicircular curved reinforced concrete girder with uniform load), Beton und Eisen, Vol. 29, No. 8, April 20, 1930, pp. 149-154.

7.4 "Curved Box Girders for Highway Overpass," Engineering News-Record, Vol. 129, No. 21, Nov. 19, 1942, pp. 698-699; see also Concrete and Constructional Engineering, Vol. 38, No. 10, Oct. 1943, pp. 327-328.

7.5 Foley, E. R. and G. D. Gilbert, "Box Girder on Single Columns Supports Curved Bridge Deck," Engineering News-Record, Vol. 140, No. 24, June 10, 1948, pp. 942-944.

7.6 Morgan, V. A., "The Design of an Unusual Bow Girder," Concrete and Constructional Engineering, Vol. 47, No. 2, Feb. 1952, pp. 47-55.

7.7 Johannson, J., "Räumlich gekrümmte Rahmenbrücke in Caracas," (Curved framed bridge in Caracas), Beton- und Stahlbetonbau, Vol. 55, No. 1, Jan. 1960, pp. 1-6.

7.8 Leonhardt, F. and W. Andrä, "Stützungsprobleme der Hochstrassenbrücken," (Problems of supporting elevated roadway bridges), Beton- und Stahlbetonbau, Vol. 55, No. 6, June 1960, pp. 121-137.

7.9 Bechert, H., "Zur Berechnung gekrümmter einfeldriger Brücken," (On the analysis of curved bridges on two supports), Beton- und Stahlbetonbau, Vol. 58, No. 12, Dec. 1963, pp. 279-284.

7.10 Bretthauer, G. and H. Kappei, "Zur Querverteilung bei unsymmetrisch geraden und gekrümmten zweistegigen Plattenbalkenbrücken," (On load distribution of straight and curved plate and girder bridges with two girders), Beton- und Stahlbetonbau, Vol. 58, No. 12, Dec. 1963, pp. 288-295.

7.11 O'Gara, M. B. and T. J. Bezonska, "Field Study of Curved Continuous Prestressed Bridge," PCI-Journal, Vol. 8, No. 6, Dec. 1963, pp. 14-23.

7.12 Menn, C., "Zur Berechnung gekrümmter Brücken," (On the analysis of curved bridges), Schweizerische Bauzeitung, Vol. 82, No. 12, March 19, 1964, pp. 185-191.

7.13 "23rd Avenue Overpass at Oakland, California," Constructional Review, Vol. 36, No. 9, Sept. 1963, pp. 10-12; see also Engineering News-Record, Vol. 173, No. 17, Oct. 22, 1964, pp. 34-36.

7.14 Grover, J. R., "Fabricating and Testing a 49-ft. Curved Pretensioned Concrete Beam," PCI-Journal, Vol. 10, No. 5, Oct. 1965, pp. 28-48.

7.15 Wittfoht, H., "Die Autobahnbrücke über das Siegtal in Siegen-Eiserfeld," (Freeway bridge over the Sieg-valley in Siegen-Eiserfeld, Germany), Bauingenier, Vol. 41, No. 10, Oct. 1966, pp. 393-399.

7.16 Renard, J., "Etude des Ponts Courbes," (Study of Curved Bridges), Annales des Travaux Publics de Belgique, No. 1, Feb. 1967, pp. 49-74.

7.17 Bassi, K. G., Lin, W. L. and B. S. Richardson, "Continuous Post-Tensioned Torsionally Stiff Concrete Bridges," First International Symposium on Concrete Bridge Design, Toronto, April 5, 1967, ACI Publication, SP-23, pp. 563-577.

7.18 Witecki, A. A., "Simplified Method for the Analysis of Torsional Moments as an Effect of a Horizontally Curved Multi Span Continuous Bridge," First International Symposium on Concrete Bridge Design, Toronto, April 5, 1967, ACI Publication SP-23, pp. 193-204.

7.19 Tamberg, K. G., "Aspect of Torsion in Concrete Structure Design," Torsion of Structural Concrete, ACI Publication SP-18, pp. 7-68.

7.20 Schreck, P., "Fertigteilbrücken mit gekrümmten Längsträgern," (Precast curved girder bridges), Bautechnik, Vol. 44, No. 2, Feb. 1967, pp. 68-69.

7.21 Chung, H. W. and N. J. Gardner, "Model Investigation of Tsing Fung Street Flyover," Department of Civil Engineering, University of Hong Kong, July 1968.

7.22 Chung, H. W. and N. J. Gardner, "Model Tests of a Curved Prestressed Concrete Cellular Bridge," Civil Engineering and Public Works Review, Vol. 63, No. 748, Nov. 1968, pp. 1253-1259.

8. Dynamic Analysis of Curved Beams and Bridges

8.1 Michell, H., "The Small Deformations of Curves and Surfaces with Application to the Vibration of a Helix and a Circular Ring," Messenger of Mathematics, Vol. 19, 1890, pp. 68-83.

8.2 Federhofer, K., "Dynamik des Bogenträgers und Kreisringes," (Dynamic analysis of the bow girder and circular ring beam), Springer-Verlag, Wien, 1950.

8.3 Volterra, E., "The Equations of Motion for Curved Elastic Bars Deduced by the Use of the 'Method of Internal Constraints,'" Ingenieur-Archiv, Vol. 23, No. 6, 1955, pp. 402-409.

8.4 Schumpich, G., "Beitrag zur Kinetik und Statik ebener Stabwerke mit gekrümmten Stäben," (Contribution to the dynamic and static analysis of plane frames with curved members), Österreichisches Ingenieur-Archiv, Vol. 11, No. 3, 1957, pp. 194-225.

8.5 Bielewicz, E. and H. Mikolajezak, "A Certain Case of a Moving Load Effect on a Curved Bar," Archiwum Inzynierii Ladowej, Vol. 7, No. 4, 1961, pp. 523-534.

8.6 Volterra, E. and J. D. Morell, "Lowest Natural Frequencies of Elastic Arcs," Journal of the Acoustical Society of America, Vol. 33, No. 12, Dec. 1961.

8.7 Volterra, E. and J. D. Morell, "Lowest Natural Frequency of Elastic Arc for Vibrations Outside the Plane of Initial Curvature," ASME - Transactions, Journal of Applied Mechanics, Vol. 28, Dec. 1961, pp. 624-627.

8.8 Yonezawa, H., "Moments and Free Vibrations in Curved Girder Bridges," Journal of the Engineering Mechanics Division, ASCE, Vol. 88, No. EM1, Feb. 1962, pp. 1-22.

8.9 Ojalvo, I. U., "Coupled Twist-Bending Vibrations of Incomplete Elastic Rings," International Journal of Mechanical Sciences, Vol. 4, 1962, pp. 53-72.

8.10 Kolousek, V., "Vibrations of Systems with Curved Members," IABSE, Publications, Vol. 23, 1963, pp. 219-232.

8.11 Hammoud, A. S. and R. R. Archer, "On the Free Vibration of Complete and Incomplete Rings," Developments in Mechanics, ed. by S. Ostrach and R. H. Scanlan, Pergamon Press, New York, April 1963.

8.12 Lang, T. E., "Vibration of Thin Circular Rings," Technical Report No. 32-261, Jet Propulsion Laboratory, Caltech, Pasadena, Calif., March 1, 1963.

8.13 Guto, H. et al., "Model Dynamical Studies on S-Shaped Curved Girder Bridges," 19th Annual Conference of the Japan Society of Civil Engineers, May 1964.

8.14 Hirai, A. and Y. Fukazawa, "Analysis of the Dynamical Problem of Curved Girder Bridges," 19th Annual Conference of the Japan Society of Civil Engineers, May 1964.

8.15 Ojalvo, I. U. and N. Newman, "Natural Frequencies of Clamped Ring Segments," Machine Design, Vol. 36, No. 12, May 1964, pp. 219-222.

8.16 Ojalvo, I. U. and N. Newman, "Natural Frequencies of Cantilevered Ring Segments," Machine Design, Vol. 37, No. 7, March 1965, pp. 191-195.

8.17 Massoud, M. P., "Vectorial Derivation of the Equations for Small Vibrations of Twisted Curved Bars," ASME - Transactions, Journal of Applied Mechanics, Vol. 32, June 1965, pp. 439-440.

8.18 Tan, C. P. and S. Shore, "Dynamic Response of Horizontally Curved Beam Subjected to Travelling Forces and Spring Masses," Proceedings, 5th U.S. National Congress of Applied Mechanics, 1966.

8.19 Komatsu, S. and H. Nakai, "Study on Free Vibration of Curved Girder Bridges," Japan Society of Civil Engineers - Transactions, No. 136, Dec. 1966, pp. 35-60.

8.20 Tan, C. P., "Dynamic Response of a Horizontally Curved Beam Subjected to Simulated Highway Loadings," Ph.D. Dissertation, University of Pennsylvania, Philadelphia, Pa., 1966.

8.21 Culver, C. G., "Natural Frequencies of Horizontally Curved Beams," Journal of the Structural Division, ASCE, Vol. 93, No. ST2, April 1967, pp. 189-203.

8.22 Christiano, P. P., "The Dynamic Response of Horizontally Curved Bridges Subjected to Moving Loads," Ph.D. Dissertation, Carnegie-Mellon University, Pittsburgh, Pa., 1967.

8.23 Tan, C. P. and S. Shore, "Dynamic Response of a Horizontally Curved Bridge," Journal of the Structural Division, ASCE, Vol. 94, No. ST3, March, 1968, pp. 761-781.

8.24 Tan, C. P. and S. Shore, "Response of Horizontally Curved Bridge to Moving Load," Journal of the Structural Division, ASCE, Vol. 94, No. ST9, Sept. 1968, pp. 2135-2151.

8.25 Reddy, M. N., "Lateral Vibrations of Plane Curved Bars," Journal of the Structural Division, ASCE, Vol. 94, No. St10, Oct. 1968, pp. 2197-2212.

8.26 Oestel, D. J., "Dynamic Response of Multi-Span Curved Bridges," M.S. Thesis, Carnegie-Mellon University, Pittsburgh, Pa., 1968.

8.27 Christiano, P. P. and C. G. Culver, "Dynamic Studies and Impact Factors for Curved Girder Bridges," Paper presented at the Annual ASCE Meeting on Structural Engineering, Pittsburgh, Pa., Sept. 30 - Oct. 4, 1968.

8.28 Christiano, P. P. and C. G. Culver, "Horizontally Curved Bridges Subject to Moving Load," Journal of the Structural Division, ASCE, Vol. 95, No. ST8, Aug. 1969, pp. 1615-1643.

8.29 Culver, C. G. and D. J. Oestel, "Natural Frequencies of Multi-span Curved Beams," Journal of Sound and Vibration, Vol. 10, No. 3, Nov. 1969, pp. 380-389.

9. Miscellaneous References on Curved Beams and Bridges

9.1 Mayer, R., "Über Stabilität und Elastizität des Kreisbogens," (On stability and elasticity of circular beams), Zeitschrift für Mathematik und Physik, Vol. 61, 1913, p. 302.

9.2 Timoshenko, S. P., "Kippsicherheit des gekrümmten Stabes mit kreisförmiger Mittellinie," (Safety of circularly curved bar against lateral buckling), Zeitschrift für angewandte Mathematik und Physik, Vol. 23, 1923.

9.3 Federhofer, K., "Kippsicherheit des kreisförmig gekrümmten Trägers mit einfachsymmetrischem, dünnwandigem und offenem Querschnitte bei gleichmässiger Radialbelastung," (Lateral buckling of circular curved girders with singly-symmetric thin-walled and open cross sections under uniform radial load), Österreichisches Ingenieur-Archiv, Vol. 4, No. 1, 1950, pp. 27-44.

9.4 Boulton, N. S. and B. Boonsukha, "Plastic Collapse Loads for Circular-Arc Bow Girders," Institution of Civil Engineers, Proceedings, Vol. 13, June 1959, pp. 161-178.

9.5 Vlasov, V. Z., "Thin-Walled Elastic Beams," 2nd Ed., Moscow, 1959, Israel Program for Scientific Translations, Jerusalem, 1961.

9.6 Goldberg, J. E. and J. L. Bogdanoff, "Out-of-Plane Buckling of I-Section Rings," IABSE, Publications, Vol. 22, 1962, pp. 73-92.

9.7 Chu, K. H. and A. Thelen, "Plastic Analysis of Circular Balcony Girders," Journal of the Structural Division, ASCE, Vol. 89, No. ST6, Part 1, Dec. 1963, pp. 159-186.

9.8 Imegwu, E. O., "Ultimate Strength of Plane Curved Girders," Structural Engineer, Vol. 42, No. 4, April 1964, pp. 129-134.

9.9 Washizu, K., "Some Considerations on a Naturally Curved and Twisted Slender Beam," Journal of Mathematical Physics, Vol. 43, No. 2, June 1964, pp. 111-116.

9.10 Jackson, N., "The Automatic Calculation of Collapse Loads for Circular-Arc Beams," Structural Engineer, Vol. 43, No. 12, Dec. 1965, pp. 413-421.

9.11 Chu, Y. K., "Beuluntersuchung von ebenen Stegblechen kreisförmig gekrümmter Träger mit I-Querschnitt," (Study on buckling of plane webs of circular curved I-beams), Stahlbau, Vol. 35, No. 5, May 1966, pp. 129-142.

9.12 Jackson, N., "Collapse Loads for Circular-Arc Beams," Journal of the Structural Division, ASCE, Vol. 92, No. ST5, Oct. 1966, pp. 1-12.

9.13 Roll, F. and I. Aneja, "Model Tests of Box-Beam Highway Bridges with Cantilevered Deck Slabs," ASCE Transportation Engineering Conference, Philadelphia, Pa., Oct. 17-21, 1966, Preprint 395.

9.14 Aneja, I., "Experimental and Analytical Study of a Horizontally Curved Box-Beam Highway Bridge Model," Ph.D. Dissertation, University of Pennsylvania, Philadelphia, Pa., 1968.

9.15 Frampton, R., "Local Instability of Horizontally Curved Members," M.S. Thesis, Carnegie-Mellon University, Pittsburgh, Pa., 1968.

9.16 McManus, P. F., G. A. Nasir, and C. G. Culver, "Horizontally Curved Girders - State of the Art," Journal of the Structural Division, ASCE, Vol. 95, No. ST5, May 1969, pp. 853-870.

9.17 Ojalvo, M., E. Demuts, and F. Tokarz, "Out-of-Plane Buckling of Curved Members," Journal of the Structural Division, ASCE, Vol. 95, No. ST10, Oct. 1969, pp. 2305-2316.

9.18 Culver, C. G. and R. Frampton, "Local Instability of Horizontally Curved Members," Journal of the Structural Divison, ASCE, Vol. 96, No. ST2, Feb. 1970, pp. 245-265.

10. Selected References on Prismatic Folded Plates and Miscellaneous Topics

10.1 Scordelis, A. C., "Analysis of Simply Supported Box Girder Bridges," Structural Engineering and Structural Mechanics Report No. SESM 66-17, University of California, Berkeley, Calif., Oct. 1966.

10.2 Scordelis, A. C., "Analysis of Continuous Box Girder Bridges," Structural Engineering and Structural Mechanics Report No. SESM 67-25, University of California, Berkeley, Calif., Nov. 1967.

10.3 Scordelis, A. C. and C. Meyer, "Wheel Load Distribution in Concrete Box Girder Bridges," Structural Engineering and Structural Mechanics Report No. SESM 69-1, University of California, Berkeley, Calif., Jan., 1969.

10.4 Willam, K. J. and A. C. Scordelis, "Analysis of Orthotropic Folded Plates with Eccentric Stiffeners," Structural Engineering and Structural Mechanics Report No. SESM 70-2, University of California, Berkeley, Calif., Feb. 1970.

10.5 Meyer, C. and A. C. Scordelis, "Computer Program for Prismatic Folded Plates with Plate and Beam Elements," Structural Engineering and Structural Mechanics Report No. SESM 70-3, University of California, Berkeley, Calif., Feb. 1970.

10.6 Willam, K. J., "Finite Element Analysis of Cellular Structures," Ph.D. Dissertation, University of California, Berkeley, Calif., Dec. 1969.

10.7 Abu Ghazaleh, B. N., "Analysis of Plate Type Prismatic Structures," Ph.D. Dissertation, University of California, Berkeley, Calif., 1966.

10.8 Lo, K. W., "Analysis of Cellular Folded Plate Structures," Ph.D. Dissertation, University of California, Berkeley, Calif., 1967.

10.9 Felippa, C. A., "Refined Finite Element Analysis of Linear and Nonlinear Two-Dimensional Structures," Ph.D. Dissertation, University of California, Berkeley, Calif., 1966.

10.10 Zienkiewicz, O. C., "The Finite Element Method in Structural and Continuum Mechanics," McGraw-Hill Publ. Comp. Ltd., London-New York, 1967.

10.11 Dunham, R. S. and R. E. Nickell, "Finite Element Analysis of Axisymmetric Solids with Arbitrary Loadings," Structural Engineering and Structural Mechanics Report No. SESM 67-6, University of California, Berkeley, Calif., June 1967.

10.12 Grafton, P. E. and D. R. Strome, "Analysis of Axisymmetric Shells by the Direct Stiffness Method," AIAA Journal, Vol. 1, 1966, pp. 2342-2347.

10.13 Percy, J. H., T. H. H. Pian, S. Klein, and D. R. Navaratna, "Application of Matrix Displacement Method to Linear Elastic Analysis of Shells of Revolution," AIAA Journal, Vol. 3, No. 11, Nov. 1965, pp. 2138-2145.

10.14 Rüdiger, D., "Die strenge Theorie anisotroper prismatischer Faltwerke," (Rigorous theory of prismatic anisotropic folded plates), Ingenier-Archiv., Vol. 23, 1955.

10.15 Goldberg, J. E. and H. L. Leve, "Theory of Prismatic Folded Plate Structures," IABSE, Publications, Vol. 17, 1957, pp. 59-86.

10.16 DeFries-Skene, A. and A. C. Scordelis, "Direct Stiffness Solution for Folded Plates," Journal of the Structural Division, ASCE, Vol. 90, No. ST4, Aug. 1964, pp. 15-47.

10.17 Cheung, Y. K., "The Finite Strip Method in the Analysis of Elastic Plates with Two Opposite Simply Supported Ends," Proceedings, Institution of Civil Engineers, Vol. 40, May 1968, pp. 1-7.

10.18 Cheung, Y. K., "Folded Plate Structures by Finite Strip Method," Journal of the Structural Division, ASCE, Vol. 95, No. ST12, Dec. 1969, pp. 2963-2979.

10.19 Powell, G. H. and D. W. Ogden, "Analysis of Orthotropic Steel Plate Bridge Decks," Journal of the Structural Division, ASCE, Vol. 95, No. ST5, May 1969, pp. 909-922.

10.20 Popov, E. P., J. Penzien, and Z. A. Lu, "Finite Element Solution for Axisymmetric Shells," Journal of the Engineering Mechanics Division, ASCE, Vol. 90, No. EM5, pt. 1, Oct. 1964, pp. 119-145.

10.21 Flügge, W., "Stresses in Shells," Third Printing, Springer-Verlag, New York, 1966.

10.22 Novozhilov, V. V., "Theory of Thin Shells," 2nd Ed., Groningen, P. Noordhoff, 1964.

10.23 Kraus, H., "Thin Elastic Shells," John Wiley & Sons, Inc., New York, 1967.

10.24 Fox, L., "An Introduction to Numerical Linear Algebra," Oxford University Press, New York, 1965.

10.25 Guyon, Y., "Calcul des Ponts Larges a Poutres Multiples Solidarisees par des Entretoises," Annales des Ponts et Chaussees, No. 24, Paris, 1946.

10.26 Massonet, C., "Methode de Calcul des Ponts a Poutres Multiples Tenant Compte de Leur Resistance a la Torsion," IABSE Publications, Vol. 10, 1950.

10.27 Rowe, R. E., "Concrete Bridge Design," John Wiley & Sons, 1962.

10.28 Przemieniecki, J. S., "Theory of Matrix Structural Analysis," McGraw-Hill Book Co., New York, 1968.

10.29 "Standard Specifications for Highway Bridges," American Association of State Highway Officials, Ninth Edition, Washington, D.C., 1965.